TU Delft

Delft University of Technology

Document Version
Final published version

Citation (APA)
Kopka, T. (2026). *Modular Power System Control for Fuel Cell-Battery Ships*. [Dissertation (TU Delft), Delft University of Technology]. https://doi.org/10.4233/uuid:5edaa16a-ea1c-49d8-89a0-9a357cf9b316

Important note
To cite this publication, please use the final published version (if applicable).
Please check the document version above.

Copyright
In case the licence states “Dutch Copyright Act (Article 25fa)”, this publication was made available Green Open Access via the TU Delft Institutional Repository pursuant to Dutch Copyright Act (Article 25fa, the Taverne amendment). This provision does not affect copyright ownership.
Unless copyright is transferred by contract or statute, it remains with the copyright holder.

Sharing and reuse
Other than for strictly personal use, it is not permitted to download, forward or distribute the text or part of it, without the consent of the author(s) and/or copyright holder(s), unless the work is under an open content license such as Creative Commons.

Takedown policy
Please contact us and provide details if you believe this document breaches copyrights.
We will remove access to the work immediately and investigate your claim.

This work is downloaded from Delft University of Technology.

Modular Power System Control for Fuel Cell–Battery Ships



Timon Kopka

Modular Power System Control for Fuel Cell-Battery DC Ships

Modular Power System Control for Fuel Cell-Battery DC Ships

Dissertation

for the purpose of obtaining the degree of doctor
at Delft University of Technology
by the authority of the Rector Magnificus,
Prof.dr.ir. H. Bijl,
chair of the Board for Doctorates
to be defended publicly on
Thursday, 24 September 2026 at 12:30

by

Timon KOPKA

This dissertation has been approved by the promotors.

Composition of the doctoral committee:

Rector Magnificus,	chairperson
Dr.ir. H. Polinder,	Delft University of Technology, promotor
Dr.ing. A. Coraddu,	Delft University of Technology, promotor
Independent members:	
Prof.dr.ir. B.H.K. De Schutter,	Delft University of Technology
Prof.dr. T. Batista Soeiro,	University of Twente
Prof.Dr.-Ing. A. Monti,	RWTH Aachen University of Technology, Germany
Dr.ir. L.M. Ramirez Elizondo,	Delft University of Technology
Dr.ir. L. van Biert,	Delft University of Technology
Prof.dr. R.R. Negenborn,	Delft University of Technology, *reserve member*

The research in this thesis was supported by the Sustainable Hydrogen Integrated Propulsion Drives (SH2IPDRIVE) Project, which has received funding from Netherlands Enterprise Agency (RvO) through the R&D Mobility Sectors (RDM) Regulation of the Ministry of Economic Affairs and Climate Policy under Grant MOB21013.





Keywords Adaptability, DC Microgrids, Distributed Optimization, Energy Storage Systems, Energy Management, Fuel Cells, Model Predictive Control, Power Sharing, Resilience, Shipboard Power Systems, Voltage Control

ISBN 978-94-6384-991-3

Copyright ©2026 by Timon Kopka

An electronic version of this dissertation is available at http://repository.tudelft.nl.

"The longer you live, the more you fail.
Failure is the mark of a life well lived.
In turn, the only way to live without failure
is to be of no use to anyone.
Trust me, I've practiced."

— *Wit*, in *Oathbringer*
by *Brandon Sanderson*

Contents

Summary xi

Samenvatting xiii

Acknowledgments xv

1 Introduction 1
- 1.1 Background . . . 2
- 1.2 Challenges for the Power System Control . . . 2
- 1.3 Research Opportunities . . . 6
- 1.4 Thesis Outline . . . 7

2 Review of Power System Control in Shipboard Power Systems 11
- 2.1 Control Hierarchy . . . 12
  - 2.1.1 Local Control. . . . 13
  - 2.1.2 Coordinated Control . . . 13
  - 2.1.3 High-Level Control. . . . 13
- 2.2 Control Architectures . . . 14
  - 2.2.1 Centralized Control . . . 14
  - 2.2.2 Decentralized Control . . . 14
  - 2.2.3 Distributed Control . . . 14
  - 2.2.4 Communication Network . . . 15
- 2.3 Local Control. . . . 15
- 2.4 Coordinated Control . . . 16
  - 2.4.1 Decentralized Coordinated control . . . 18
  - 2.4.2 Centralized Coordinated Control . . . 20
  - 2.4.3 Predictive Coordinated Control . . . 21
  - 2.4.4 Distributed Coordinated Control . . . 21
  - 2.4.5 Coordinated Control in Zero-Emission Ships . . . 23
- 2.5 Energy Management . . . 23
  - 2.5.1 Energy Management in Automotive Sector . . . 24
  - 2.5.2 Energy Management in Microgrid Applications . . . 25
  - 2.5.3 Energy Management for Ships . . . 25
  - 2.5.4 Optimization-based Energy Management . . . 28
  - 2.5.5 Predictive Energy Management . . . 29
  - 2.5.6 Distributed Energy Management . . . 30
  - 2.5.7 Energy Management for Zero-Emission Ships . . . 32
- 2.6 Conclusions for the Control of Shipboard Power Systems . . . 35

3 Energy-based Voltage Stabilization in DC Shipboard Power Systems 37
3.1 Introduction . . . 38
3.2 System Description and Modeling . . . 39
3.2.1 Power Sources . . . 39
3.2.2 DC-DC Converters . . . 39
3.2.3 DC Distribution System and Power Loads . . . 41
3.3 Conventional Droop Control . . . 41
3.3.1 Local Control . . . 41
3.3.2 Voltage Droop . . . 42
3.3.3 Voltage Restoration . . . 43
3.3.4 Dual Loop Control Design . . . 43
3.4 Energy-based Voltage Control . . . 44
3.4.1 Energy-based Droop . . . 44
3.4.2 Dual Loop Control Design . . . 45
3.4.3 Disturbance Rejection . . . 46
3.4.4 Sensitivity to Bus Capacitance Estimate . . . 46
3.4.5 Sensitivity to Current Control Bandwidth . . . 48
3.5 Parallel Control . . . 49
3.5.1 Power Sharing Among Parallel ESS . . . 49
3.5.2 Communication Failure . . . 50
3.5.3 Power Split Between ESS and Main Power Supplies . . . 50
3.6 Results . . . 51
3.6.1 HiL Testbed . . . 51
3.6.2 Single Converter . . . 53
3.6.3 Parallel Control . . . 58
3.7 Conclusions . . . 61

4 Coordinated Control for Fuel Cell-Battery Power Systems 63
4.1 Introduction . . . 64
4.2 System Description . . . 65
4.2.1 Reference Vessel . . . 65
4.2.2 Virtual Retrofit . . . 66
4.2.3 Modeling . . . 67
4.3 Power System Control . . . 70
4.3.1 Coordinated Control . . . 71
4.3.2 Centralized Control . . . 71
4.3.3 Decentralized Control . . . 72
4.3.4 Low-Bandwidth Communication and Reconfiguration . . . 75
4.4 Numerical investigations . . . 77
4.4.1 Centralized Control with Low-Pass Filter . . . 78
4.4.2 Decentralized Control Strategy . . . 79
4.4.3 Mission Simulation . . . 81
4.4.4 Droop Parameter Adaptation . . . 86
4.4.5 Reconfiguration After Fault . . . 87
4.5 Conclusions . . . 90

5 Mission-Scale Optimization for Modular Fuel Cell-Battery Power Systems 91
5.1 Introduction . . . 92
5.2 Modeling . . . 93
5.2.1 System Dynamics . . . 94
5.2.2 Fuel Cell Consumption and Degradation . . . 94
5.3 Optimal Energy Management . . . 95
5.3.1 Dynamic Programming . . . 95
5.3.2 Energy Management Optimization . . . 97
5.4 Simulation and Results . . . 99
5.5 Conclusions . . . 102

6 Predictive Energy Management for Fuel Cell-Battery Power Systems 103
6.1 Introduction . . . 104
6.2 System Description . . . 107
6.2.1 Original System . . . 107
6.2.2 System Retrofit . . . 109
6.3 Power System Model . . . 110
6.3.1 Fuel Cell . . . 110
6.3.2 Energy Storage System . . . 112
6.3.3 State Space Modeling . . . 112
6.3.4 Hydrogen Consumption . . . 113
6.3.5 Fuel Cell Degradation . . . 114
6.3.6 Cost Model . . . 116
6.4 Load Forecasting . . . 118
6.4.1 Problem Description and Available Data . . . 118
6.4.2 Methods . . . 118
6.4.3 Application to Case Study . . . 121
6.5 Power System Control . . . 125
6.5.1 Filter-based Control . . . 125
6.5.2 ECMS . . . 125
6.5.3 MPC . . . 127
6.6 Numerical Investigations . . . 128
6.6.1 Rectangular Load Profile . . . 128
6.6.2 Mission Simulation . . . 131
6.6.3 Variation of Prediction Horizon . . . 133
6.7 Conclusions . . . 134

7 Distributed Energy Management for Modular Fuel Cell-Battery Power Systems 137
7.1 Introduction . . . 138
7.2 Modular Power System . . . 141
7.2.1 Fuel Cells . . . 141
7.2.2 Energy Storage Systems . . . 143
7.2.3 DC System and Loads . . . 143

7.3 Modular Energy Management . . . 144
7.3.1 Instantaneous Optimization . . . 144
7.3.2 Predictive Optimization . . . 146
7.4 Numerical Investigations . . . 149
7.4.1 Implementation . . . 150
7.4.2 Central vs Distributed . . . 151
7.4.3 Modular System Topology . . . 152
7.4.4 Predictive Optimization . . . 152
7.4.5 Individual FC State Switching . . . 156
7.5 Real-Time Controller Deployment . . . 159
7.5.1 Optimal Dispatch . . . 159
7.5.2 Convergence at Load Step . . . 162
7.5.3 Convergence at Component Fault . . . 163
7.6 Conclusions and Discussion . . . 164

8 Distributed Optimization in Multi-Bus DC Shipboard Power Systems 167
8.1 Introduction . . . 168
8.2 Distributed Energy Management for Single-Bus Systems . . . 169
8.2.1 Problem Description . . . 169
8.2.2 ADMM for Constrained Convex Optimization . . . 170
8.2.3 Stopping Criteria . . . 171
8.3 Network-Coupled ADMM for Optimization in Multi-Bus Systems . . . 171
8.3.1 Coupled Problem Description . . . 172
8.3.2 BTS Agent Updates . . . 172
8.3.3 BTS Cost Function . . . 173
8.3.4 Additional Stopping Criterion . . . 173
8.4 Case Study . . . 173
8.4.1 Single Bus Topology . . . 176
8.4.2 Dual Bus Topology . . . 176
8.5 Conclusion . . . 181

9 Synthesis and Future Directions 183
9.1 Contributions . . . 184
9.1.1 Findings . . . 184
9.1.2 Recommendations . . . 188
9.2 Future Research . . . 189
9.3 Reflection . . . 190

Bibliography 191

Acronyms 215

About the Author 217

List of Publications 219

Summary

This dissertation addresses the emerging challenge of controlling electric power systems on hydrogen-powered ships equipped with fuel cells and energy storage systems. As the maritime sector faces stringent decarbonization targets, electrification, hybridization and hydrogen as a fuel have become central concepts in future ship designs. Modern shipboard power systems are becoming more complex in topology and componentry, with heterogeneous power generation and storage technologies, facing high power availability and reliability requirements. These ambitions are met with enabling technologies, most prominently DC distribution technology and power electronics converters, that lay the groundwork for a highly efficient and controllable power system. The key is thus not necessarily whether we are able to control the system but in how we should control it. Yet, existing control strategies are not designed for the real-time coordination of multiple power system components with individual characteristics, leaving untapped potential for leveraging the high controllability. Even less attention has been given to the specific challenge of coordinating multiple fuel cells and batteries in DC architectures.

This topic encompasses a multitude of system-level challenges, covering aspects of power availability, stability, safety, efficiency, resilience, and scalability. Handling these requires specific attention when investigating the integration of fuel cells and energy storage systems into DC shipboard power systems. Beyond the vast discrepancy in operational characteristics between fuel cells and batteries, each component carries individual parameters, due to differences in design, rating and state-of-health. In addition, the trends of containerizing components and aiming at increased resilience shift the design paradigm from an integrated to a more modular approach. This raises the question of how modular hardware architectures can be matched with equally modular control strategies. The main challenge in the operation of complex hydrogen-based ship power systems lies in the coordination of components with different characteristics. This motivates the central research question on how to design real-time control and energy management strategies that ensure power availability and efficient resource utilization in modular, hydrogen-based DC ship power systems.

The dissertation contains contributions for a comprehensive, multi-layered control framework spanning all levels of the power system hierarchy. At the lowest level, it develops an energy-based voltage stabilization method for parallel DC-DC converters, enabling adaptive power sharing among batteries and ensuring DC bus stability. Building on this, it introduces a decentralized coordination strategy for fuel cell-battery hybrid systems using virtual-impedance-based frequency decoupling, allowing components with different dynamic capabilities to share load effectively while maintaining voltage restoration and state-of-charge management. At the energy-management level, the work presents both offline and real-time optimization strategies. An offline dynamic programming approach computes globally optimal dispatch schedules that minimize hydrogen consumption and component degradation, including integer decisions such as fuel cell on-off switching.

For real-time operation, the dissertation proposes a predictive, degradation-aware energy management system that uses load forecasting to optimize power allocation over medium-length horizons. The work further extends these methods to modular and distributed architectures. Through Lagrangian dual decomposition, the dissertation develops a distributed predictive energy management strategy in which each module optimizes its own power output while a coordinating agent enforces system-level feasibility. This architecture enhances scalability and resilience, enabling fault-tolerant operation and adaptation to heterogeneous component characteristics. The final contribution introduces topology-aware distributed energy management for multi-bus DC systems, allowing the energy management strategy to adapt to bus faults, switch states, and spatial distribution of loads and generators.

Collectively, this dissertation delivers a modular and optimization-based control and energy management framework. It advances the field by demonstrating that scalable, resilient, and real-time coordination of multiple fuel cells and energy storage systems is feasible through a combination of adaptive functionalities, predictive optimization, and distributed architectures. Overall, the work forms a modular power system control and energy management for fuel cell-battery DC shipboard power systems. This positions the research as a significant step toward efficient and resilient, zero-emission maritime power and energy systems capable of meeting future operational and regulatory demands.

Samenvatting

Dit proefschrift behandelt de opkomende uitdaging elektrische energiesystemen op waterstof-aangedreven schepen die zijn uitgerust met brandstofcellen en energieopslagsystemen aan te sturen. Aangezien de maritieme sector momenteel wordt geconfronteerd met strenge doelstellingen voor decarbonisatie, zijn elektrificatie, hybridisatie en waterstof als brandstof centrale concepten geworden in toekomstige scheepsontwerpen. Moderne boordsystemen voor elektrische energie worden steeds complexer in zowel topologie als componentopbouw, met heterogene opwek- en opslagtechnologieën die moeten voldoen aan hoge eisen aan de beschikbaarheid van vermogen en betrouwbaarheid. Deze ambities worden mogelijk gemaakt door faciliterende technologieën, met name DC-distributietechnologie en vermogenselektronica, die de basis leggen voor een zeer efficiënt en goed regelbaar energiesysteem. De kernvraag is daarom niet zozeer óf we het systeem kunnen inregelen, maar hoe we het zouden moeten inregelen. Bestaande regelstrategieën zijn echter niet ontworpen voor de real-time coördinatie van meerdere energiesysteemcomponenten met individuele eigenschappen, waardoor potentieel onbenut blijft om de hoge regelbaarheid te benutten. Nog minder aandacht is besteed aan de specifieke uitdaging van het coördineren van meerdere brandstofcellen en batterijen in DC-architecturen.

Dit onderwerp omvat een veelheid aan systeemniveau-uitdagingen, waaronder vermogensbeschikbaarheid, stabiliteit, veiligheid, efficiëntie, weerbaarheid en schaalbaarheid. Het omgaan hiermee vereist specifieke aandacht bij het onderzoeken van de integratie van brandstofcellen en energieopslagsystemen in DC-scheepsenergiesystemen. Naast de grote discrepantie in operationele eigenschappen tussen brandstofcellen en batterijen heeft elke component individuele parameters, voortkomend uit verschillen in ontwerp, nominale waarden en staat van degradatie. Daarnaast verschuiven trends zoals functionele modularisatie van componenten en het streven naar grotere weerbaarheid het ontwerpparadigma van geïntegreerde naar meer decentrale systemen. Dit roept de vraag op hoe een modulaire hardwarearchitectuur kan worden gecombineerd met een even modulaire regelstrategie. De belangrijkste uitdaging in de werking van complexe waterstofgebaseerde scheepsenergiesystemen ligt dan ook in de coördinatie van componenten met verschillende eigenschappen. Dit motiveert de centrale onderzoeksvraag: hoe kunnen real-time regel- en energiemanagementstrategieën worden ontworpen die zowel vermogensbeschikbaarheid als efficiënte inzet van middelen waarborgen in modulaire, waterstofgebaseerde DC-scheepsenergiesystemen?

Het proefschrift bevat bijdragen aan een uitgebreid, gelaagd regelraamwerk dat alle niveaus van de energiesysteemhiërarchie omvat. Op het laagste niveau ontwikkelt het een energiegebaseerde spanningsstabilisatiemethode voor parallelle DC-DC-omzetters, waarmee adaptieve vermogensdeling tussen batterijen mogelijk wordt gemaakt en de stabiliteit van de DC-bus wordt gewaarborgd. Hierop voortbouwend introduceert het een gedecentraliseerde coördinatie voor hybride brandstofcel-batterijsystemen, gebaseerd op frequentieontkoppeling via virtuele impedantie, waardoor componenten met verschillende dynamische eigen-

schappen effectief vermogen kunnen delen, terwijl spanningsherstel en laadtoestandbeheer behouden blijven. Op het niveau van energiemanagement presenteert het werk zowel offline als real-time optimalisatiestrategieën. Een offline dynamische-programmeringsbenadering berekent globaal optimale vermogensverdelingsschema's die het waterstofverbruik en de degradatie van componenten minimaliseren, inclusief discrete beslissingen zoals het in- en uitschakelen van brandstofcellen. Voor real-time werking stelt het proefschrift een voorspellend, degradatiebewust energiemanagementsysteem voor dat gebruikmaakt van belastingvoorspelling om de vermogensverdeling over de middellange tijdshorizon te optimaliseren. Het werk breidt deze methoden verder uit naar modulaire en gedistribueerde architecturen. Via Lagrangiaanse duale decompositie ontwikkelt het proefschrift een gedistribueerde voorspellende energiemanagement waarbij elke module zijn eigen vermogensoutput optimaliseert, terwijl een coördinerend element de haalbaarheid op systeemniveau afdwingt. Deze architectuur verhoogt de schaalbaarheid en weerbaarheid, en maakt fouttolerante werking en aanpassing aan heterogene componenteigenschappen mogelijk. De laatste bijdrage introduceert topologie-bewust gedistribueerd energiemanagement voor multi-bus DC-systemen, waardoor de energiemanagementstrategie zich kan aanpassen aan busstoringen, schakeltoestanden en de ruimtelijke verdeling van belastingen en generatoren.

Gecombineerd levert dit proefschrift een modulair en optimalisatie-gebaseerd regel- en energiemanagementraamwerk. Het werk toont aan dat schaalbare, weerbare en real-time coördinatie van meerdere brandstofcellen en energieopslagsystemen haalbaar is door een combinatie van adaptieve functionaliteiten, voorspellende optimalisatie en gedistribueerde architecturen. Concluderend presenteert het onderzoek een modulair regel- en energiemanagementconcept voor brandstofcel-gebaseerde DC-scheepsenergiesystemen. Daarmee positioneert het zich als een belangrijke stap richting efficiënte, weerbare en emissieloze maritieme energie- en vermogenssystemen die voldoen aan toekomstige operationele eisen en regelgeving.

Acknowledgments

I was privileged with the opportunity to spend the past four years at TU Delft to work on my research leading up to this dissertation. It has been quite a break, returning to academia after some years in industry, and not all was as imagined. Quite a few new challenges were suddenly building up in front of me, and I had to rediscover myself to handle this new stage. However, there were so many unexpected upsides to be taking this step, that no regrets remain. In a way, this felt like coming home. The environment at the department with all my new colleagues, many of whom in the same situation as me, boosted my motivation and made me feel welcome. Quite a few of those colleagues I can call friends now. And last but not least, the change in scenery, moving to the Netherlands, gave me more than I could have asked for.

I have many to thank and would like to start with my supervisors, Henk Polinder and Andrea Coraddu, for opening up this opportunity to me and keeping an eye on me during this journey. They allowed me to shape my research as I saw fit, and I could count on their opinion and input to nudge me in the right direction.

My thanks go out to my wonderful colleagues, who made their way through their own projects with their ups and downs alongside my own. I appreciate the casual chats, the spirited exchanges, the nonsense talking, the mutual support, the occasional trip, and all those other moments. Also, the shared doubts about whether it all makes sense, yet finding a way in the end. I am glad to take all those memories with me.

And finally, most importantly, my thanks go out to my family. My parents, for their support and immediate excitement when I told them that my next project would be to move to the Netherlands and do a PhD. And to my wife Sibel, thank you for joining me on this journey to the Netherlands, for making the decision to build the first years of our life in this new place, for never doubting my plans to pursue this PhD, and for always being there for me!

Timon Kopka
Delft, July 2026

1

Introduction

In this dissertation, I am investigating the power system control for shipboard power systems equipped with hydrogen fuel cells and energy storage systems. Before delving into the matter, this introductory chapter provides context on the relevance of this topic. I am looking at the challenges arising from integrating new technologies into increasingly complex ship power systems. But I am also looking at the opportunities of electrified ships, DC distribution technology, power electronics converters, and modern communication and computation capabilities. The key is thus not necessarily whether we are able to control the system but in how we should control the system. In my dissertation the focus lies on how to do this for ships with multiple fuel cells and energy storage systems. The aim of this chapter is to make the reader familiar with these challenges and opportunities, and to indicate for which specific problems our current means are insufficient. This leads up to the formulation of my research questions, pointing at where we lack answers. Not yet, since that is where my work comes into play; to find these answers.

"Journey before destination.
It cannot be a journey
if it doesn't have a beginning."

— *Dalinar*, in *The Way of Kings*
by *Brandon Sanderson*

1

This first chapter presents the motivation and context for conducting research on decarbonizing the maritime sector, and specifically why the power system control and energy management are key aspects of this endeavor. The topics of ship power system design and control, with focus on hydrogen-based applications, are introduced in Section 1.1. To provide background for further investigations within this dissertation, the main challenges are described in Section 1.2. Finally, in Section 1.3 a problem statement is formulated based on the identified short-comings of state-of-the-art approaches.

1.1 Background

The transport and energy sectors are confronted with a series of challenges, pushing the industries to develop innovative and sustainable alternatives. The European Commission [1] and the United Nations [2, 3] have set ambitious goals to reduce greenhouse gas emissions, prompting the International Maritime Organization [4, 5] to define targets for the reduction of the carbon impact of ships. Hence, the maritime industry is under pressure to provide solutions for lowering its dependency on fossil fuels.

Accordingly, more and more effort is put into research for emission-free ships equipped with alternative power generation and storage technologies, e.g. fuel cells (FCs) and battery storage systems [6, 7]. A centerpiece of this concept is the utilization of hydrogen. Green hydrogen, produced from renewable energy sources (RESs), has the potential to serve as the main power supply onboard a ship. Beyond the environmental aspects, the European Commission has identified green hydrogen as a key strategic technology to be developed as a means for the security of energy supply and for the European Union's vision of the future energy and transport system [8].

With the SH2IPDRIVE project, a consortium has been brought to life whose goal is to lead the way for hydrogen in the Dutch maritime sector. A key idea here is the integration of hydrogen FCs into ships' power systems. To increase the efficient operation and mitigate the slow dynamic capabilities of these FCs, they are typically deployed together with energy storage systems (ESSs) [9]. Such hybrid shipboard power system (SPS) designs are promising for decarbonizing maritime transport. An overarching challenge for fully exploiting this technology is the coordination of components. This includes short-term power sharing and long term power scheduling of FCs and ESSs, the charge management of storage units, and further aspects such as power reserve allocation [10]. The objectives are multi-faceted and cover aspects related to availability, stability, safety, efficiency, and resilience. The design of high-level power system control and energy management strategies (EMSs) boils down to the minimization of operational costs while still meeting all ship- and mission-specific requirements. In essence, this is a constrained optimization problem, interspersed with uncertainties that arise from the nature of operating a ship.

1.2 Challenges for the Power System Control

Hydrogen FCs are emerging as the prominent solution in state-of-the-art applications of emission-free power generation on board ships [11, 12]. These are usually hybridized with ESSs since FCs have limited dynamic capabilities and are subject to specific operation characteristics [6]. In order to mitigate the effects of high load gradients and relieve stress on batteries, several designs additionally add a fast-response ESS, e.g. an ultra-capacitor

(UC), to form a hybrid energy storage system (HESS) [7, 13]. Due to the nature of FCs and ESSs, the regarded vessels feature an electric propulsion system with an integrated power system, with all components including various loads connected to one single power system [14, 15].

For various reasons, e.g. efficiency, size, modularity and operational flexibility, DC power systems are deemed an appropriate alternative to the conventional AC technology in SPSs [16, 17], especially with many DC sources on board, e.g. FCs, batteries and UCs. Moreover, ship electrification allows the integration of RESs as zero-emission auxiliary power supplies [12]. A further notable trend is the modularization of generation and storage components. This facilitates an easy integration and reconfiguration of the SPS as well as an adaptation to each component's characteristics. A key challenge in modern SPSs lies in the coordination of these energy resources, i.e. heterogeneous power supplies and storage technologies. In the following, relevant criteria for the operation of the power system are elaborated.

Power Availability: The main goal for the power system design and control strategy is to ensure sufficient power availability for its subsystems at all times, so that their proper functionality according to system requirements can be ensured. This encompasses both the availability of energy for the mission duration, and sufficient dynamic capabilities to cover peaks and high load ramps.

System Stability: The stability of the DC power system forms the foundation for an operable and resilient electric distribution. With power generation and loads in balance, the voltage is kept stable. However, tightly controlled and fluctuating loads as well as generation are a challenge for the stabilization. The control strategy is tasked to keep the DC voltage within a specified band to prevent a black-out and maintain a sufficient quality of supply.

Safety: Both on a component- and system-level, the system operation is constrained by certain limitations. On a component-level, source-specific limits, e.g. maximum currents, must be respected. Additional requirements apply on the system-level in order to ensure safe operation of the equipment.

Efficiency: A key measurement of performance for the assessment of a control strategy is the total energy consumption. In a hydrogen-based SPS, the main contributors are the hydrogen consumption and additionally consumed shore power. Energy consumption is a central factor in the operation costs and a limiting factor for the reach of a vessel. Another emphasis aspect related to the efficiency is the component wear. Specifically, FC systems and battery systems degrade based on their operation, which should be accounted for in the control design.

Resilience: The system's resilience refers to the ability of the SPS to minimize the effect of uncertainties on the performance of the power system. A key aspect here is its adaptability to altered circumstances, e.g. faults, topology changes, parameter uncertainties, and external influences. This specifically includes the ability to reconfigure and continue operation after a fault.

Scalability: An important criterion for an operation strategy to be viable for a broad range of ship types and technologies is its scalability. In this context, this refers to the integration of additional power supplies and storage systems of both the same type as well as new technologies. For the control strategy to be flexible in this regard, it needs to be able to

1

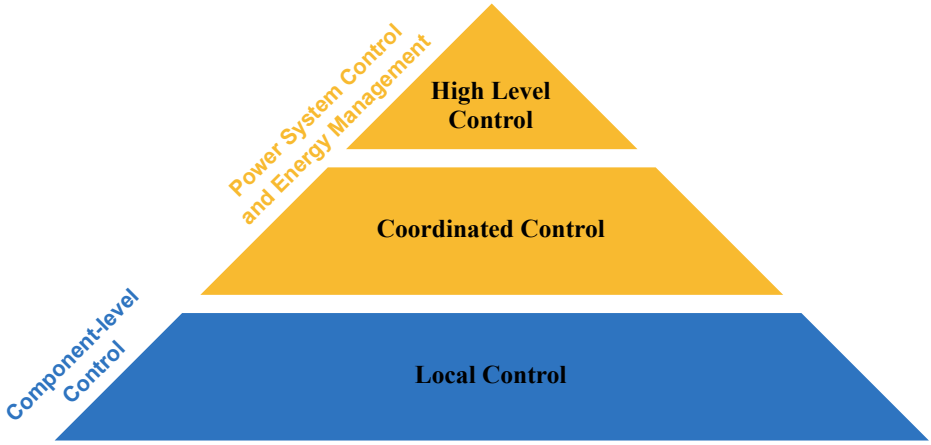


Figure 1.1: Division of control hierarchy into local, coordinated and high-level control layers

adapt to a scaling and reconfiguration of the SPS. A specific aspect is the modularity of a control strategy, allowing an extension of the power system in a plug-and-play fashion with minimal required changes for the system-level control.

The control of the SPS is usually divided into different layers, forming a hierarchical control [16, 18], as shown in Figure 1.1. In the following, a generalized overview of these layers and their objectives is given in order to contextualize the proposed research.

On the bottom layer, control loops for the components' current and voltage outputs are implemented. In modern SPSs, this is realized via power electronics interfaces, connecting the components to the distribution bus [10, 19]. Additionally, this layer includes control loops for the components' inner state variables, balance of plant, and component level protection functions. Local control is usually encapsulated and does not require communication, although target values are normally received from a higher control layer.

One layer above, the coordinated control is situated. It manages the interaction between the different generation, storage and load components. An efficient power sharing strategy is needed to mitigate imbalances between load and generation in both steady-state and dynamic conditions. Power flows are controlled to stabilize and regulate the DC voltage, and manage the state-of-charge (SoC) of ESSs. The coordinated control works on dynamic processes and accordingly the differing characteristics and limitations of all components need to be considered [16]. E.g. FCs with low dynamic capabilities can be complemented by ESSs providing high power gradients [6, 9]. Various functionalities of the coordinated control can be realized in a decentralized, distributed or centralized fashion and require low- or high-bandwidth communication depending on the specific strategy.

On a higher level, the energy management is responsible for the scheduling of power generation and storage components to meet the required load. The resources are allocated so that each component can operate in an efficient operating range, while respecting their

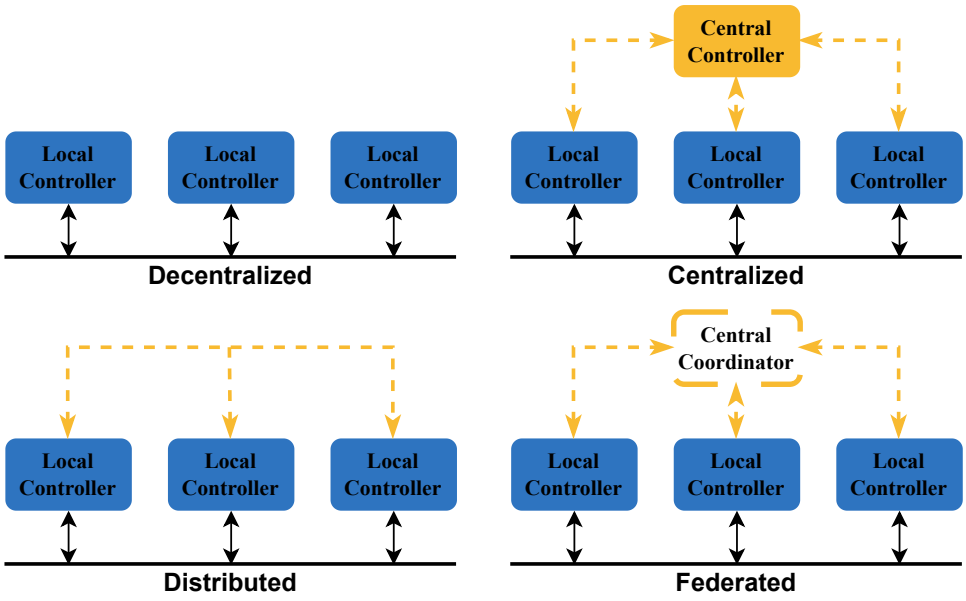


Figure 1.2: Overview of archetypal control architectures for power systems

limited generation and storage capabilities. Hence, the EMS is responsible for an optimized use of energy resources, usually following economic objectives [16].
The cyber-physical system is equipped with local controllers for each component and one or multiple central control units. Each power system control function can be distributed in various ways among these controllers. Archetypal control architectures are decentralized, centralized, and distributed approaches. A federated architecture is an additional, hybrid type where distributed control methods are deployed, yet information sharing is handled via a central coordinator. An overview is shown in Figure 1.2. Typically the fast, low-level control loops are implemented in a decentralized fashion whereas long-timescale, computation-heavy energy management is conventionally handled centrally [10]. However, these approaches are not fixed. Especially distributed implementations have emerged as a more resilient and scalable alternative for coordination in cyber-physical systems [20]. Accordingly, the investigation of control architectures to realize coordinated control and energy management functionalities offers an opportunity to shape a modular power system control onboard ships.
Currently, most applications and case studies for hydrogen-based SPSs are limited to small passenger ships and ferries [21–24]. Those ship types have comparably low power levels and operate over short distances. Furthermore, their power systems are usually simple due to low redundancy requirements. The development of viable and competitive solutions for high energy and high power applications, as well as more complex system layouts, would mean a decisive step forward for zero-emission shipping. This furthermore includes the necessary coordination of multiple, different parallel generation components in a multi-bus configuration. Additionally, a modular approach for the power system design

promises benefits regarding an easy integration, retrofit and extension with new power system technologies, and an increased resilience towards faults, parameter changes and operational uncertainties.

1.3 Research Opportunities

A literature review on the design and control of zero-emission SPSs has been conducted in order to identify current trends and research opportunities. A more detailed analysis follows in Chapter 2. Key developments include the electrification and integration of the power system, the use of DC technology and the introduction of ESSs. A next aim is the decarbonization, with much attention on the FC as main power supply and the exploitation of renewable energy resources. Moreover, a modular approach in the ship design and control has been identified as a key trend. The main challenge in the operation of complex hydrogen-based ship power systems lies in the coordination of components with different characteristics. Multi aspects need to be accounted for with the key being high power availability and efficiency providing a safe, resilient and adaptable platform. With an increasing number of heterogeneous components with unique characteristics, the challenge grows and begs the questions, whether a modular approach to the power system control is viable. The proposed research focuses on real-time applicable methods covering all required aspects to implement power system control and energy management in system- and component-level controllers. The problem statement is formulated as follows:

How can the real-time control for the electric power system in a hydrogen-based ship with DC distribution integrating modular generation and storage devices be designed to ensure power availability and an efficient utilization of its resources?

The problem statement is broken down into a series of research questions, which are being addressed over the course of this thesis.

1. *What are suitable methods and architectures for the power system control in shipboard DC distribution systems and for the energy management of fuel cell-battery ships?*

2. *How can a stable bus voltage, in DC shipboard power systems with parallel converter-interfaced batteries, be ensured?*

3. *How can the multiple fuel cells and batteries in a hybrid ship energy system be coordinated such that each component is operated based on its static and dynamic characteristics and constraints?*

4. *How can the energy management in a fuel cell-battery shipboard power system be optimized under consideration of efficiency and component degradation?*

5. *How can an optimized energy management strategy be implemented in a modular DC shipboard power system considering its resilience towards parameter uncertainties, faults, and scalability?*

1.4 Thesis Outline

This thesis covers multiple aspects of the power system control and energy management for SPSs. A common aspect among the investigations is the power system design, namely an electrified system with DC distribution technology. FCs and batteries are connected to the system via DC-DC converters, facilitating full control of current flows among the system. A further aspect is the modularity of the system design, with specific interest in methods able to handle a broad range of generation and storage modules with different characteristics and capabilities, and to adapt to flexible system constellations. Figure 1.3 shows a graphical representation of the thesis outline and the connection between research questions and chapters.

Chapter 2 provides an overview of the state-of-the-art when it comes to power system control in shipboard power systems with a specific interest in hydrogen-based power systems. This covers methods from local control of DC-DC converters, over fast timescale coordination of parallel components for voltage stabilization, all the way up to predictive power dispatch optimization in the top-layer. It also covers a variety of control architectures and communication layouts with an interest in methods that meet the modularity and adaptability aspects. This chapter culminates in the identification of research gaps, which have served in the formulation of research questions and design of investigations presented in further chapters.

Chapter 3 investigates the fastest power system control layer. It presents a method for parallel control of DC-DC converters aiming at voltage stabilization and restoration. This is intended to be used with components that support high power gradients, specifically aimed at the batteries. In addition, this method manages the power sharing among batteries according to their power availability, realizing the adaptability aspect.

Chapter 4 builds on the previous chapter and includes the FC in the coordinated control. Here, a decentralized power sharing method for FCs and batteries is presented that handles the varying dynamic capabilities by introducing virtual impedance-based droop controllers that results in a frequency-based separation of the load into high- and low-frequency parts, which are met by the respective components. This investigation further covers voltage restoration and SoC management functionalities, thus providing a comprehensive power system control method for FC-battery hybrid ships.

Chapter 5 moves the focus to long-term operation and optimization, presenting an offline-computed global optimization of the energy management. It aims at the minimization of operational costs, consisting of hydrogen consumption and cell degradation in a system with multiple FCs. A specific emphasis of this study is on the on- and off switching of individual modules, which introduces an integer-valued decision-making in the power system operation. The study solves the formulated problem through an efficient implementation of dynamic programming.

Opposed to the previous offline computation, Chapter 6 investigates the real-time application of energy management methods, providing a method for the high-level control layer. It shows an optimization-based and degradation-aware EMS for a FC-battery SPS, albeit with a centralized architecture. In a first step, an equivalent cost minimization strategy is formulated for instantaneous optimization of the power split. Then, leveraging data-driven load forecasting, the instantaneous strategy is extended into a predictive EMS optimizing over medium-length time intervals of up to an hour.

1

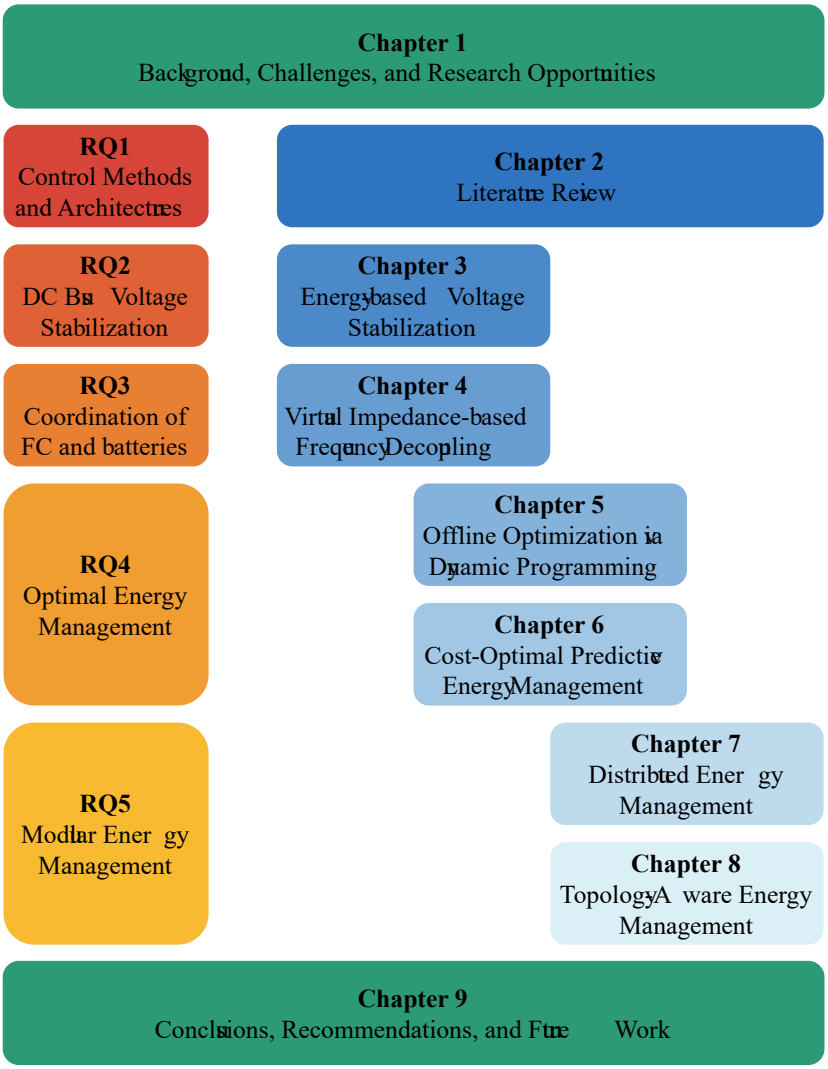


Figure 1.3: Graphical overview of thesis outline

Chapter 7 connects the findings of the predictive optimization from the previous chapter with the modularity aspect by defining a predictive EMS with a distributed architecture. Through Lagrangian dual decomposition, each module is enabled to optimize their own locally-feasible power output, while a federating agent ensures power balance via a gradient-based solver. In addition, a local decision-making heuristic is implemented for the state of each FC module. The method is demonstrated for a modular FC-battery SPS where each component has unique ratings and parameters, and finally the fault-tolerant operation with this strategy underscores the resilience of distributed control approaches.
Chapter 8 extends the distributed energy management by topology-awareness, making it applicable to multi-bus architectures. This incorporates an adaptation to the physical topology determined by location of power loads and generation, the states of bus-ties, and an optimization of power flows through closed switches. These aspects further enhance the resilience of the the energy management for meshed DC systems, allowing an adaptation to bus faults.
Chapter 9 concludes this dissertation by reviewing its investigations, highlighting the findings, and reflecting on the progress in context of the original problem statement. The focus lies on connecting each contribution to the research questions posed in the introductory chapter, with the aim of providing comprehensive answers.

2

Review of Power System Control in Shipboard Power Systems

This chapter provides context on the state-of-the-art of power system control onboard ships. Through a literature review, I investigated what control functionalities are relevant for the electric system, specifically for DC distribution. This gives an overview of the various layers and objectives in a control hierarchy, and in which architectures these can be organized. For each generic approach, I list a series of relevant studies that apply them for ships, ranging from simple rule-based strategies to elaborate predictive, optimization-based strategies. My focus lies on singling out strategies applicable to hydrogen-based power systems and promising for the modular integration of heterogeneous components. The findings from this chapter were the driving element in defining the direction of my research and formulating my problem statement.

"I seek the truth.
Wherever it may be,
whoever may hold it.
That's who I am."

— *Shallan*, in *Words of Radiance*
by *Brandon Sanderson*

This chapter is published with minor modifications as *Power System Control in DC Shipboard Power Systems: A Review of Methods and Architectures, in: IEEE Access, 2025* [25]

2

The design of modern shipboard power systems (SPSs) features an increasing system complexity due to its number of power generation, energy storage, and demanding loads, while requirements on availability, reliability, and other factors put additional strain on the power system. On the other side, modern equipment, especially due to power converters, high computational power, and fast communication technology, yield an increasing plethora of opportunities for the control of the SPS. This chapter is dedicated to giving an overview of the underlying challenges and functionalities for the operation of a vessel's power distribution system. It presents typical control hierarchies, architectures, and methods, with a specific focus on approaches that support the operation of electrified DC SPSs with heterogeneous power system resources. A proper coordination of the power system components is not only required to ensure power availability and an efficient utilization of resources, but also for the system's reliable and fault-tolerant operation. For the control of the SPS, many parallels can be drawn to the terrestrial power system, especially regarding the system design and control architectures. In the same regard, mission- or trip-based energy management strategies are pioneered in automotive systems. However, the specific demands arising from the operation in a maritime environment lead to dedicated control strategies. As a first step, the prevalent control architectures and archetypal communication layouts in ships are reviewed. Moreover, the SPS control is dissected into distinct layers whose tasks and functionalities are identified, leading to a differentiation between local control, coordinated control and energy management. This chapter presents an overview of methods applied on different layers and with differing communication layouts. A specific interest in control approaches suitable for modular and zero-emission SPSs designs is brought forward.

2.1 Control Hierarchy

Whereas small-scale power systems can be approached with a very simple control strategy, the control architecture in complex power systems is commonly organized in a hierarchical structure. Hierarchical control is state-of-the-art in terrestrial power grids [26], and commonly also adopted in shipboard power grids [10]. Typically, the bandwidth of control loops is increasing towards the lower layers, with high-speed control algorithms typically implemented in the component level control.

The literature provides various definitions and nomenclatures for the tasks and scope of control layers. A general description of a standardized three-level control hierarchy in power systems is brought forward by [26], usually adopted in microgrid control [27–29], and also in several maritime studies [18, 30]. However, other researchers prefer to separate between low-level and high-level control [31, 32] or between local and coordinated control [16]. The coordinated control is further divided into power and energy management in [33]. In this thesis, I will follow the nomenclature from [33, 34], differentiating between power system control and a high-level control layer, in which the energy management functions are located. The power system control is further divided into local and coordinated control. The hierarchy is sketched in Fig. 2.1. The tasks, scope and functionalities of these three layers are described as follows.

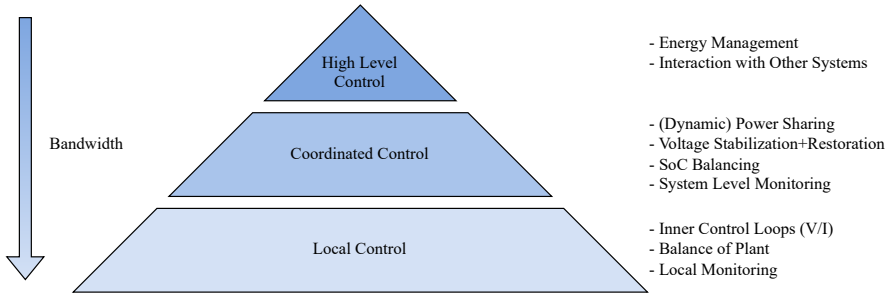


Figure 2.1: Hierarchical Control Layers

2.1.1 Local Control

On the component level, control-loops for the output current and voltage of power generation, storage systems and controllable loads are implemented. In modern DC SPSs, the current and voltage control is usually realized via a power electronics interface, connecting the component to the distribution bus [10, 19]. Additionally, this layer includes controllers for the components' inner state variables, balance of plant, as well as component level protection functions. The local control is usually encapsulated and does not require communication. However, information exchange with a higher-level is required for receiving reference values and providing local states and measurements.

2.1.2 Coordinated Control

The coordinated control is mainly responsible for establishing an efficient power sharing among the generation devices and establishing an instantaneous power balance in the system. Moreover, this layer is responsible for operation within system-level operational constraints, e.g. DC bus voltage regulation [10], battery state-of-charge (SoC) balancing, and protection functions. An overview on fault detection, protection and reconfiguration methods in SPSs is described in [35].

2.1.3 High-Level Control

On the high-level control layer, functions for the monitoring, optimization and decision-making in the operation of the system and its interaction with other systems are implemented. My dissertation focuses predominantly on the energy management, responsible for the dispatch of power system resources in order to satisfy the system's operational requirements, usually involving economic or strategic objectives. Furthermore, several works incorporate maneuvering control [36, 37] and voyage scheduling [38]. In most cases, due to the limited size of SPSs, a central controller is preferred for the energy management strategy (EMS). Thus, all information can be taken into account for optimal control actions. However, depending on the size and, furthermore, redundancy requirements of a vessel, a distributed approach for the energy management can be feasible as well [39].

2.2 Control Architectures

The cyber-physical system includes local and centralized controllers. Control architectures differ in how functions are allocated to the controllers and how the communication network between the controllers is established. The distinct schemes follow either a centralized, a decentralized or a distributed approach. A review of power system control strategies and their categorization into these three schemes is presented in [19] where the focus is on stabilization techniques on the coordinated control layer for DC micro-grids. The different architectures are shown in Fig. 2.2.

2.2.1 Centralized Control

An architecture employing a centralized layout is able to benefit from a central optimization of the energy management or power system control, due to a global information awareness in one central controller [40]. However, such a system requires an extensive communication infrastructure enabling high-bandwidth data exchange between the central controller and all local controllers. Especially in systems that are large in size or amount of controlled components, this can become unfeasible [41]. Furthermore, the central controller poses a single point of failure, leading to a low fault-tolerance of the control system.

2.2.2 Decentralized Control

A decentralized architecture is characterized by a lack of dedicated communication infrastructure. Instead, the system elements operate based on local measurements of system wide quantities, such as bus voltage or frequency [19]. The absence of a dedicated communication network for a coordinated control of the power system makes this approach inexpensive, simple to set up, robust and easily scalable. Especially for primary control in systems with long distances, such as terrestrial power grids, a decentralized control approach is preferred [41].

2.2.3 Distributed Control

In applications where coordination is required but a centralized unit is either not feasible or not desired, distributed control offers a promising alternative [42]. In this architecture, the main computations are implemented locally while a communication network is used for exchanging information. A key for the application lies in the minimization of communication overhead and information exchange. [27] notes that distributed control for coordinated functionalities attracts interest due to its reliability, stability, and facilitation of easy network expansion (plug-and-play characteristic [15]). [43] discusses the implementation of distributed EMSs as a candidate solution to enhance the survivability and robustness of the power system to meet the increasing requirements in naval vessels. Architectures can be further divided into federated and fully distributed implementations [44]. The former features a central coordinator that aggregates and broadcasts information from distributed units. A fully distributed setup only has communication among local controllers, typically with a sparse network. This setup requires consensus algorithms for determining shared control variables.

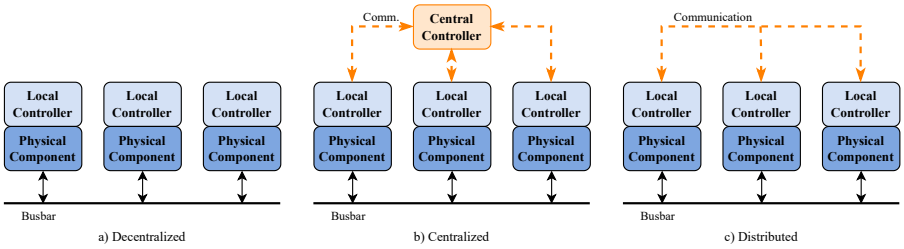


Figure 2.2: Archetypal control architectures, from [19]

2.2.4 Communication Network

One can typically differentiate between high- and low-bandwidth communication networks for the coordinated control in a power system. Information exchange for real-time control of distributed components requires a high bandwidth communication, e.g. in a network with a centralized controller computing power references for all local controllers. The required communication would be expensive, especially with increasing system size and the communication network posing a single point of failure [45]. Alternatively, a low-bandwidth (LBW) communication network can be used for the exchange of information, while considerably faster control functions are implemented locally, shaping a federated setup. For instance, [46] uses low-bandwidth communication to realize adaptive functionalities in a central controller, so a communication failure would only result in a loss of adaptability. Distributed control architectures typically use low-bandwidth communication for implementing consensus-based algorithms [20, 47, 48], completely bypassing a central coordinator. Moreover, decentralized control can be considered to be communication-less, using only the DC bus voltage as information carrier [49].

2.3 Local Control

The various power system resources in a DC power system are typically interfaced by a power converter, depending on the source type. Most relevant zero-emission technologies, e.g. fuel cells (FCs), batteries, capacitors, provide a DC output and are therefore connected with a DC-DC converter. This is typically a uni- (for power supplies) or bi-directional (energy storage) boost converter. In order to regulate the output of the source, the power electronics interface is current or voltage controlled, depending on the chosen strategy. Furthermore, component- or converter-specific local constraints, e.g. on the current, voltage or ramp rates are respected by the local control. A recent review on advanced control strategies for DC-DC converters in DC systems is presented by [50].

The common approach for tracking the current reference in power electronics converters is via proportional-integral (PI) control and pulse-width modulation (PWM) to set the voltage, which is easy to implement and tune. However, for systems with specific requirements for high control accuracy or robustness, more advanced methods might be required [51]. Especially non-linearities in the components lead to instabilities and performance degradation with conventional methods. [52] reviews various non-linear control strategies for DC-DC converters to stabilize the DC-grid voltage under the influence of constant power

loads (CPLs).
A popular method for the control of DC-DC converters is sliding-mode control due to its robustness when implemented in non-linear systems. [46] employs such a controller to track the reference output voltage and current in a DC-DC converter interfacing an energy storage system (ESS). However, due to its fast switching it is typically limited to low power applications.
[51] uses distributed model predictive control (MPC) controllers for the current control of DC-DC converters which serve as interfaces for photovoltaic (PV) and FC systems to the DC-link. This solution is presented as an alternative to classic PI control and uses a simplified MPC with a prediction model for the inductor current. A prediction horizon of one switching period is implemented where the control inputs are chosen so that the deviation from the reference current is minimized. [53] additionally presents local MPC controllers for batteries and diesel generators (DGs). A challenge for MPC arises from the high computational requirements in real-time control, especially with increasing complexity and prediction horizon of the optimization problem.
The researchers in [54] investigate the accuracy of control algorithms for the DC-DC converters in a DC power system. In a case study, the boost converter supplying a CPL is investigated and a sliding-mode controller based fuzzy-logic approach is proposed for the current control. A conventional PI controller and an MPC approach are used as benchmark solutions and it was shown that the used approach yields significantly improved power and voltage tracking and stabilization of the DC-link voltage under changing operation conditions.
The reference values for current and voltage control of the distributed components is dependent on the source-dependent functions. While main power supplies and ESSs are typically involved in the coordinated control for power sharing, auxiliary power supplies, especially renewable energy sources (RESs), are often operated with maximum power point tracking [12, 55]. However, curtailment of RESs can be a supportive function in the system stabilization [31].
Loads are subject to inputs from the user or a high-level control layer. The current of power electronics interfaced loads is tightly controlled, making them appear as CPLs to the DC system [52, 56]. Load limiting control can be utilized as a tool in power system control by degrading the height or gradient of the power demand [36, 57, 58].
A challenge with many advanced DC-DC converter control strategies is their scalability. Complex stabilization methods that are designed for a single power supply are not applicable to multiple parallel supplies, and much less for a modular power system with heterogeneous resources.

2.4 Coordinated Control

As already outlined in section 2.1, the primary objective of the power system control is to maintain operational constraints, e.g. voltage stability and power availability, and to achieve an accurate steady-state and dynamic power sharing [59]. With the introduction of ESSs, the management and balancing of SoC has become an additional challenge. The parallels between SPSs and islanded microgrids are regularly pointed out in the literature, however, the challenge of power system control in SPSs meets additional, specific challenges [60]. E.g., high load fluctuations and environmental influences as well as short

lines with low impedances are notable differences. Moreover, ships have to deal with specific reliability and power quality requirements. In the following, the challenges for the coordinated control to achieve power sharing and voltage stability in SPSs are summarized:
Fluctuating loads and intermittent generation: An essential difference between shipboard and terrestrial power systems is the high amount of fluctuating loads in the MW-range [60] for propulsion and service equipment. It is important to maintain sufficient quality of power supply while ensuring power availability. While terrestrial grid applications focus on steady-state power sharing, an efficient dynamic power sharing is a necessity in SPSs. [61] points out that intermittent generation from renewables effectively functions as a negative load, since these are typically current-controlled to supply maximum power. Although rarely used in SPSs, these sources can further de-stabilize the power system.
Constant and pulsed power loads: One major challenge for the stability in DC power systems is the presence of CPLs [37]. These are tightly regulated loads which draw a constant power, resulting in an increasing current when the DC-link voltage falls [52]. This problem is reviewed in detail by [56] who furthermore presents strategies for the mitigation of effects from CPLs. Another type of load, which is extensively discussed in the literature, are pulsed power loads. Especially in the naval field, advanced weaponry systems and sensors have a high, intermittent power draw with a detrimental effect on power system stability [15]. Mitigation methods for these adverse effects of pulsed loads are accordingly studied in several works [62, 63].
Lack of inertia: Systems with a high share of converter-interfaced generation and low inertia are particularly susceptible to voltage instabilities. For this reason, suitable strategies for stabilizing the grid are needed [64, 65].
Quality of power supply: [14] mentions frequency and voltage deviations and harmonic distortions as main challenges for the coordinated control in ships. Power quality is increasingly becoming important as a design target for ships [15]. An extensive review on power quality and energy efficiency issues in maritime micro-grids is conducted in [66].
Fault handling: Depending on specific reliability requirements, the power system is required to ride through fault scenarios. Therefore, the coordinated control needs to mitigate the effects from faults and re-establish stable operation [55, 57].
Heterogeneous capabilities: A decisive factor in the coordinated control is the consideration of differing characteristics of power sources and storage systems [10]. Power sources, such as conventional DGs and FCs, have low dynamic capabilities and are preferably operated in their efficient operation range. ESSs show varying power and energy characteristics, hence both their available power, power gradients and SoC range play an important role in their optimal utilization [7].
Component degradation: The lifetime of many components is influenced significantly by their operating profile. Especially FCs [67, 68] and batteries [7] are expensive to replace and susceptible to degradation. Hence, lifetime prolongation by keeping their power output and the batteries' SoC steady and within an efficient range, is key for the reduction of operating costs [10].

As described in section 2.2, control approaches can be categorized into centralized, decentralized and distributed methods. In the following, common approaches for coordinated control in DC SPSs with power electronics interfaced generation, storage and load components are reviewed. The main question here is what methods are appropriate to overcome

the prevalent challenges for power system stability and efficient power sharing in DC SPSs and what conclusions we can draw for coordinated control in zero emission ships (ZESs). The focus lies on methods for (dynamic) power sharing, voltage restoration, and SoC balancing. Overviews of their applications in SPSs are listed in Tables 2.1, 2.2, 2.3, and 2.4.

2.4.1 Decentralized Coordinated control

A common decentralized method for power sharing in microgrids is droop control. Various modified droop methods are commonly used for load sharing and system stabilization as part of primary control [41], and typically implemented as a P/V or I/V droop in DC power systems [10, 64]. This method uses the DC bus voltage as information carrier. However, challenging issues are unknown line impedances, inefficient dynamic power sharing and a residual bus voltage deviation. This method is easy to set up with the droop gain of generators normally proportional to their power rating [19]. As noted by [18], conventional droop control for power sharing and voltage stabilization is not recommended in diesel-dominant systems due to the efficiency drops and slow transients of the internal combustion engine. This can be extended to ZESs with FC systems which should preferably be operated steadily and within their optimal operation range. However, the inclusion of ESSs presents additional opportunities for efficient power system control methods.
[69] presents a decentralized droop for power sharing between parallel DGs in an SPS, embedded within a hierarchical control scheme. However, as noted in [18], limitations of conventional droop arise due to efficiency drops at off-design conditions and low transients of the DGs. In addition, droop control leads to inefficiencies in dynamic conditions and the power sharing problem becomes more complex as soon as power generation and storage with differing dynamic characteristics are added. To handle this, different component types are equipped with specific local controls, depending on their characteristics. [70] and [18] assign low or even zero gain to DGs and FCs, leaving the batteries to cover large power mismatches. These schemes then rely on the EMS to provide an efficient references for the main power supplies. Various methods for power sharing in DC SPSs are listed in Table 2.1.

Power System	Communication	Method	Ref.
DG	Decentralized	Droop	[69]
DG-Bat	Decentralized	Droop	[70]
GT-Bat-UC	Decentralized	Inverse droop	[18]
GT-Bat	Federated	Adaptive droop	[71]
DG-Bat-CI	Federated	Adaptive droop	[60]
DG-Bat	Federated	Adaptive droop	[72]
Bat	Federated	Adaptive droop	[46]
GT-FC-Bat	Centralized	PI	[73]
DG-Bat	Centralized	Master-Slave	[74]

Table 2.1: Power sharing approaches in DC ships

These droop control schemes with virtual resistances are primarily designed for steady-state power sharing, which is inefficient under fluctuating loads. To mitigate this, [75, 76] propose a virtual impedance to achieve a frequency separation, based on the dynamic characteristics

of power system components. Accordingly, fast-response components, e.g. batteries or ultra-capacitors (UCs) can react immediately to voltage deviations, while energy-dense technologies, e.g. DGs or FCs, can be tuned to change their output efficiently, matching their capabilities. [77] uses virtual capacitances for UC control in a DC microgrid for stabilization under surge loads, showcasing the plug-and-play capability of this approach. The remaining voltage deviation created by droop control is not necessarily critical, but can lead to undesired side-effects. A decentralized method for voltage restoration is via local PI controllers [18, 78]. Table 2.2 lists applications for the voltage regulation in DC ships. However, fully decentralized control for the voltage restoration with multiple parallel units is challenging due to stability issues and circulating currents.

Power System	Communication	Method	Ref.
DG-Bat	Decentralized	Local PI loop	[78]
GT-Bat-UC	Decentralized	Local PI loop	[18]
DG	Centralized	Central PI loop	[69]
GT-FC-Bat	Centralized	Central PI loop	[73]
DG	Distributed	Voltage shifting	[20]
Bat-PV	Distributed	Voltage shifting	[48]

Table 2.2: Voltage restoration approaches in DC ships

In addition to power sharing and voltage regulation, the balancing of SoCs among parallel ESSs is required. One option is to employ adaptive droop coefficients based on each storage's SoC [79, 80]. This approach is quite popular in the maritime sector for power sharing and voltage stabilization as observed in [60, 71, 78]. The virtual impedance of the droop controllers is adjusted based on the SoC so that batteries with a high charge contribute more to the power sharing. In [81], this approach is extended to a DC seaport microgrid for communication-less power sharing among multiple ships. As an alternative to adapting droop coefficients, SoC management can be done by voltage switching [48] or current correction [75]. However, for improved accuracy, these approaches usually include aggregated information, e.g. average SoC, from a federating agent. The different strategies for SoC management are summarized in Table 2.3.

Power System	Communication	Method	Ref.
DG-Bat	Decentralized	Adaptive Droop	[78]
GT-Bat	Federated	Adaptive Droop	[71]
DG-Bat-CI	Federated	Adaptive Droop	[60]
DG-Bat-UC-FW[1]	Federated	Current Correction	[75]
Bat	Centralized	Voltage shifting	[46]
Bat-PV	Distributed	Voltage shifting	[48]

Table 2.3: SoC balancing approaches in DC ships

[1] fly-wheel

2.4.2 Centralized Coordinated Control

The availability of information in a central controller with high-bandwidth communication enables a more efficient coordination of all power system components. [69] implements a central PI controller for voltage restoration by adjusting the output voltage of the synchronous generators, while power sharing is still realized with droop control. Similarly, in [73] a central PI controller determines the required total DC-link current for stabilizing the voltage. This current is split to the power sources based on a given ratio from an EMS. An application of power sharing with a central controller, implemented in a master-slave configuration with the ESS controller as master controller, is shown in [74]. The power sharing is taken over by the energy storage devices while the main supplies can operate in their efficient operating point. Constraints on the SoC of the ESS are disregarded here, and this approach requires a sufficiently sized storage to function efficiently.

A frequency-based separation of the load power in order to assign differing frequency bands to generating devices with differing response times is presented in [82]. A series of low-pass filters is employed to compute power references with differing band-widths to DGs, batteries and UCs, according to their capabilities. A much-discussed measure for the enhancement of dynamic capabilities is the combination of an energy-dense with a power-dense ESS technology into a hybrid energy storage system (HESS). The coordination of dynamic power generation and storage in both systems is a challenge for which typically a central HESS-controller is used. Some of the proposed approaches can be extended to include the main power supply as well. [45] uses a filter-based approach for separating high frequency load fluctuations to be mitigated using the UC while the battery is covering low frequency load changes. Here, the load power is directly transferred to power references. Similarly, [61] employs a HESS with load frequency-separation in order to mitigate effects of fluctuating PV generation. In the same fashion the frequency separation of load fluctuations is achieved using a wavelet transform in [83] where a semi-active HESS topology is used. In [18] the filter-based approach is combined with an underlying droop control for parallel connected HESSs. An alternative approach aiming for voltage stability is proposed in [45] where deviations from the DC-link reference voltage are used to generate PI-controlled current references for the battery and UC. Table 2.4 lists the described methods for dynamic power sharing in DC SPSs.

Power System	Communication	Method	Ref.
DG-UC	Decentralized	Resistive-Capacitive Droop	[77]
Bat-UC	Decentralized	Resistive-Capacitive Droop	[76]
DG-Bat-UC-FW	Decentralized	Resistive-Capacitive Droop	[75]
DG-Bat-UC	Centralized	Load-filtering	[82]
Bat-UC	Centralized	Load-filtering	[45]
DG-Bat-UC-PV	Centralized	Load-filtering	[61]
GT-Bat-UC	Centralized	Load-filtering	[18]
FC-Bat-UC	Centralized	Adaptive load filter	[84]
FC-Bat-UC-PV	Centralized	Wavelet transform	[61]
DG-Bat-UC	Centralized	PI loop	[45]

Table 2.4: Dynamic power sharing approaches in DC ships

2.4.3 Predictive Coordinated Control

Several researchers investigate the utilization of predictive control for optimal coordination of power system resources by explicitly formulating control objectives and constraints and leveraging predictions. MPC is able to realize multiple functions simultaneously, e.g. dynamic power sharing and voltage regulation. In [37] the stabilization of the DC-link voltage with MPC under the effects of CPLs and sudden changes in loading conditions of a diesel-electric power system is demonstrated. Load forecasts are obtained from a higher-level motion controller. An extension to a battery hybrid system is shown in [53], implementing a multi-level MPC. Here, a system-level MPC computes current set-points for all components, which are tracked by component-level predictive controllers. [85] expands the problem formulation to holistically include system efficiency, component wear, thrust production and DC voltage deviations. [86] conducts a joint optimization of switching actions in parallel active front-end rectifiers and DC-DC converters to minimize the deviation from power and voltage setpoints.

MPC also receives much attention for the control of HESSs. Proposed methods for HESS control can also be expanded to systems incorporating a broader variety of technologies. [13] coordinates the power flows with a battery and UC using an MPC with the aim of minimizing the total losses of the HESS while keeping the system states within its defined boundaries. [87] proposes a real-time MPC approach for addressing both fluctuating loads as well as pulsed power loads. This work is later expanded upon by an adaptive MPC considering uncertainties of the HESS parameters [88].

[62] uses MPC for real-time generation control of gas turbines (GTs) and voltage stability of a naval DC power system with pulsed loads. The power system analyzed in [63] additionally incorporates a HESS to improve voltage stabilization and load leveling for the main power supplies. The results show that such an approach is effective in providing voltage stability under extreme load fluctuations while keeping system variables within defined limits. Various studies on MPC for coordinated control are summarized in Table 2.5.

2.4.4 Distributed Coordinated Control

Whereas the previously mentioned approaches rely on a high-bandwidth communication and computation in a centralized controller, concerns for system scalability, reliability and survivability constitute the development of distributed approaches. In [47], power sharing in a DC microgrid is implemented in the local controllers, enhanced by low-bandwidth information exchange via a common bus. [92] describes how cooperative control can be employed in DC microgrids, e.g. for voltage restoration.

[20] presents a hierarchical control scheme with distributed voltage regulation for a medium-voltage DC power system with parallel DGs. Power sharing is decentralized via droop control, while a consensus-based algorithm introduces corrective terms on the output voltage reference of the rectifiers to regulate voltage and increase fuel efficiency of the engines. An application for distributed control using a multi-agent system for power sharing and balancing of SoC among distributed ESSs is presented in [48]. Through communication with neighboring ESSs and a consensus algorithm, agents estimate the average SoC and DC-link voltage in the system. An underlying droop control scheme is extended using these system wide variables for SoC balancing and DC bus voltage regulation. Table 2.6 lists distributed approaches for coordinated control in SPSs.

Power System	Scope	Ref.
DG-FC-Bat-PV	Local current control	[51]
DG-Bat	DC voltage stabilization and local current control	[53]
Bat-UC	Voltage stability and loss minimization	[13, 89]
DG	DC voltage stabilization with CPL	[37]
GT	Non-linear MPC for stability under pulsed loads	[62]
DG-Bat	Non-linear MPC for power smoothing using load power spectral density	[90]
DG-Bat	Adaptive MPC for stability and loss minimization	[85]
GT-Bat-UC	Voltage stability under pulsed loads	[63]
DG-Bat-UC	Adaptive MPC for prediction and mitigation of torque fluctuations	[85]
Bat-UC	Stability, Loss Minimization, SoC tracking	[87]
DG-Bat	Voltage stability	[86]
GT-Bat	MILP-based MPC for load shedding and mode switching	[91]

Table 2.5: Predictive coordinated control in SPSs

Power System	Scope	Ref.
-	Consensus to ensure accurate power sharing and voltage regulation in DC microgrids	[47]
GT-Bat	Distrib. PSO for power reference tracking in naval ships	[93]
DG	Consensus on voltage regulation and power sharing for parallel DGs	[20]
ESS	Consensus on SoC balancing and voltage regulation	[48]
ESS	Consensus on unified state factor for SoC balancing, voltage regulation and current sharing in DC microgrid	[94]
ESS	SoC balancing, voltage regulation and current sharing via multi-objective fusion and dynamic diffusion	[95]
GT	Unified power tracking and voltage control for improved transient response	[96]
GT-Bat	Dynamic power allocation under ramp-rate and servicing constraints via ADMM	[97]

Table 2.6: Applications of distributed coordinated control

2.4.5 Coordinated Control in Zero-Emission Ships

Among applications of power system control in ships using fuel cells, e.g. [73, 84, 98], it can be observed that FCs are preferably not participating in voltage stabilization due to their limited transient capabilities. Instead, it is necessary to combine fuel cells with more dynamic technologies, typically batteries [98] or HESSs [84].

Studies considering the coordinated control with FC systems are usually focusing on the power balance in a small-scale or simplified systems consisting of a single FC and one ESS. For instance, [22, 99], propose a PI-based power system control for distributing the load power to the FC and battery. Such an approach is only applicable for a small system with a central controller. Hence, scalability to a larger system with parallel power generation is not given. Furthermore, the FCs serve as quasi-steady current sources in these studies, while voltage stability and fast load fluctuations are responsibility of the batteries. Methodologies for coordinated control in diesel-electric (e.g. [69]) and diesel-hybrid systems (e.g. [18]) can potentially be adapted to FC-hybrid systems, with alterations catering for the changed characteristics of the main power supply and accounting for the replacement of rectifiers by DC-DC converters. Also, methodologies for the control of HESSs, such as [87], do not consider the main power supply and are, therefore, applicable to ZESs as well.

For future research, it will be necessary to investigate the coordinated control in ships with multiple parallel FCs as main power supplies as a prerequisite for utilizing this technology as sole power sources in more complex ZESs. It can be expected that various ESSs and possibly RESs and demand-side management need to be considered for an efficient coordinated control. Hence, with SPSs incorporating a broader spectrum of power system technologies, the approach for coordinated control should adapt to the available power system resources. A control architecture that accounts for the modular integration of technologies with differing characteristics facilitates the adoption of new technologies and scalability of the system. Furthermore, it benefits the system's reliability and adaptability for handling uncertainties, e.g. component faults, parameter alterations, and topology changes.

2.5 Energy Management

An efficient energy management is a major challenge in maritime vessels with multiple energy sources, especially with a heterogeneous set of components [100]. Dedicated EMSs are typically situated on the high-level control layer. However, energy management functionalities can also be intertwined with the coordinated control, blending the boundary between the functional layers. In the literature, a plethora of differing approaches for optimal and robust EMSs can be found. [101] points out the similarity of the energy management problem for ships and hybrid-electric vehicles. The research literature on EMSs in the automotive sector is significantly more extensive than for maritime applications. Moreover, additional references for EMS solutions can be observed in power system, building and microgrid applications [102–104].

Many authors attempt a classification of these methodologies [101, 105]. However, varying definitions of the energy management functions and the broad variety of differing EMS designs make an exhaustive classification challenging. The aim in this review is to provide an overview of common and promising approaches for designing the EMS, with a specific interest for solutions in all-electric ships and utilization of FCs. A generic classification of types is portrayed in Fig. 2.3. The methods can generally be divided into optimization-

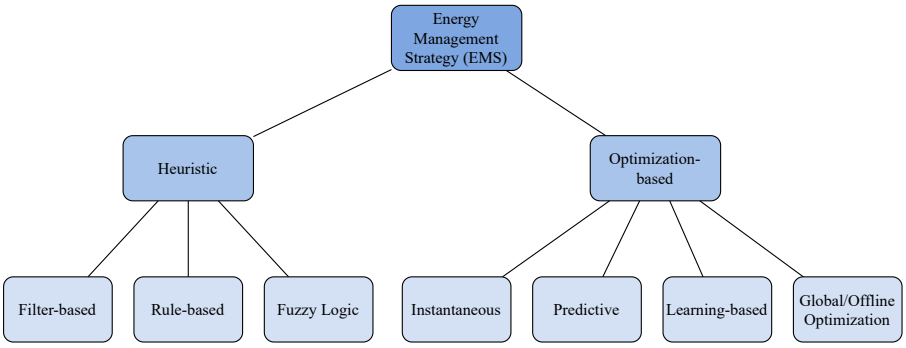


Figure 2.3: Classification of energy management strategies

based and rule-based or heuristic approaches [33]. Heuristic or rule-based approaches can further be split into state-based, PI-based and fuzzy logic-based approaches [106, 107]. These approaches are usually simple, easily implemented and computationally efficient. However, the design and consequently the performance of these approaches rely heavily on human experience as input. Some approaches incorporate adaptive features to overcome their shortcomings in performance [107], however, for complex and novel systems a more elaborate EMS is required.

Among optimization-based methods, a differentiation must be made between global and real-time optimization methods. Real-time capable solutions include instantaneous methods, such as an equivalent consumption minimization strategy (ECMS) [30] or sequential dynamic programming (SDP) [67, 105], which do not require any knowledge about the future mission profile. In contrast to these approaches are predictive methods which incorporate knowledge or predictions of future states and use results from explicit optimization for real-time control of the system [27]. This is especially interesting for energy management challenges with load predictions [108]. Moreover, learning-based and data-driven control add to the possible approaches for an optimized energy management in ships [101].

Global optimization is possible for offline computation of the optimal dispatch of energy resources. Methods include classic analytical, numerical (e.g. dynamic programming) and meta-heuristic approaches. Even though the online application of a pure global optimization is not possible, their outputs can be used for the design of an online EMS or these methods can be combined with predictive and learning-based control approaches. Using knowledge from global optimization in a real-time application is e.g. proposed for future research in [33]. Finally, offline generated control inputs can serve as a benchmark for the performance of real-time strategies.

2.5.1 Energy Management in Automotive Sector

It is worthwhile to investigate which methods are applied in other fields in order to assess what the maritime sector can learn from them. The challenge of optimizing the power split for SPSs has similarities to the challenge in the automotive field [101]. Especially relevant is the research on hybrid electric vehicles, incorporating combustion engines and

batteries [107, 109], as well as FC-powered vehicles [67, 110]. In fact, many of the methods we see in maritime applications today originate in the automotive field, such as ECMS [111], SDP [67] and applications of predictive control [112].
Nevertheless, it must be noted that there are several distinguishing characteristics between maritime and automotive applications. Hence, the challenge differs and methods need to be adapted. Some of the most notable differences are listed here:

- Larger variety and number of generation and storage devices in SPSs than in vehicles [113], where one main supply and an optionally an ESS are standard [114]. The coordination of multiple parallel generators and storage systems increases the problem complexity [33].
- Different reliability requirements, standards and legislation apply [66]. Hence, there are unique operational requirements for ships [115].
- Vastly different power ratings between vehicles (kW-level) and ships (MW-level). Automotive systems primarily supply traction power [116], whereas ships often feature service equipment with high and specific load profiles [11]. Consequently, load ramp rates are significantly higher and follow different patterns [13].
- The EMS in hybrid electric vehicles relies heavily on the ability to regenerate energy under braking, which cannot be applied to a significant effect in ships [7, 114]
- The load requirements in ships are heavily influenced by environmental factors, e.g. wind and waves. In addition, large drive shaft torque fluctuations occur at wave frequency and propeller rotational frequency [13].

2.5.2 Energy Management in Microgrid Applications

The topology and technology in SPSs shares some resemblances with terrestrial microgrids, especially islanded microgrids [14]. Hence, both coordinated control and EMSs from such applications serve as an additional reference for control in ships. [102] provides an overview of heuristic and optimization-based approaches for the EMS in terrestrial micro-grids as well as a brief review of control architectures. For residential micro-grids, in which the use of distributed energy sources and smart control systems are vital, the energy management problem is analyzed by [104] and [103]. However, once again it is important to point out the decisive dissimilarities in the challenge between microgrid and maritime applications. Different standards, legislation and reliability requirements apply [66, 115]. Furthermore, SPSs need to supply high power gradients and continually fluctuating loads [14]. Another difference is the limited space requirement and constant movement of the ship [117, 118]. Finally, ships follow a mission-based operation profile with distinctive tasks and a limited duration [66], whereas microgrids need to provide power indefinitely and usually follow a stochastic load distribution [27].

2.5.3 Energy Management for Ships

In SPSs, a broad variety of different EMSs and methods can be found, many of which are application-specific. The following overview aims at providing an overview of general approaches and challenges in the energy management.

Power split between parallel main power supplies: A key challenge for the energy management is the allocation of power generation among parallel power supplies, conventionally, DGs or GTs, whereas in a hydrogen-based ship, FC systems are the predominant technology. A conventional approach is the tuning of droop gains to ensure proper balance of load and generation while operating generators according to their power ratings [18]. Similarly, [69] employs virtual impedance control-based on generator ratings as a method for an efficient steady-state power split among DGs. For improved efficiency and adaptability and incorporating further objectives, e.g. emissions and component wear, more elaborate strategies are needed. Those are discussed below, among the optimization-based techniques.

Power split between main power supply and ESS: The EMS becomes significantly more complex by the introduction of ESSs. A large amount of studies on energy management in all-electric ships focuses on the utilization of ESSs to assist the power generation for minimal operation costs or fuel consumption. A common aim when managing power flows between battery and the main power supply is to level the load profile of the main supply so that it can operate in its efficient loading. [78] proposes to operate DGs at their rated power and leave voltage regulation and thereby all fluctuating loads to the batteries. In [60], the power allocation between diesel generators and batteries is using a rule-based approach, aiming at operation of DGs with a steady profile within an efficient operation range. Power fluctuations and deviations between DGs and loads are covered by the battery packs. For the ESS an additional set of rules is employed to manage their SoC. [55] uses a rule-based approach for determining the charge and discharge of the ESS. Such rule-based approaches are often implemented as decision trees, whose output is based on net power demand and SoC of the ESSs [51, 55]. Another possibility to leverage expert knowledge is to employ a fuzzy logic controller in the EMS. Similar to rule-based approaches, the inputs to the controller are usually the power demand and SoC, yielding an efficient instantaneous power split [21]. In [119], a fuzzy logic control strategy is applied to a small diesel-battery ship. As an alternative to expert knowledge, [83] uses an offline optimization for the fuzzy logic design.

On-off switching of main power supplies: A key decision in the operation of each individual component is their on- and off switching, which poses an integer-valued decision variable. Conventionally, the state reference is determined heuristically through rules or more recently using fuzzy control. [120] presents a methodology to determine an optimal number of running generators so that the loading and consequently fuel consumption of each generator is optimized. For FC systems there generally is a trade-off between component wear and system efficiency [121].

Power split between FC and conventional power supply: A further issue arises in SPSs where different types of power supply systems are integrated. Such is the case when combining FC systems together with conventional power supplies. A power system design with DG and FC is proposed in [51]. However, the FC is serving as an auxiliary power supply in this study by providing a constant power at the system's maximum efficiency. Such a solution can be beneficial for retrofits so that the original EMS of the diesel-battery

hybrid system can be kept. [122] investigates the EMS for a dredging vessel incorporating FCs together with GTs and batteries. In this approach, power fluctuations are covered by the ESSs, as in a normal hybrid system. The remainder, a moving average of the load power, is split between gas turbines and solid-oxide FCs, so that the instantaneous equivalent fuel consumption is minimized, resembling an ECMS.

Renewable Energy Integration: One special type of power system resource is given by RESs. Their power profile is subject to environmental conditions and therefore intermittent rather than controlled. The maximum power point tracking of RESs yields a stochastic power output, which can be seen as a negative load. In [51], which investigates PV integrated in the SPS, the EMS aggregates the power demand and RES generation to a net power load. In [118], the fluctuations of PV generation are estimated and the ESS is sized and operated to compensate for the fluctuating generation, hence explicitly anticipating the renewable energy influx. A further means to account for the uncertainties related to renewable energy generation is to employ a predictive energy management strategy as shown in [123].

Voyage and Propulsion Control: One promising addition to the energy management problem is the inclusion of voyage or propulsion control. A joint optimization of both control levels offers the possibility to adapt the propulsive load demand in a manner which is beneficial for the energy management. For instance, the propulsion control can flatten load gradients or shift load peaks. [34] optimizes the propulsion shaft speed and load demand of aship-based on a reference trajectory and predicted environmental uncertainties. This consequently has an influence on the energy management by providing a load forecast and smoothing the load profile. In a similar fashion, [36] proposes an MPC formulation for maneuvering control through trajectory tracking. The work aims at optimizing the ship's voyage for maximum efficiency.

Power System	Method	Scope	Ref.
DG	Virt. impedance	Steady state power sharing	[69]
DG-Bat	PI[1] loop	Voltage regulation by ESS	[78]
DG-Bat-CI	Rule-based	Power split for DG and ESS	[60]
DG-FC-Bat-PV	Rule-based	Power split for DG and ESS	[51]
DG-Bat-RES	Rule-based	Charge-discharge of ESS and fault-tolerant operation	[55]
DG-Bat	Fuzzy logic, PSO	Power split for DG and ESS for DG and ESS with param. optimization	[119]
FC-Bat-PV-UC	Fuzzy logic, DP[2]	Power split for DG and ESS leveraging global opt.	[83]
GT-FC-Bat	Equiv. SFC[3] min.	Split of moving average power between GT and SOFC	[122]
DG-Bat-PV	Load Leveling	Mitigating PV fluctuations with ESS	[118]

Table 2.7: Heuristic energy management in ship applications

[1] proportional-integral [2] dynamic programming [3] specific fuel consumption

2.5.4 Optimization-based Energy Management

As described above, a main distinction can be made between conventional and optimization-based energy management methods. Conventional energy management strategies, mainly consisting of rule-based, deterministic and fuzzy logic formulations, are listed in Table 2.7.

Optimization-based control methods can be characterized on whether they are instantaneous or predictive. Applications of instantaneous optimization predominantly focus on the challenges of optimal loading of parallel power supplies as well as the power split between main power supplies and ESSs. A minimization of the instantaneous fuel consumption in a diesel-electric ship is proposed in [120], where ESSs are used to shift the total power demand for the generators for minimizing their specific fuel consumption. The predominant optimization-based approach for instantaneous allocation in hybrid systems is ECMS [109, 124, 125]. An application of this method to a battery-hybrid SPS is proposed in [126] and [127]. The equivalence factor, describing the cost ratio between power from the main supply and the ESS, can be adapted based on the SoC in order to manage the ESS's charge [128]. [129] expands the ECMS with an additional cost term for the degradation of the ESS. An overview of optimization-based EMS methods for ships is provided in Table 2.8.

Power System	Method	Scope	Ref.
DG-Bat	SFC min.	Optimal fuel eff. for 4 DG with ESS	[120]
DG-Bat	ECMS	Power split for DG and ESS	[126]
DG-Bat	ECMS	Power split for DG and ESS	[127]
DG-Bat	ECMS	Power split for DG and ESS	[130]
DG-Bat	ECMS, ACO[1]	ECMS with opt. equivalence factor	[131]
GT-FC-Bat	Equiv. SFC min.	Split of moving average power between GT and SOFC[2]	[122]
GT	MPC	Fuel efficiency of parallel GT	[132]
DG-Bat	MPC	Optimal DG dispatch and SoC management with short-term load prediction	[133]
DG-Bat	MPC	Fuel eff. of DG and SoC management	[134]
GT-Bat-UC	MPC, OPF[3]	Generation scheduling leveraging load predictions	[76]
DG-Bat-PV	Stochastic MPC	Scenario-based optimization	[123]
GT-Bat	2-level MPC	Set-based MPC to guarantee operation in state and input constraints	[135]
DG-Bat-UC	2-level MPC	Decoupled steady-state and dynamic MPC problems	[136]
DG-FC-Bat	3-level MPC	Decomposition of control problem in multiple MPC	[137, 138]
DG-Bat-UC	2-level MPC	Propulsion control + opt. power split	[34]
DG-Bat	MPC	Maneuvering and optimal power split	[36]
DG-Bat-CI	2-level MPC	Mission-scale SoC trajectory	[139]
DG-Bat-UC	MPC, ECMS	ECMS with equivalence factor based on MPC output	[140]

Table 2.8: Optimization-based energy management in ship applications

Power System	Method	Scope	Ref.
DG	DP	Global opex minimization with DSM[1]	[141]
DG	DP	Global opex minimization with DC system	[142]
DG-Bat	DP	Global opex minimization with ESS	[143]
DG	PSO	Global multi-objective opt. for parallel DG	[144]
DG-Bat	MINLP[2]	Sizing and operation for min. TCO[3]	[145]
DG-Bat-CI	GA[4]	Global joint voyage schedule and EMS optimization	[146]
DG-Bat-CI	MILP[5]	Global joint voyage schedule and EMS with electricity price prediction	[147, 148]
DG-Bat-UC-CI	GA	Scenario-based global joint route plan, voyage schedule and EMS optimization	[149]
DG-Bat-CI-PV	PSO	Large-scale global optimization	[150]
DG-Bat	MILP	Optimal power dispatch and voyage scheduling incl. power reserve management	[151]

Table 2.9: Applications of mission-scale optimal ship operation

2.5.5 Predictive Energy Management

Predictive methods can be employed to leverage knowledge on future system states and disturbances. MPC allows to explicitly formulate objectives and constraints while accounting for the system's dynamics. Various strategies are listed in Table 2.8.

A simple, conventional power system in a naval vessel with parallel GTs is controlled using an MPC in [132]. A perfect load prediction is assumed, and the turbines are operated so that total fuel consumption is minimized over the prediction horizon, considering the non-linear efficiency characteristics of the turbines. [134] additionally regards batteries next to the conventional generators in the SPS. The MPC formulation aims at operating the internal combustion engines in their most efficient operating point while keeping a steady battery SoC. As in [132], no prediction model is implemented. Instead, the load is assumed to be constant over the prediction horizon, which can be feasible in ships with an unknown operating profile.

An optimal power flow calculation, as typically conducted in terrestrial power systems, leveraging load predictions in a medium-voltage DC SPS with GTs, batteries and UCs is proposed in [76]. Although the solution yields minimized operation costs, the constructed optimization problem is computationally expensive and subject to prediction and model errors. In [136], a two-level MPC with frequency decoupling is proposed. A high-level MPC optimizes the power system in quasi steady-state operation to match the slow load dynamics, while a low-level MPC with higher band-width optimizes the dynamic dispatch of generation power to meet the load requirements. A load prediction based on propulsion torque estimation is proposed in [85]. The formulated problem involves a broad range of objectives for voltage stability, component wear, efficiency, and propeller thrust, with the

[1] ant colony optimization [2] solid-oxide fuel cell [3] optimal power flow [1] demand-side management [2] mixed-integer non-linear programming [3] total cost of ownership [4] genetic algorithm [5] mixed-integer linear programming

aim of mitigating the effects of torque oscillations on the propulsion shaft. A three-level MPC is proposed by [137] for a naval vessel with GTs, FCs and batteries. The three layers operate with different band-widths from optimizing long-term generation scheduling, over optimal static power split between power sources of different types, to short-term disturbance rejection at the highest bandwidth.

In [34] and [36], the maneuvering control is included in the problem formulation. The authors present a two-level MPC in which the top layer determines an optimized shaft speed and torque, from which a load power prediction can be derived as input for the bottom layer MPC. The latter optimizes the power split between a DG, battery and UC to minimize the overall losses and the deviation from the required load power.

For ships with a known operation profile, knowledge over the entire mission duration can be used for predictive control. [139] uses this knowledge for the control of a diesel-hybrid ship with a charge-depleting-charge-replenishing strategy for the ESSs. A top-level mission-scale optimization regularly updates the optimal trajectory for the battery SoC. The authors in [140] implement an ECMS whose equivalence factor is updated based on inputs from a predictive controller.

Although an offline optimization of the power scheduling is not real-time applicable due to computational constraints and required a-priori knowledge, it is able to provide a benchmark for the optimal achievable control strategy, as showcased in [83] and [139]. Generally, mission-scale optimization is relevant for predictive control, as they can be employed within a multi-timescale MPC scheme [140]. Applications of a global optimization commonly focus on cost optimization via quasi-static dispatch of resources, while neglecting faster dynamics. An investigation of optimized power generation control in a conventional cruise ferry with DC distribution is conducted in [141–143]. The authors formulate the dispatch of energy resources as a non-linear constraint optimization problem in steady state conditions with a known mission profile and employ dynamic programming to solve this. The work of [145] occupies itself with the optimized operation planning of a hybrid diesel-battery ship. The authors use mixed-integer non-linear programming to simultaneously solve the optimal power generation scheduling and sizing of the battery energy storage system for minimization of the total cost of ownership. Complex and large scale optimization problems are commonly approached using meta-heuristics. In [150], the authors optimize the energy management strategy for a diesel-battery ship with additional RESs and cold ironing (CI) capability using particle swarm optimization (PSO). Applications of global optimization for ship operation are listed in Table 2.9.

2.5.6 Distributed Energy Management

The EMS methods above assume availability of all information in a central controller. However, in more complex power system architectures, a distributed energy management is promising to achieve a higher degree of reliability and reduction of computational load. Generally, distributed EMSs are proposed for zonal distribution architectures, typically in naval applications where survivability is a critical design target [115].

Specifically with the aim of creating a modular energy management solution, [152] describes a distributed EMS for electric vehicles. Generally, power systems and especially microgrid applications provide a range of methods for distributed optimization, with several relevant references listed in Table 2.10. The most widespread methods for distributed optimization

in multi-agent systems are Lagrangian dual decomposition solved via iterative gradient-based methods [44, 153–155] and alternating direction method of multipliers (ADMM) which uses an augmented Lagrangian formulation [155–158]. These methods allow for local optimization and feasibility while ensuring global feasibility through consensus. Global optimality is guaranteed for modules with convex cost functions. One prevalent method for incorporating non-convex functions and decision-making is through market- or auction-based algorithms [159, 160], albeit without guarantee for global optimality.
Applications for SPSs generally follow these methods, implementing dual decomposition [20, 161, 162] and ADMM [45]. EMSs that are both distributed and predictive use the same methods, i.e. dual decomposition [163, 164] and ADMM [165–167]. Whereas most studies focus on economic dispatch or balancing of marginal costs among parallel generators, several researchers incorporate specific objectives. Especially for naval vessels, more focus is placed on resilience and mission fulfillment. Researchers utilize distributed optimization for reconfiguration [168, 169] and load utilization [170]. Especially for increasing survivability and load servicing in emergency situations these aspects are relevant [171]. A range of distributed methods for ship energy management are listed in Table 2.11.

Power System	Method	Scope	Ref.
Distrib. gen.+loads	Auction-based	Federated buying-selling for economic dispatch	[159]
Distrib. gen.+loads	Auction-based	Federated buying-selling for economic dispatch	[172]
Quadratic costs	Dual decomposition	Consensus on marginal cost	[153]
Convex gen. costs	Dual decomposition	Consensus on marginal cost	[44]
Convex gen. costs	Diffusion Strategy	Diffusion of marginal cost	[173]
Convex gen. costs	Lambda iteration	Federated economic dispatch	[154]
GT-Bat-PV-WT[1]	Dual decomposition	Consensus on marginal cost	[155]
Convex gen. costs+ESS	ADMM	Economic dispatch	[155]
Convex gen. costs	ADMM	Economic dispatch with limited communication	[156]
Convex gen. costs	Relaxed ADMM	Increased convergence speed and robustness	[157]
Convex gen. costs	Scenario-based MPC	Robust, ECMS-based economic dispatch	[174]
Convex gen. costs	ADMM+DRA[2]	Simult. static and dynamic dispatch	[158]
Distrib. gen.+loads	Market emulation	Predictive, trading-based multi-agent system	[160]

Table 2.10: Applications of distributed energy management in microgrids

[1] wind turbine [2] distributed resource allocation

Power System	Method	Scope	Ref.
-	Maximum flow	Automatic reconfiguration with load priorization	[171]
-	Flocking	Optimal load utilization in zonal SPS	[175]
Ship-Harbor	Dual decomposition	Consensus on marginal cost	[161]
DG	Dual decomposition	Consensus on marginal cost for DC SPS	[20]
DG-ESS	Dual decomposition	Marginal cost balancing and ESS mode	[162]
DG-ESS	Leader-follower	Min. loss and economic dispatch in zonal SPS	[176]
DG-Bat-UC	ADMM	Distributed ECMS for zonal SPS	[45]
GT-Bat	Predictive heuristics	SoC management in zonal SPS with high ramped loads	[177]
GT-Bat	Flocking, predictive	Predictive distributed crow search for economic dispatch	[97]
DG-Bat	MPC, dual decomp.	Battery degradation-aware economic dispatch	[163]
GT-Bat	MPC, dual decomp.	Fault-tolerant load and SoC management	[164]
DG-Bat	MPC, ADMM	Load leveling and SoC management in zonal system with pulsed loads	[165]
DG-Bat	MPC, ADMM	Economic dispatch in zonal SPS + reserve allocation	[166]
DG-Bat-PV	MPC, ADMM	Static economic dispatch with load forecasting	[167]

Table 2.11: Applications of distributed energy management for ships

2.5.7 Energy Management for Zero-Emission Ships

The energy management in ZESs, especially with integrated FCs, has received little attention in the past. In this section, case studies for the energy management in ZESs are reviewed in order to identify challenges and trends for the control of hydrogen-based power systems on ships. Whereas the focus in conventional ships mainly on fuel efficiency and power balance, an additional objective that is often regarded in the EMS for ZESs is the degradation of the FCs and batteries. Table 2.12 presents an overview of studies on EMSs for ZESs in the literature. And the following subsection provides a categorization of archetypal energy management methods applied in FC-based SPSs.

Power System	Method	Scope	Ref.
Bat-UC	Constr. progr.	Minimal stress on battery	[23]
FC-Bat	PI	Peak-shaving for FC by ESS	[99]
FC-Bat	PI	Peak-shaving for optimal fuel efficiency and component wear	[24, 178]
FC-Bat-UC	PI	Load leveling and SoC management	[84]
FC-Bat	PI, rule-based	Rule-based FC operation and PI voltage regulation	[22]
FC-Bat	Rule-based	Optimal fuel efficiency	[98]
FC-Bat	Rule-based	Load-leveling for optimal fuel efficiency and component wear	[24, 178]
FC-Bat	Rule-based	Optimal fuel efficiency and component aging with CDCR strategy	[24, 178]
FC-Bat	Rule-based	TCO minimization through optimal sizing and operation	[179]
FC-Bat-UC	ECMS, SDP[1]	Optimal fuel efficiency and component degradation	[105]
FC-Bat-CI	Multi-scheme	Minimized opex and component degradation	[180]
FC-Bat-UC	Fuzzy-logic	Voltage regulation and SoC management for ESS	[21]
FC-Bat-UC-PV	Fuzzy-logic	Optimal fuel efficiency and SoC management for ESS	[83]
FC-Bat-CI	MPC	Optimized power scheduling for opex minimization	[181]
FC-Bat-CI-PV	Stochastic MPC	Opex minimization	[123]
FC-Bat-CI	Stochastic MPC	Minimized opex and degradation of components	[182]
FC-Bat	ANFIS[2]	Optimal fuel efficiency and SoC management	[183]
FC-Bat-CI	Deep RL[3]	Optimized power scheduling for opex minimization	[184]
FC-Bat	MILP	Global multi-objective optimization	[185]
FC-Bat-CI	SCA[4]	Global opex minimization	[186]

Table 2.12: Energy management in hydrogen-based power systems

Rule-based control: A rule-based EMS is proposed by [22]. Here, the FC system does not follow the demanded load, but instead a PI controller tracks a power reference determined based on load power and battery SoC. The scheme aims at operating the FC with an optimized and smoothed reference. In a similar fashion [98] presents a rule-based EMS for a small FC-battery passenger ferry aiming at a steady FC operation within an efficient

[1] sequential dynamic programming [2] adaptive neuro fuzzy inference system [3] reinforcement learning
[4] sine cosine algorithm

operating band. A multi-scheme approach, combining of four distinct EMSs into with heuristic rules for mode switching is proposed by [180]. Rule-based approaches generally yield satisfactory results, but the rule definition relies on expert knowledge, and is typically applied only to small-scale systems. Rules and heuristics appear in varying shapes and complexities. Increased complexity, however, should be motivated and requires more extensive input for parameter definition.

Load leveling approaches: A common goal of EMSs incorporating FCs is to level the load for the main power supply. [23] proposes constraint programming for an optimal power split between main power supply and auxiliary energy storage. This work points out the trade-off between storage sizing and degree of load leveling. A FC-battery hybrid system is regarded in [99], proposing load leveling via a central PI-controller. The power reference follows the load demand via a PI feedback loop. Since the dynamic capabilities of the FCs are limited, the deviation between load and FC output is compensated by the batteries. In [84] a HESS is proposed for load leveling. The storage system absorbs power fluctuations, while the SoC of the storage components is maintained using PI controllers, hence decoupling the FCs from the immediate load demand. [178] and [24] implement a load-leveling, a peak-shaving and a charge-depleting-charge-replenishing strategy, observing FC degradation, hydrogen consumption, power balance and space requirements. Generally, the strategies underscore the required trade-off between fuel consumption, FC aging and component sizing.

Fuzzy-logic control: Fuzzy logic offers an alternative method for applying expert knowledge into the control strategy. For a ZES with an FC-battery-UC system, a fuzzy logic strategy is designed in [21], and with additional RESs in [83]. Generally, fuzzy logic in FC-ESS systems derives a power reference for the FCs or power split between multiple units based on instantaneous load and SoC. Results generally show promising performance regarding energy consumption and FC lifetime degradation. As shown in [183]., fuzzy logic control can be combined with adaptive elements to improve the performance over time, which is especially beneficial with insufficient expert knowledge.

Equivalent consumption minimization: Whereas ECMS strategies are common for hybrid SPSs with DGs, their application for hydrogen-based systems is much less developed. An elaborate approach for a FC-battery-UC ship, inspired by an ECMS, is applied in [105]. A real-time control strategy is realized by formulating an instantaneous multi-objective optimization problem considering hydrogen consumption of the FC and an equivalent consumption for battery and UC utilization. Additionally, FC and battery degradation costs are included in the problem formulation. The optimization problem is consequently solved via SDP, a powerful tool for the energy management, which had already been applied to FC-hybrid electric vehicles [67].

Predictive control: As for the EMS in conventional ships, MPC is promising for the optimized control of zero-emission power systems. [181] investigates the generation scheduling of an FC-battery hybrid passenger ferry with CI capability, focusing on the minimization of operation costs. In [123], a PV system is additionally included in the

power system, for which generation predictions are leveraged in the MPC formulation. This work is later expanded upon [182] with a stochastic MPC in order to account for environmental uncertainties represented as probabilistic scenarios. In these works, hourly time intervals are used, while any kind of dynamics is disregarded. Hence, current literature lacks predictive energy management solutions for ZESs that incorporate system dynamics and handles load fluctuations.

Global optimization: Several studies investigate the global optimization of the power dispatch in ZESs, typically in a joint effort with component sizing and overall cost minimization. A simultaneous component sizing and energy management for a FC-Battery passenger ferry has been conducted by [185]. The authors take into account the total costs based on investment and operation costs for component acquisition and fuel consumption and further representing fuel cell degradation by considering replacement costs. The large-scale problem is formulated as a mixed-integer linear program (MILP), which is consequently solved in a multi-objective optimization. Another study for cost optimization is conducted in [186], presenting a feasibility study of a tourist boat. Due to the problem complexity, the authors employ a meta-heuristic sine-cosine algorithm, commonly used for complex, large-scale optimization problems.

Learning-based control: The hourly power scheduling with the aim of minimizing operation costs is approached using deep reinforcement learning in [184]. The authors regard a tourist boat powered by FCs and batteries with possibility for charging the ESSs when berthed. For this purpose, the scheduling of energy resources is modeled as a Markov Decision Process (MDP). The resulting EMS based on reinforcement learning is applied for real-time power scheduling on a test-bench. Currently, little attention lies on learning-based approaches, which, given sufficient data, is a promising research avenue for the future studies.

2.6 Conclusions for the Control of Shipboard Power Systems

The ongoing changes in the design of modern SPSs impose new challenges on the power system control and energy management for the operation of these vessels. The research literature provides novel methods to meet the requirements of increasingly complex power system architectures and technologies. In this chapter, the challenges for the overall control of SPSs have been analyzed and suitable control architectures and methods for local, coordinated and high-level control have been reviewed. This literature research was carried out with a specific interest in DC power systems and the modular integration of zero-emission technologies. The main conclusions resulting from this chapter are summarized as follows:

- SPSs are incorporating a growing variety of technologies. This necessitates control strategies that account for the varying characteristics of these power system resources. Generation and storage components differ in dynamic capabilities, efficiency, power and energy density and should be operated accordingly.

- A trend in power system design is pointing towards modular integration of power system components, which should be reflected in the control strategies as well. It is key to develop methods that facilitate a simple integration of new technologies. DC distribution is deemed to be an enabler for this plug-and-play capability in both design and control of the SPSs.
- Studies on control for ZESs with FCs focus on small passenger ships and ferries. There is a clear lack in research for the control of FC-based ships with a larger number of parallel generation and storage systems. Applications with high energy needs and significant service loads and reliability requirements need to be addressed.
- The literature on energy management for FC-hybrid vessels is focused on deterministic and rule-based approaches. Optimization-based EMSs, especially predictive and learning-based methods, show high potential for improving the performance.
- Distributed methods are a promising solution for tying together complex power systems with heterogeneous resources in a modular fashion. The adaptability of this approach is able to increase the system resilience and adaptation under faults and uncertainties.
- With new ship designs incorporating FCs and batteries, component degradation is becoming an increasingly important objective for the control of SPSs, next to the minimization of fuel consumption and operating costs.
- Several studies include adaptive elements in their control strategies. Adaptive control, demand-side management and mode-based operation can play an important role in enhancing the resilience of the ship.
- An often overlooked aspect in power system control is the consideration of faulty and degraded sub-systems. The coordinated control and energy management should be designed to support fault-tolerant operation while meeting load servicing requirements and efficient utilization of resources.
- Current literature studies lack experimental validation of control strategies. Most studies rely on numerical investigations. Especially for the real-time control of SPSs, experimental work will create valuable insights and showcase the methods' applicability in the field.

Future research must focus on these aspects to develop methods that meet the requirements of modern SPSs and to take on the challenges the maritime sector is currently facing. Faced with the challenge of integrating and coordinating vastly different novel technologies, the power system control is subject to a series of requirements. Whereas power availability and efficiency play an important role, resilience, safety and adaptability are gaining in relevance. DC distribution, power electronics converters and modern computing and communication equipment provide opportunities to handle these challenges. Reviewing control architectures and the distribution of control functionalities is a promising ingredient in developing suitable control methods. The research opportunities identified in this chapter are directly linked to the formulation of the problem statement and research questions in Section 1.3 and thereby serve as the foundation for further investigations in this thesis.

3

Energy-based Voltage Stabilization in DC Shipboard Power Systems

As part of the literature review in the preceding chapter, control architectures and hierarchical control layers were described and analyzed. As in a typical control hierarchy, I would like to build my overarching approach from the bottom up. Before spending time on fancy energy management and coordination algorithms, this chapter is dedicated to building a solid foundation. For DC systems, this means to stabilize the voltage such that it is not overburdened by the load demands. Before even thinking about increasing the efficiency of power generation, I want to make sure that the loads can be serviced according to their requirements, without the system falling apart. The voltage stabilization is also the fastest of system-level control tasks, directly affected by the local current controllers. In a fuel cell-battery system, this is the responsibility of the batteries due to their higher dynamics. This chapter describes a control strategy for parallel batteries, interfaced via DC-DC converters to a DC distribution system. Its purpose is to provide a bus voltage stabilization and simultaneously allocates power targets among batteries according to their capabilities. The result is a stable and resilient platform, on top of which more advanced control layers can be built.

"The winds will blow,
the storms will come.
You cannot stop them.
But you can stand."

— *Kaladin*, in *The Way of Kings*
by *Brandon Sanderson*

This chapter is published with minor modifications as *Energy-Based Voltage Stabilization in DC Shipboard Power Systems With Dual Loop Control, in: IEEE Access, 2025* [187]

3.1 Introduction

Modern shipboard power systems (SPSs) are subject to a multitude of developments in the context of decarbonizing the maritime sector. Key changes encompass ship electrification, DC distribution technology [17], as well as the introduction of energy storage systems (ESSs) and zero-emission power supplies [11, 12]. Such systems can be regarded as islanded DC microgrids [10]. Several aspects set SPSs apart from terrestrial power systems. The number and variety of components are considerably lower, and the network's impedances are often negligibly small. The main loads are subject to high fluctuations and are typically power-controlled, e.g., propulsion machinery and service equipment. In addition, SPSs must follow special requirements for power availability, influencing the power system architecture and its control. In an integrated DC power system, it is key to maintain the bus voltage around its nominal value, and to prevent a loss of load or even a blackout. Hence, fast and accurate voltage stabilization and restoration are crucial objectives, which are further aggravated in systems with constant power loads (CPLs), low inertia and negligibly low line impedances. This study focuses on the primary and secondary control layers, as described in [19, 59], covering the voltage stabilization and restoration with parallel power sources.

The conventional primary control strategy is voltage droop, a decentralized method that does not require any communication [49]. Droop-based strategies are generally favored since they allow a system extension and require no high-bandwidth communication, thereby offering modular characteristics [47]. In the context of voltage stability with CPLs, a comparative analysis of standard droop schemes in DC microgrids is conducted in [188]. The effect of the negative incremental impedance of CPLs and the consequent weak damping of the power system is analyzed in [189]. Several studies delve into non-linear control approaches for the stabilization with CPLs [52]. However, these approaches typically investigate a single converter supplying one CPL [190–194]. Several works attempt to increase the stability of droop-controlled systems with CPLs by extending the standard droop scheme with virtual impedances and filters [189, 195–197]. Although these studies address stability with a CPL in droop-controlled systems, a decentralized method for parallel control of power converters that directly addresses the non-linearity between the voltage-based controller and the power load is lacking. Passivity-based approaches for DC link stabilization regard the power system control from an energy-based perspective [191–194]. Following this concept, this study proposes the adaptation of an energy-based scheme for stabilizing low-inertia, low-impedance DC power systems. The energy-based approach offers the scalability and modularity of conventional droop control, due to its decentralized architecture, while improving the system stability and voltage restoration speed by explicitly accounting for the non-linearity of CPL.

As a drawback, standard droop control yields a steady-state voltage deviation, which requires the implementation of a secondary control layer for voltage restoration. Conventionally, this function is centralized and reference changes are broadcast via communication links [49, 59, 198]. The centralized voltage restoration is accurate [47], but slow, especially without a high-bandwidth communication [59, 199]. To increase the control speed, this study considers a local implementation of the voltage restoration, yielding a dual loop controller. Several studies attempt a local implementation of PI loops, increasing the speed of voltage restoration [46, 200], albeit at a loss of power sharing accuracy. However,

inaccuracies in the power sharing can be compensated by additional methods utilizing low-bandwidth information sharing, e.g., via average current sharing [47], droop coefficient adaptation [80, 201], or voltage reference shifting [202, 203]. In this work, an adaptive power sharing control loop supported by a low-bandwidth communication network is proposed. This facilitates a compensation of power sharing imbalances arising from the decentralized control architecture and ensures that the power ratio of parallel components is accurately tracked while maintaining a fast voltage stabilization and restoration.

To summarize, the main contributions of this work are as follows. 1) An energy-based dual loop control scheme to increase stability and damping of the bus voltage with fluctuating loads in DC SPSs with CPLs; 2) An adaptive power sharing loop utilizing low-bandwidth communication to ensure accurate power sharing among parallel power supplies.

This chapter first introduces the considered SPS topology and the modeling approach for the system and its components in Section 3.2. In Sections 3.3 and 3.4, the conventional and the proposed energy-based droop scheme are analyzed, and the controllers are tuned via pole placement. Section 3.5 describes the adaptive power sharing for parallel control with the energy-based approach. A HiL testbed for the validation is presented in Section 3.6, where the performance and applicability of the proposed control strategies are demonstrated. For this purpose, two test setups, for control of a single converter and for parallel control, are deployed on the testbed. Finally, the results and conclusions of these contributions are summarized in Section 3.7.

3.2 System Description and Modeling

This study considers the primary systems of a fully electrified SPS with DC distribution and power converter-interfaced components. The load-side converters follow a power demand, while the generation-side converters stabilize the bus voltage. Here, batteries are implemented as ESSs and fuel cells (FCs) are incorporated as zero-emission power supplies. Accordingly, no inertia from conventional engines remains. An exemplary topology is shown in Fig. 3.1. This section describes the modeling approach for the power sources, DC-DC converters, DC distribution system, and power loads.

3.2.1 Power Sources

For the power sources, i.e., the ESSs and FCs, dynamic simulation models are implemented using static current-voltage curves and first-order transfer functions. The models are parameterized based on manufacturer data. The ESSs are represented by Li-ion batteries using standard parameters following the approach in [204]. Hydrogen proton-exchange membrane FCs are represented using a similar model from [205].

3.2.2 DC-DC Converters

The DC-DC converters are modeled as half-bridges, as implemented in [178]. This topology allows bi-directional power flows, although the operation of the FCs is limited to positive power flows into the DC bus. Since this work focuses on the coordinated control of multiple sources, the high-frequency switching actions of the transistors are neglected. Hence, the converters are implemented as averaged models, as in [206] and [73].

Fig. 3.2 shows the equivalent circuit of a synchronous boost converter connected to the DC

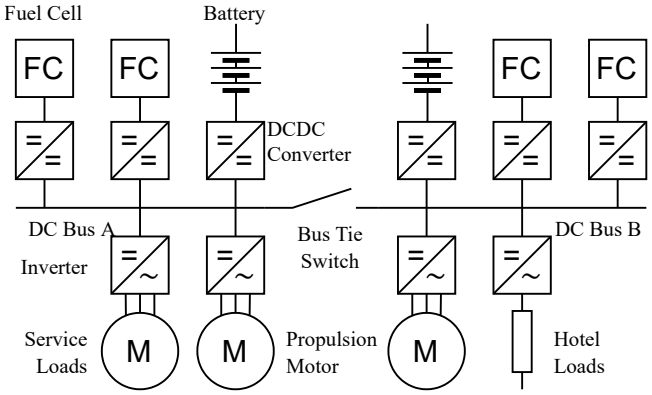


Figure 3.1: Exemplary shipboard power system topology with FC-battery hybrid energy system with DC distribution and power electronics-interfaced subsystems

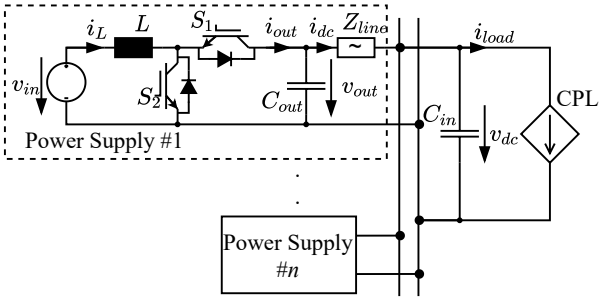


Figure 3.2: Equivalent circuit of the modeled DC system with constant power load and multiple idealized power supplies connected via half-bridge DC-DC converters

bus. The dynamics of the averaged inductor current i_L in this topology can be computed as

$$\frac{di_L}{dt} = \frac{1}{L}(v_{in} - (1-d)v_{out}) \tag{3.1}$$

where v_{in} and v_{out} signify the source and output voltages where $v_{in} < v_{out}$, and L the converter's inductance. d is the duty cycle of switch S_2, serving as the control input in boost mode. In buck mode, switch S_1 is operated with duty cycle $\tilde{d} = 1 - d$. Each converter is additionally equipped with an output capacitance C_{out} such that the output voltage is given as

$$\frac{d}{dt}v_{out} = \frac{1}{C_{out}}(i_{out} - i_{dc}) = \frac{1}{C_{out}}((1-d)i_L - i_{dc}) \tag{3.2}$$

where i_{out} is the current flowing from the power supply to the DC bus. The local current controller is implemented as a PI feedback controller, tracking a reference for i_{out} obtained from the primary control level. Multiple half-bridges in parallel can be used to connect a power supply as an interleaved converter. In this case, each phase leg is controlled individually following the method above.

3.2.3 DC Distribution System and Power Loads

The most significant system loads are constituted by the propulsion motors and service equipment. These loads are typically interfaced with inverters are regulated such that they draw a constant power. Hence, on the system level, these loads can be seen as CPLs, which are characterized by their negative incremental resistance, i.e., a voltage drop yields an increasing current draw at constant power. All loads are modeled as an aggregated CPL given as an exogenous input p_{load}. Using the DC bus voltage v_{dc} over the load's input capacitance C_{in}, the power demand can be translated to a load current $i_{load} = p_{load}/v_{dc}$. The interconnection of power supplies, loads, and the DC bus is depicted in Fig. 3.2. Each power supply is connected to the DC bus via a line impedance Z_{line}, modeled as a series RL-element. The output current of each i-th converter connected to the bus can be denoted as $I_{dc,i}$, and the time derivative of the DC-link voltage $\frac{d}{dt}v_{dc}$ can then be computed as

$$\frac{d}{dt}v_{dc} = \frac{1}{C_{in}}(\sum_{i=1}^{N} I_{dc,i} - i_{load}) \tag{3.3}$$

3.3 Conventional Droop Control

This section introduces voltage-based droop as the conventional primary control method, including an extension by an integral action for bus voltage restoration. Assumptions for the local control and a simplification of the plant model for the controller synthesis are presented. Subsequently, transfer functions for the conventional control are derived and control parameters are determined via pole placement.

3.3.1 Local Control

Each power converter has a local controller regulating its output current. Local PI current controllers are implemented, which are tuned such that they meet the designed bandwidth of the current control loop (see [46]). In the context of a modular system design, we assume

the utilization of off-the-shelf power converters with a fixed switching frequency and limited current control speed which, for SPSs, is typically in the range of 1000 Hz [207]. For the controller synthesis, the current control transfer function H_{cc} is simplified as a first-order low-pass filter with unitary gain and current control bandwidth ω_{cc}.

3.3.2 Voltage Droop

In SPS, line impedances are typically very low. In the considered power system, the time constants comprised of each module's output filter and line impedance are significantly faster than the current control speed of the power electronics converters. This means that the voltage balances faster among the distributed capacitances than the decentralized controllers act. This allows the simplified representation of the entire DC bus as a lumped capacitance C_{dc}, which is approximated as the sum of all power supplies' output capacities and the load's input capacitance. This assumption requires that the electrical distance between components is sufficiently small such that the balancing of voltages between the distributed capacitances occurs faster than the current control dynamics. This approach is in line with the model description for DC SPSs proposed in [10]. Hence, for the control, the DC bus is modeled with transfer function

$$\frac{v_{act}}{i_{act} - i_{load}} = \frac{1}{sC_{dc}} \tag{3.4}$$

where v_{act} is the DC bus voltage, i_{act} the total current from all power supplies, and i_{load} the current drawn by the load.

The conventional droop scheme operates in voltage-mode, where each device computes a target output voltage as

$$v_{ref} = V_{nom} - R_d i_{out} \tag{3.5}$$

where V_{nom} is the nominal bus voltage, R_d is a virtual resistance and i_{out} is the measured output current. Power sharing among parallel devices is realized by tuning the virtual resistances inversely proportional to the source's rating.

The same scheme can be transformed such that a current reference is obtained based on the output voltage measurement, which is more appropriate for the considered SPS with negligibly small line impedances. This scheme's block diagram for a single power supply is shown in Fig. 3.3. The current reference i_{ref} is determined as

$$i_{ref} = (v_{ref} - v_{msr}) H_{vc} \tag{3.6}$$

where H_{vc} is the transfer function of the droop controller. Furthermore, the real measured feedback signal v_{msr} of the bus voltage includes measurement noise d_m, and the power load p_{load} acts as an input disturbance on the plant. Conventionally, a proportional gain is used, such that $H_{vc} = \frac{1}{R_v}$. Both the voltage- and current-mode droop schemes yield an equivalent steady-state behavior and similar dynamic responses. A more detailed comparison, including stability analysis, is presented in [188]. In this work, the current-mode droop control is considered the baseline approach.

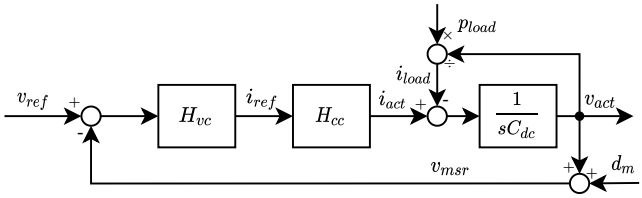


Figure 3.3: Block diagram of conventional voltage-based scheme in current-mode including input and measurement disturbances

3.3.3 Voltage Restoration

In steady state, conventional droop schemes yield a non-zero voltage error $\Delta v = v_{\text{ref}} - v_{\text{msr}}$. This can be mitigated by implementing an integral gain on the voltage error, yielding a dual loop approach with PI feedback control. The integral action is often realized in a central, secondary control layer [59]. To achieve a fast voltage restoration, however, a local implementation is more desirable, as in [200]. Accordingly, instead of a virtual resistor, as in the standard voltage droop in (3.6), a PI controller with proportional gain k_{p} and integral gain k_{i} is implemented. The current reference is then generated according to

$$i_{\text{ref}} = k_{\text{p}} \Delta v + \frac{k_{\text{i}}}{s} \Delta v \tag{3.7}$$

3.3.4 Dual Loop Control Design

To analyze the dynamic behavior and tune the control parameters, we first simplify the system shown in Fig. 3.3. The voltage control bandwidth ω_{vc} should be sufficiently slower than the current control ($\omega_{\text{vc}} << \omega_{\text{cc}}$). Hence, in the controller synthesis, we disregard the transfer function of the current controller and assume $H_{\text{cc}} \approx 1$, yielding $i_{\text{act}} = i_{\text{ref}}$ We further disregard measurement noise in this study, such that $v_{\text{msr}} = v_{\text{act}}$. For the performance of the voltage stabilization, the controller's ability to compensate for input disturbances is decisive for minimizing the set point error, while the reference voltage typically does not change Hence, we consider the transfer function G_{do} from disturbance, i.e., the unknown CPL, to the actual bus voltage. Due to the negative incremental resistance of power-controlled loads, the CPL introduces a non-linear feedback loop from the DC bus voltage to the load current. Hence, we linearize the load current around the nominal voltage V_{nom} as $\tilde{I}_{\text{load}} = p_{\text{load}}/V_{\text{nom}}$. The voltage dynamics can then be described as

$$v_{\text{act}} = (v_{\text{ref}} - v_{\text{act}}) H_{\text{vc}} \frac{1}{sC_{\text{dc}}} \tag{3.8}$$

The transfer function of the voltage-based dual loop control is then obtained as

$$G_{\text{do}} = \frac{v_{\text{act}}}{i_{\text{load}}} = -\frac{1}{sC_{\text{dc}} + H_{\text{vc}}} = -\frac{s}{s^2 C_{\text{dc}} + s k_{\text{p}} + k_{\text{i}}} \tag{3.9}$$

By analyzing the denominator of (3.9), it can be derived that the poles of G_{do}, lie at

$$s_{1,2} = -\frac{k_{\text{p}}}{2C_{\text{dc}}} \pm \sqrt{(\frac{k_{\text{p}}}{2C_{\text{dc}}})^2 - \frac{k_{\text{i}}}{C_{\text{dc}}}} \tag{3.10}$$

We select the PI gains to place the poles of G_{do} at the desired voltage control bandwidth ω_{vc}. Eliminating the term under the square root in (3.10) ensures a fast voltage restoration while ensuring the poles do not contain imaginary parts. This yields

$$k_{\mathrm{p}} = \omega_{\mathrm{vc}} \hat{C}_{\mathrm{dc}} \quad \text{and} \quad k_{\mathrm{i}} = \frac{k_{\mathrm{p}}^2}{4\hat{C}_{\mathrm{dc}}} \tag{3.11}$$

Although popular due to its simplicity, ease of implementation, and decentralized architecture, the voltage-based approach has a series of limitations. One key challenge is posed by the operation of loads in SPSs at constant power. Fig. 3.3 outlines the dependence of the load current on the actual DC bus voltage. The conventional scheme attempts to reject disturbances originating from a power load via the current as an input variable. However, the real system contains a non-linearity due to the feedback of the power load on the bus voltage. For this reason, we introduce an energy-based droop scheme, generating a power reference to stabilize the disturbance, in the following section.

3.4 Energy-based Voltage Control

This section describes the proposed energy-based droop. The concept of energy-based control is introduced in the context of droop control, and subsequently, a dual loop controller is designed via pole placement, analogously as in Section 3.3. The stability of the proposed schemes are assessed, and finally the sensitivity of the proposed schemes to an inaccurate DC bus capacitance estimate and the underlying current control speed are analyzed.

3.4.1 Energy-based Droop

The key step for setting up an energy-based droop scheme is transforming the voltage- and current-based control into a system where the energy in the DC bus is controlled via the input power. Using the voltage-energy relationship of capacitances and regarding the DC bus as a single capacitance C_{dc}, we can define a reference energy e_{ref}, as well as an estimate energy in the DC bus e_{est}

$$e_{\mathrm{ref}} = \frac{\hat{C}_{\mathrm{dc}}}{2} v_{\mathrm{ref}}^2 \quad \text{and} \quad e_{\mathrm{est}} = \frac{\hat{C}_{\mathrm{dc}}}{2} v_{\mathrm{msr}}^2 \tag{3.12}$$

$\hat{C}_{\mathrm{dc}}$ is an estimate of the system's DC bus capacitance. In the energy-based scheme, the local controller computes a power reference, as opposed to a current reference in the conventional scheme. Since the lower level current control loop requires a current reference, the power reference is then transformed back. Using a proportional controller yields the energy droop scheme

$$p_{\mathrm{ref}} = k_{\mathrm{p}}(e_{\mathrm{ref}} - e_{\mathrm{est}}) \quad \text{and} \quad i_{\mathrm{ref}} = p_{\mathrm{ref}} / v_{\mathrm{msr}} \tag{3.13}$$

This scheme is visualized in Fig. 3.4. Here, the linear relationship between controller output and input disturbance, which are power quantities, can be seen, setting the energy-based droop apart from the conventional strategy.

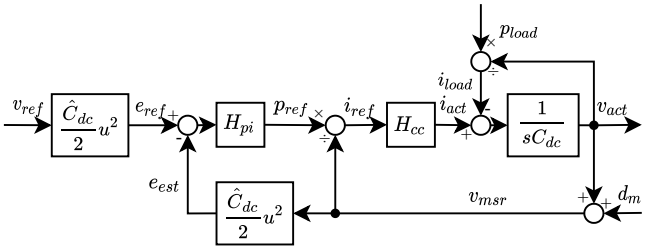


Figure 3.4: Block diagram of proposed energy-based control including input and measurement disturbances

3.4.2 Dual Loop Control Design

As the conventional droop, the energy-based droop yields a steady-state voltage deviation without an integral action. As before, this is mitigated by feeding the energy error $\Delta e = e_{\text{ref}} - e_{\text{est}}$ through a PI loop.

$$p_{\text{ref}} = (k_{\text{p}} + \frac{k_{\text{i}}}{s})\Delta e \tag{3.14}$$

For the derivation of the transfer functions, no linearization of the CPL is required in the energy-based scheme since now the disturbance and controller output are both power quantities. In the relationship between disturbance and output G_{do}, the squared bus voltage is regarded:

$$v_{\text{act}}^2 = \frac{2}{C_{\text{dc}}} e_{\text{act}} = 2\frac{p_{\text{ref}} - p_{\text{load}}}{sC_{\text{dc}}} \tag{3.15}$$

$$p_{\text{ref}} = -H_{\text{pi}} \frac{\hat{C}_{\text{dc}}}{2} v_{\text{act}}^2 \tag{3.16}$$

$$G_{\text{do}} = \frac{v_{\text{act}}^2}{p_{\text{load}}} = -\frac{s}{s^2 \frac{C_{\text{dc}}}{2} + s\frac{\hat{C}_{\text{dc}}}{2} k_{\text{p}} + \frac{\hat{C}_{\text{dc}}}{2} k_{\text{i}}} \tag{3.17}$$

Hence, we see that the disturbance has a linear effect on the stored energy, or alternatively, on the squared DC bus voltage. Again, the voltage controller shall be tuned to reject disturbances according to the desired voltage control bandwidth ω_{vc}. The poles of the transfer function G_{do} in (3.17) are located at

$$s_{1,2} = -\frac{\hat{C}_{\text{dc}}}{2C_{\text{dc}}} k_{\text{p}} \pm \sqrt{(\frac{\hat{C}_{\text{dc}}}{2C_{\text{dc}}} k_{\text{p}})^2 - \frac{\hat{C}_{\text{dc}}}{C_{\text{dc}}} k_{\text{i}}} \tag{3.18}$$

With an accurate DC bus capacitance estimate, i.e., $\hat{C}_{\text{dc}} = C_{\text{dc}}$, the poles can be placed as desired by setting

$$k_{\text{p}} = \omega_{\text{vc}} \quad \text{and} \quad k_{\text{i}} = \frac{k_{\text{p}}^2}{4} \tag{3.19}$$

Inserting (3.19) into (3.17) and (3.18) yields the closed-loop transfer function of the designed controller and the location of its poles:

$$G_{\mathrm{do}} = -\frac{s}{s^2\frac{C_{\mathrm{dc}}}{2} + s\frac{\hat{C}_{\mathrm{dc}}}{2}\omega_{\mathrm{vc}} + \frac{\hat{C}_{\mathrm{dc}}}{8}\omega_{\mathrm{vc}}^2} \tag{3.20}$$

$$s_{1,2} = -\frac{\omega_{\mathrm{vc}}\hat{C}_{\mathrm{dc}}}{2C_{\mathrm{dc}}} \pm \frac{\omega_{\mathrm{vc}}}{2}\sqrt{(\frac{\hat{C}_{\mathrm{dc}}}{C_{\mathrm{dc}}})^2 - \frac{\hat{C}_{\mathrm{dc}}}{C_{\mathrm{dc}}}} \tag{3.21}$$

3.4.3 Disturbance Rejection

To analyze the stability of the proposed controller, we regard the disturbance transfer function G_{do} of voltage- and energy-based schemes, with and without voltage restoration, to assess the deviation of the bus voltage as a function of the load. Fig. 3.5 shows the corresponding gain for the different control schemes, over varying load frequencies. The data in this figure is generated via numerical simulations, injecting a load power with varying frequency and magnitude to the modeled system, and logging the bus voltage.
All controllers reject load disturbances with frequencies significantly smaller than the voltage control bandwidth very well, whereas the DC bus capacitance filters out high-frequency loads. The gain of energy-based scheme is only affected by the load frequency but remains unaffected by the load magnitude. The transfer function of voltage-based control shows an additional dependency on the load amplitude. At low magnitudes, its gain matches those of the energy-based schemes. However, at higher load magnitudes, the gain increases, due to the non-linear relationship to the constant power load. Beyond a certain magnitude, the voltage-based control becomes unstable and tends towards infinity, as indicated in Fig. 3.5. Purely proportional voltage droop becomes unstable in the low-frequency range for load magnitudes beyond a certain threshold. With an added integral action the controller shows instabilities around the voltage control frequency.
Generally, the results show that energy-based control rejects load disturbances of all magnitudes with a limited gain, which can be designed such that the bus voltage constraints are not violated under maximum load. The maximum gain can be decreased and shifted towards higher frequencies by increasing the voltage control bandwidth.
For practical implementation, it is furthermore important to regard the effect of measurement noise on the controller performance. Fig. 3.6 shows the noise-to-output gain for the proposed controllers for noise added to the bus voltage measurement. For all schemes, the gain is independent of the noise magnitude and no difference was observed between voltage- and energy-based schemes. For all schemes, the gain is 0 dB in the low-frequency region and dropping off beyond the voltage control frequency. For controllers with voltage restoration, the gain peaks at ca. 2 dB increased gain around the voltage control frequency. The results show that measurement noise has no additional adverse effect on the proposed energy-based controller, compared to conventional voltage-based control, and that all schemes are robust against measurement noise significantly faster than the voltage control bandwidth.

3.4.4 Sensitivity to Bus Capacitance Estimate

The actual location of the poles of the closed-loop system is dependent on the quality of $\hat{C}_{\mathrm{dc}}$ as an estimate of the DC bus capacitance. In the previous sections, it was assumed that $\hat{C}_{\mathrm{dc}} = C_{\mathrm{dc}}$, which in reality is not necessarily true. Furthermore, the real DC bus is not a

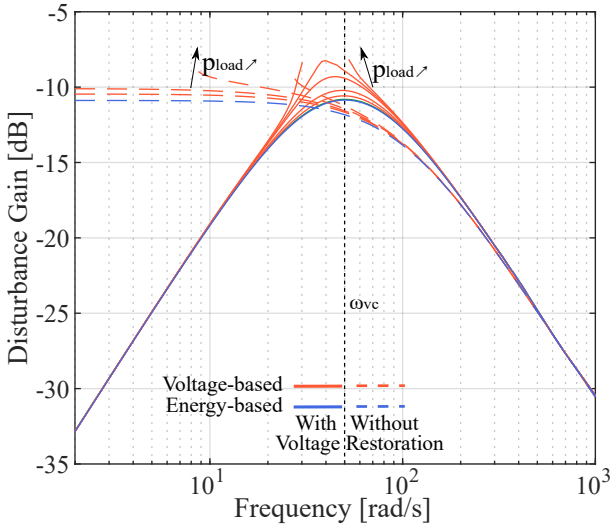


Figure 3.5: Gain of closed-loop disturbance transfer function $[V^2/W]$ over disturbance frequency

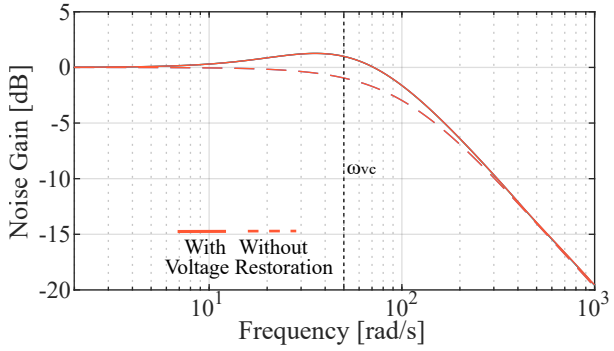


Figure 3.6: Gain of closed-loop transfer function from measurement noise to output $[V/V]$ over noise frequency

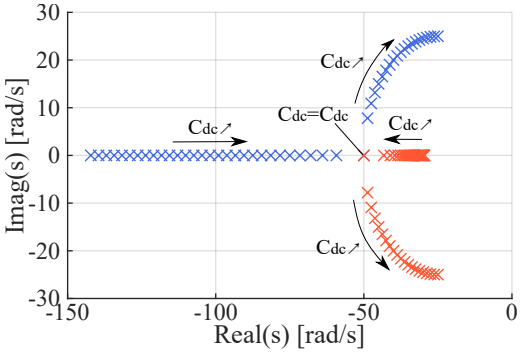


Figure 3.7: Root locations of disturbance-output transfer functions of energy-based controller for variation of the DC bus capacitance estimate

lossless, lumped capacitance, but actually consists of multiple, distributed capacitances. To analyze the effect of a non-ideal capacitance estimation, we consider the root locations of the transfer functions for a variation of $\hat{C}_{\mathrm{dc}}$, as displayed in Fig. 3.7. We can observe that an underestimation of the capacitance moves one pole close to the imaginary axis, yielding a slower voltage control response. An overestimation, however, makes the controller overly aggressive, introducing voltage oscillations.

3.4.5 Sensitivity to Current Control Bandwidth

It has so far been assumed that the underlying inner loop for current control is sufficiently fast ($H_{\mathrm{cc}} \approx 1$) so that it does not interfere with the outer voltage or energy loop. In reality, the current control bandwidth and the output current are limited so that the cascaded loops to interfere with one another.

Including the current controller H_{cc} in the transfer function of the energy-based dual loop scheme with PI loop, and inserting the designed values for k_{p} and k_{i} from (3.19), we obtain

$$G_{\mathrm{do}} = -\frac{s^2 + \omega_{\mathrm{cc}} s}{s^3 \frac{C_{\mathrm{dc}}}{2} + s^2 \frac{C_{\mathrm{dc}}}{2} \omega_{\mathrm{cc}} + s \frac{\hat{C}_{\mathrm{dc}}}{2} \omega_{\mathrm{vc}} \omega_{\mathrm{cc}} + \frac{\hat{C}_{\mathrm{dc}}}{8} \omega_{\mathrm{vc}}^2 \omega_{\mathrm{cc}}} \tag{3.22}$$

We observe that the speed of the inner current control influences can interfere with the outer energy loop, compromising its performance. In Fig. 3.8, the effect of a variation of the current control bandwidth ω_{cc} on the location of the poles for both schemes is shown. This analysis shows that an reduced current control speed shifts the pole locii, lowering the frequency of the slowest pole and possibly introducing imaginary pole pairs. This highlights the importance of ensuring that the inner control loop is sufficiently fast enough. In practice, the achievable or available speed of the the inner loop limits the realizable voltage control speed.

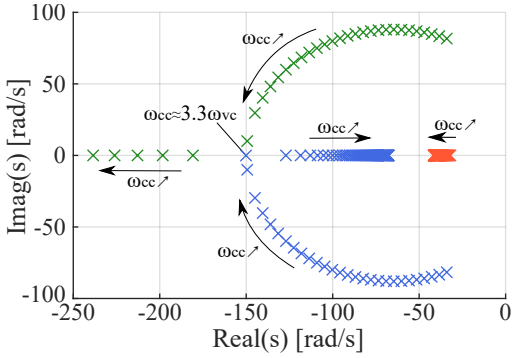


Figure 3.8: Root locations of disturbance-output transfer functions for variation of the current control bandwidth for energy-based control with PI loop

3.5 Parallel Control

In the previous sections, the bus stabilization with a single controlled power supply has been investigated. The decentralized design requires applying the proposed strategy to the parallel control of multiple power sources. This section discusses the design of a coordinated control between multiple parallel ESS, and coordination with main power supplies for bus stabilization and efficient dispatch of resources.

3.5.1 Power Sharing Among Parallel ESS

We assume that multiple ESS systems are connected to the DC SPS and are responsible for the stabilization of the bus voltage. Every system has an individual available power $P_{\mathrm{av},i}$. The total available power in the system follows from the sum of all N units as

$$P_{\mathrm{av,tot}} = \sum_{j \in N} P_{\mathrm{av},j} \tag{3.23}$$

The actual supplied power of each unit can be computed locally as

$$p_{\mathrm{act},i} = v_{\mathrm{out},i} i_{\mathrm{out},i} \tag{3.24}$$

and the sum of all power outputs yields the total supplied power

$$p_{\mathrm{act,tot}} = \sum_{j \in N} p_{\mathrm{act},j} \tag{3.25}$$

We define the goal of the power sharing among parallel power supplies to ensure that the ratio of power output to available power is equal for all units. For this we define the actual power sharing gain as

$$\gamma_{\mathrm{act},i} = \frac{p_{\mathrm{act},i}}{p_{\mathrm{act,tot}}} \tag{3.26}$$

whereas the desired reference for the power sharing gain is

$$\gamma_{\mathrm{ref},i} = \frac{P_{\mathrm{av},i}}{P_{\mathrm{av,tot}}} = \frac{P_{\mathrm{av},i}}{\sum_{j \in N} P_{\mathrm{av},j}} \tag{3.27}$$

Since the local controllers cannot measure the power output of other units, we introduce a central control unit connected via a low-bandwidth communication network. This controller collects the individual power outputs $p_{\mathrm{act},i}$ and available power levels $P_{\mathrm{av},i}$ from all units and broadcasts $p_{\mathrm{act,tot}}$ and $P_{\mathrm{av,tot}}$. Thus, the required information is made available for all local controllers to compute $\gamma_{\mathrm{ref},i}$ and $\gamma_{\mathrm{act},i}$. The control architecture and signal exchange is visualized in Fig. 3.9 To realize the power sharing according to the available power, each local energy control loop is modified by multiplying the PI-controller output with $\gamma_{\mathrm{ref},i}$, as can be seen in Fig. 3.9.

In a real system, multiple factors influence the accuracy of the desired power sharing. These encompass sensor noise and bias, parallel processing on different controller hardware, unequal line impedances, and further effects. To compensate for a mismatch between $\gamma_{\mathrm{ref},i}$ and $\gamma_{\mathrm{act},i}$, we introduce an adaptive droop gain $r_{\mathrm{d},i}$ which shifts the individual reference energy $e_{\mathrm{ref},i}$. Adaptive techniques with droop gain variation have been shown to be effective in compensating imbalances [59]. Here, we initially set the droop gain to zero and only use small values to compensate for power sharing imbalances. The gain is then controlled using a PI loop as

$$r_{\mathrm{d},i} = (\gamma_{\mathrm{act},i} - \gamma_{\mathrm{ref},i})(k_{\mathrm{p}\gamma,i} + \frac{k_{\mathrm{i}\gamma,i}}{s}) \tag{3.28}$$

with control gains $k_{\mathrm{p}\gamma,i}$ and $k_{\mathrm{i}\gamma,i}$. Following the nominal voltage V_{nom}, the adjusted energy reference is obtained as

$$e_{\mathrm{ref},i} = \frac{\hat{C}_{\mathrm{dc}}}{2} V_{\mathrm{nom}}^2 - r_{\mathrm{d},i} p_{\mathrm{out},i} \tag{3.29}$$

3.5.2 Communication Failure

A key challenge of a centralized controller, as proposed here for the power sharing control loop, is its vulnerability towards faults in the high-level control or communication. To mitigate this, the system can safely transition to a purely decentralized fallback mode after a communication fault. In fallback mode, the power sharing control switches to a droop-based approach that affects the reference voltage $e_{\mathrm{ref},i}$ with a fixed droop gain $R_{\mathrm{fb},i}$:

$$e_{\mathrm{ref},i} = \frac{\hat{C}_{\mathrm{dc}}}{2} V_{\mathrm{nom}}^2 - R_{\mathrm{fb},i} p_{\mathrm{out},i} \tag{3.30}$$

That droop gain is set inversely proportional to the unit's power rating. This approach resembles a conventional droop approach in voltage mode, albeit transformed to an energy-based framework. The approach is known to provide accurate power sharing at high droop resistances, with the drawback of a steady-state voltage deviation from the nominal value [208].

3.5.3 Power Split Between ESS and Main Power Supplies

This study focuses on the stabilization of the DC bus using fast-responding power system components, e.g., batteries, to compensate for imbalances between load and generation dispatch. Considering an all-electric SPS with ESSs and FCs, as shown in Fig. 3.1 this is required due to low transient capabilities of the FCs. The generation dispatch is an output from the energy management layer, giving set-points to the main power supplies to meet

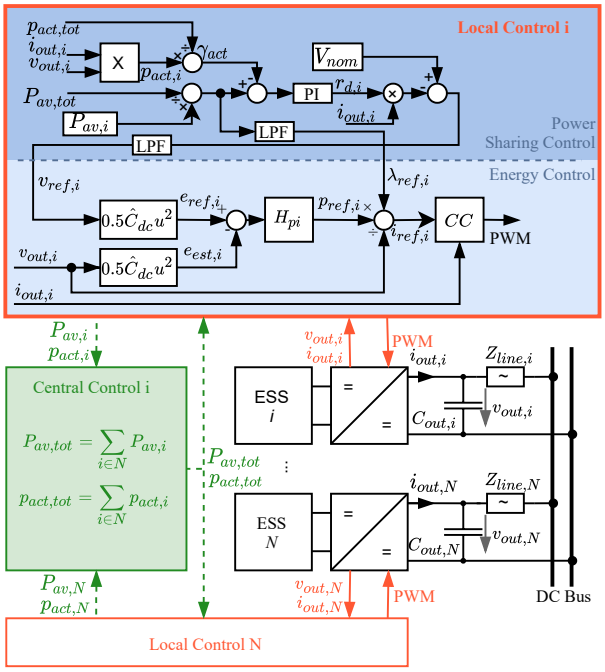


Figure 3.9: Control and communication architecture for parallel control of multiple power sources

the estimated load, and to ESSs for state-of-charge (SoC) management additional support. The energy management and SoC management are out of scope for this study, since their time-frame is considerably slower than the voltage stabilization and restoration, and in a hierarchical control architecture, each layer may be addressed individually. However, important for the method presented in Section 3.5.1, is that the available power values $P_{\text{av},i}$, $P_{\text{av,tot}}$, $p_{\text{act},i}$, and $p_{\text{act,tot}}$ only account for available and supplied power to compensate for power imbalances. Otherwise, the energy management set-points would interfere with the voltage stabilization and vice-versa.

3.6 Results

For validation of the proposed control methods, a hardware-in-the-loop (HiL) simulation environment is used. This section introduces the HiL test setup, describes the deployment of controllers and plant model and discusses the results of various test-cases for a single-converter and parallel control setups.

3.6.1 HiL Testbed

The HiL testbed used for the investigations is shown in Fig. 3.10. The plant model, comprised of energy source(s), power converter(s), DC distribution system, and loads, is implemented in a Plexim RT Box CE [209], a dedicated real-time simulation platform for power electronics systems. The digital control is deployed on the STM32 Nucleo-G474RE I/O Board [210],

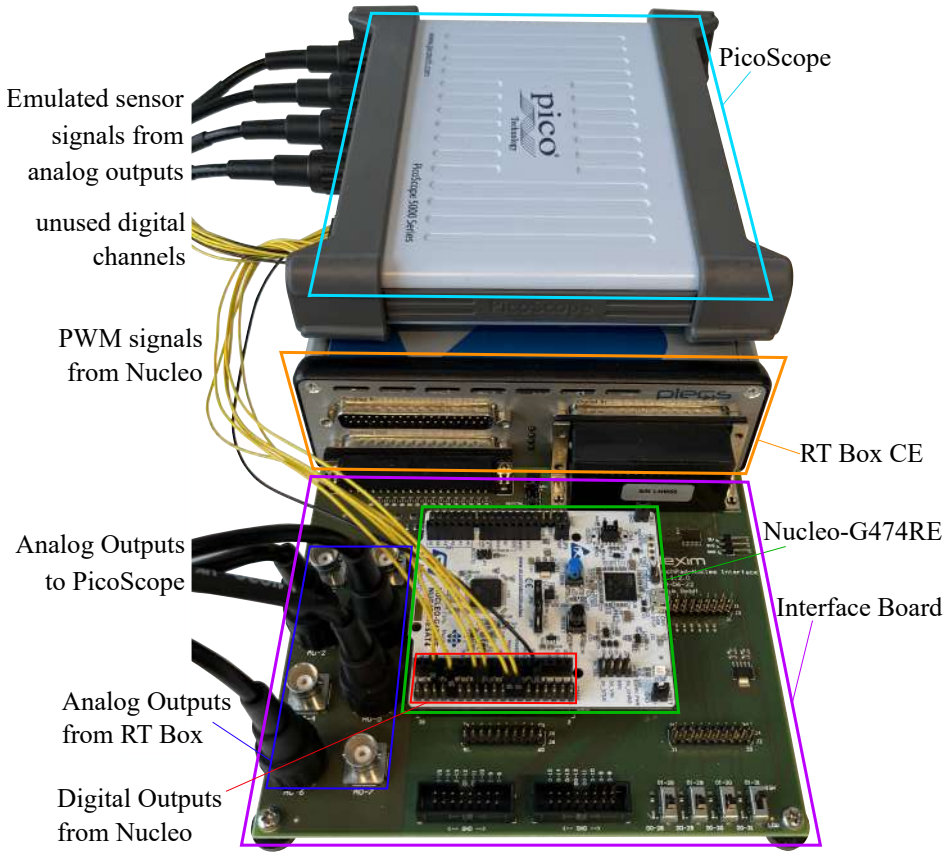


Figure 3.10: HiL simulation test setup consisting of Plexim RT Box CE real-time target machine, STM32 Nucleo-G474RE I/O Board, a dedicated interface board, and PicoScope oscilloscope for measurement logging.

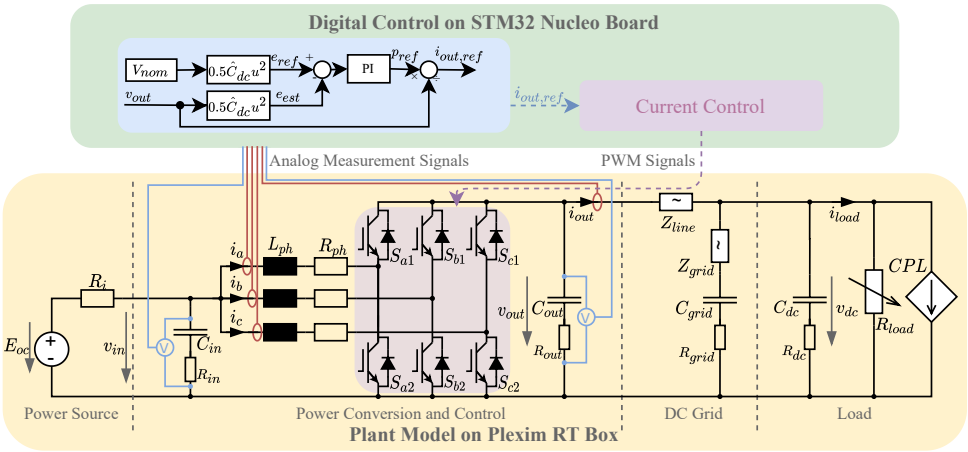


Figure 3.11: Plant model and digital control implementation for HiL simulation of single power source connected to DC grid via three-phase interleaved converter feeding resistive and constant power loads.

which is able to capture the emulated sensor signals from the RT Box and generate pulse-width modulation (PWM) signals for the actuation of the virtual power switches in the plant model. Both the plant model as well as the digital control are implemented in PLECS, using available block-sets for the RT Box and STM32 Nucleo board to handle inputs and outputs. The analog and PWM signals are measured directly on the I/O board pins via a PicoScope oscilloscope [211].

3.6.2 Single Converter

In a first step, the performance of the proposed controllers is tested in a single converter topology, as shown in Fig. 3.11. For this purpose, a power source is connected to the DC system via a three-phase interleaved DC-DC converter, whose output current i_{out} is to be controlled to stabilize the DC bus voltage v_{dc}. The power converter is connected to the DC grid via a line impedance Z_{line}. The capacitances of the remaining grid components, which in this case are not participating in the voltage stabilization, are modeled as an aggregated capacitance C_{grid} series-connected with an equivalent impedance Z_{grid}. The system loads are modeled as an aggregation of resistive loads R_{load} and power controlled loads CPL. These are connected to a capacitance C_{dc} which is the reference point for the DC bus voltage v_{dc}.

An output filter capacitance C_{out} is attached to the converter output to reduce its voltage ripple and, similarly, an input capacitance is connected on the source-side. The voltages v_{out} and v_{in} over the respective output and input terminals, are measured and captured by the digital control. In addition, the total output current i_{out}, as well as the three phase currents are measured. The parameters for this test setup are listed in Table 3.1.

The digital control is comprised of a voltage or energy control loop and a current control loop, which receives a current reference $i_{\text{out,ref}}$ from the former. The current control translates this into references for the inductor currents, which are realized as three individual PI-controllers with anti-windup via back propagation. The PWM generation of the three

phase legs is shifted symmetrically such that the current ripple at the output is minimized.

Step Response

For the operation of the power system, it is crucial to ensure that the DC bus voltage stays within its required limits. A critical case is the possibility of an undervoltage due to a sudden load step or a loss of generation. Due to its limited size, compared to terrestrial power systems, the loss of a power generation system can account for a significant share of the total installed power. In the reference design shown in Fig. 3.1, 50 % of the FC systems can be disconnected instantaneously due to a single fault. To test the voltage stabilization and restoration via the proposed control scheme, we test the system response to an application of a load step as a fraction of the total installed FC power, mimicking the disturbance occurring due to a severe loss of generation while operating at full power. Fig. 3.12 shows the voltage stabilization after load steps of 650 kW and 1300 kW, amounting to half and full load power, for voltage and energy based droop control schemes without voltage restoration. The controllers are tuned such that the voltage droop controller yields a 10 % voltage deviation at half load, and the energy droop is tuned to match the control bandwidth. Results show that the energy-based droop, when tuned for the same control bandwidth, achieves a lower voltage drop due to its non-linear characteristics. The relative difference between the two control schemes, increases progressively with the magnitude of the load.

Fig. 3.13 shows the results for the same test case with dual loop controllers to restore the voltage. As before, a difference of the voltage stabilization speed and voltage sag becomes clear when we consider power loads. With an increase in load step magnitude, the voltage sag of the conventional controller becomes progressively larger while the energy-based scheme keeps the voltage drop roughly proportional to the load magnitude.

Frequency Response

Apart from ensuring the maintenance of the bus voltage within critical limits, it is key to evaluate the controller's stability and its overall disturbance rejection capabilities. To this end, we analyze the open-loop output impedance of the controller by applying a sinusoidal voltage disturbance to the DC bus voltage v_{dc} and measuring the output current as a reaction to the voltage variation. Fig. 3.14 show the impedance of the four control schemes, computed as $-\frac{\Delta v_{\mathrm{dc}}}{i_{\mathrm{out}}}$. The region below the target control bandwidth shows an increased impedance of the energy-based controller, compared to the conventional voltage-droop, meaning that a lower output current is supplied by the power converter. The real part of the impedance is positive over the tested frequency interval and voltage magnitude, meaning that the converter is passive in this test case and no shortage of stability has been observed for either control approach.

In addition, we test the closed-loop frequency response of the bus voltage when applying a sinusoidal power controlled load to the system. The resulting bode plot of the disturbance rejection is displayed in Fig. 3.15. We see that the amplification is limited for all controllers and the dual loop schemes peak around the implemented control bandwidth. As expected, the voltage-based controller has a slightly elevated gain in the high-amplification region, which explains the increased voltage sag observed after a load step.

Table 3.1: Plant model and control parameters for HiL simulation

Parameter	Description	Value
V_{nom}	Nominal DC-link voltage	700 V
E_{oc}	Voltage source	400 V
L_{ph}	Phase inductance	500 µH
C_{in}	Input capacitance	10 mF
C_{out}	Output capacitance	20 mF
C_{dc}	DC link capacitance	20 mF
C_{grid}	Remaining grid capacitance	40 mF
Z_{line}	Line impedance single unit	63.9 µΩ, 3.2 µH
$Z_{\text{line,A}}$	Line impedance to unit A	63.9 µΩ, 3.2 µH
$Z_{\text{line,B}}$	Line impedance to unit B	319.5 µΩ, 16 µH
Z_{grid}	Line impedance to remaining grid	31.9 µΩ, 1.6 µH
R_{ph}	Phase resistance	0.5 µΩ
R_{i}	Power source resistance	10 mΩ
R_{in}	ESR of C_{in}	15 mΩ
R_{out}	ESR of C_{out}	15 mΩ
R_{dc}	ESR of C_{dc}	15 mΩ
R_{grid}	ESR of C_{grid}	7.5 mΩ
$P_{\text{load,max}}$	Maximum CPL load	1300 kW
$R_{\text{load,full}}$	Resistive load at full power	376.9 mΩ
$P_{\text{av,A}}$	Available power unit A	650 kW
$P_{\text{av,B}}$	Available power unit B	325 kW
f_{sim}	Sampling rate of RT Box	250 kHz
f_{sw}	Switching frequency	10 kHz
ω_{cc}	Current control bandwidth	1000 rad/s
ω_{vc}	Voltage control bandwidth	100 rad/s
$k_{\text{p}\gamma,i}$	γ-control proportional gain	$-\frac{2500}{P_{\text{av},i}}$
$k_{\text{i}\gamma,i}$	γ-control integral gain	$-\frac{25000}{P_{\text{av},i}}$
$R_{\text{fb},i}$	Droop gain in fallback mode	$\frac{1500}{P_{\text{av},i}}$

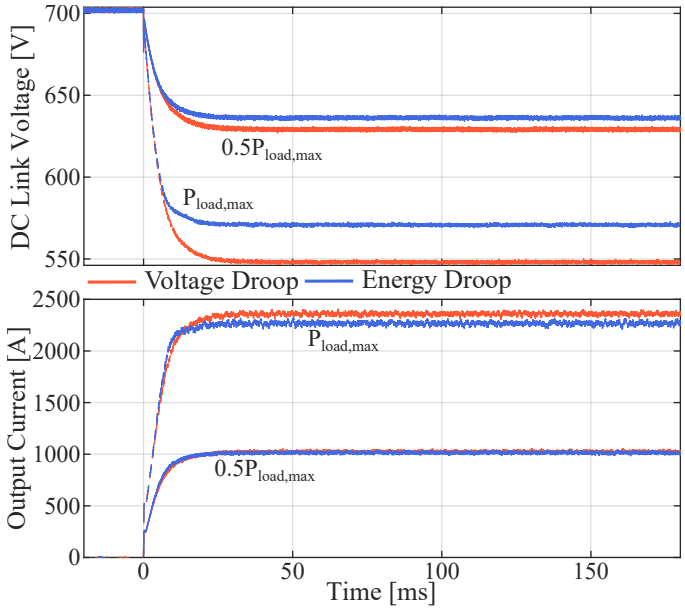


Figure 3.12: Voltage and energy droop with power load

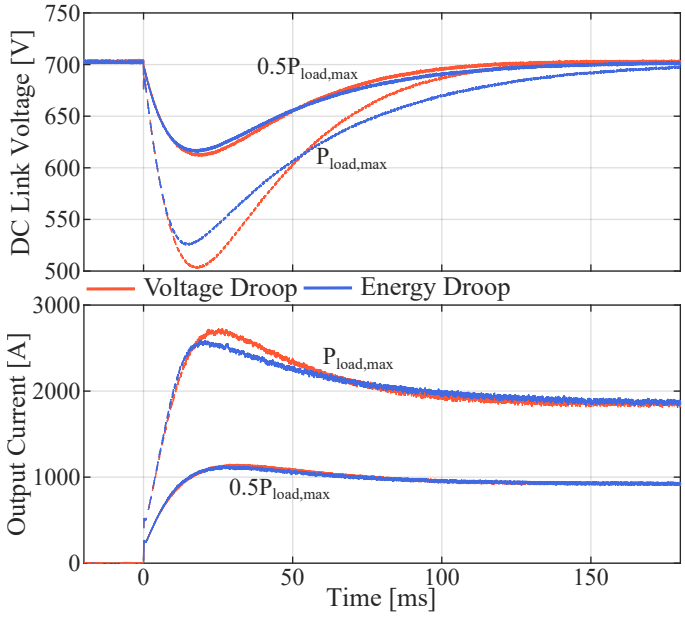


Figure 3.13: Voltage and energy dual loop control with power load

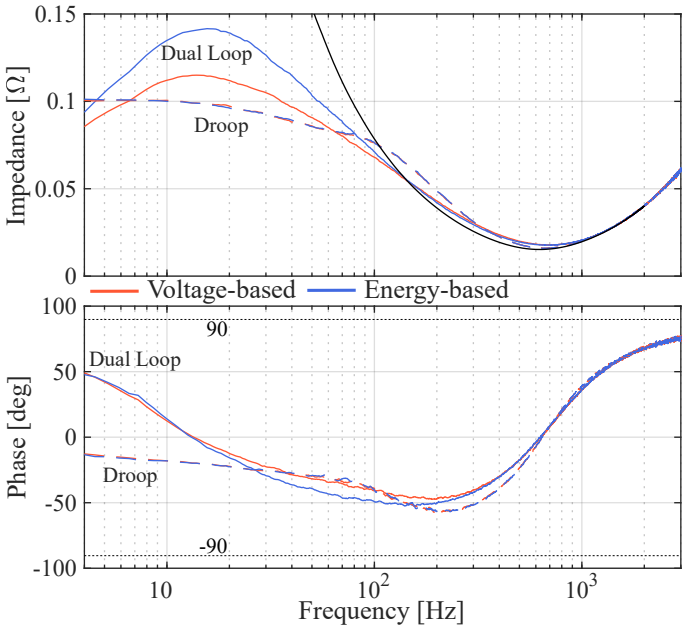


Figure 3.14: Observed controller output impedance at DC bus in HiL simulation via injection of voltage error (v_{dc}/i_{out})

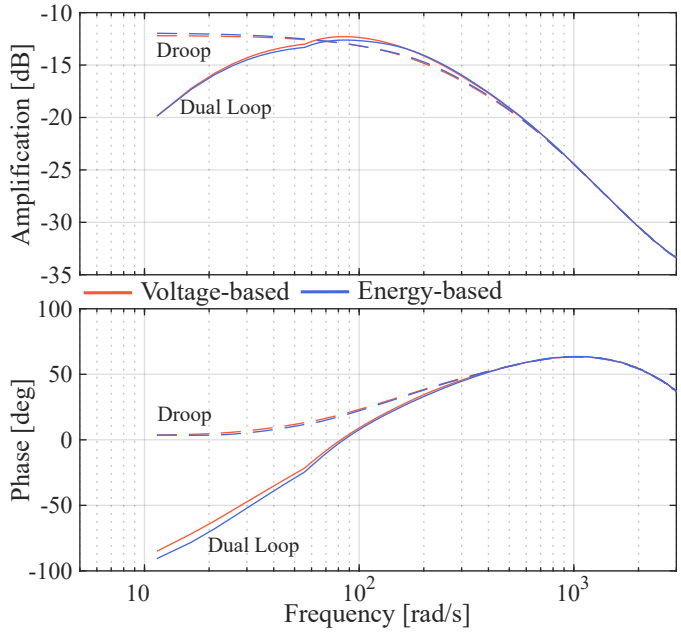


Figure 3.15: Observed controller disturbance rejection in HiL simulation via injection of oscillating load power (amplification in $[V^2/W]$)

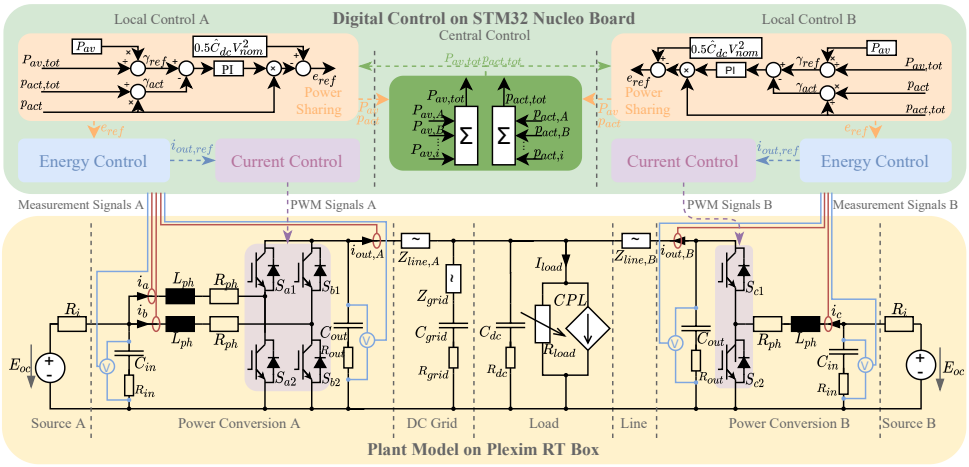


Figure 3.16: Plant model and digital control for HiL simulation of parallel power sources connected to DC grid with differently rated converters feeding resistive and constant power loads.

3.6.3 Parallel Control

The parallel control of multiple DC-DC converters is tested via a different plant model. Fig. 3.16 shows the HiL simulation test setup with two differently rated sources and power converters feeding the DC system. Power source A is interfaced via a two-phase interleaved converter, while power source B, rated at half the power of source A, is connected via a single-phase synchronous converter. As for the previous case, the parameters for this test setup are listed in Table 3.1. The goal is to ensure that the overall voltage stabilization is achieved with the same quality as with a single converter while keeping the power sharing between the sources at the desired ratio.

Each converter has a local controller deployed on the STM32 Nucleo board, which have only access to the measurements belonging to their respective emulated hardware. In addition, a central control unit is implemented in the digital control, which receives information signals from the local controllers and periodically broadcasts information accessible to all local units.

Load Step

The total system response the load is intended to be independent of the number of stabilizing power supplies, achieved by introducing the power sharing gain into the control loop, as shown in Fig. 3.9. To test this, the power system is subjected to a load step of 975 kW, equaling total power rating of power supplies A and B. The resulting output currents and DC bus voltage in this scenario are shown in Fig. 3.17. It can be seen that the voltage is restored within the same time frame as in the single-converter scenario. This shows that multiple parallel converters are able to stabilize and restore the voltage in the same manner as a single converter could.

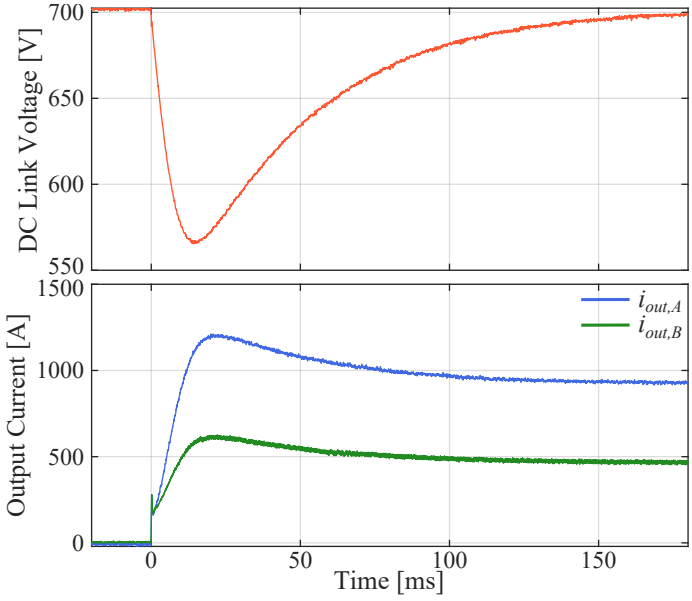


Figure 3.17: Voltage stabilization after load step with two parallel converters

Power Sharing

Each local controller has only its local output voltage $v_{\text{out},i}$ available. Furthermore, $Z_{\text{line,B}}$ is set to five times $Z_{\text{line,B}}$. Hence, even in steady-state operation, minor differences in measurements and voltage drops over the line will results in imbalances in power-sharing. The accuracy of the power sharing control described in Section 3.5.1 is tested by holding the load from the previous test case at a constant level for 30 s, and observing the ratio of output currents from power supplies A and B. The resulting measurements of currents for the parallel control without power sharing control and with power sharing control are shown in Fig. 3.18. The results show that, without intervention, the output currents of parallel converters diverge from the desired setpoint and already after less than a minute, the power sharing ratio has changed significantly (here: ca. 1.2:1 instead of the desired 2:1 after 30 s). However, including the central controller for power sharing control, the currents of both controllers are quickly stabilized at the desired setpoint. Here, this means a current ratio of two-to-one between units A and B.

Fault Considerations

During the operation of the SPS, a fault can occur at any given time, affecting the ideal power sharing among parallel power supplies. The power sharing control is intended to adapt to such changes by modifying the local power sharing gains. To demonstrate this, we consider a fault in power supply A that leads to a reduction of its available power by 50 %. The currents of the parallel power supplies before and after the degradation of unit A are shown in Fig. 3.19. As intended, before the fault ($t < 0\,\text{s}$), unit A is carrying twice the current of unit B, matching the ratio of their available power. After the fault ($t > 0\,\text{s}$), the power availability of both units is equal. Hence, the currents converge to the new, desired

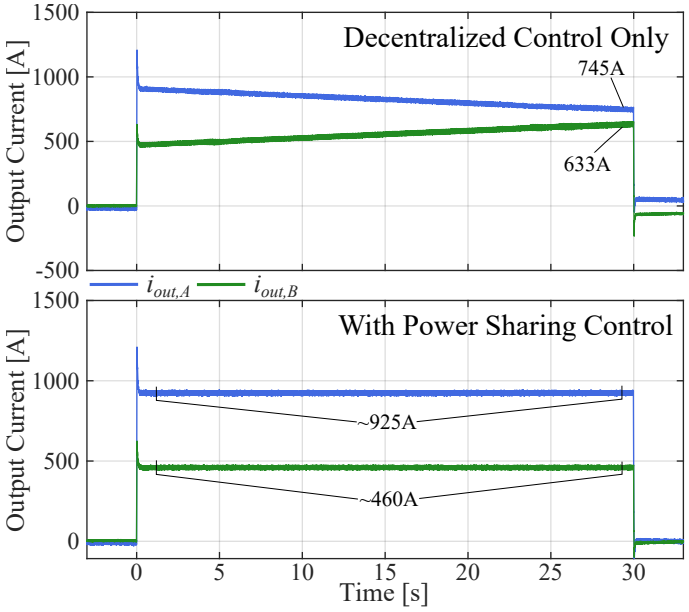


Figure 3.18: Power sharing between two parallel converters without and with adaptive power sharing loop

power sharing ratio, equally divided among both units. Following the same concept, the power sharing control can also adapt to deliberate variations of the available power of each units, e.g., arising from an optimized allocation of power reserve from a high-level controller.

The transition to fallback mode, as described in Section 3.5.2, is displayed in Fig. 3.20. At time $t = 0\,\text{s}$, a load step occurs with the original power sharing control still intact. At $t = 1\,\text{s}$, the communication fails and both units switch to fallback mode, employing a fixed droop constant. As a result, the bus voltage is reduced, requiring both units to increase their currents to deliver the power demand. However, due to the comparably low droop gains, as

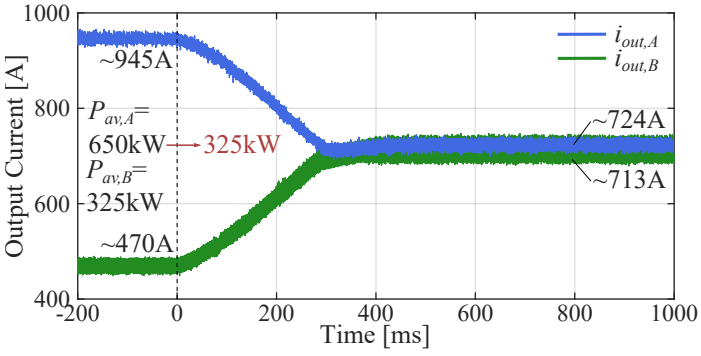


Figure 3.19: Adaptive power sharing between parallel converters during change of available power

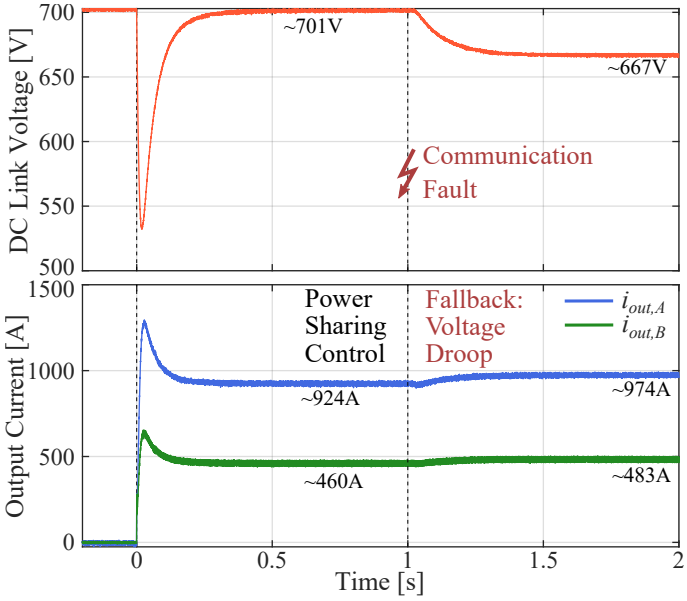


Figure 3.20: Current outputs of parallel converters before and after fallback mode due to communication failure

opposed to the adaptive control regime, the power sharing ratio is still close to the desired value of two-to-one between units A and B.

3.7 Conclusions

The decentralized voltage control for DC systems is a specific challenge for shipboard applications due to minimal line impedances and highly fluctuating CPLs, setting it apart from terrestrial DC microgrids, as well as DC links in automotive applications. Voltage-based droop as the state-of-the-art solution for decentralized power sharing is challenged due to the negative incremental resistance of CPLs, resulting in low damping and possibly voltage instability at high load steps. This study proposes a transformation of the voltage droop to an energy-based control scheme, eliminating the non-linear relationship between the power load and the controlled variable, where a power reference replaces the current reference of the state-of-the-art approach. HiL test results highlight the energy-based controller's improved performance in stabilizing the bus voltage even at high load steps, and its accurate voltage restoration according to the specified bandwidth, while conventional voltage-based control leads to increased voltage sags due to the low damping with CPLs. Assuming a fixed current controller of an off-the-shelf power converter, this enables fast restoration of the DC bus voltage with minimal deviations during transients. Hence, the proposed energy-based scheme serves as a crucial element for securing the power availability in decentralized systems with critical loads and a network with low capacitances and low line impedances. An adaptive power sharing loop lets parallel power supplies accurately track their desired power sharing ratio without compromising the control speed. This yields a stable and flexible voltage control, suitable for the implementation in modular

power systems where number and rating of power supply units are variable.
Future work will see the proposed method embedded into complete hierarchical control schemes to investigate its interaction with energy and power management strategies. The flexibility of the proposed method is very suitable to interact with optimal power and reserve power allocations from a higher-level controller. Additionally, the proposed control design can further be fine-tuned and optimized with attention to application-specific performance criteria. Whereas this study focuses on voltage stabilization and regulation using an energy-based control scheme, the next step should expand the focus to include optimized power sharing, and battery SoC management, leveraging the low-bandwidth communication links in the system.

4

Coordinated Control for Fuel Cell-Battery Power Systems

The previous chapter has shown how the voltage stabilization using fast-acting sources interfaced with DC-DC converters can look like. In the scope of my research, this is applicable for the batteries. However, the ships I am investigating also feature fuel cells, which have vastly different characteristics. In this chapter I am staying on the coordinated control layer, looking into the interaction between these two types of components. Whereas the voltage stabilization shown in the previous chapter lays the foundation, it is not sufficient yet to run the power system over the course of a mission. With a fuel cell-battery system, we need to find an efficient power sharing strategy, both under static and dynamic loads, and manage the charge of batteries. The work I present in this chapter does exactly that, thereby providing an applicable strategy for the power system control with multiple fuel cells and batteries in a DC shipboard power system.

"A man's emotions are what define him,
and control is the hallmark of true strength.
To lack feeling is to be dead,
but to act on every feeling is to be a child."

— *Teft*, in *The Way of Kings*
by *Brandon Sanderson*

This chapter is published with minor modifications as *Virtual impedance-based frequency decoupling for modular fuel cell-battery DC shipboard power systems, in: Journal of Marine Engineering & Technology, 2025* [212]

4.1 Introduction

The design of modern shipboard power systems (SPSs) is driven by multiple factors, including technological advances, new regulations, as well as economic and environmental aspects [11]. A key development is the electrification of ships, away from conventional diesel-mechanic propulsion and towards a utilization of novel energy sources and energy storage systems (ESSs) [7]. The goal to decrease carbon emissions has increased interest in alternative energy carriers and converters, among which hydrogen fuel cells (FCs) are a promising option [12, 68].

In this context, DC distribution with power electronics interfaces is a fitting solution for the integration of multiple different energy supply and storage technologies [17]. This yields high controllability of power flows in the system [16]. The efficient coordination of all devices, based on their respective characteristics is key [10]. The system control must facilitate the balance between the fluctuating load and generation while keeping fuel consumption and degradation on the components at a minimum [59]. Especially the FCs' lifetime is affected by their operation, which ideally is at low current gradients within its efficient output range [6].

DC distribution and power converters facilitate an easy expansion and reconfiguration of the power system topology, promoting a modular design with plug-and-play characteristics [213, 214]. This also requires the control system to be modular, and adapt to a reconfiguration, e.g. during regular operation, after a fault, or system retrofit.

To implement a scalable and reconfigurable control strategy, a decentralized architecture can be used [19, 69]. Doing so removes the need for an extensive communication architecture, enables the local implementation of main control functionalities, and reduces vulnerability to faults. The conventional decentralized method is virtual impedance-based droop control [59, 70], in DC systems implemented as voltage droop. Major drawbacks of droop control are a steady-state deviation from the set-point and imbalances in power-sharing. Further, standard voltage droop does not consider the time response of different sources, which is an important aspect in the control design with ESS [215]. It is desirable to decouple the main power source from the load using the ESS, so the main supply can operate at low power gradients and in an efficient operating point [7].

The literature on coordinated control and system stabilization for FC-battery SPS is dominated by centralized approaches, focusing the power split between a single FC system and ESS. This is realized, e.g., using PI-controllers as in [24, 84, 99] or via rule-based approaches as in [21, 24, 98, 180].

The above-mentioned load-frequency separation is also an important objective for the power split in hybrid ESS including both batteries and ultra-capacitors, as proposed by [45, 82, 216] which can be adapted for the control in FC-battery designs.

The proposed solutions, however, do not cover investigations of larger power systems with multiple FCs and batteries, or even a modular topology. A centralized controller computing all power references is not applicable here due to the overhead required for fast communication. For this reason, this study proposes a decentralized method for dynamic power sharing among multiple power sources with different time characteristics. The proposed scheme can adapt to the system reconfiguration in a plug-and-play manner.

This article expands on the previous work by [200], whose contributions are summarized as follows.

1. A virtual impedance-based approach with both capacitive and inductive elements to achieve a decentralized voltage stabilization with frequency decoupling in a FC-battery DC SPS.

2. An extension of local controllers by voltage restoration and state-of-charge (SoC) management functionalities via adaptation of the reference voltage.

3. Demonstration of the control strategy using real measurements at the example of a virtually retrofitted short-sea cargo vessel

In addition, this article delves into the concept of modularity and proposes an extension of the previously developed strategy by a low-bandwidth communication network to adapt the control parameters following a topology reconfiguration. For this purpose, how the local control parameters can be adapted after a component fault is investigated in order to maintain the desired power system dynamics. Furthermore, this work presents additional simulation results using high-frequency measurements from multiple operating scenarios. This chapter is organized as follows. A virtual retrofit and the modeling of a reference vessel with a FC-battery hybrid system is introduced in Section 4.2. Subsequently, the proposed decentralized control strategy for coordinating FCs and batteries is laid out in Section 4.3. Section 4.4 describes the simulation environment for numerical investigations and discusses the obtained results. The main conclusions are presented in section 4.5.

4.2 System Description

The work in this article focuses on all-electric ships with a hybrid energy system, as defined in [30], consisting of multiple main power supplies and ESSs. The emphasis is on FC-battery hybrid SPS, however, the method is applicable to alternative generation and storage technologies as well. This section describes the case study used in this work and introduces the models used for numerical investigations of the SPS.

4.2.1 Reference Vessel

The originally diesel-driven short-sea cargo vessel *Ankie* operating in the Baltic and North Seas serves as the reference vessel for the case study. The main specifications of the vessel are listed in Table 4.1. The original power system utilizes a main diesel engine, mechanically connected to a controllable pitch propeller. Additionally, a shaft generator is used as a power take-off to feed the bow thruster, auxiliary, and hotel loads via an electric AC distribution network. The system is equipped with an auxiliary engine that can be used for supplying the electric system while the main engine is turned off.

The reference vessel is equipped with measurement devices, continually logging the power generation of main and auxiliary engines, main consumers, as well as mechanical power working on the propulsion shaft. Figures 4.1 and 4.2 show the histograms of total power consumption and speed over ground for one month of continuous logging. Time spent at low power (<100 kW; 41.7 % of samples) and at low speed (<1 kn; 44.0 % of samples) are not shown in the figures. The measurements are available with a sampling time of 200 ms, which is considerably faster than typical ramp times of power generators and conventional propulsion systems in ships. Power profiles for different operation scenarios can be derived

Table 4.1: Specifications of reference vessel. Adapted from [217].

Parameter	Info
Type	General cargo ship
Length	90.0 m
Width	12.6 m
DWT	3638 t
Propulsion	Diesel-mechanic
Main Engine	Wärtsilä 9L20 (1.6 MW)

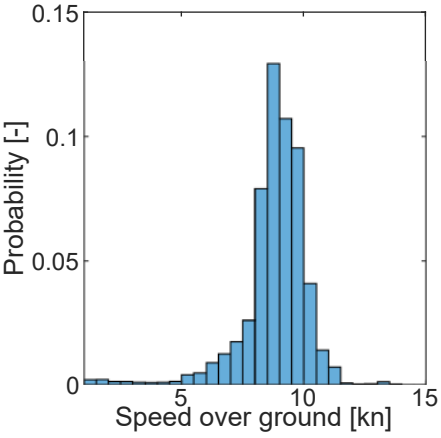


Figure 4.1: Histogram of speed over ground of reference vessel derived from continuous measurements over one month.

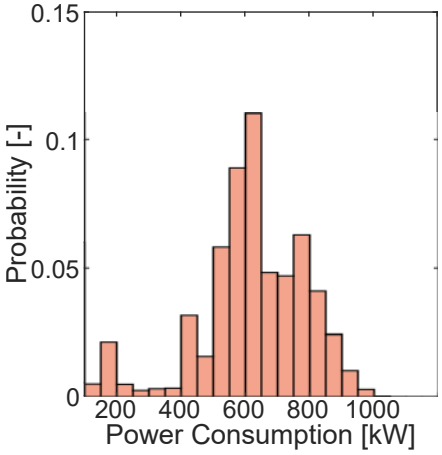


Figure 4.2: Histogram of power consumption of reference vessel derived from continuous measurements over one month.

from the measurements and used as input for the re-design and simulation of a retrofitted vessel.

4.2.2 Virtual Retrofit

Since the SPS of the original vessel does not match the scope of this work, a virtual retrofit of the power system was conducted to make it usable as a case study. In the virtual retrofit the vessel is fitted with an FC-battery hybrid system. Hence, all diesel-generators are removed from the system, and an electric-driven propeller replaces the mechanic propulsion. The resulting system, equipped with four FC and two battery systems in a dual-bus configuration, is shown in Fig. 4.3. This constellation creates a redundancy to compensate for a component or bus fault, and the number of FCs in the system gives operational flexibility. All power generation devices and loads are connected to the electric system, forming an integrated power system. DC distribution is used for the on-board grid, as it matches the outputs of FCs and batteries, among further advantages, such as increased efficiency [120] and operational flexibility [16]. Neglecting the enhanced operational capabilities of electric propulsion drives, it is assumed that the load requirements of the

Table 4.2: Parameters of retrofitted power system components.

Parameter	Description	Value
$P_{\mathrm{r,fc}}$	FC power rating	4x325 kW
E_{bat}	Battery energy capacity	2x225 kWh
$C_{\mathrm{bat,chg}}$	Battery max. charge C-rate	1.5
$C_{\mathrm{bat,dis}}$	Battery max. discharge C-rate	1.5
$P_{\mathrm{r,bat}}$	Battery power rating	2x337.5 kW
P_{em}	Prop. motor rating	2x600 kW

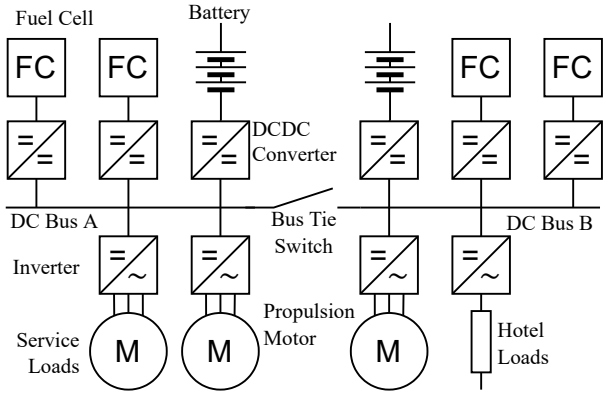


Figure 4.3: Topology of retrofitted hydrogen-based system with electric propulsion and DC distribution.

vessel remain the same as in the original topology.
The power and energy ratings of the components are listed in Table 4.2. The FC and battery ratings are based on a newly developed short-sea cargo vessel fueled by liquid hydrogen that has similar operational characteristics as the *Ankie*. The power rating of the batteries is sufficient such that the ESS can compensate for the fault of FC system while having surplus capacity for covering transient loads. Furthermore, the energy rating allows short-time strategic charging and load leveling to reduce the power gradients of the FCs.

4.2.3 Modeling

The focus of this work is the development of control strategies. Power system and component models are required to evaluate these strategies. Because the emphasis is on system-level control, simple dynamic models are implemented to build a simulation environment for the complete SPS. The following sections describe the approaches for modeling FCs, batteries, converters, and loads and how they interact with one another via the DC bus.

Proton exchange-membrane fuel cells

The FC models used in this work were implemented according to [205]. A beneficial feature of this model is that it can be parameterized using manufacturer data. Hence, the real

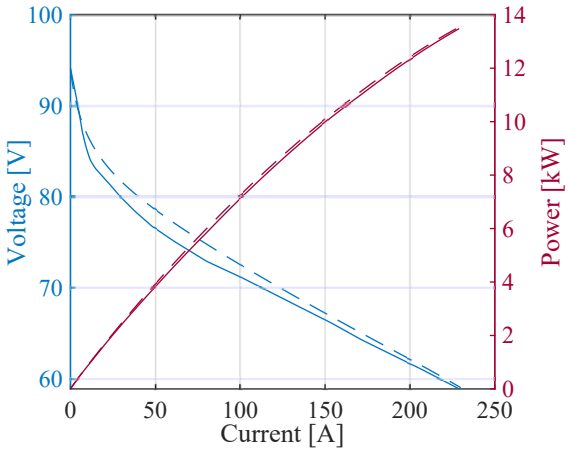


Figure 4.4: Polarization curve and power output of Nedstack FCS 13 XXL module, from data-sheet and simulation in steady-state.

components can be easily represented.
The FC systems investigated in this chapter are based on the Nedstack FCS 13 XXL, a proton-exchange membrane fuel cell (PEMFC) module with a maximum output power of 13.6 kW [218]. Figure 4.4 shows the polarization curves and power outputs of a single module from the manufacturer's data-sheet against the simulation results obtained using the described model in steady-state operation. The graph describes the relationship between the FC current $I_{\mathrm{fc,in}}$ and voltage V_{fc}, as indicated in Fig. 4.5 a). The mean absolute percentage error (MAPE) of the output voltage between the simulation and data-sheet is 1.6 %, which is sufficiently accurate for the purpose of this research. To achieve the targeted 325 kW per FC system in the SPS, 24 modules are stacked together.
The voltage efficiency and hydrogen consumption of the FC stack can be computed as defined and described in [219]. The calculation is based on a theoretically achievable cell potential derived from the lower heating value of hydrogen H_{lhv}, Faraday's constant F, and the number of elementary charges per H2-molecule $n = 2$. The efficiency of a FC is proportional to its cell potential V_{cell} and consequently also to the module's voltage V_{mod} with N_s series connected cells. Hence, the voltage efficiency is estimated as

$$\eta_{\mathrm{fc}} = \frac{V_{cell} nF}{H_{lhv}} = \frac{V_{mod} nF}{N_s H_{lhv}} \tag{4.1}$$

The hydrogen consumption per cell is proportional to its cell current I_{cell}. In extension, a FC module's hydrogen use $\dot{m}_{H2}$ in g/s is derived from the total current I_{mod}:

$$\dot{m}_{H2} = \frac{I_{cell} N_p N_s}{F} = \frac{I_{mod} N_s}{F} \tag{4.2}$$

where N_p is the number of parallel connected cell stacks. Several sources compute the voltage efficiency based on the higher heating value or Gibbs free energy instead [220].
It is important to note that the voltage efficiency is idealized and neglects crossover currents, oxygen starvation, and auxiliary power consumption. Hence, the computed efficiency at

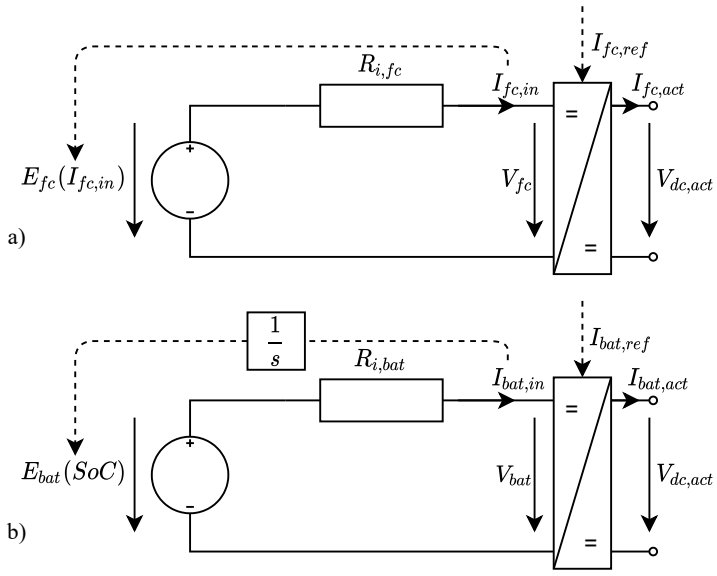


Figure 4.5: Equivalent circuit models of FC (a) and battery (b) including DC-DC converter and interface to the DC bus.

low currents is unrealistically high, whereas a real FC efficiency would drop when operated at low power. For this reason, the FC operation shall be limited to the linear Ohmic loss region, as suggested in [6], while operation close to zero output power is avoided.

Li-Ion batteries

For the batteries, a model of similarly low fidelity as that for the FCs was used, as reported in [204], shown here in Fig. 4.5 b). It is based on single cell modeling, and in this study, generic values for Li-ion battery cells, as reported in the source, are used. Opposed to the FC model, the voltage source E_{bat} is a function of the SoC, which is obtained via Coulomb counting. Multiple cells are connected in series and parallel to achieve the desired voltage, power, and energy levels of the battery packs.
The terminal voltage V_{bat} is obtained as

$$V_{\text{bat}} = E - R_i I_{\text{bat}} \tag{4.3}$$

DC-DC converters

A dynamic model of a DC-DC converter for maritime power systems is presented in [206]. It is an averaged model that describes the current dynamics while neglecting any losses in the system. Similarly, an averaged representation of a half-bridge is used in [73].
Conventionally, the converter is current-controlled using PI feedback control, as outlined in [46]. For DC SPSs, the current control bandwidth is typically in the range of 1000 Hz [207]. Whereas transient analysis requires a high-fidelity model of the power converters, the system-level simulation and investigation of voltage droop control allow the simplified

representation of the current control using a first-order low-pass filter [202]. The converter output current $I_{out,act}$ as a function of reference current $I_{out,ref}$ and current control time constant τ_{cc} is realized according to

$$I_{out,act} = \frac{1}{s\tau_{\text{cc}} + 1} I_{out,ref} \tag{4.4}$$

Consequently, the input-side current I_{in} as a function of $I_{out,act}$ as well as input and DC bus voltages V_{in} and $V_{\text{dc,act}}$, as indicated in Fig. 4.5 is computed as

$$I_{\text{in}} = \frac{V_{\text{dc,act}}}{V_{\text{in}}} I_{out,act} \tag{4.5}$$

Loads

All system loads are aggregated and represented as a power load P_{load} acting on the electric system. The load profile obtained from the measurements represents the actual consumed power and is modeled as an exogenous input disturbance. Assuming that all loads are tightly power-controlled, the current drawn by the loads I_{load} depends on the actual bus voltage $V_{\text{dc,act}}$. Accordingly, the current drawn by the loads is derived as

$$I_{\text{load}} = \frac{P_{\text{load}}}{V_{\text{dc,act}}} \tag{4.6}$$

DC distribution

The DC distribution system in a ship is characterized by short power lines with low impedance. Following the approach described in [10], the bus in DC SPS can be simplified as a lumped capacitor, neglecting the losses and inductances in the network. The DC-link capacity C_{dc} is the sum of the output capacitors of all N adjacent DC-DC converters $C_{out,i}$. Accordingly, the time derivative of the DC-link voltage $\dot{V}_{\text{dc,act}}$ can be computed as

$$\dot{V}_{\text{dc,act}} = \frac{1}{C_{\text{dc}}} \left(\sum_{i=1}^{N} I_{out,i} - I_{\text{load}} \right) \tag{4.7}$$

$$C_{\text{dc}} = \sum_{i=1}^{N} C_{out,i} \tag{4.8}$$

4.3 Power System Control

The control of the power system covers multiple functionalities, of which this work focuses on the coordinated control for stabilizing the DC bus voltage and managing the power flows between the different components.

On the generation side, each primary system, i.e., the FC systems and batteries, is interfaced to the bus via a DC-DC converter. Whereas the FCs can only provide positive current, the battery converter needs to be bi-directional to enable both discharging and charging. The converters are current-controlled, tracking a given reference value, as described in 4.2.3. Additionally, the local controllers ensure the operation of each device within its technical

limitations, e.g., voltage and current limits. The balance-of-plant and inner control loops of the FC battery systems are not explicitly considered here.
This section leads through the proposed implementation of local controllers for FCs and batteries. A more detailed elaboration can be found in [200]. This work additionally introduces a method for parameter adaptation after a topology change.

4.3.1 Coordinated Control

The coordinated control layer covers a multitude of functionalities. This work focuses on the voltage stabilization and restoration, battery SoC management, and power sharing among parallel devices. Additionally, this work explores the adaptation of control parameters to a reconfiguration of the power system topology.
For the control of the regarded SPS, FCs and batteries are required to match the power demand in dynamic conditions, stabilizing the DC bus voltage. The FCs benefit from operation within a specific power band and at low power gradients to limit their lifetime degradation and operate them at a high efficiency [221]. The batteries can provide high power gradients and thereby cover load fluctuations, but cycling at high power and high depth-of-discharge also degrades their lifetime.
In this section, first a centralized controller is described as a benchmark strategy. Subsequently, a decentralized control architecture is proposed, employing virtual impedances for frequency decoupling between FCs and batteries.

4.3.2 Centralized Control

Ideally, the current references for the coordination of FCs and batteries can be generated in a centralized controller. All required information about the system's states is available to the central controller so that it can compute a target for each component in real-time while accounting for their different characteristics. As a benchmark strategy, a PI feedback controller with a filter-based frequency decoupling is considered, similar to [82]. The PI feedback loop with gains k_p and k_i is employed for the voltage control, determining a total required current for bus stabilization and restoration $I_\mathrm{tot,ref}$ as a function of the voltage set-point error $V_\mathrm{dc,nom} - V_\mathrm{dc,act}$:

$$I_\mathrm{tot,ref} = (V_\mathrm{dc,nom} - V_\mathrm{dc,act})(k_\mathrm{p} + \frac{k_\mathrm{i}}{s}) \tag{4.9}$$

Low-frequency elements of this reference current are forwarded as a reference current for the FCs $I_\mathrm{fc,ref}$, while the remaining high-frequency parts of the reference $I_\mathrm{bat,ref}$ are to be covered by the batteries. The control strategy is illustrated in Fig. 4.6. For the frequency decoupling, the filter is tuned using the time constant τ_fd.

$$I_\mathrm{fc,ref} = \frac{I_\mathrm{tot,ref}}{s\tau_\mathrm{fd} + 1} \tag{4.10}$$

$$I_\mathrm{bat,ref} = I_\mathrm{tot,ref} - I_\mathrm{fc,ref} \tag{4.11}$$

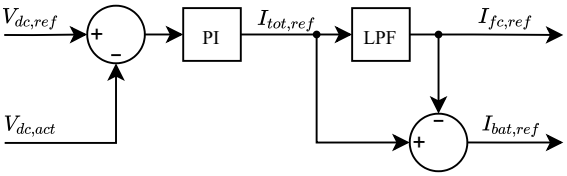


Figure 4.6: Centralized power sharing strategy with PI controller and low-pass filter.

4.3.3 Decentralized Control

Several issues make the implementation of real-time control in a centralized unit challenging. The acquisition of measurements and real-time distribution of reference signals to local controllers requires high-bandwidth communication, which can be costly, prone to faults, and introduce latencies. Hence, this work proposes the implementation of a decentralized architecture. No communication between local controllers is required for the real-time voltage stabilization and restoration. This provides a control strategy which can be scaled to a modular reconfiguration of the power system topology. In the following, virtual impedance-based droop is introduced as a method for voltage stabilization and frequency decoupling between the different sources. This method is subsequently extended by a voltage restoration and an SoC management functionality.

Virtual impedance-based droop

The state-of-the-art solution for decentralized voltage stabilization in DC power systems is voltage droop [49]. Whereas conventional, resistive droop control is appropriate for power sharing under steady-state conditions, additional capacitive or inductive droop elements can be used to include an additional time-response of the controllers [75, 76]. Whereas a capacitive droop controller serves as a high-pass filter, this work proposes an extension of droop schemes with an inductive element to create a low-pass filter. Such a droop controller is an appropriate tool for controlling the power output of power supplies with slow dynamic capabilities, such as FCs. Figure 4.7 shows the equivalent circuits describing the functioning principle of different droop schemes. The corresponding transfer functions of the DC link voltage deviation $\Delta V = V_{\mathrm{d,ref}} - V_{\mathrm{dc,act}}$ to the current reference are as follows:

$$\frac{I_{\mathrm{d,rc}}}{\Delta V} = \frac{sC_{\mathrm{d,rc}}}{sR_{\mathrm{d,rc}}C_{\mathrm{d,rc}} + 1} \tag{4.12}$$

$$\frac{I_{\mathrm{d,rl}}}{\Delta V} = \frac{1}{R_{\mathrm{d,rl}} + sL_{\mathrm{d,rl}}} \tag{4.13}$$

where $I_{d,x}$ is the computed reference current for the droop-controlled source. $R_{d,x}$, $C_{d,x}$, and $L_{d,x}$ describe the virtual resistance, capacitance and inductance, C_{dc} is the total dc bus capacity; $V_{\mathrm{d,ref}}$ and $V_{\mathrm{dc,act}}$ are the reference and actual dc bus voltages, respectively.

Voltage restoration

The aforementioned droop control schemes lead to a voltage drop on the main bus proportional to the delivered power [222]. To restore the voltage and maintain the modular

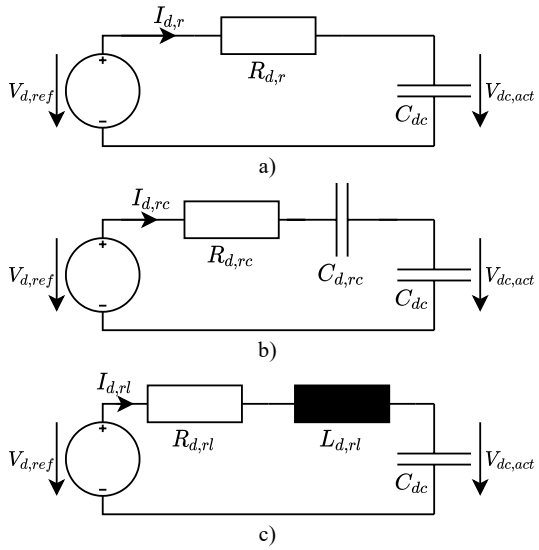


Figure 4.7: Equivalent circuit representations of decentralized droop controllers with a) resistive b) resistive-capacitive, and c) resistive-inductive virtual impedance.

power system design, the voltage reference $V_{\mathrm{d,ref}}$ in the local droop controllers is adapted based on an integral action on the set-point error and is computed as

$$V_{\mathrm{d,ref}} = V_{\mathrm{dc,nom}} + k_{\mathrm{v}} \int (V_{\mathrm{dc,nom}} - V_{\mathrm{dc,act}}) dt \tag{4.14}$$

where k_{v} is the integral coefficient for voltage regulation.

SoC management

Due to the ESSs' limited energy capacity, the SoC of each device needs to be maintained within specified limits, e.g. between 20 % and 80 % as in [223]. Additionally, different SoCs in parallel devices need to be balanced. The local battery controllers are further extended to include the SoC management in the decentralized control strategy. Each local battery controller is enhanced by an SoC-dependent term $V_{\mathrm{SoC,ref}}$, which manages the additional charge and discharge of the device. The reference voltage $V^{*}_{\mathrm{d,ref}}$ is manipulated for this purpose and is computed as

$$V^{*}_{\mathrm{d,ref}} = V_{\mathrm{d,ref}} + V_{\mathrm{SoC,ref}} \tag{4.15}$$

$$V_{\mathrm{SoC,ref}} = k_{\mathrm{SoC}} \int (\mathrm{SoC_{ref}} - \mathrm{SoC_{act}})^{\alpha} dt \tag{4.16}$$

where $\mathrm{SoC_{ref}}$ and $\mathrm{SoC_{act}}$ are the reference and actual SoC values and k_{SoC} is the integral coefficient of the SoC management strategy. An additional shape factor α describes the relationship between SoC deviation and charging current. Figure 4.8 shows the imposed discharge current for an ESS based on its SoC for different α. To ensure that the ESS

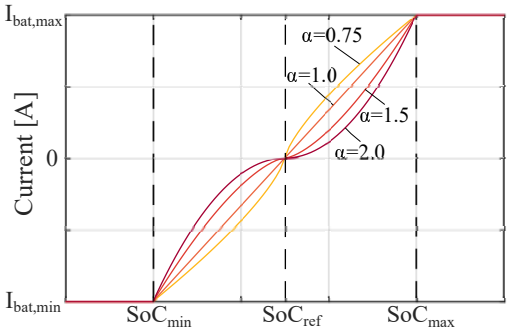


Figure 4.8: SoC-dependent charging current for each ESS for different shape factors α to track the reference value while avoiding over- and undercharging.

current reaches its respective maximum and minimum values when the SoC reaches its limits k_{SoC} is computed as following. Here, it is assumed that the reference SoC is centered around maximum and minimum SoC and that the batteries maximum charge and discharge currents are equal at $I_{\text{bat,max}}$:

$$k_{\text{SoC}} = -\frac{I_{\text{bat,max}}}{C_{\text{d,rc}}(\frac{SoC_{\text{max}} - SoC_{\text{min}}}{2})^{\alpha}} \tag{4.17}$$

Implementation

Figure 4.9 shows a graphical representation of the local controllers for the FCs and ESSs. Since no real-time communication takes place between the decentralized controllers, it is crucial to carefully tune all control parameters so that the overall system performance meets the desired requirements. To achieve the desired frequency separation, the resistive-inductive droop scheme from Eq. (4.13) is used to control each individual FC system's output current, while each ESS is controlled according to the resistive-capacitive droop Eq. (4.12).

For the consistent behavior of the power system under dynamic operation, a series of guidelines for tuning the control parameters are proposed. Following these guidelines ensures a coherent design of all local controllers:

- The total droop resistance of the main power supplies should equal the total droop resistance of the ESS and match a reference value $R_{\text{d,ref}}$ so that a consistent response of the power system in dynamic and steady-state operation is obtained.

- The total droop resistance should be selected such that the bandwidth of the DC bus voltage regulation is at least one order of magnitude slower than the current control of the DC-DC converters ($\tau_{\text{vc}} >> \tau_{\text{cc}}$).

- The droop resistances of the FC controllers should be inversely proportional to their rated power. The same approach shall be applied for the ESS.

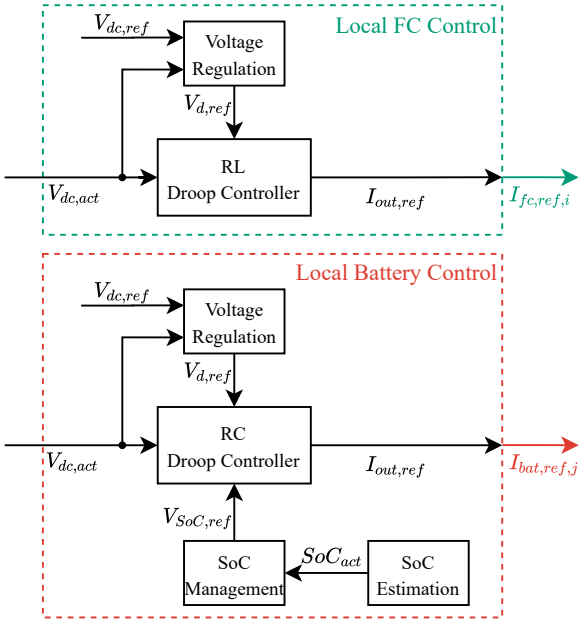


Figure 4.9: Synthesis of local controllers for FCs and batteries.

- In the proposed FC-hybrid system, the time constants of the RC and RL filters should be equal and match the desired frequency decoupling time constant τ_{fd}. This allows a smooth transition from batteries to FC as a power source.

- Reducing the time constant τ_{fd} will yield a higher dynamic capability, allowing the generation-side to cover higher load gradients, which would otherwise be inhibited by the limited power of the batteries. However, a higher time constant lowers the output gradients of the FCs, reducing their degradation.

4.3.4 Low-Bandwidth Communication and Reconfiguration

The proposed control strategy from [200] has a series of challenges due to the lack of information-sharing. The system's dynamics will differ from the designed characteristics once the topology changes, e.g., due to a component fault or an extension of the power system. It is furthermore inflexible towards a change in the topology. To mitigate this, this study proposes the extension of the decentralized strategy by a central controller and low-bandwidth communication and leveraging shared information for an adaptation of control parameters. It is important to note that the central controller is used only for slow information sharing, whereas all essential computations for coordinated control remain in the local controllers.

The response of each local controller is determined based on its virtual resistance and the time constant of the low- or high-pass filter constituted by the virtual impedance. The goal is for each local controller to adapt its parameters so that the total droop gain of the system

matches its target value $R_{\mathrm{d,ref}}$ independent of the system topology. Hence, the guidelines listed in section 4.3.3 should hold true even if the topology is reconfigured.
Each FC system and battery shares its available power rating, $P_{\mathrm{r,fc},i}$ and $P_{\mathrm{r,bat},j}$ respectively, via the communication network. Accordingly, the central controller can determine the total available FC power $P_{\mathrm{r,fc,tot}}$ and total available battery power $P_{\mathrm{r,bat,tot}}$ as

$$P_{\mathrm{r,fc,tot}} = \sum_{i \in N} P_{\mathrm{r,fc},i} \tag{4.18}$$

$$P_{\mathrm{r,bat,tot}} = \sum_{j \in M} P_{\mathrm{r,bat},j} \tag{4.19}$$

In case a component fails, is degraded, or the system is reconfigured, the effect of the altered topology is visible in a change of the total available power ratings. The central controller broadcasts $P_{\mathrm{r,fc,tot}}$, $P_{\mathrm{r,bat,tot}}$, and reference values for τ_{fd} and k_{v}, as well as $R_{\mathrm{d,ref}}$. Since a low-bandwidth communication is assumed here, and to avoid jumps in the parameters, the local controllers apply a low-pass filter with time constant 10 s on the received values. Each local controller is then able to compute its local virtual impedance parameters $R_{\mathrm{d,rl}}$ and $C_{\mathrm{d,rl}}$, or $R_{\mathrm{d,rc}}$ and $C_{\mathrm{d,rc}}$. The i-th FC computes its control parameters as

$$R_{\mathrm{d,rl}} = R_{\mathrm{d,ref}} \frac{P_{\mathrm{r,bat,tot}}}{P_{\mathrm{r,bat},j}} \tag{4.20}$$

$$L_{\mathrm{d,rl}} = \tau_{\mathrm{fd}} R_{\mathrm{d,rl}} \tag{4.21}$$

The j-th battery computes its control parameters as

$$R_{\mathrm{d,rc}} = R_{\mathrm{d,ref}} \frac{P_{\mathrm{r,bat,tot}}}{P_{\mathrm{r,bat},j}} \tag{4.22}$$

$$C_{\mathrm{d,rc}} = \frac{\tau_{\mathrm{fd}}}{R_{\mathrm{d,rc}}} \tag{4.23}$$

Additionally, it needs to be considered that the DC bus capacitance changes upon disconnection of a source, assuming that the switch is situated between the converters' output filter and the DC bus. As the total virtual droop $R_{\mathrm{d,ref}}$ is dimensioned to reach a specific control time constant for the voltage stabilization τ_{vc}, the total droop should be adjusted to achieve a consistent voltage control speed. Assuming that the central controller has an estimate of the total capacity in the bus $C_{\mathrm{dc,est}}$, the total droop is adapted as

$$R_{\mathrm{d,ref}} = \tau_{\mathrm{vc}} C_{\mathrm{dc,est}} \tag{4.24}$$

The information exchange between the central and local controllers in the power system is visualized in Fig. 4.10. Since no vital computation is being done in the central controller and all adaptations based on information broadcast is low-bandwidth, a failure of the communication network has no immediate effect on the voltage stability of the system.

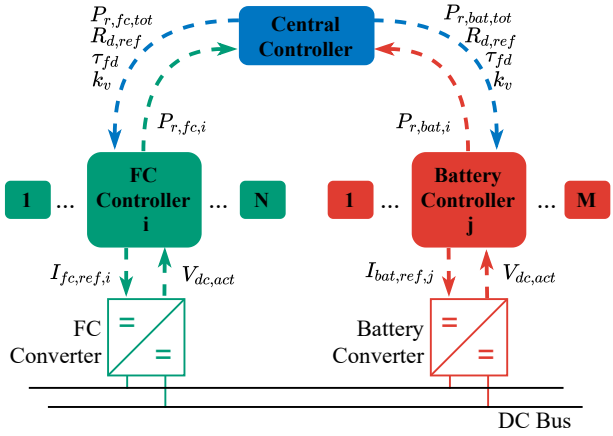


Figure 4.10: Control architecture of local FC and battery controllers and central controller communicating via low-bandwidth interface.

4.4 Numerical investigations

A power system model as outlined in section 4.2.3 is implemented in Matlab/Simulink to create a simulation environment where control strategies can be tested. This section describes the case study and system parameterization in more detail, introduces test scenarios for the control of the reference vessel and evaluates the numerical results obtained through the simulations. Table 4.3 provides an overview of system level parameters used throughout the simulations. The 700 V DC bus voltage stems from a reference design within the *SH2IPDRIVE* project [224] and falls within the low voltage DC range [17]. The current control time constant of 1 ms matches typical control bandwidths of 1000 Hz as mentioned in [207]. The voltage control bandwidth is chosen ten times slower to avoid interferences between the cascaded control loops. The output capacitances were estimated following the approach outlined in [225].

Table 4.3: System and control parameterization for numerical investigations.

Parameter	Description	Value
$V_{\mathrm{dc,nom}}$	Nominal DC bus voltage	700 V
$C_{\mathrm{out,fc}}$	FC converter output capacity	25 mF
$C_{\mathrm{out,bat}}$	Battery converter output capacity	25 mF
τ_{cc}	Current control time constant	1 ms
τ_{vc}	Voltage control time constant	10 ms
α	SoC shape factor	2.0 –
τ_{fd}	Frequency decoupling time constant	variable

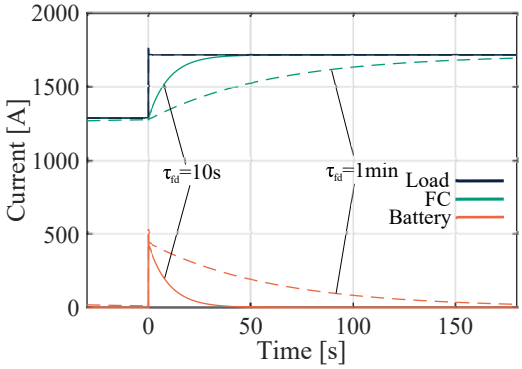


Figure 4.11: Total output current of FC and battery systems after a load step using the centralized PI control with low-pass filter (LPF) and time constants of 10 s(dashed) and 1 min(solid)

4.4.1 Centralized Control with Low-Pass Filter

As outlined in section 4.3.2, a centralized PI controller with low-pass filter is implemented as a benchmark. The PI gains are tuned via pole placement to match the desired voltage control bandwidth:

$$k_\mathrm{p} = C_\mathrm{dc}\,\tau_\mathrm{vc} \tag{4.25}$$

$$k_\mathrm{i} = \frac{k_\mathrm{p}^2}{4C_\mathrm{dc}} \tag{4.26}$$

Eq. (4.25) and (4.26) show that the feedback gains are dependent on the estimate of the total DC bus capacitance. The estimation may differ from the real value. An overestimation will lead to a more aggressive control action, and vice versa. This fact should be accounted for in the control design to ensure sufficient stability margins. The low-pass filter is parameterized with the frequency decoupling time constant as $\tau_\mathrm{LPF} = \tau_\mathrm{fd}$. The reference currents are distributed among parallel components of the same type proportional to their power rating. Initially, all FCs and batteries are rated equally and accordingly the current is shared equally among parallel components. The figures with results show the summed currents of all components of the same type.

In the first simulation, the step response of the power system was investigated. Measurements of the propulsive power, taken during a mission of the reference cargo vessel, show an average load of 900 kW during cruising. Taking this value as the starting point, the step to full propulsive power of 1200 kW was investigated, matching load current increase from 1286 A to 1714 A at 700 V. Two cases with $\tau_\mathrm{fd} = 10\,\mathrm{s}$ and 1 min were analyzed to compare the effects of different time constants. The resulting trajectories are displayed in Fig. 4.11. The FCs react to the load change according to the low-pass filter; therefore at $t = \tau_\mathrm{fd}$ the output current reaches 63.2 % of the step. The battery supplies the remaining difference between load and FC power, and additionally stabilizes the DC link voltage, which remains within 20 V of the nominal DC link voltage of 700 V.

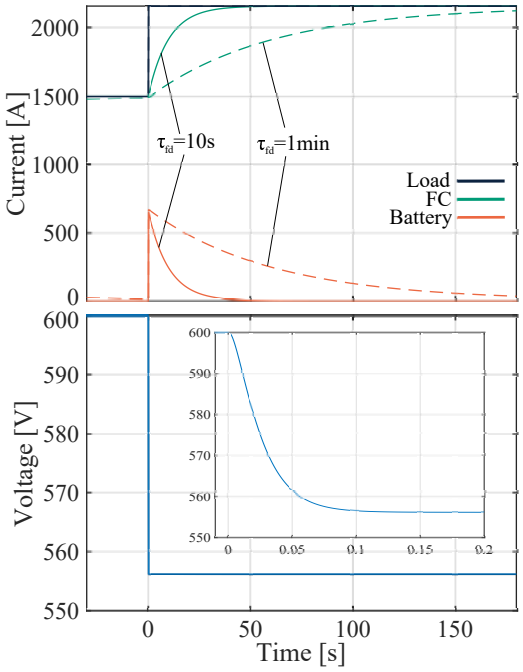


Figure 4.12: Load step response with decentralized strategy with τ_{fd}=10 s(dashed) and 1 min(solid) a) FC, battery and load currents, b) DC bus voltage

4.4.2 Decentralized Control Strategy

The proposed strategy aims to achieve the same performance as the central controller using a decentralized architecture. For this purpose, the total droop resistance was chosen to equal the inverse of the proportional factor of the PI controller in the benchmark strategy. Furthermore, the time constant for frequency decoupling τ_{fd} is adjusted by sizing the virtual inductances and capacitances such that $\tau_{\mathrm{fd}} = R_{\mathrm{d,rc}} C_{\mathrm{d,rc}} = L_{\mathrm{d,rl}} / R_{\mathrm{d,rl}}$.

In the first step, voltage regulation and SoC management are not implemented and the power system with the virtual impedance-based droop is subjected to the same load step as the benchmark strategy in section 4.4.1. The simulation results in Fig. 4.12 show that frequency decoupling is achieved as accurately as with the benchmark, matching the chosen τ_{fd}. Since the load before the step is non-zero, the bus voltage has already decreased to 600 V due to the absence of an integral action. The steady-state deviation further increases to 144 V at full load. The reduced DC bus voltage requires higher currents and, therefore, increases conduction losses. In this case, the voltage drop is beyond 10 %, which would be a typical lower voltage limit. Furthermore, the power quality can be insufficient for sensitive loads, and a sudden change in voltage is challenging for accurate current control in DC-DC converters.

In the next step, the same step response as before was simulated with the proposed strategy, including the voltage regulation described in section 4.3.3. The gain k_{v} in (4.14) was selected to match the integral action of the benchmark's PI controller:

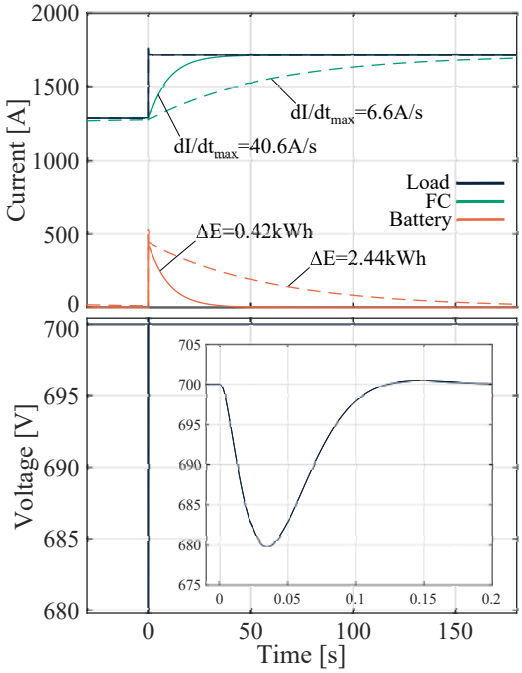


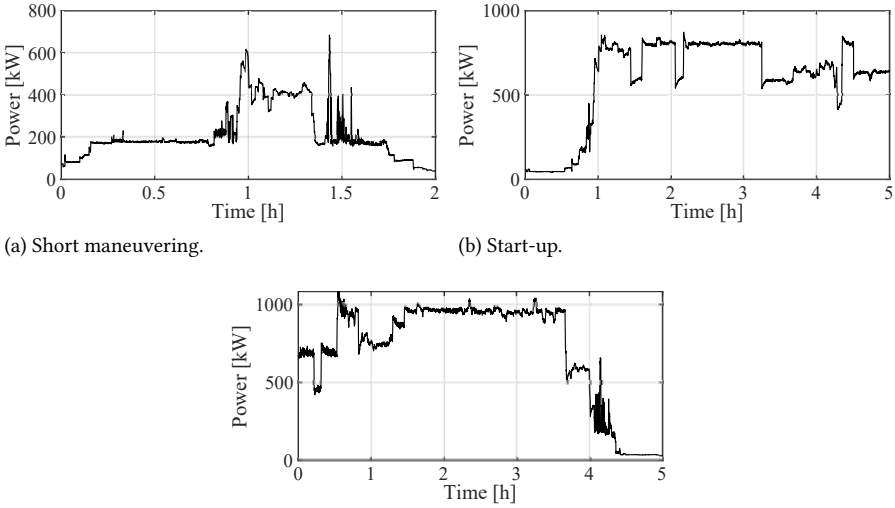
Figure 4.13: Load step response with decentralized strategy incl. voltage regulation with τ_{fd}=30 s(dashed) and 300 s(solid) a) FC, battery and load currents, b) DC bus voltage

$$k_{\mathrm{v}} = \frac{\tau_{\mathrm{vc}}}{4} \tag{4.27}$$

Note that the squared term present in the denominator in Eq. 4.26 is not present here, since the adjusted voltage $V_{\mathrm{d,ref}}$ is still passing through the droop controller. The step response obtained using this strategy is displayed in Fig. 4.13. The resulting curves of the FC and battery currents are equal to those of the benchmark, indicating that the same behavior of a centralized PI controller with a low-pass filter can be achieved in a decentralized architecture. Additionally, this method achieves accurate tracking of the nominal DC bus voltage. Initially, after the load step, an acceptable voltage drop of 20.1 V can be observed, and the steady-state deviation could be eliminated.
Furthermore, Fig. 4.13 shows the implications of changing the time constant τ_{fd}. With 1 min, a total of 2.44 kWh of battery charge is required to compensate for the difference between load and FC power, while the maximum current gradient of the FC systems is limited to 6.6 A/s. Reducing the time constant by a factor to 10 s proportionally reduced the required battery charge to 0.42 kWh. However, the current gradient of the FCs increased by the same factor to 40.6 A/s, leading to higher degradation. This comparison highlights the underlying trade-off between the required battery charge and dynamic operation of the FCs when selecting the time constant.

4.4.3 Mission Simulation

The application of the proposed control strategy in an SPS is demonstrated using parts of real mission profiles as inputs. The challenging operation periods of the vessel occur during maneuvering, start-up and shutdown sequences, or other situations demanding highly fluctuating loads. Three scenarios are selected for which power profiles of the real operation are available. The first scenario represents a relatively short maneuvering sequence of ca. 2 h, which covers high power gradients. The second scenario covers the start-up and maneuvering out of harbor sequence until cruising. The third scenario, in turn, is the shutdown from cruising into the harbor. The latter two cover ca. 5 h of operation each. Fig.4.14 shows the power demand over time for all three scenarios.
Three mission simulations were performed for each scenario with different time constants τ_{fd} of 10 s, 1 min, and 10 min. Because multiple control functionalities act on the power system, it is key to ensure that they do not interfere with each other. An increased time constant aims at smoothening the FCs' output power while requiring the batteries to provide more power and depth-of-discharge for achieving the load-generation-balance. The current and voltage control bandwidths are separated by tuning the control parameters to meet the values listed in Table 4.3. In the same manner, the slower control loops, i.e., the frequency decoupling and the SoC management, need to be separated to avoid them interfering with one another. The shape factor α was set to 2.0 so that the slope of the charging current around the target SoC was flat. Doing so ensures that the SoC management acts more slowly than the frequency decoupling.
Resulting current trajectories of total FC and battery power, as well as battery SoC over time, are shown in Figs. 4.15, 4.16, and 4.17, for the three scenarios respectively. The plots with the results are zoomed in on the time period where the highest load fluctuations occur. For the simulation, running at 1 ms steps, the measured values, sampled at 200 ms, were linearly interpolated.



(a) Short maneuvering.

(b) Start-up.

(c) Shut-down.

Figure 4.14: Exemplary power profiles obtained from measurements taken during the reference vessels' operation.

Table 4.4: Key values of simulation results with different frequency decoupling time constants for short maneuvering/start-up/shutdown profiles.

	Frequency decoupling time constant τ_{fd}		
Value	10 s	1 min	10 min
SoC_{min} [%]	49.7/49.7/49.5	48.4/47.6/47.8	42.1/32.3/33.0
SoC_{max} [%]	50.0/50.1/50.2	50.1/50.1/51.9	57.2/58.7/63.9
$P_{\mathrm{bat,min}}$ [kW]	-255/-221/-325	-212/-256/-319	-274/-471/-435
$P_{\mathrm{bat,max}}$ [kW]	232/159/252	387/287/262	320/468/409
$\lvert\dot{P}_{\mathrm{fc}}\rvert_{\mathrm{avg}}$ [W/s]	1083/1605/3148	731/1494/2929	693/1431/2841

Table 4.4 summarizes the key numbers from the simulations, including the batteries' SoC ranges, as well as maximum charge and discharge currents. Load cycling is reported to be detrimental to the health of PEMFC [226, 227]. In [67], a linear degradation factor for transient loads on the cell voltage decay was used. Hence, the average absolute value of the FC power gradient $|\dot{P_{\mathrm{fc}}}|_{\mathrm{avg}}$ is listed as a proxy for assessing the effect of transient FC operation on degradation. Given the FC output $P_{\mathrm{fc},n}$ and time at the n-th simulation step t_n, it is computed as

$$|\dot{P_{\mathrm{fc}}}|_{\mathrm{avg}} = \frac{1}{N}\sum_{n=1}^{N}\frac{|P_{\mathrm{fc},n} - P_{\mathrm{fc},n-1}|}{t_n - t_{n-1}} \tag{4.28}$$

The results show that the FC follows the load closely, and little power and energy are demanded from the batteries with a low time constant. However, a higher time constant

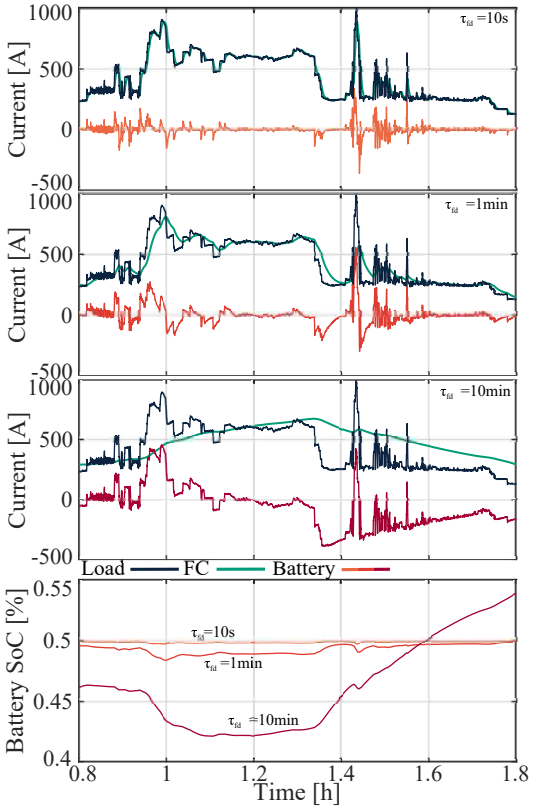


Figure 4.15: Power split between FCs and batteries and battery SoC during short maneuvering for different frequency decoupling time constants

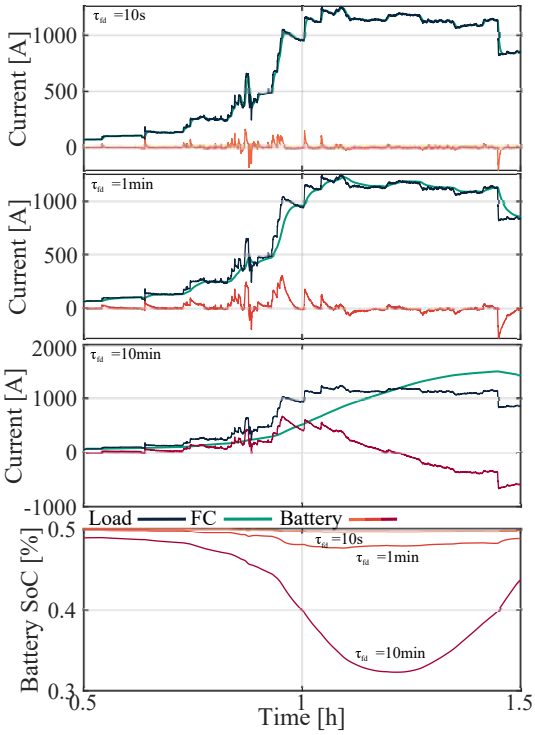


Figure 4.16: Power split between FCs and batteries and battery SoC start-up for different frequency decoupling time constants

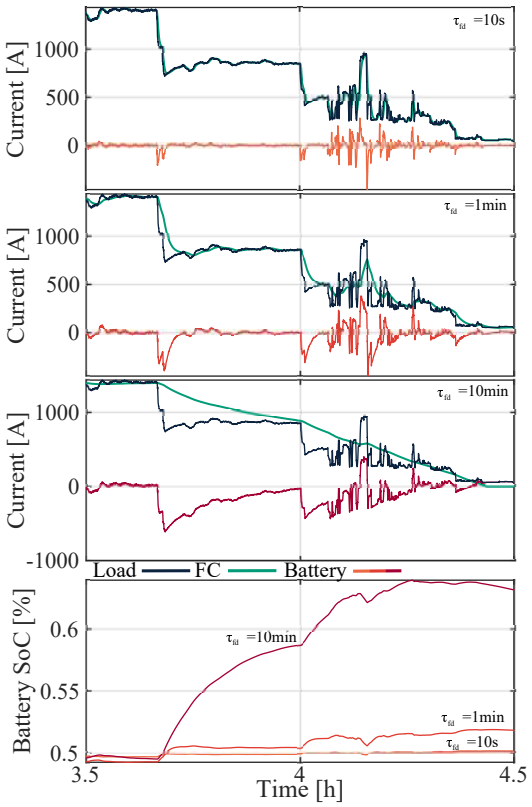


Figure 4.17: Power split between FCs and batteries and battery SoC during shutdown for different frequency decoupling time constants

Table 4.5: Asymmetric component ratings and control parameterization.

Parameter	Description	Value
$P_{\mathrm{r,fc,A}}$	Power rating FC A	325.0 kW
$P_{\mathrm{r,fc,B}}$	Power rating FC B	292.5 kW
$P_{\mathrm{r,fc,C}}$	Power rating FC C	260.0 kW
$P_{\mathrm{r,fc,D}}$	Power rating FC D	227.5 kW
$E_{\mathrm{bat,A}}$	Energy capacity battery A	300 kWh
$P_{\mathrm{r,bat,A}}$	Power rating battery A	450 kW
$E_{\mathrm{bat,B}}$	Energy Capacity battery A	150 kWh
$P_{\mathrm{r,bat,B}}$	Power rating battery B	225 kW
τ_{fd}	Frequency decoupling time constant	10 min

smoothens the power output of the FCs, reducing their power gradients and, consequently, their degradation. With a higher time constant, the SoC-limits are exploited to a higher degree, leading to a reduced transient operation of the FCs. During maneuvering (Fig. 4.15), the average FC power gradient is reduced by 32.5 % by increasing the time constant from 10 s to 1 min and even 36.0 % at 10 min. In the start-up (Fig. 4.16) and shut-down (Fig. 4.17) profiles, a minimum is reached when the FC power is monotonously increasing or decreasing, respectively. It is to be noted that this metric does not consider the rate-of-change of the FC but the absolute change in output power.
The increased ESS discharge depth at higher time constants negatively influences the battery lifetime. The results underscore the importance of selecting the time constant to trade off the discharge depth of the batteries and the transient loading of the FCs. The simulated operation range of the batteries also shows that they may be sized significantly smaller when a small time constant is chosen to reduce capital expenditure.

4.4.4 Droop Parameter Adaptation

One key goal of the decentralized architecture is its adaptability to configuration changes and in this work the low bandwidth communication is leveraged to realize said adaptation. Accordingly, components with different ratings and characteristics should behave differently. To highlight this, the characteristics of the FC systems are changed to emulate aged components, which is done by shifting their polarization curves down. Thereby their output voltage, and in turn their output power at a given current, is decreased. The voltage of FCs A, B, C and D are reduced by 0 %, 10 %, 20 % and 30 %, respectively. In addition, the batteries' capacities are changed to different ratings, and their initial SoCs are set to 40 % for battery A and 60 % for battery B. Accordingly, each component has an individual power rating, which influences the droop parameter calculation described in Section 4.3.4. Table 4.5 lists the parameters of the altered configuration. Non-listed parameters remain unchanged from the previous Section.
The power system is simulated with the short maneuvering power profile in Fig. 4.14a) to demonstrate the effectiveness of the proposed control architecture. The resulting output currents of all components and battery SoC are shown in Fig. 4.18. Generally, the configuration changes lead, as expected, to an unequal current sharing among both the FCs as well

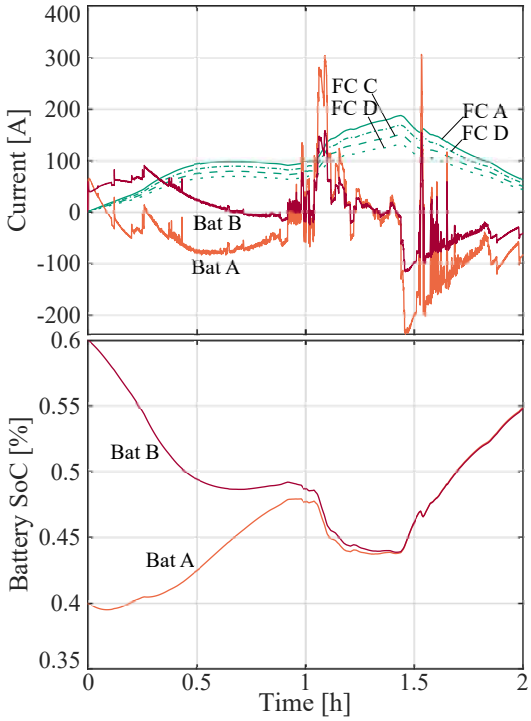


Figure 4.18: Power sharing and battery charge during mission simulation of short maneuvering with asymmetric component ratings and different initial SoC

as among the batteries. For both type of components, the current sharing is proportional to their power rating such that the FCs with higher maximum power carry higher currents. Analogously, battery A provides twice the current as battery B for voltage stabilization, due to its doubled capacity and power rating. Additionally, it can be observed, that the SoC management strategy of both batteries lets both charges converge over time.

4.4.5 Reconfiguration After Fault

The reconfiguration of the power system control is investigated by emulating component faults. As described in Section 4.3.4, the fault itself has three immediate effects on the coordinated control. First, the power output of the disconnected component drops to zero, creating a power imbalance which needs to be compensated. Second, the total DC bus capacity is reduced by the output capacity of the disconnected converter. Third, the total virtual resistance of the control strategy is increased since one local controller is missing. Thus, the time-response of the voltage stabilization is slowed down.
Here, two successive faults of a battery system and a FC system are emulated. The disconnection of an ESS leads to an increased total virtual resistance of the high frequency power supplies, while the low-frequency resistance is affected by the FC fault. Three adaptation strategies are compared. First, no adaptation of parameters is done. Second, the parameters are adapted to track a reference value $R_{\mathrm{d,ref}}$ with the total virtual resistance. Third, $R_{\mathrm{d,ref}}$ is

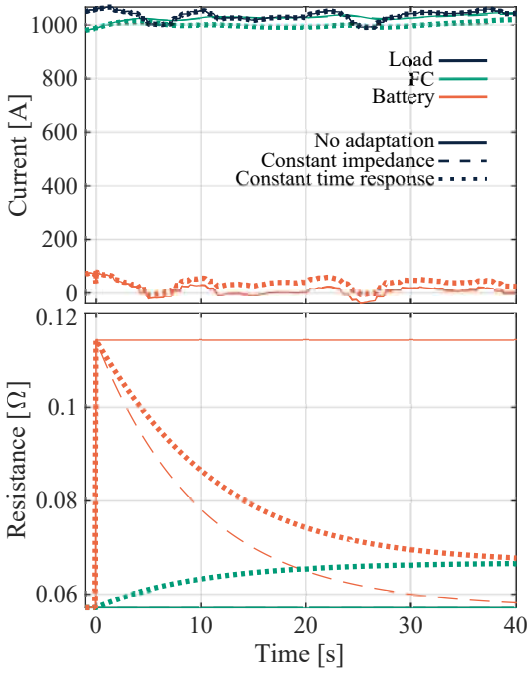


Figure 4.19: Droop resistances and current sharing immediately after battery fault for different adaptation scenarios

adapted according to Eq.4.24 to keep the voltage control at the desired bandwidth.

The two faults are sufficiently far apart, such that the first parameter adaptation is completed at the time of the second fault. Fig. 4.19 shows the battery disconnection at $t = 0\,\mathrm{s}$. Since the fault instance the battery output is close to zero, the remaining battery is only required to compensate for a minor imbalance, yielding a voltage drop of ca. $3\,\mathrm{V}$. Figure 4.19 shows the low- and high frequency elements of the total virtual resistance over time. The battery disconnection instantly doubles the high frequency element. This value remains unchanged if no adaptation is undergone, yielding differing virtual resistances of the low- and high frequency controllers. In the second case, the resistance converges back to its target value by decreasing the droop parameter of the remaining battery controller. In the third case, due to the decreased DC bus capacity, the total droop resistance is led to a slightly higher value than originally. Here, the low frequency components also adapt their droop parameters, reacting to the adapted DC bus capacity estimation. In the second and third cases, the final virtual resistance of all low- and high-frequency components matches, as intended in the implementation guidelines in section 4.3.3.

During the subsequent FC system fault, the local controllers are parameterized differently, depending on the adaptation strategy. The results are shown in Fig. 4.20, with the fault occurring at $t = 0\,\mathrm{s}$. A quarter of the delivered power is suddenly cut back and is required to be compensated by the remaining battery.

Figure 4.20 shows the voltage trajectories during the stabilization for the three described

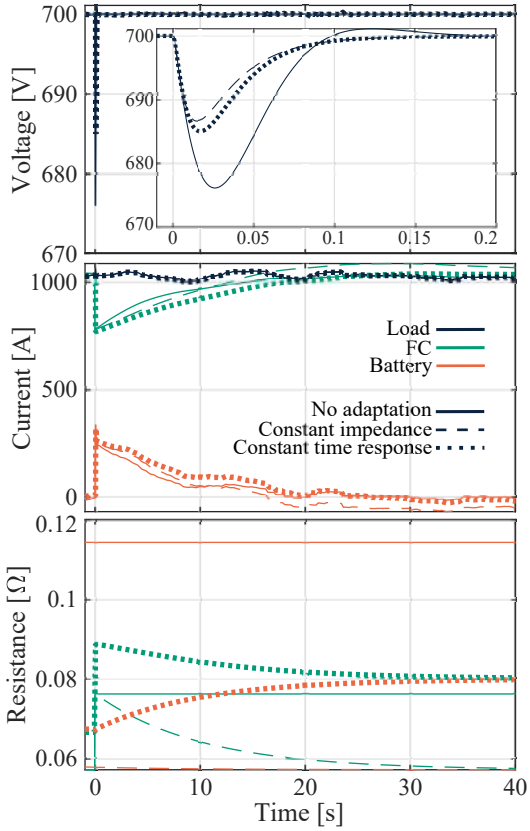


Figure 4.20: Voltage stabilization, droop resistances and current sharing immediately after fuel cell fault with previous battery fault for different adaptation scenarios

strategies. With no adaptation, the total droop resistance is too high, leading to an increased voltage dip of 24 V and a subsequent overshoot after stabilization. With a constant droop resistance in the second case, the voltage stabilization becomes more aggressive, since the total droop resistance is lower than required to achieve the desired voltage control bandwidth, yielding a voltage dip of 13 V. Finally, in the third case, the voltage stabilization is achieved as designed according to the voltage control bandwidth ω_{vc}, yielding a voltage dip of 15 V, 37.5 % lower than without parameter adaptation.

Figure 4.20 shows the droop parameter adaptation for the high bandwidth droop resistance after the fault. With the adaptation enabled, low- and high-frequency resistances converge towards the same value. The low bandwidth resistance remains constant except for the third case, where the system reacts to the change in DC bus capacity. Accordingly, for consistent behavior, regardless of the system topology, an adaptation of the droop parameters following the desired voltage control bandwidth is recommended.

4.5 Conclusions

Although FC-battery hybrid power systems with DC distribution are emerging as a promising solution for zero-emission shipping, the coordinated control of multiple power system resources remains a challenge. In larger systems, a modular approach for integration and control is a viable approach, as it can facilitate the reconfiguration and extension of the SPS.

This work presented a decentralized coordinated control strategy using virtual impedance-based droop achieving low DC bus voltage deviations and fast restoration as well as a load frequency decoupling. It could be shown that the decentralized solution can achieve the same quality in dynamic power sharing and voltage control as a centralized PI controller with a low-pass filter. The controller tuning affects the power gradients and load changes demanded from the FC systems, as well as the required depth-of-discharge for the ESS. Accordingly, a trade-off must be made between FC and ESS degradation arising from their dynamic operation. This study further presented an approach for automatic parameter adaptation after system reconfiguration utilizing a low-bandwidth communication network. The adaptation is proposed as a means to facilitate a modular power system control. It could be shown the the power sharing among components is adapting to configuration and parameters alterations and furthermore the voltage dynamics of the electric system could be maintained after disconnection of multiple components.

Whereas a low-bandwidth communication network facilitates parameter adaptation, its full potential has not yet been leveraged. The consideration of varying component parameters, e.g., owing to aging effects, and the consideration of different component types remain unaddressed topics for future research. This study considers simple component models for FCs and batteries, which allows parameterization with limited manufacturer data. Such models are sufficient for this work's focus on the system dynamics of the electric distribution system. However, models with higher fidelity will enable to generate deeper insights in the component-level behavior. Accurate quantification of FC and battery degradation, as well as hydrogen consumption of the proposed methodology, and a comparison to an optimized control strategy will be valuable additions in the future.

5

Mission-Scale Optimization for Modular Fuel Cell-Battery Power Systems

The studies so far, described in the previous chapters, were dedicated to fast-timescale objectives, namely system stabilization and dynamic power sharing, making out the lower layers of the hierarchy. Next, I am moving on to the high-level layer. The first question to answer is how an optimal dispatch of fuel cells and batteries looks like when considering a full mission. So before investigating implementable energy management strategies, this chapter provides an offline method for the cost-optimal dispatch of multiple fuel cells and batteries. The aim is to provide a benchmark and showcase the benefits from a modular fuel cell integration and control. This will serve as a performance comparison for real-time applicable methods and gives incentives for including optimal on-off decision-making in the energy management.

"It is not the destination that matters,
but how one arrives there."

— *Dalinar*, in *The Way of Kings*
by *Brandon Sanderson*

This chapter is published with minor modifications as *Optimal Energy Management of FC- Battery Shipboard Power System using Dynamic Programming, in: Proceedings of IEEE ESARS-ITEC, 2024* [121].

5.1 Introduction

The targets defined for the decarbonization of the maritime sector [4] demand the investigation of clean technologies as an alternative carbon-based power generation. One promising energy supply technology is the hydrogen fuel cell (FC) [6]. Combined with energy storage systems (ESSs), they are a viable solution for zero-emission shipping in specific applications. A key challenge for these systems lies in the optimal utilization of FCs and batteries to supply the load demand, while minimizing fuel consumption and component degradation.

In the literature, the proposed solutions for the degradation-aware control of FC-battery hybrid systems are mostly not based on an optimization, e.g., filter-based [200], rule-based [22, 180] and fuzzy-logic control [21, 83]. Equivalent consumption minimization strategies for instantaneous optimization are applied in [22, 24] and, similarly, in [228] for a modular setup. These, however, neglect the FC degradation. In addition, predictive control can be employed to include load predictions for the optimal power dispatch [182]. Both instantaneous and predictive optimization-based approaches must trade-off the quality of solutions with computational efficiency and do usually not yield the actual optimal energy management solution. The multi-objective optimization of energy management is generally complex, typically shaping a mixed-integer non-linear problem. Simplified, it can be solved using conventional numerical methods [145]. Meta-heuristic methods can be employed to provide sufficient results, however, without guarantee to find the optimum [150]. Alternatively, dynamic programming is a suitable method for finding the global optimum solution to a control problem [229, 230]. An offline multi-objective optimization with dynamic programming of hybrid ships is proposed by [231]. An optimization-based approach for FC-battery vehicles considering FC degradation is proposed by [110] using stochastic dynamic programming. However, degradation-aware offline optimization of shipboard power systems with a FC-battery hybrid energy system has not yet been investigated. Furthermore, existing studies do not include the optimized on- and off-switching of multiple FC modules.

This chapter investigates the offline computation of the optimal dispatch of multiple FC modules and batteries for a given load profile. Dynamic programming is used to determine the optimized power outputs of each component. This method is suitable for handling non-linearities and mixed-integer problems. The optimization covers multiple objectives, considering both fuel consumption and FC degradation, aiming to minimize total operational costs. Battery degradation is neglected for this study, as its impact is expected to be considerably smaller than FC degradation. Furthermore, the developed method allows the selective on-off switching of FC modules as an additional degree of freedom in the optimization.

The following Section 5.2 describes the regarded system and the models used in this study. Section 5.3 elaborates on the problem formulation and implementation of dynamic programming algorithm. Simulation results are presented in Section 5.4, and key takeaways of this study are given in Section 5.5.

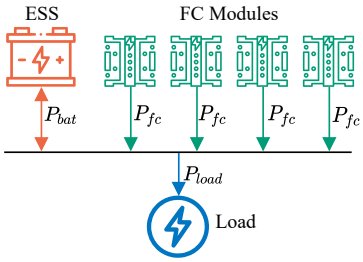


Figure 5.1: System topology with four FC modules, one ESS, and load connected to common bus

Table 5.1: Fuel Cell and Battery Parameters

Parameter	Description	Value
$P_{\mathrm{fc,max}}$	Max. FC power	316 kW
$\dot{P}_{\mathrm{fc,max}}$	Max. FC power gradient	10 kW/s
N_{fc}	Available FC modules	4
C_{bat}	Battery Capacity	1125 Ah
V_{nom}	Nominal voltage	440 V
R_{i}	Internal resistance	6.8 mΩ
$I_{\mathrm{bat,max}}$	Maximum current	3.37 kA

5.2 Modeling

The energy system contains multiple FC modules and one ESS, which together supply an electric load. An exemplary power system with four FC modules is shown in 5.1. The output power of all active FC modules plus the discharge of the ESS must match the demanded load in each instant.

At a given time, the state of the system can be characterized by the state-of-charge (SoC) $\xi(t)$, and the number of active FC modules $n_{\mathrm{fc}}(t)$, defining the state vector

$$\boldsymbol{x}(t) = [\xi(t)\ n_{\mathrm{fc}}(t)]^T \tag{5.1}$$

The input vector is defined as

$$\boldsymbol{u}(t) = [P_{\mathrm{fc}}(t)\ \Delta n_{\mathrm{fc}}(t)]^T \tag{5.2}$$

containing the power output of each FC module $P_{\mathrm{fc}}(t)$ and the switching action $\Delta n_{\mathrm{fc}}(t)$, changing the number of active FC modules.

The power load $P_{\mathrm{load}}(t)$ acts as an input disturbance, yielding a disturbance vector

$$\boldsymbol{d}(t) = [P_{\mathrm{load}}(t)] \tag{5.3}$$

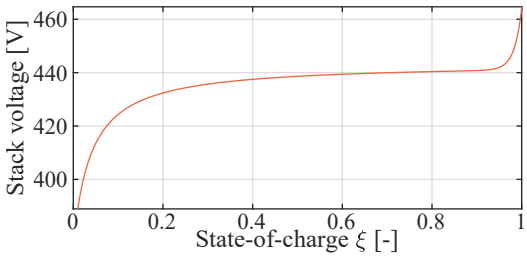


Figure 5.2: Battery polarization curve

5.2.1 System Dynamics

The number of active FC modules is directly influenced by the corresponding input to switch modules on and off.

$$\frac{d}{dt} n_{\mathrm{fc}}(t) = \Delta n_{\mathrm{fc}}(t) \tag{5.4}$$

where $\Delta n_{\mathrm{fc}}(t)$ is either zero, or a positive or negative unit impulse. The change in ESS SoC depends on the battery current $I_{\mathrm{bat}}(t)$ and the battery capacity C_{bat} such that

$$\frac{d}{dt} \xi(t) = -\frac{I_{\mathrm{bat}}(t)}{C_{\mathrm{bat}}} \tag{5.5}$$

Assuming a simple quasi-static battery model with an SoC-dependent open circuit voltage $V_{\mathrm{oc}}(\xi(t))$ and an internal resistance R_{i}, the battery current is obtained as a function of battery parameters and delivered power P_{bat} as

$$I_{\mathrm{bat}}(t) = \frac{V_{\mathrm{oc}}(\xi(t))}{2R_{\mathrm{i}}} - \sqrt{-\frac{P_{\mathrm{bat}}(t)}{R_{\mathrm{i}}} + \left(\frac{V_{\mathrm{oc}}(\xi(t))}{2R_{\mathrm{i}}}\right)^2} \tag{5.6}$$

Specified parameters for the $LiFePO_4$ battery, obtained from a manufacturer data-sheet [232], are listed in Table 5.1, with $V_{\mathrm{oc}}(\xi)$ shown in 5.2. The battery power is constituted by the system's power balance as

$$P_{\mathrm{bat}}(t) = P_{\mathrm{load}}(t) - P_{\mathrm{fc}}(t) n_{\mathrm{fc}}(t) \tag{5.7}$$

5.2.2 Fuel Cell Consumption and Degradation

The hydrogen consumption of each FC module depends its power output, as shown in Fig. 5.3, next to the module's efficiency over its power range. Table 5.1 lists the modules' specifications based on manufacturer data [218]. The total hydrogen consumption $\dot{m}_{\mathrm{h2}}$ is computed as

$$\dot{m}_{\mathrm{h2}}(t) = n_{\mathrm{fc}}(t) f(P_{\mathrm{fc}}(t)) \tag{5.8}$$

In addition, the FC modules' voltage degrades based on their operation. Three degradation modes have been identified in literature [67, 233, 234], and are modeled as contributors to the cell voltage decrease. Cyclic degradation is modeled as a fixed voltage decrease per activation of a FC module. Dynamic degradation is modeled as a linear function of

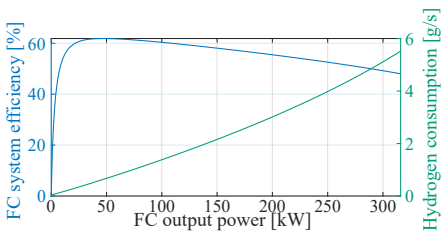


Figure 5.3: FC module polarization curve

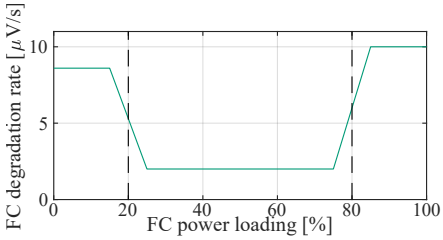


Figure 5.4: FC module static degradation rate

Table 5.2: FC Degradation Parameters

Param.	Description	Value	Ref.
dv_{hi}	Static degradation high power	10.0 μV/h	[234]
dv_{lo}	Static degradation low power	8.6 μV/h	[234]
dv_{base}	Baseline static degradation	2.0 μV/h	[235]
p_{lo}	Low power threshold	20 %	[6]
p_{hi}	High power threshold	80 %	[67]
dv_{sw}	Cyclic degradation factor	13.79 μV	[234]
dv_{dyn}	Dynamic degradation factor	0.212 μV/cycle	[67]

the load change of each module. Static degradation is modeled as a piece-wise linear function, depicting an hourly degradation rate depending on the operation in a low-power, high-power, and base-power region, as depicted in Fig. 5.4. The degradation parameters, referred to a single cell, are listed in Table 5.2.

5.3 Optimal Energy Management

The energy management refers to the time-varying dispatch of power generation and energy storage over the duration of a mission. In this study, the performance of the energy management is assessed based on hydrogen consumption and FC degradation. Dynamic programming is employed to find an offline-computed optimal trajectory of the control inputs, assuming a-priori knowledge of the load profile.

5.3.1 Dynamic Programming

Applying dynamic programming as a solver for this optimization problem requires quantizing the time-state space.

Time Discretization

Inputs and states of the system must be time-discrete. The discrete system dynamics, as applied in the dynamic programming algorithm, are described in Section 5.3.2. Furthermore, the disturbance posed by the load profile must be transformed into a discrete time series. The time-continuous input $P_{\text{load}}(t)$ is obtained from measurements. The discretization with

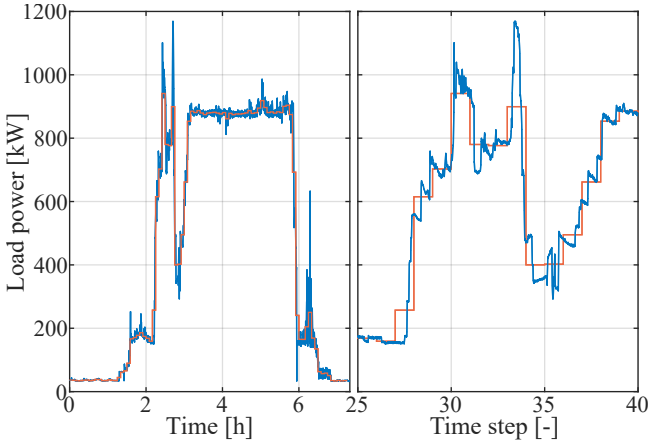


Figure 5.5: Time discretization of load profile

time steps of length Δt is done by computing the average value of the time-continuous input over the k-th time interval as

$$P_{\text{load}}(k) = \frac{1}{\Delta t} \int_{(k-1)\Delta t}^{k\Delta t} P_{\text{load}}(t)dt \tag{5.9}$$

$\forall k \in \mathbb{N}^{+}_{\leq N_k}$, where

$$N_k = \lfloor \frac{\Delta t}{t_{\text{max}}} \rfloor \tag{5.10}$$

and t_{max} being the total duration of the measured load profile. The discretization from a continuous-time to a discrete-time load profile is depicted in Fig. 5.5.

State Discretization

The valid SoC range of the ESS is quantized into N_{soc} discrete SoC levels. This yields a set $\mathcal{M}$ of valid SoC states ξ at equidistant intervals between the minimum and maximum allowable SoC ξ_{min} and ξ_{max}.

$$\mathcal{M} = \{\xi = \xi_{\text{min}} + \frac{(\xi_{\text{min}} - \xi_{\text{min}})(n_{\text{soc}} - 1)}{N_{\text{soc}} - 1} | n_{\text{soc}} \in \mathbb{Z}^{+}_{\leq N_{\text{soc}}}\} \tag{5.11}$$

The number of active FC modules n_{fc} is discrete, as it is an integer value of the set $\mathcal{N}$ defined as

$$\mathcal{N} = \{n_{\text{fc}} | n_{\text{fc}} \in \mathbb{Z}^{0}_{\leq N_{\text{fc}}}\} \tag{5.12}$$

where N_{fc} is the number of available FC modules. All possible states are spanned up in the state space $\mathcal{X}$ as

$$\mathcal{X} = \mathcal{M} \times \mathcal{N} \tag{5.13}$$

The i-th element in $\mathcal{X}$ can be expressed as a tuple

$$(\xi_i, n_{\mathrm{fc},i}) \tag{5.14}$$

where $i \in \{1, 2, 3, ..., N_{\mathrm{soc}}(N_{\mathrm{fc}} + 1)\}$. Accordingly, the quantized time-state space is spanned up by state space over time $\mathcal{X} \times \mathbb{N}^{+}_{\leq N_k}$. Each trajectory with increasing time signature from $k = 1$ to $k + N_k$ that does not violate any constraint describes a possible solution candidate for the energy management problem. It is important to note that the choice of time interval Δt and number of SoC states N_{soc} poses a trade-off between accuracy of the optimization model versus the size of the solution space and thereby computational complexity.

5.3.2 Energy Management Optimization

To find an optimal energy management solution, a cost function $J(\boldsymbol{x}(k), \boldsymbol{u}(k), \boldsymbol{d}(k))$ must be defined. In this case it is the summation of the fuel consumption and FC degradation over all N_k time steps:

$$J(\boldsymbol{x}(k), \boldsymbol{u}(k), \boldsymbol{d}(k)) = \sum_{k=1}^{N_k} c_{\mathrm{h2}} \dot{m}_{\mathrm{h2}}(k) \Delta t + c_{\mathrm{deg}}\, dV_{\mathrm{deg}}(k) \tag{5.15}$$

where c_{h2} and c_{deg} are cost parameters for the hydrogen consumption and FC degradation, respectively. The states and inputs are subject to the following constraints:

$$\xi_{\min} \leq \xi(k) \leq \xi_{\max} \tag{5.16}$$

$$0 \leq P_{\mathrm{fc}}(k) \leq P_{\mathrm{fc,max}} \tag{5.17}$$

$$|\dot{P}_{\mathrm{fc}}(k)| \leq \dot{P}_{\mathrm{fc,max}} \tag{5.18}$$

$$P_{\mathrm{fc}}(k = 1) = P_{\mathrm{fc}}(N_k) = 0\,\mathrm{kW} \tag{5.19}$$

$$n_{\mathrm{fc}}(k) \in \{0, 1, ..., N_{\mathrm{fc}}\} \tag{5.20}$$

Further, the final SoC is required to match the initial value:

$$\xi(k = 1) = \xi(N_k) = \xi_{\mathrm{init}} \tag{5.21}$$

Implementation

The dynamic programming algorithm computes transition costs T_{ij} for the transition from node i at time k to node j at time $k + 1$, as outlined in Fig. 5.6. The inputs P_{fc} and Δn_{fc} required for a specific transition at time k are computed using the discretized model equations and the change of state variables x_i and n_{fc}. The battery current is obtained from the change in SoC from ξ_i to ξ_j as

$$I_{\mathrm{bat}}(i, j) = -\frac{(\xi_j - \xi_i) C_{\mathrm{bat}}}{\Delta t} \tag{5.22}$$

Accordingly, the battery power is derived following (5.6)

$$P_{\mathrm{bat}}(i, j) = I_{\mathrm{bat}}(i, j) V_{\mathrm{oc}}(\xi_i) - I_{\mathrm{bat}}(i, j)^2 R_{\mathrm{i}} \tag{5.23}$$

The necessary FC power per module at time k for the transition, according to (5.7) is computed as

$$P_{\mathrm{fc}}(k,i,j) = \frac{(P_{\mathrm{load}}(k) - P_{\mathrm{bat}}(i,j))}{n_{\mathrm{fc},i}} \tag{5.24}$$

Accordingly, the FC power gradient is

$$\dot{P}_{\mathrm{fc}}(k,i,j) = \frac{P^*_{\mathrm{fc}}(k+1,j) - P_{\mathrm{fc}}(k,i,j)}{\Delta t} \tag{5.25}$$

The input Δn_{fc} is derived as

$$\Delta n_{\mathrm{fc}}(i,j) = n_{\mathrm{fc},i} - n_{\mathrm{fc},j} \tag{5.26}$$

For each transition, hydrogen consumption $\dot{m}_{\mathrm{h2}}$ and FC degradation dV_{deg} are computed. The degradation is averaged over all cells, and is the sum of static, dynamic, and cyclic degradation dV_{stat}, dV_{dyn}, and dV_{sw}.

$$\dot{m}_{\mathrm{h2}}(k,i,j) = n_{\mathrm{fc},i} f(P_{\mathrm{fc}}(k,i,j)) \tag{5.27}$$

$$dV_{\mathrm{stat}}(k,i,j) = \frac{n_{\mathrm{fc},i}}{N_{\mathrm{fc}}} f(P_{\mathrm{fc}}(k,i,j)) \tag{5.28}$$

$$dV_{\mathrm{dyn}}(k,i,j) = \frac{n_{\mathrm{fc},i}}{N_{\mathrm{fc}}} dv_{\mathrm{dyn}} \frac{\dot{P}_{\mathrm{fc}}(k,i,j)\Delta t}{P_{\mathrm{fc,max}}} \tag{5.29}$$

$$dV_{\mathrm{sw}}(i,j) = \frac{dv_{\mathrm{sw}} \Delta n_{\mathrm{fc}}(i,j)}{N_{\mathrm{fc}}} \tag{5.30}$$

$$dV_{\mathrm{deg}}(k,i,j) = dV_{\mathrm{stat}}(k,i,j) + dV_{\mathrm{dyn}}(k,i,j) + dV_{\mathrm{sw}}(i,j) \tag{5.31}$$

Finally, the transition cost is computed as

$$T_{ij}(k) = c_{\mathrm{h2}} \dot{m}_{\mathrm{h2}}(k,i,j)\Delta t + c_{\mathrm{deg}} dV_{\mathrm{deg}}(k,i,j) \tag{5.32}$$

Dynamic programming iterates backward through all time steps and determines the minimal cost and optimal trajectory for each time-state node to reach the final state. For each node i at time step k, a value $W(k,i)$ can be computed, defining the minimal cost to reach the final state. This value is obtained by finding the target node $j^*(k,i)$ that minimizes

$$W(k,i) = \min_{j \in \mathcal{X}} W(k+1,j) + T_{ij}(k) \tag{5.33}$$

At the final time step, the terminal cost of each state is pre-defined as

$$W(N_k,i) = \begin{cases} 0 & \text{if } \xi_i = \xi_{\mathrm{init}} \wedge n_{\mathrm{fc},i} = 0 \\ \infty & \text{otherwise} \end{cases} \tag{5.34}$$

The algorithm is implemented as following:

1. initialize cost-to-end of nodes i at $k = N_k$
2. iterate through time steps from $k = N_k - 1$ to 1

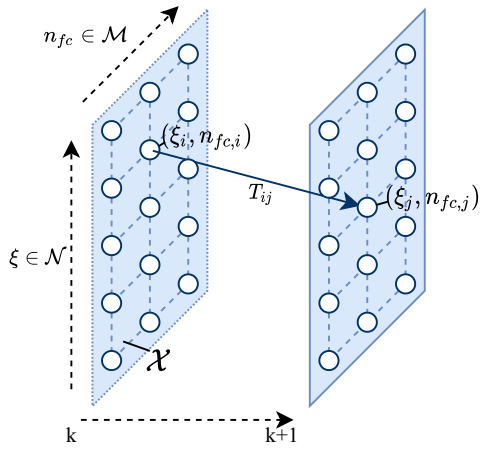


Figure 5.6: Transition from node i to j at time k in quantized time-state space

(a) iterate through all nodes i at step k

i. Determine transition cost to all valid target nodes j

ii. Determine minimal cost-to-end $W(k,i)$

iii. Store optimal transition $j^*(k,i)$, and inputs $P^*_{\mathrm{fc}}(k,i)$ and $\Delta n^*_{\mathrm{fc}}(k,i)$

3. resolve optimal trajectory through quantized time-state space forwards through time from initial node $\{\xi_{\mathrm{init},0}\}$

4. determine total hydrogen consumption $m_{\mathrm{h2,tot}}$ and fuel cell degradation dV_{tot} for optimal state trajectory

5.4 Simulation and Results

The model described in Section 5.2 and the dynamic programming algorithm from Section 5.3 are implemented in Matlab. For the simulations, the parameters listed in Table 5.3 are applied. Three scenarios are investigated to assess the effect of an optimized on-off switching of FC modules. In the first scenario, all modules are constantly active. The second scenario allows the simultaneous on-off switching of all modules. Finally, in the third scenario, a selective on-off switching of each module is possible. The load profile shown in Fig. 5.5 is investigated for the simulations.

The power balance for the three scenarios is shown in Figs. 5.7, 5.8, and 5.9, respectively. The resulting optimal hydrogen consumption and FC degradation, with the specified factors c_{h2} and c_{deg} from Table 5.3, are given in Table 5.4. In this specific investigation, the optimal timing of switching the FC systems on and off allows a significant reduction of their degradation by 41.8 %, whereas the effect on fuel consumption is marginal. Selective switching additionally improves both metrics to a negligible extent.

The factor c_{deg} is varied between 10 % and 1000 % of its listed value to assess the sensitivity of the results to the cost parameters. The resulting Pareto-fronts for the second and third scenarios are displayed in Fig. 5.10. This comparison shows that the additional freedom to

Table 5.3: Simulation Parameters

Parameter	Description	Value
c_{h2}	H2 cost factor	4.95 €/kg [236, 237]
c_{deg}	FC deg. cost factor	12.64 €/μV [238]
Δt	Time step	60 s
ξ_{min}	Min. SoC	25 %
ξ_{max}	Max. SoC	75 %
ξ_{init}	Initial SoC	50 %
N_{soc}	Number of SoC states	2001

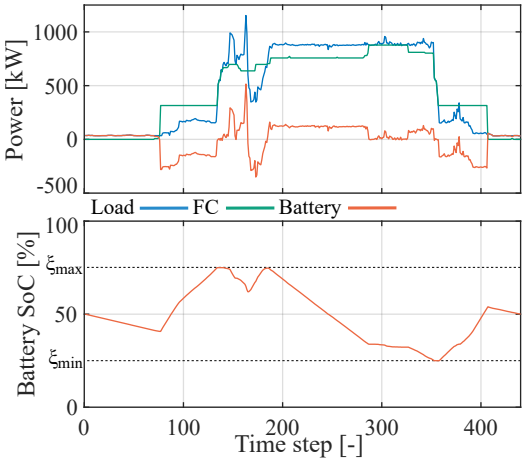


Figure 5.7: Power sharing between FCs and batteries, and battery SoC for minimized operational costs with constantly active FCs

selectively switch modules can significantly reduce the FC degradation, which becomes optimal when stack replacement is considerably more costly than hydrogen. Both the second and third scenarios significantly reduce the FC degradation for all cost factor combinations compared to the first scenario.

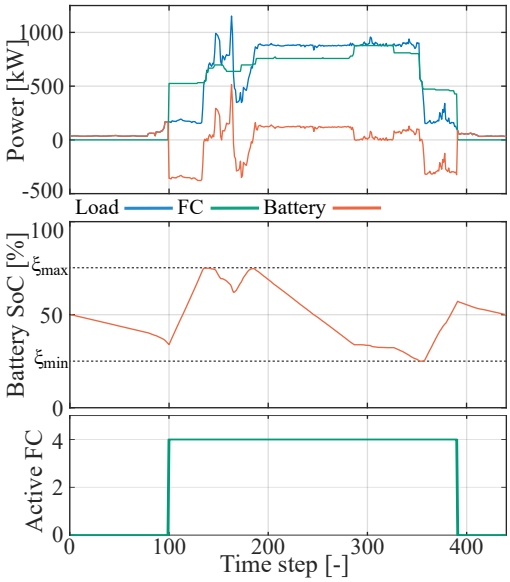


Figure 5.8: Power sharing between FCs and batteries, battery SoC, and number of active FCs for minimized operational costs with simultaneous on-off switching of all FCs

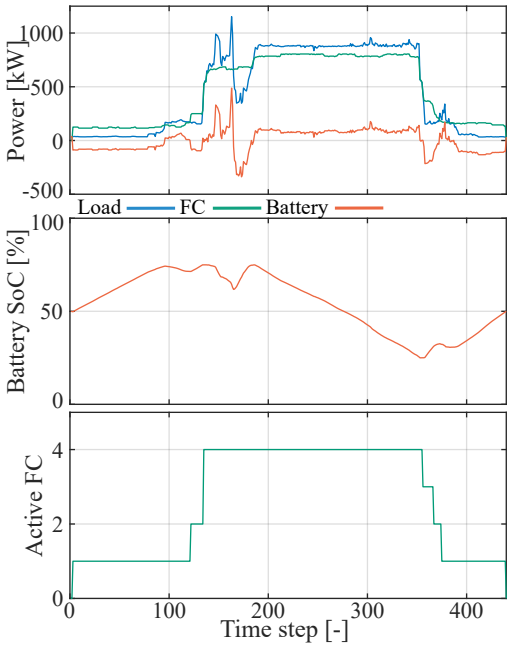


Figure 5.9: Power sharing between FCs and batteries, battery SoC, and number of active FCs for minimized operational costs with selective on-off switching of FCs

Table 5.4: Simulation Results

	Fuel Consumption	FC degradation
All Active	180.02 kg	40.74 μV
All On-Off	179.87 kg	23.72 μV
Selective On-Off	179.58 kg	23.69 μV

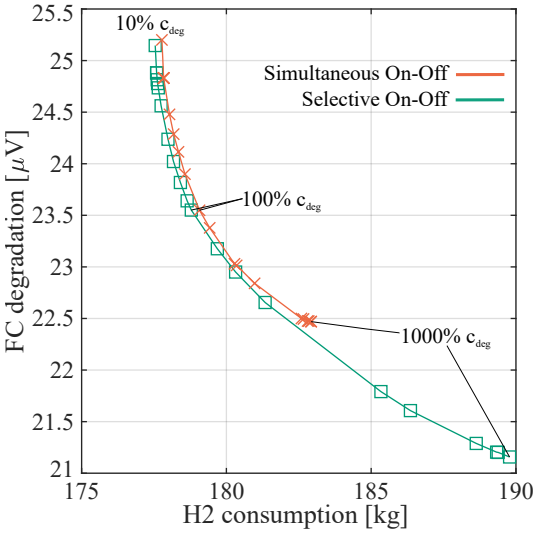


Figure 5.10: Sensitivity of optimal solution to a variation of the FC degradation costs between 10 % and 1000 % of original value

5.5 Conclusions

In this work, dynamic programming has been applied for the offline computation of the optimal trajectories of power outputs and on-off switching for multiple FC modules to supply the load of a FC-battery zero-emission ship. Results indicate that the optimal timing of switching the FCs on and off significantly reduces their degradation, while fuel consumption is much less affected. Enabling selective on-off switching further reduces the FC degradation at the cost of increased hydrogen use. The optimal trade-off between the two values depends on the ratio of hydrogen and FC stack replacement costs, whereas minimizing the total operational expenditure should be goal of the ship operator. In future work, the offline optimal energy management can serve for benchmarking real-time strategies, as well as support in the design of new control approaches. Offline optimization can also assist in mission planning, assuming that information on the mission profile is available beforehand. Obtained results can then be utilized to inform the real-time controller to improve its performance. Furthermore, an efficient implementation of the optimization can be used in a predictive controller if load predictions can be made during ship operation.

6

Predictive Energy Management for Fuel Cell-Battery Power Systems

In earlier chapters, I have shown methods for the lower control layers, and presented an offline-computed optimal power dispatch. This chapter moves on to a real-time applicable energy management strategy. The method and study presented in this chapter define an approach for a centralized architecture that minimizes total operational costs. By defining cost functions for a fuel cell and a battery, involving not only fuel costs but also cell degradation costs, an optimal power split can be found. Initially, I describe an equivalent cost-based approach as an instantaneous optimization, which I later on extend into a predictive energy management strategy. Using outputs from a data-driven load forecasting model, this strategy can be applied for optimization over a 15-minute horizon, but assuming a perfect load prediction shows high potential over longer horizons as well.

"Strength does not make one capable of rule;
it makes one capable of service."

— *Teft*, in *The Way of Kings*
by *Brandon Sanderson*

This chapter is submitted for publication with minor modifications as *Degradation-aware Predictive Energy Management for Fuel Cell-Battery Ship Power System with Data-driven Load Forecasting, preprint accessible on arXiv* [239]

6.1 Introduction

Electrification and hybridization are two key enablers for increasing the operational flexibility and capability of onboard energy systems in ships [12]. Fuel cells (FCs) are a prominent candidate for the replacement of conventional diesel engines as main generators, aiming at the decarbonization of maritime transport [6]. Energy storage systems (ESSs) allow for the decoupling of the load and generation, making it possible to operate the main supplies more steadily and efficiently, while high power gradients and power peaks can be compensated by, e.g., batteries [7]. This can be especially beneficial in ship types whose load profile is highly volatile, changing quickly within a short time frame, e.g. harbor tugs.

One fundamental line of research for hybrid vessels is the coordination of the generation and storage systems, as the batteries introduce additional degrees-of-freedom for the control system. The main challenge for the energy management strategy (EMS) is the optimal dispatch of power sources over time, ensuring that each component- and system-level constraints are respected [30]. Typically, the EMS aims at the minimization of the fuel consumption, while ensuring that the load power can always be supplied by the generation side [101]. However, with the introduction of FCs, an additional key performance criterion is the cell degradation, which is required to be minimized such that their lifetime is extended, keeping stack replacement costs low [6, 233]. Hence, the optimal energy management of FC-battery shipboard power system (SPS) poses a multi-objective optimization problem.

In the literature, a multitude of approaches attempts to solve this problem. Generally, methods can be divided into heuristic and optimization-based approaches [33]. Many studies on the energy management for FC-battery based SPS focus on PI or filter-based controllers [24, 178, 212] to achieve peak-shaving for steady FC operation or on efficiency improvement via rule-based controllers [22, 98]. Similarly, fuzzy-logic controllers are utilized to translate expert insights into rules for a functioning EMS [21, 83].

More advanced EMSs are optimization-based, which can either be instantaneous or predictive, where the latter attempts to include knowledge of future system states and disturbances, e.g. the load power, in the solution of the energy management problem. An example of instantaneous optimization is equivalent consumption minimization strategy (ECMS), which conventionally is applied to hybridized diesel-based power systems [109, 126, 127], but has also been shown to be applicable to zero-emission ships [105, 228]. [131] shows the implementation of ECMS for multi-objective optimization. The advantage of instantaneous optimization is that no knowledge of future system disturbances is required. However, in case a prediction of the future mission profile is possible, it can be incorporated in the EMS to improve the controller performance and explicitly include system limitations. An example of this is the use of model predictive control (MPC), which can be utilized in various functions, such as optimal control of parallel prime movers [132], and optimal power split for hybrid systems [36, 76]. [140] and [139] formulate ECMS implementations whose parameters are set by overarching predictive or mission-scale optimizers. MPC is commonly implemented in multiple layers, decomposing the optimization problem into varying timescales. [36, 136] decouple the optimal steady-state dispatch from the dynamic power sharing in two-level MPC formulations whereas a three-level implementation is proposed by [137]. Predictive energy management for zero-emission ships is much less investigated. In [123, 181] an MPC is applied to determine the steady-state economic dispatch for a zero-emission ferry. The work in [182] further incorporates FC degradation

as an objective. However, the mentioned applications for FC-battery systems apply the optimization for large time steps while assuming a mission-scale quantification of load uncertainties. This disregards both the highly fluctuating load dynamics, as well as the optimal power split in dynamic conditions and uncertainties between predicted and actual load.

Most studies dedicated to the optimized control of hydrogen-based SPS only optimize for fuel consumption. Besides the cost of hydrogen, the cell degradation and eventual stack replacement of the FCs, as well as increased consumption due to degradation, are key drivers of the overall operating costs of a hydrogen FC-based system. An explicit quantification of the cell degradation and its minimization during dynamic operation is done by [67]. Similarly, [180] analyzes the cell degradation for various rule-based EMS in an SPS. However, these studies lack an attempt to quantify the costs arising from the cell degradation and, furthermore, do not include their degradation function in a predictive EMS.

The implementation of an MPC requires an estimate of future states, inputs and/or disturbances. Many sources assume perfect knowledge of future load to showcase the effectiveness of predictive control. Typically, this approach leads to promising results. However, in practice, knowledge of future system states and disturbances is limited. Accordingly, real systems require designers of a predictive EMS to develop methods for predicting the load, which can be based on heuristics, arise from the mission planning, or be based on operational data. A promising approach is the utilization of data-driven techniques for predicting the load profile over a certain time interval into the future, denoted as the prediction horizon. This challenge can be characterized as a Time Series Forecasting (TSF) problem [240–242]. Many approaches exist for solving TSF [240–242]. Classical methods such as Autoregressive Integrated Moving Average (ARIMA) and Exponential Smoothing often yield good results [243], but Machine Learning (ML) has become an increasingly attractive option due to its potential to improve model accuracy and scale to larger datasets with higher dimensionalities. ML models can be broadly categorized into two main families. The first is Shallow ML, which can achieve reasonably good performance with small to medium-sized datasets, provided that domain-specific features are carefully engineered [241]. The second family, Deep ML, can automatically learn features, i.e., representations without the need for manual feature engineering. However, leveraging Deep ML models can be challenging due to the large number of architectural design choices and the substantial amount of data required [242]. Recent studies have demonstrated that ML-based approaches, particularly those using Deep ML, can outperform classical methods on a variety of TSF tasks [244, 245].

Unfortunately, Deep ML models rely on massive labeled datasets, and constructing such datasets is challenging due to limited data availability (i.e., data may not be available at all) or high data annotation costs (i.e., data must be labeled by humans). To address these challenges, Foundation Models (FMs), such as Large Language Models in Natural Language Processing [246] and advanced models in Computer Vision [247], have emerged as powerful paradigms capable of achieving state-of-the-art performance in their respective fields. The success of these FMs stems from their ability to leverage vast amounts of data to learn general-purpose representations, enabling them to be fine-tuned or even used directly in a zero-shot manner across a diverse range of downstream tasks [248]. This approach

not only reduces the need for task-specific model development but also encapsulates a broad understanding of the world, endowing these models with exceptional versatility and efficiency. Motivated by this success, researchers have started exploring the development of Time Series Foundation Models (TSFMs) to harness the potential of the foundation model paradigm for time series data. By capitalizing on large-scale time series datasets, TSFMs aim to achieve superior performance across a variety of TSF tasks, offering a unified framework that can accelerate research and application development in this field [249]. The no-free-lunch theorem [250] asserts that identifying the optimal algorithm for a specific application requires evaluating multiple approaches.

This work formulates an MPC that handles second-scale load fluctuations and continuously prescribes optimized power references for FCs and batteries considering their dynamic and steady-state constraints and operational costs.

In our work, we explored several state-of-the-art methods and, based on their performance, proposed a novel approach that combines their strengths.

In our work, we propose the following contributions to address the gaps which have been identified in the literature and the state-of-the art for predictive energy management of hydrogen-based SPS:

- First, a degradation-aware optimization for a FC-battery hybrid SPS is constructed and applied in an ECMS-based EMS in real-time. The optimization minimizes operational costs arising from hydrogen consumption and cell degradation as main cost drivers.

- Second, several state-of-the art TSF methods are explored for the load forecasting of a harbor tug, utilizing the system's available real-time measurements. Based on their performance, a novel approach that combines their strengths is proposed to provide accurate load predictions.

- Third, the data-driven load forecasting and degradation-aware cost function are formulated in an MPC which explicitly minimizes the operating costs over the prediction horizon.

The remainder of this chapter is organized as follows. Section 6.2 introduces the original layout and measurement of the harbor tug and describes the virtual retrofit for obtaining an all-electric FC-battery hybrid vessel which serves as the case study in this work. Dynamic component and system models as well as a derivation of a complete state-space model are presented in Section 6.3. Further, this chapter introduces cost functions for hydrogen consumption and cell degradation and introduces system constraints. Section 6.4 describes the development of the data-driven load forecasting method and showcases its performance in predicting the future load of the harbor tug. The optimization function for the degradation-aware energy management is derived in Section 6.5. Both an ECMS-based and a model predictive EMS as well as a filter-based benchmark controller are described here. Numerical results of mission simulations for the display of performance using the proposed strategies are analyzed and discussed in Section 6.6. Finally, Section 6.7 summarizes the main conclusions of this work.

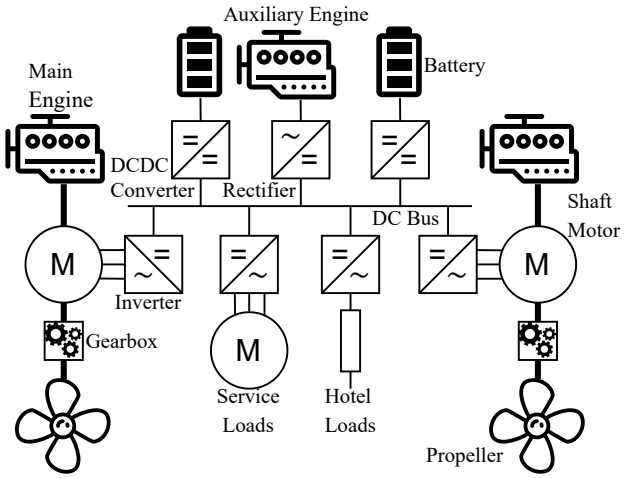


Figure 6.1: Primary systems of original diesel-based SPS

6.2 System Description

The EMS developed for this study is applicable to fully electric SPS with FCs and ESS on the generation side. Here, a harbor tug is considered, whose operating profile is characterized by a highly volatile load, with distinct operating modes and short mission profiles. As tugs typically operate in fleets and stay within the harbor space, they are a viable candidate for FC-battery systems, assuming that a hydrogen bunkering infrastructure is present. This chapter first describes the original diesel-hybrid harbor tug and the available measured data from its operation. In the next step, based on original design and mission requirements, virtual retrofit of the tugboat's power system with FCs and batteries is described, yielding the vessel regarded in this work.

6.2.1 Original System

The original harbor tug is equipped with a hybrid propulsion architecture and hybrid energy system with its specifications listed in Table 6.1. The main diesel engines are sized to carry the bulk of the propulsive load while the shaft motors and batteries allow for load leveling, gradient support, and full-electric operation at low load as well as a power take-off for feeding electric consumers.

Twelve months of operational data has been analyzed to determine the required power of the considered vessel for broad variety of actual mission profiles. Over this period, a total number of 167 missions have been logged with a logging rate of 5 s. Decisive for the power system control, as outlined in Section 6.5, is the time-dependent total power load. However, a broader array of real-time measurements is available and required for an accurate data-driven load forecasting. More detailed descriptions of the available data-sets and their utilization for the load forecasting are given in Section 6.4.

Table 6.1: Specifications of original diesel-hybrid power system.

Parameter	Info
Type	Harbor tug
Length	29.0 m
Width	10.5 m
Displacement	575 t
Max. Speed	13.5 kn
Propulsion	Diesel-hybrid
Main Engine	2x1840 kW
Shaft Motor	2x115 kW
Auxiliary Engine	800 kW
Battery Pack	2x120 kWh

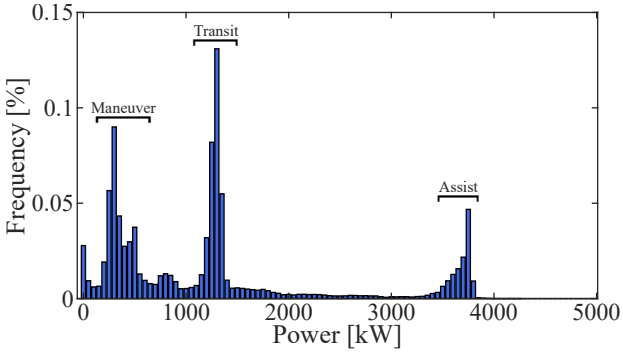


Figure 6.2: Histogram of total load measured during operation of the harbor tug

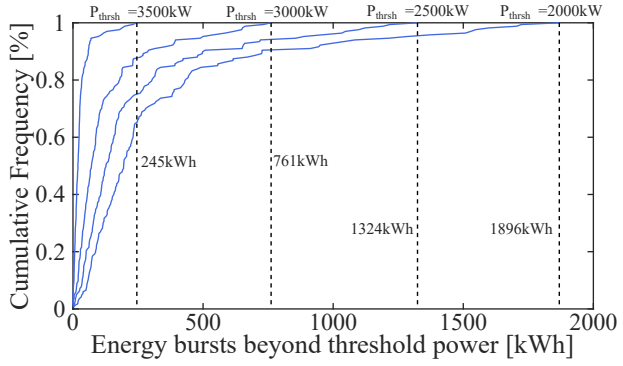


Figure 6.3: Cumulative frequency of energy bursts beyond specified threshold power during assist

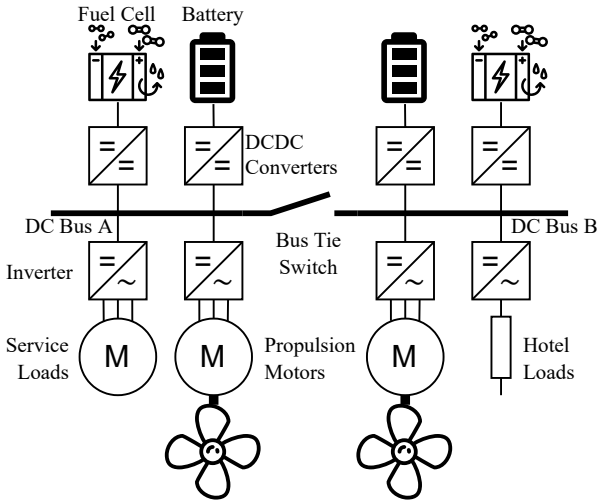


Figure 6.4: Primary systems of retrofitted full electric FC-hybrid power system

6.2.2 System Retrofit

Based on the original power system and the operational requirements, a hydrogen FC-based re-design has been conceptualized. Two interconnected DC busses, each attached to an FC and a battery system comprises the complete energy generation system. All loads are electrified, and fed by power converters. The resulting topology is displayed in Fig.6.4 and the specifications listed in Table 6.2.

Regarding the sizing of components, the total FC power at end-of-life (EOL) shall be sufficient for providing the maximum required power during assist. The maximum measured power, safe for negligibly short peaks, is 3800 kW, covering both the propulsive and auxiliary power load. Assuming that the EOL power of the FC systems is at 90 % of the system's original power rating [251], two proton-exchange membrane FC (PEMFC) systems, each with a maximum power output of 2125 kW at begin-of-life (BOL), are selected. This leaves a total of 3825 kW available generative power before a stack replacement.

FC systems show increased degradation at high power operation beyond 80 % of their maximum rating. Hence, it is desirable to size the energy storage such that the FCs are rarely forced above this threshold. At EOL, this amounts to 3060 kW of total power from the FCs. Bursts of energy that require power beyond a certain threshold P_{thresh} are shown in Fig. 6.3. For the desired operation limit of the FCs, an additional energy of up to 761 kWh is required to cover all observed mission profiles. With an assumed depth-of-discharge of 60 %, this requires 1268 kWh of installed energy storage capacity. For the ESS sizing, we round this value to 1250 kWh, distributed over two units. To achieve sufficient capability for compensating short-term power bursts, and power gradient support, a charge and discharge rating of 1.5 C is sufficient. Here, we select lithium iron phosphate (LFP) batteries due to their high efficiency and stable degradation behavior.

Table 6.2: Specifications of re-designed full-electric FC-battery power system.

Parameter	Info
Type	Harbor tug
Propulsion	Full-electric
Fuel Cells	2x2125 kW (BOL)
Battery Pack	2x625 kWh (BOL)
Propulsion Motors	2x1840 kW

6.3 Power System Model

This section describes the dynamic models used for the primary components of the SPS which encompasses the FC, the ESS, electric load and the power distribution system. From these models, a state-space representation of the complete system is derived, to be used for the optimization-based formulation of the system's energy management. In addition, approximations of the hydrogen consumption and the cell degradation of the FCs, and a cost model for aggregating both factors in the operating costs are described.

6.3.1 Fuel Cell

In this work PEMFCs serve as main power generation devices. The equivalent circuit of the simulation model consisting of an equivalent voltage source and internal resistance is shown in Fig. 6.5 a), as proposed by [205] for dynamic simulation of FC-based systems. The voltage source e_{fc} is current-dependent and computed as

$$e_{\mathrm{fc}}(i_{\mathrm{fc}}) = E_{\mathrm{oc,fc}} - N_{\mathrm{s,fc}} E_{\mathrm{ts}} ln(\frac{i_{\mathrm{fc}}}{N_{\mathrm{s,fc}} I_0}) \cdot \frac{1}{s T_{\mathrm{d}}/3 + 1} \tag{6.1}$$

where stack settling time T_{d}, Tafel slope E_{ts}, exchange current I_0, number of series-connected cells $N_{\mathrm{s,fc}}$, and open circuit voltage $E_{\mathrm{oc,fc}}$, as well as the internal resistance $R_{\mathrm{i,fc}}$, accounting for the linear voltage decrease, are extracted from the manufacturer datasheet [218] according to the method described by [205]. With this parameterization, the output voltage v_{fc} follows the polarization curve of the PEMFC module as described in its datasheet. Table 6.3 lists the FC model parameters. The voltage and power curves over output current for the system at BOL and EOL are shown in Fig. 6.6.

Table 6.3: Fuel Cell and Battery Parameters

Parameter	Description	Value
$P_{\mathrm{fc,max}}$	Max. net FC power	4150 kW
$\dot{P}_{\mathrm{fc,max}}$	Max. FC power gradient	212.5 kW/s
$R_{\mathrm{i,fc}}$	FC resistance (BOL/EOL)	23.2/28.0 mΩ
C_{bat}	Battery Capacity	3125 Ah
$R_{\mathrm{i,bat}}$	Bat. internal resistance	2.4 mΩ
$I_{\mathrm{bat,max}}$	Maximum current	9.4 kA

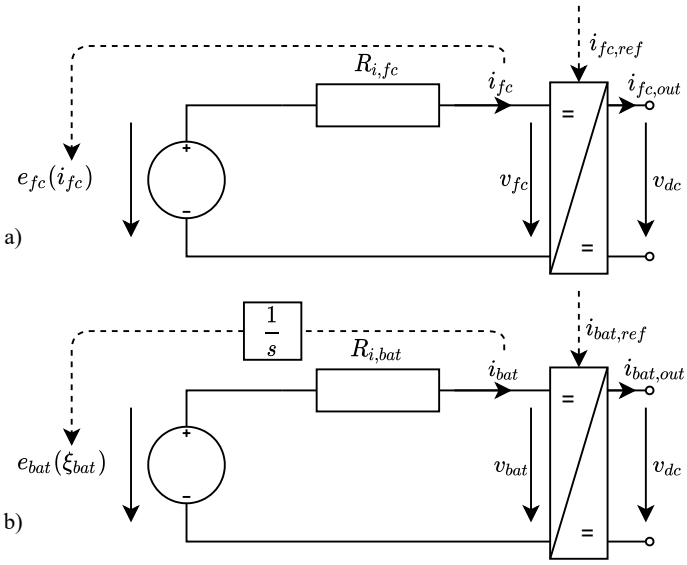


Figure 6.5: Simulation models for the PEMFC (a) and battery (b) including current-controlled power electronics converter

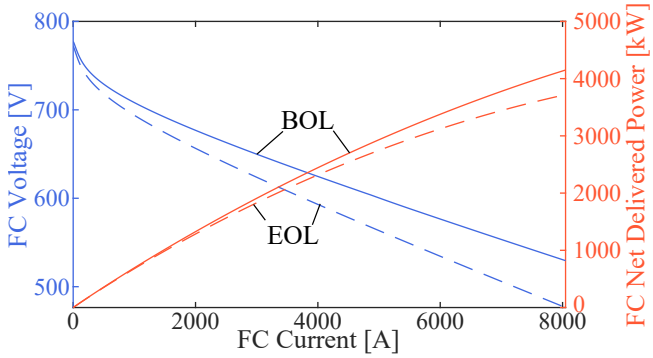


Figure 6.6: PEMFC voltage v_{fc} and net output power as functions of output current i_{fc} for BOL and EOL conditions

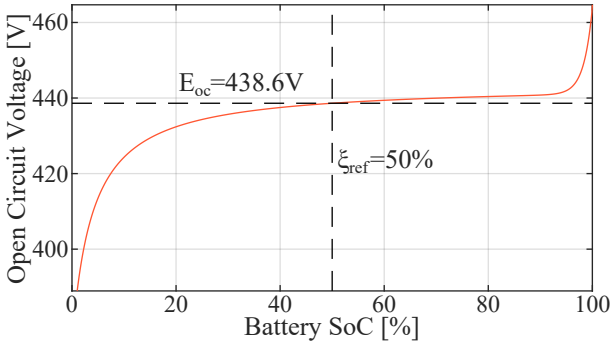


Figure 6.7: Open-circuit voltage of LFP battery system

6.3.2 Energy Storage System

An LFP battery system is integrated into the power system as ESS. The simulation model, proposed by [204], is similar to the FC model and is shown in Fig. 6.5 b). Here, the equivalent voltage source e_{bat} is depending on the battery state-of-charge (SoC), which is calculated via Coulomb counting. The system is parameterized based on the manufacturer datasheet [232] and its open-circuit voltage is displayed in Fig. 6.7. The battery model parameters are shown in Table 6.3. The LFP technology is characterized by its flat SoC-dependency curve. This enables the approximation of the open-circuit voltage with a constant value $E_{\text{oc}} = e_{\text{bat}}(\xi_{\text{bat}} = 50\%)$.

6.3.3 State Space Modeling

For the energy management, the control model of the SPS is simplified as a single-node system connected to a PEMFC, a battery, and an aggregated electric load, as shown in Fig. 6.8. The FC model generates an estimate of hydrogen consumption $\dot{m}_{\text{H2}}$ and cell voltage degradation ΔV_{deg}, as described in the modeling section 6.3. Both values are taken into account as objectives to be minimized in the energy management.
Furthermore, the PEMFC and the LiFePO battery feed power into the bus, denoted as p_{fc} and p_{bat}, respectively. We define the FC power p_{fc} and the battery SoC ξ_{bat} as system states. Our control input is the FC power gradient $\dot{p}_{\text{fc}}$. Whereas p_{fc} must always be ≥ 0, p_{bat} may be negative, indicating a charging of the battery. Furthermore, a limit is set on the input, i.e., $\dot{p}_{\text{fc}}$. Hence, system inputs and states must adhere to the following constraints

$$|\dot{p}_{\text{fc}}(n)| \leq \dot{P}_{\text{fc,max}} \tag{6.2}$$

$$0 \leq p_{\text{fc}}(n) \leq P_{\text{fc,max}} \tag{6.3}$$

$$SoC_{\text{min}} \leq \xi(n) \leq SoC_{\text{max}} \quad \forall \quad n \in [k, k+N] \tag{6.4}$$

The FC power dynamics are simply computed as

$$p_{\text{fc}}(n+1) = p_{\text{fc}}(n) + \dot{p}_{\text{fc}}(n) T_s \tag{6.5}$$

where T_s is the discretization interval. The power generation must always be in balance with the load power p_{load}. The latter is modeled as an external disturbance and since p_{fc} is

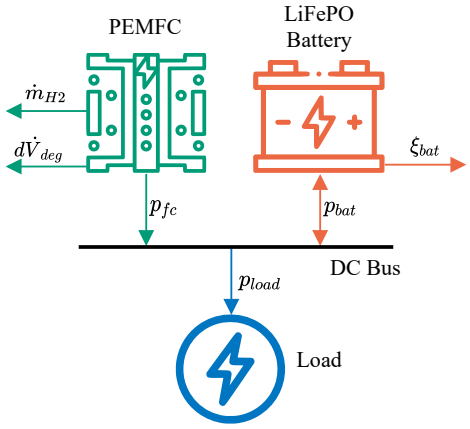


Figure 6.8: Simplified one-node control model for the EMS

defined as a system state, we can compute the battery power and current as

$$p_{\text{bat}}(n) = p_{\text{load}}(n) - p_{\text{fc}}(n) - \frac{T_s}{2}\dot{p}_{\text{fc}}(n) \tag{6.6}$$

$$i_{\text{bat}}(n) = \frac{E_{\text{oc}}}{2R_{\text{i,bat}}} - \sqrt{-\frac{p_{\text{bat}}}{R_{\text{i,bat}}} + \left(\frac{E_{\text{oc}}}{2R_{\text{i,bat}}}\right)^2} \tag{6.7}$$

$$\xi_{\text{bat}}(n+1) = \xi_{\text{bat}}(n) - \frac{i_{\text{bat}}(n)}{C_{\text{bat}}} T_s \tag{6.8}$$

for $i_{\text{bat}} R_{\text{i,bat}} << E_{\text{oc}}$ we can observe that $v_{\text{bat}} \simeq E_{\text{oc}}$ and simplify (6.7) with a linearized function for the battery current

$$i_{\text{bat}}(n) \simeq \frac{p_{\text{bat}}}{E_{\text{oc}}} = \frac{p_{\text{load}}(n) - p_{\text{fc}}(n) - \frac{T_s}{2}\dot{p}_{\text{fc}}(n)}{E_{\text{oc}}} \tag{6.9}$$

We can rewrite the complete system dynamics as

$$[p_{\text{fc}}(n+1),\ \xi_{\text{bat}}(n+1)]^T = A[p_{\text{fc}}(n),\ \xi_{\text{bat}}(n)]^T + B\dot{p}_{\text{fc}}(n) + B_d p_{\text{load}}(n) \tag{6.10}$$

$$A = \begin{bmatrix} 1 & 0 \\ \frac{-T_s}{E_{\text{oc}} C_{\text{bat}}} & 1 \end{bmatrix} \qquad B = \begin{bmatrix} T_s \\ \frac{-T_s}{2E_{\text{oc}} C_{\text{bat}}} \end{bmatrix} \qquad B_d = \begin{bmatrix} 0 \\ \frac{T_s}{E_{\text{oc}} C_{\text{bat}}} \end{bmatrix} \tag{6.11}$$

6.3.4 Hydrogen Consumption

The hydrogen consumption of the stack is directly connected to the FC current $I_{\text{fc,in}}$, as laid out in [228]. In addition, hydrogen is lost due to hydrogen crossover and internal short-circuits in the cells [252]. On a system level, the FC consumes auxiliary power for its balance-of-plant, which depends on the operation of the system [6]. Since it is relevant for

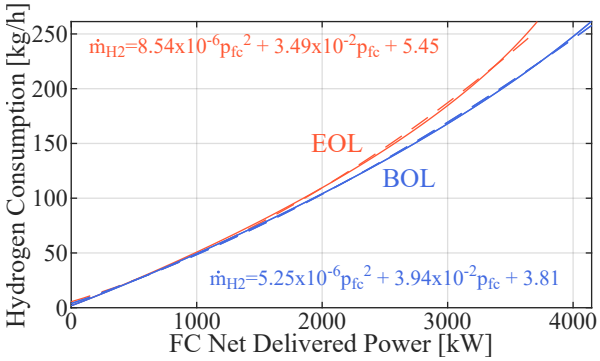


Figure 6.9: Hydrogen consumption and quadratic approximation for FC system at BOL and EOL

the power balance, this work regards the FC power p_{fc} as the net delivered power, which is the power delivered by the stack minus the auxiliary power.
For the optimization-based power system control, the hydrogen consumption can be approximated with a second-order polynomial as a function of net delivered power $\dot{m}_{\mathrm{H2}}(p_{\mathrm{fc}})$. The modeled hydrogen consumption and its quadratic approximations at BOL and EOL are shown in Fig. 6.9. The curves show the effect of degradation on the increased hydrogen need, which becomes especially apparent in the high power region.

6.3.5 Fuel Cell Degradation

Apart from the hydrogen consumption, a key performance indicator for the control is the FC degradation, affecting the state-of-health and lifetime of the PEMFC. PEMFC degradation is a complex combination of mechanisms, affected by several causes, which ultimately results into a decrease of the delivered output power. In this work, degradation is evaluated in terms of voltage decrease over time at a rated current. On an operational level, the load is considered the main cause affecting PEMFC degradation. To distinguish its effects on the PEMFC system, the load is typically broken down into three main categories, i.e., degradation arising from static operation, dynamic load changes, and system start-up cycles. In literature, different degradation rates are reported for operation in low and high current operation regions, and a considerably lower static degradation in between those regions. Representative degradation values and region limits are listed in Table 6.4. The change of degradation rate between the regions is approximated with a linear function around the region limit. To make the static degradation function easier to handle in an optimization, it is approximated via a second-order polynomial, enforcing its convexity over the power range. The static degradation of the FC over its operation range and its quadratic optimization at BOL and EOL are shown in Fig. 6.10. Since the power thresholds are relative to the maximum power, the curve is compressed towards the origin with increased degradation.
The dynamic degradation is a result of load changes. [253] reports an average of 19 μV per complete power cycle from idling to full power and back. No studies were made on the effect of the current gradient in dynamic degradation studies. However, we assume a quadratic relationship between the gradient and the degrading effect, meaning the faster

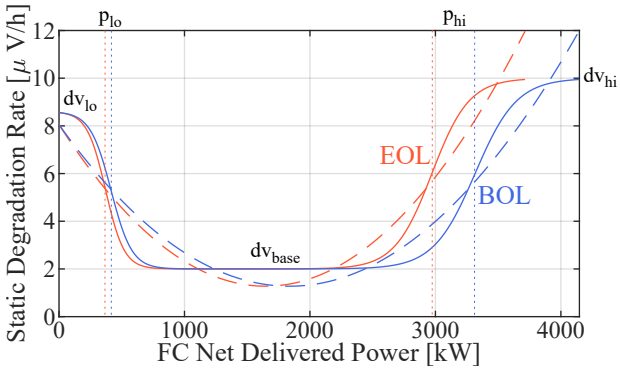


Figure 6.10: Cell-level static voltage degradation of FC system (solid) and approximation with second-order polynomial (dashed) at BOL and EOL

Table 6.4: FC Degradation Parameters (per cell)

Param.	Description	Value	Ref.
p_{lo}	Low power threshold	20 %	[6]
p_{hi}	High power threshold	80 %	[67]
dv_{hi}	High power deg. ($>p_{\text{hi}}$)	10.0 μV/h	[234]
dv_{lo}	Low power deg. ($<p_{\text{lo}}$)	8.6 μV/h	[234]
dv_{base}	Base degradation	2.0 μV/h	[235]
dv_{dyn}	Dynamic degradation	0.5·19 μV	[253]
dt_{dyn}	Reference ramp time	10 s	(assumed)

Table 6.5: Cost Parameters for hydrogen consumption and cell degradation

Parameter	Description	Value
c_{H2}	Hydrogen cost	8 €/kg
$c_{fc,capex}$	FC system cost	1500 €/kW
$r_{fc,stack}$	FC stack cost ratio	50 %
r_{eol}	FC power loss at EOL	10 %
c_{deg}	Degradation cost	50.6 €/μV

the change in output current, the higher the degrading effect of the dynamic change. For this study, we assume a reference time of 10 s at which the reported degradation rate is realized. Additionally, the dynamic degradation is scaled linearly for partial current cycles:

$$d\dot{V}_{dyn}(\dot{p}_{fc}) = \frac{dt_{dyn}\, dv_{dyn}}{P^2_{fc,max}} \dot{p}^2_{fc} := dv_{dyn2}\dot{p}^2_{fc} \tag{6.12}$$

Degradation due to start-up and shutdown cycles are disregarded in this study, since it is assumed that the FC is not switched during the operation, therefore not affecting the control scheme.

6

6.3.6 Cost Model

Hydrogen consumption and FC degradation are two objectives for the operation of the hybrid ship. It is essential to determine a suitable trade-off between these two for the design of the power system control. In this study, the related costs for both objectives are estimated to enable a comparison between the two. The cost estimate for hydrogen c_{deg} is straightforward since the fuel is a traded commodity.

The cost for degradation is more difficult to define. This study estimates it as the cost of reduced lifetime due to voltage degradation. Conventionally, a power loss of 10 % at rated current compared to a new system is proposed as the end-of-life of FC systems in heavy duty applications with a targeted lifetime of 25 000 h [251]. This is challenged by [254] as being too restrictive and, in dynamic applications, reached considerably earlier. Due to a lack of alternative standards, we use the limit of 10 % for this study. Accordingly, at reaching 90 % of its original maximum power rating, the FC stack needs to be replaced. The degradation-specific cost is estimated as the partial replacement costs due to operation-specific voltage degradation:

$$c_{deg} = \frac{r_{fc,stack}\, c_{fc,capex}\, P_{fc,max}\, N_s}{r_{eol}\, V_{fc,min}} \tag{6.13}$$

A comparison of hydrogen costs, static degradation costs and total costs from static operation of the FC system is displayed in Fig. 6.11. The cost parameters used in this study are listed in Table 6.5.

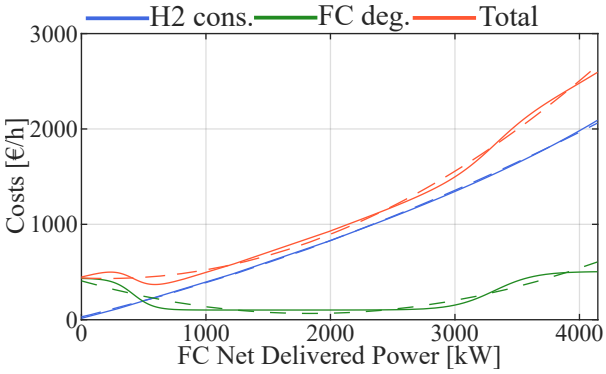


Figure 6.11: Cost curves of hydrogen consumption and static degradation. Model data (solid) and approximations with second-order polynomials (dashed) at BOL.

Table 6.6: Definition of parameters used in the fuel-cell cost model.

Symbol	Description	Unit
$r_{\text{fc,stack}}$	Fraction of total FC system cost attributed to the replaceable stack	–
$c_{\text{fc,capex}}$	Capital cost of the complete fuel-cell system	N/kW
$P_{\text{fc,max}}$	Rated maximum fuel-cell power output	kW
N_{s}	Number of cells per stack	–
r_{eol}	Relative power loss at end-of-life (EOL)	–
$V_{\text{fc,min}}$	Minimum cell voltage at EOL	V

6.4 Load Forecasting

This section deals with the problem of predicting the load power of the vessel for the future with a sampling frequency of 5 s, matching the data-logging rate of the original measurements. In particular, Section 6.4.1 will describe in detail the problem and the data available to address it while Section 6.4.2 will explain the proposed methods based on advanced ML techniques to solve the problem.

6.4.1 Problem Description and Available Data

The case study of this chapter examines a vessel featuring a hybrid propulsion system that includes diesel and electric power. The proposed methodology utilizes operational data logged by the vessel's automation system. The data under consideration comprises 5 million samples with a sampling rate of 5 seconds, spanning over one year of operational data, between 24th of April 2022 and 6th of May 2023. It consists of 18 input features, as presented in Table 6.7, where the feature total power (p_{tot}) is defined as the sum of power, i.e., the total power to be forecasted is obtained as

$$p_{tot} = (\gamma_{de,s} + \gamma_{de,p})P_{de,max} + \gamma_{aux}P_{aux,max} + p_{bat,s} + p_{bat,p}. \tag{6.14}$$

In this work, the vessel has been retrofitted as described in Section 6.2.2, and, as a result, only the information provided in Table 6.8 is available. Specifically, we assume that the retrofit to a fully electric configuration does not alter the vessel's operational profile. Consequently, parameters such as v, δ_p, δ_s, and p_{tot} are assumed to remain unchanged.
As a consequence, after the retrofitting, our scope is to predict, at time t_0, the p_{tot} for the next Δ^+ minutes with a sampling frequency of 5 s, i.e., $p_{tot}(t)$ with $t \in \{t_0 + 5s, t_0 + 10s, \cdots, t_0 + \Delta^+\}$, based on the information of v, $n_{prop,s}$, $n_{prop,p}$, δ_p, δ_s, and p_{tot} with $t \in [t_0 - \Delta^-, t_0]$ and Δ^- (see Section 6.4.2). Table 6.9 summarizes inputs and output of our TSF problem.

6.4.2 Methods

The problem in Section 6.4.1 can be effectively framed as a classical TSF problem [240–242]. TSF involves predicting future values of a variable of interest at time t_0, specifically for $t \in [t_0, t_0 + \Delta^+]$. The forecasting approach depends on the available information at time t_0. Predictions can be made based solely on the past values of the target variable (i.e., without covariates). Alternatively, forecasts can leverage both past values of the target variable and past and/or future values of related variables (i.e., with covariates). Including relevant covariates can improve forecast accuracy by providing context and capturing variations not explained by the target variable alone. In some scenarios, forecasts can be generated using only covariates if past values of the target variable are unavailable. In our specific case, as shown in Table 6.9, we have access to both past values of the target variable and past covariates.
As a first step, we tested a TSF method based on top-performing algorithms from different ML paradigms: Shallow ML (i.e., XGBoost [255]), Deep ML (i.e., Temporal Convolutional Networks - TCN [256]), and TSFMs (i.e., the TSFM proposed in [257]). The first two approaches were implemented using the Dart library [258], while the last one was implemented using the library released by [257]. Algorithms hyperparameter tuning (tougher with Δ^-) and performance evaluation, i.e., model selection and error estimation [259], were

Table 6.7: Load forecasting: available data on the original vessel.

Symbol	Definition	Unit
v	Vessel Speed	[knots]
$n_{prop,s}$	Propeller Speed - Starboard	[rpm]
$n_{prop,p}$	Propeller Speed - Port	[rpm]
$n_{em,s}$	Electric motor speed - Starboard	[rpm]
$n_{em,p}$	Electric motor speed - Port	[rpm]
$p_{em,s}$	Electric motor power - Starboard	[kW]
$p_{em,p}$	Electric motor power - Port	[kW]
$p_{bat,s}$	Battery power - Starboard	[kW]
$p_{bat,p}$	Battery power - Port	[kW]
ξ_s	State of charge - Starboard	[%]
ξ_p	State of charge - Port	[%]
$n_{de,s}$	Diesel engine speed - Starboard	[rpm]
$n_{de,p}$	Diesel engine speed - Port	[rpm]
n_{aux}	Auxiliary generator set speed	[rpm]
$\dot{m}_{de,s}$	Diesel fuel consumption - Starboard	[kg/min]
$\dot{m}_{de,p}$	Diesel fuel consumption - Port	[kg/min]
$\dot{m}_{aux}$	Auxiliary generator set fuel consumption	[kg/min]
$\gamma_{de,s}$	Diesel engine load - Starboard	[%]
$\gamma_{de,p}$	Diesel engine load - Port	[%]
γ_{aux}	Auxiliary generator set load	[%]
δ_s	Steering angle - Starboard	[°]
δ_p	Steering angle - Port	[°]
p_{tot}	Total Power	[kW]

Table 6.8: Load forecasting: available data after the vessel retrofitting.

Symbol	Definition	Unit
v	Vessel Speed	[knots]
$n_{prop,s}$	Propeller speed - Starboard	[rpm]
$n_{prop,p}$	Propeller speed - Port	[rpm]
δ_s	Steering angle - Starboard	[°]
δ_p	Steering angle - Port	[°]
p_{tot}	Total Power	[kW]

Table 6.9: Load forecasting: input and output of the forecast problem available at time t_0.

Input/Output	Symbol	Frequency	Time Span
Input	v	5 s	$[t_0 - \Delta^-, t_0]$
	$n_{prop,s}$		
	$n_{prop,p}$		
	δ_s		
	δ_p		
Output	p_{tot}	5 s	$[t_0, t_0 + \Delta^+]$

Table 6.10: Load Forecasting: MAE, MAPE, and PPMCC for XGBoost, TCN, TSFM, and XGBoost+TSFM for different time horizons.

	Model	**5s**	**1min**	**15min**	**30min**
MAE	XGBoost	0.23±0.02	0.23±0.02	2.31±0.25	28.74±3.26
	TCN	0.22±0.02	0.25±0.03	2.35±0.14	30.74±2.76
	TSFM	0.41±0.04	0.43±0.05	2.85±0.23	51.94±5.01
	XGBoost+TSFM	0.17±0.02	0.18±0.02	1.19±0.06	21.64±2.36
MAPE	XGBoost	1.2±0.1	1.6±0.1	4.4±0.5	58.0±5.9
	TCN	1.2±0.1	1.7±0.2	4.4±0.5	61.0±7.1
	TSFM	10.1±0.6	11.0±1.4	37.0±3.2	97.0±7.4
	XGBoost+TSFM	0.4±0.1	0.4±0.1	2.8±0.3	51.0±5.9
PPMCC	XGBoost	0.998±0.012	0.997±0.011	0.926±0.011	0.127±0.001
	TCN	0.999±0.008	0.998±0.009	0.928±0.010	0.129±0.001
	TSFM	0.986±0.009	0.985±0.007	0.877±0.009	0.099±0.001
	XGBoost+TSFM	0.997±0.009	0.998±0.013	0.938±0.008	0.139±0.001

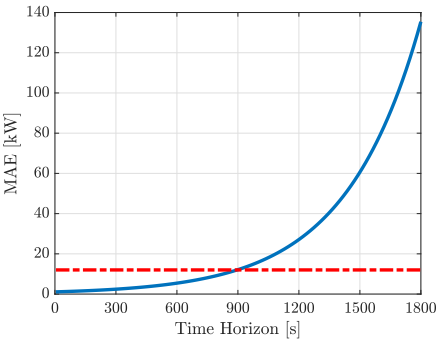


Figure 6.12: MAE varying the time horizon for XGBoost+TSFM.

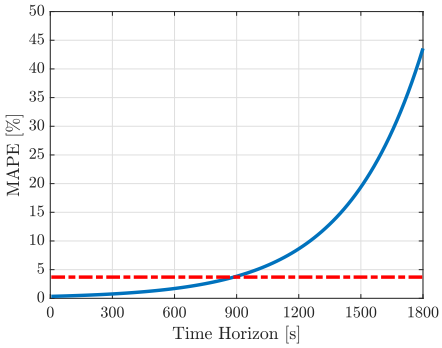


Figure 6.13: MAPE varying the time horizon for XGBoost+TSFM.

conducted using the standard temporal split of the train, validation, and test sets commonly applied in TSF [240, 243, 258]. The accuracy is evaluated using a combination of quantitative and qualitative metrics. The quantitative metrics include the Mean Absolute Error (MAE), the Mean Absolute Percentage Error (MAPE), and the Pearson Product-Moment Correlation Coefficient (PPMCC) [260]. The qualitative metrics comprise a scatter plot comparing actual versus predicted values [261], as well as an analysis of the real-time series behavior against the forecast generated by the best-performing model.

From the results of these models (Section 6.4.3), we observe that TSF methods based on XGBoost and TCN outperformed the TSFM-based approach, with XGBoost slightly surpassing TCN. Nevertheless, given the specific nature of our TSF problem, TSFM showed impressive performance. Consequently, we propose using the TSFM-based forecast as a future covariate for the XGBoost-based TSF method. This integration (see Section 6.4.3) leads to a notable performance improvement in the XGBoost-based TSF, confirming the potential of TSFM in real-world TSF applications. As a final remark, note that we set $\Delta^+ = 15\,\text{min}$ as, after that, the performance started to become too low to be used in practice.

6.4.3 Application to Case Study

In this section we will present the results of applying the method presented in Section 6.4.2 to the problem and data described in Section 6.4.1. As a first step, we report in Table 6.10 the MAE, MAPE, and PPMCC for XGBoost, TCN, TSFM, and the combination of XGBoost and TSFM for different time horizons. It is further possible to observe that XGBoost is the best-performing method among the base methods (XGBoost, TCN, and TSFM). Nevertheless, XGBoost+TSFM resulted in an improvement over the base methods. From Table 6.10, we also note that on the 30 min time horizon, the prediction starts to lose accuracy and therefore meaning. The increase of MAE and MAPE for an increased time horizon with XGBoost+TSFM is shown in Figs. 6.12 and 6.13, respectively.

To understand what time horizon can be considered meaningful, Figs. 6.12 and 6.13 show the dependency of MAE and MAPE on the time horizon for XGBoost+TSFM (best model according to Table 6.10). Figs. 6.12 and 6.13 indicate that 15 min (900 s) is the limit to have a reasonable error (around 10 kW and 5 %). For the sake of completeness we report in

Fig. 6.17 scatter plots and Fig. 6.21 the real versus predicted load for time horizons of 5 s, 1 min and 15 min with XGBoost+TSFM prediction (best performing model according to Table 6.10). From Figs. 6.17 and 6.21 it is possible to observe also qualitatively the very good agreement between the real values and the XGBoost+TSFM predictions on the considered time horizon.

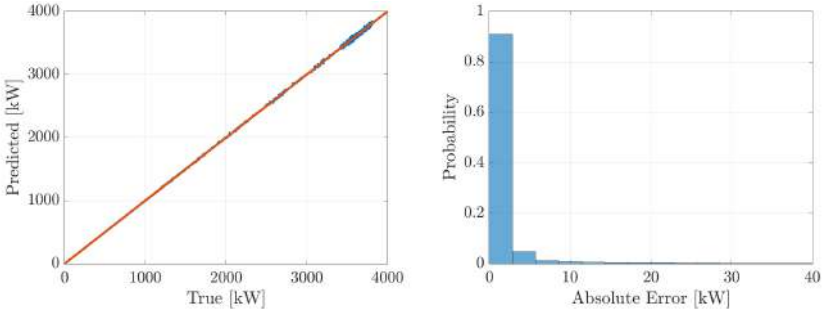


Figure 6.14: 5 s

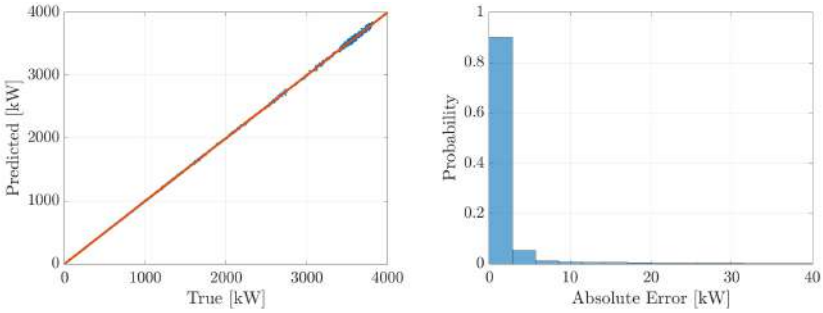


Figure 6.15: 1 min

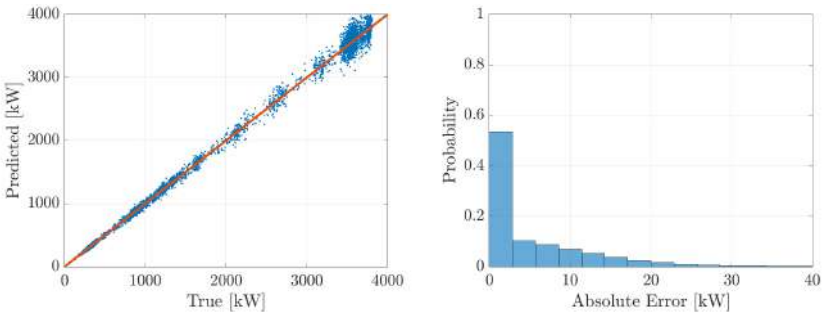


Figure 6.16: 15 min

Figure 6.17: Load Forecasting: Scatter Plot and histogram of the absolute error for time horizons of a) 5 s (a), b) 1 min, and c) 15 min for XGBoost+TSFM (best model according to Table 6.10).

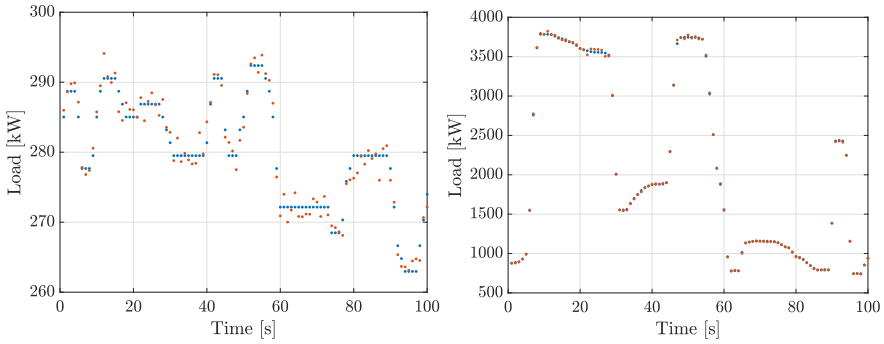


Figure 6.18: 5 s

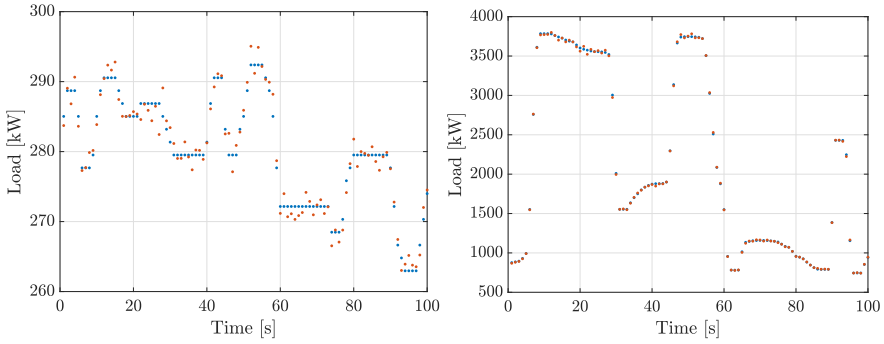


Figure 6.19: 1 min

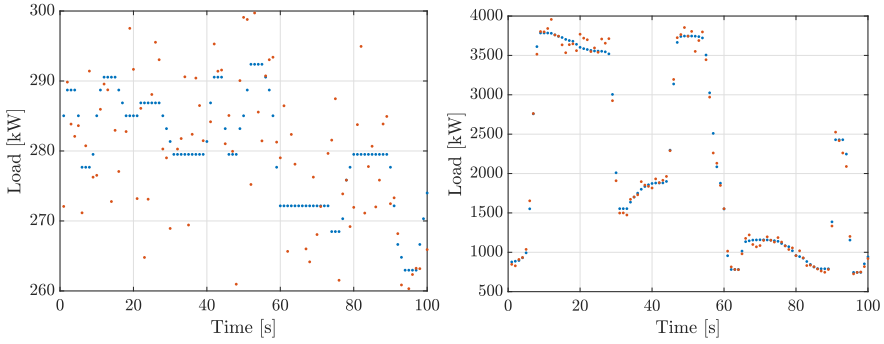


Figure 6.20: 15 min

Figure 6.21: Load Forecasting: real load (blue) and predicted one (red) with XGBoost+TSFM prediction (the best model according to Table 6.10) for time horizons of a) 5 s (a), b) 1 min, and c) 15 min at different regimes (left low load and right medium/high load).

6.5 Power System Control

This chapter describes the energy management strategies which are used in this work to minimize the operating costs accounting for hydrogen consumption and cell degradation mechanisms. The controlled system and centralized control architecture in this study is depicted in Fig. 6.23. First, a filter-based controller is introduced against which the optimization-based strategies are benchmarked. Next, a minimization problem accounting for the steady-state operating costs and the state-space model from Section 6.3 is constructed. Finally, ECMS-based approach is expanded to the predictive EMS which leverages the data-driven load forecasting from Section 6.4 and explicitly considers the dynamic costs and constraints of the system.

6.5.1 Filter-based Control

A virtual impedance-based controller for scalable FC-battery systems with DC distribution was presented in [200] and [212]. These works realized a filter-based power split between the power generation and energy storage modules, with additional control outputs for voltage restoration and SoC management. The filter-based power split and SoC management functionalities are implemented here as a benchmark control strategy. The FC's output power is determined based on the measured load power filtered through a low-pass filter such that

$$p_{\mathrm{fc}} = \frac{\tau_{\mathrm{fd}}}{s+\tau_{\mathrm{fd}}} p_{\mathrm{load}} + f(\xi_{\mathrm{bat}}) \tag{6.15}$$

where τ_{fd} is the tunable frequency decoupling time constant. Superimposed on the frequency decoupling is an SoC management strategy as laid out in [200].

6.5.2 ECMS

To determine an instantaneously optimal split between the FC and stored energy in the battery, a cost function needs to be defined. Originally, the ECMS approach assigns an equivalent fuel consumption to the energy stored in the battery [109]. Here, we instead define an equivalent cost, which allows to incorporate both the hydrogen consumption as

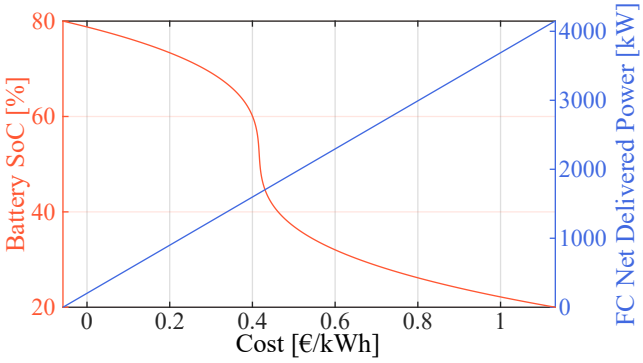


Figure 6.22: Equivalent cost of stored energy as a function of battery SoC versus marginal static cost of FC energy at BOL.

well as the FC degradation, thus making this approach health-aware. The power-dependent cost of the FC was already defined in Sections 6.3.4, 6.3.5, and 6.3.6.
The energy stored in the battery is assigned the equivalent cost λ. The optimal power split at a given time instance and load power is then defined by the FC power output minimizing the cost function

$$\min_{\dot{p}_{\mathrm{fc}}} f_{\mathrm{fc,stat}}(p_{\mathrm{fc}}) + \lambda \left(p_{\mathrm{bat}} + \left(\frac{p_{\mathrm{bat}}}{E_{\mathrm{oc}}} \right)^2 R_{\mathrm{bat,i}} \right) + \mu \dot{p}_{\mathrm{fc}}^2 \tag{6.16}$$

accounting for the system dynamics (6.10) and constraints (6.2, 6.3, 6.4). To avoid high FC power gradients and unstable dynamic behavior of the controller, an arbitrary dynamic cost μ is added to the optimization.

Equivalent Cost of Stored Energy

A further challenge for the ECMS algorithm lies in the limited energy that can be stored in the batteries. Accordingly, an additional SoC management strategy is required to avoid the violation of charge limits. This can be realized by adjusting the equivalent cost λ based on the SoC, such that ESS power is expensive at low and cheap at high charge.
Neglecting the dynamic cost μ and battery losses, the optimal power split for (6.16) lies in the intersection of the marginal cost of the FC $\frac{df_{\mathrm{fc,stat}}(p_{\mathrm{fc}})}{dp_{\mathrm{fc}}}$ with λ. Via an appropriate choice of $\lambda(\xi)$, we want to ensure that the FC power is maximal at the minimum allows charge ξ_{min}, and zero at ξ_{max}. Additionally, at a reference SoC-level ξ_{ref}, the corresponding value of $\lambda(\xi)$ shall be equal to the marginal FC cost at a reference power level $P_{\mathrm{fc,ref}}$. The function $\lambda(\xi)$ is therefore defined by the third-order polynomial displayed in Fig. 6.22 where

$$\lambda(\xi_{\mathrm{ref}}) = \frac{df_{\mathrm{fc,stat}}(P_{\mathrm{fc,ref}})}{dp_{\mathrm{fc}}} \tag{6.17}$$

$$\lambda(\xi_{\mathrm{min}}) = \frac{df_{\mathrm{fc,stat}}(P_{\mathrm{fc,max}})}{dp_{\mathrm{fc}}} \tag{6.18}$$

$$\lambda(\xi_{\mathrm{max}}) = \frac{df_{\mathrm{fc,stat}}(0)}{dp_{\mathrm{fc}}} \tag{6.19}$$

$$\frac{\lambda(\xi_{\mathrm{ref}})}{d\xi} = 0 \tag{6.20}$$

Dynamic Costs

The dynamic cost μ in (6.16) is intended to limit the magnitude of system inputs and avoid oscillations around an equilibrium point. Further, it is an implicit means to incorporate the cost of dynamic load changes. The formulation of the cost is similar to the dynamic cost in 6.12. However, μ must be considerably smaller than dv_{dyn2}, otherwise the full cost of the load change would outweigh the static components in (6.16), which only consider one time instant, yielding a sluggish controller.

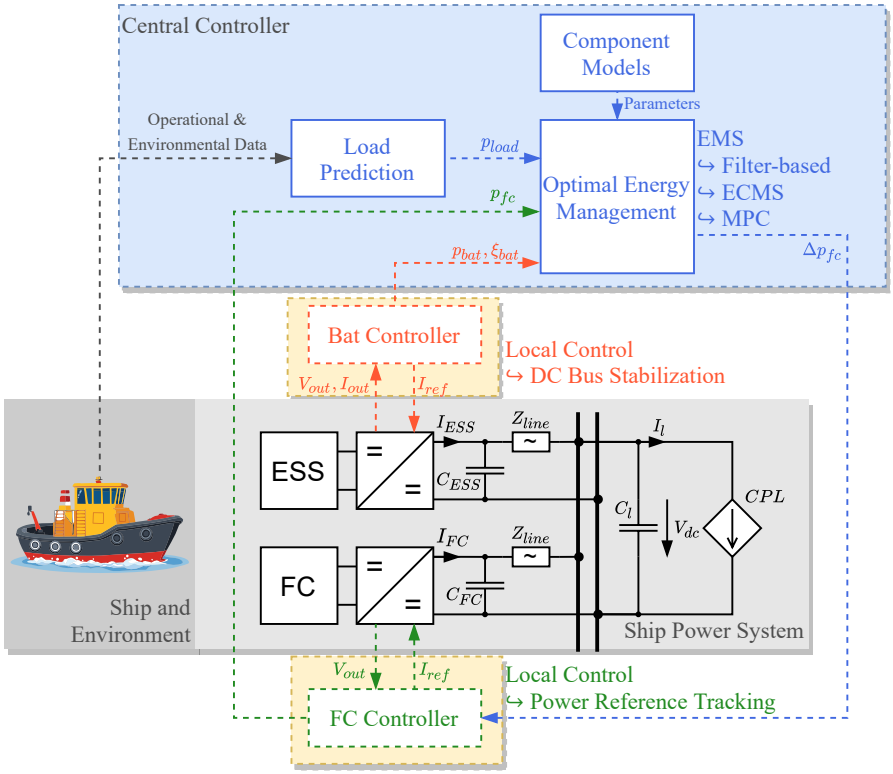


Figure 6.23: Depiction of the plant model and the control architecture for filter-based EMS, ECMS, and MPC including load predictions

6.5.3 MPC

Whereas the previous ECMS controller implements an instantaneous optimization, an MPC incorporates future inputs, states and disturbances as well. This section describes the formulation of the MPC for the energy management of the FC-hybrid vessel.

Optimization Problem

Given a prediction horizon N_{mpc}, an optimization time period of T_{mpc}, the optimal input $\dot{p}^*_{\text{fc}}(k)$ at time instance k solves the optimization problem

$$\min_{\dot{p}_{\text{fc}}} \sum_{n=k}^{k+N_{\text{mpc}}-1} T_{\text{mpc}} \Bigg(\left(f_{\text{fc,stat}}(p_{\text{fc}}(n)) + d\dot{V}_{\text{dyn}}(\dot{p}_{\text{fc}}(n)) + \lambda(\xi(k)) R_{\text{i,bat}} \left(\frac{p_{\text{bat}}(n)}{E_{\text{oc}}}\right)^2\right) - \lambda(\xi(k))\xi(k+N_{\text{mpc}}) E_{\text{oc}} C_{\text{bat}} \quad (6.21)$$

s.t. (6.2), (6.3), (6.4), and (6.10). For each time step n, the static and dynamic costs of the FC, as well as an equivalent cost for battery losses are considered. Additionally, the equivalent value of stored energy at time $k+N_{\text{mpc}}$ is implemented as a terminal cost. To avoid complex

non-linearities, the equivalent cost $\lambda(\xi)$ is evaluated for the SoC at time k rather than for each time instance, such that it is eliminated as a dependent variable. Doing so leaves only quadratic and linear terms in the cost function and linear constraints. Accordingly, this problem can be solved using quadratic programming. The optimization is run once per optimization time interval T_{mpc}.

6.6 Numerical Investigations

The described energy management strategies are implemented in a numerical simulation environment using MATLAB/Simulink. The settings for the simulation and the controllers are listed in Table 6.11. Several scenarios are tested to highlight the functioning principles and the performance of the different strategies. First, a rectangular load profile is applied to the system to highlight the working principles of the ECMS and MPC. Next, results of an exemplary mission profile for all strategies are shown for demonstrating the behavior of the respective approaches in real conditions and subsequently, aggregated results over all available mission profile are described. Finally, the effect of a variation of the prediction and control horizon on the performance of the MPC is analyzed to estimate the expected benefit of obtaining accurate predictions over a longer horizon.

6.6.1 Rectangular Load Profile

To highlight the functioning principles of the respective EMS implementations, a simple rectangular-shaped load is fed into the system. For this, we emulate a mission sequence from sailing to towing to sailing. From the load histogram in Fig. 6.2, we derive a power of 1300 kW during sailing and 3800 kW during towing. We consider a shortened duration of towing of 10 min, such that it falls within the prediction horizon and we assume a perfect power load prediction for this case.

The resulting power trajectories for the ECMS and MPC with 15 min prediction horizon are displayed in Figs. 6.24 and 6.25, respectively. The plots show both the full EMS implementations as well as a case in which the equivalent cost is not adapted to the battery SoC. For the MPC, an additional case is investigated in which the battery losses are ignored in the optimization problem.

With ECMS it can clearly be seen that the controller is acting only upon a load change. At the load step, the batteries are immediately compensating the load imbalance, while the FC

Table 6.11: Simulation Settings

Parameter	Description	Value
T_{sim}	Simulation step width	1 s
T_{ecms}	ECMS step width	5 s
T_{mpc}	MPC step width	30 s
N_{mpc}	Control horizon	30
μ	Dynamic cost in ECMS	$0.01\frac{dt_{\mathrm{dyn}}\,dv_{\mathrm{dyn}}}{P^2_{\mathrm{fc,max}}}$
ξ_{init}	Initial SoC	50 %

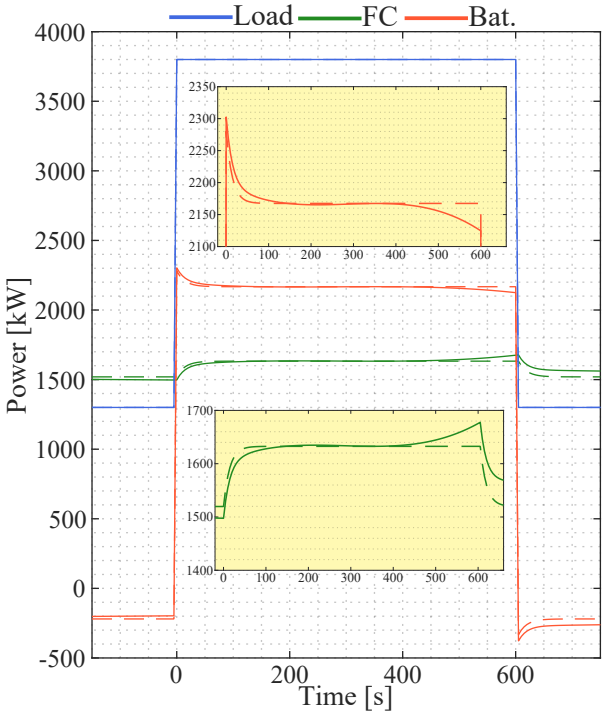


Figure 6.24: Power trajectories of FC and battery with ECMS for rectangular load shape with (solid) and without (dashed) SoC adaptation of equivalent cost. Zoom-ins (yellow-backed) on details of battery and FC trajectories.

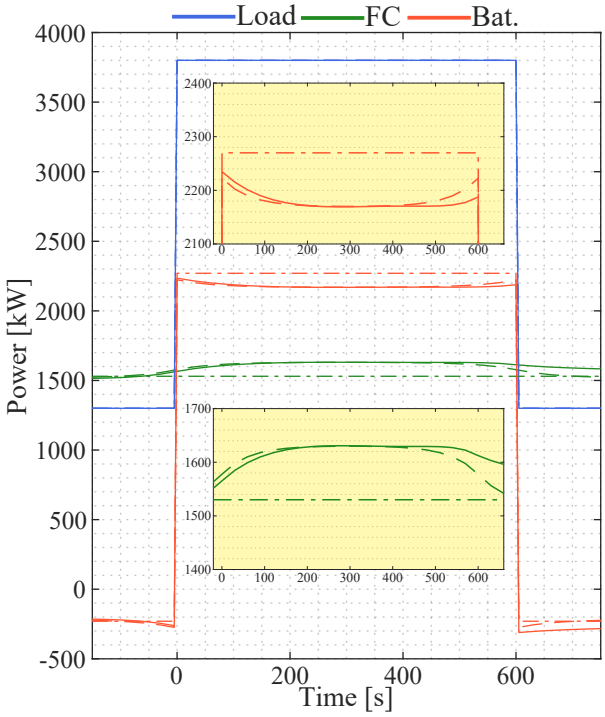


Figure 6.25: Power trajectories of FC and battery with MPC for rectangular load shape with cost adaptation (solid), without cost adaptation (dashed), and without cost adaptation plus disregard of battery losses (dash-dot). Zoom-ins (yellow-backed) on details of battery and FC trajectories.

increases its power to establish a cost balance. The speed of this adaptation is subject to the dynamic cost μ. Without a cost factor adaptation, the system stays in an equilibrium as neither the FC cost nor the battery cost change. With cost adaptation active, the FC power is constantly increasing to compensate the increased cost of stored energy due to a decreasing SoC. Over an increased amount of time, the FC power would be required to match the load power, while the SoC approaches its lower limit. After the negative load step it can be observed that the FC power is higher than initially, due to the lower SoC. Without SoC adaptation, the trajectories are symmetrical.

Employing MPC, the controllers act already before the load step occurs, anticipating the power imbalance. The trajectory smoothly approaches an equilibrium, limiting the power gradients of the FC. As with the ECMS, the cost factor adaptation leads to an asymmetrical power trajectory accounting for the decreased battery SoC. Without cost adaptation and additionally neglecting battery losses, the FC power is completely constant, since the prediction horizon is longer than the pulse. This showcases the fact that in the first two scenarios, the increase in FC power output is done to avoid increased costs of battery losses.

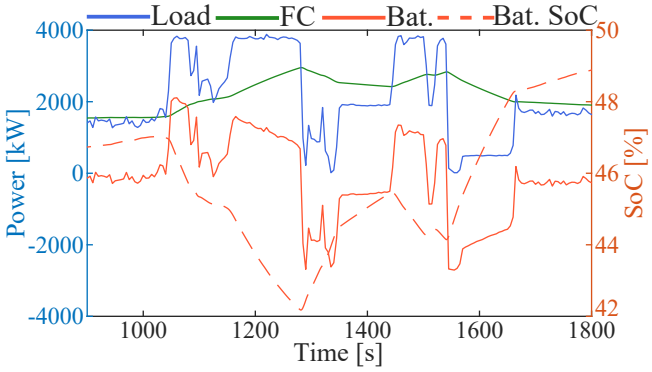


Figure 6.26: Power split between FC and battery, and battery SoC during high fluctuations with filter-based control and $\tau_{\mathrm{fd}} = 600\,\mathrm{s}$.

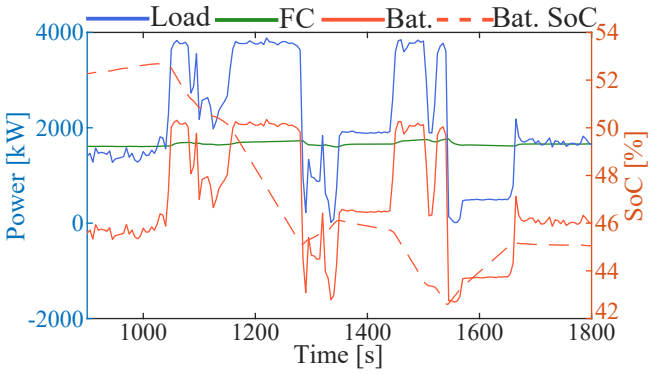


Figure 6.27: Power split between FC and battery, and battery SoC during high fluctuations with ECMS.

6.6.2 Mission Simulation

The application of the strategies is demonstrated with one exemplary mission profile. Figs. 6.26, 6.27, and 6.28 show the power trajectories during a mission phase with highly fluctuating loads. Fig. 6.29 shows the complete mission profile using MPC leveraging data-driven load predictions. The comparison shows that both optimization-based approaches yield a flattened FC power output, with clearly reduced fluctuations and peak value. The MPC further minimizes fluctuations compared to the ECMS-based controller such that fast fluctuations are almost entirely covered by the batteries.

To compare the performance of all strategies, the strategies are applied to all 167 available mission profiles, and their performance in terms of hydrogen consumption and FC degradation are compared, for BOL and EOL conditions. In total, the missions add up to a total operation time of 345.1 h. This time only accounts for active operation of the vessel and covers only the available measurements during the period described in Section 6.4.1. Fig. 6.30 shows a scatter plot indicating the results of all simulations at BOL for all described strategies, i.e. frequency decoupling with time constans of $\tau_{\mathrm{fd}} = 60\,\mathrm{s}$, $\tau_{\mathrm{fd}} = 600\,\mathrm{s}$, ECMS, and MPC with perfect and with data-driven load predictions. Fig. 6.31 shows the

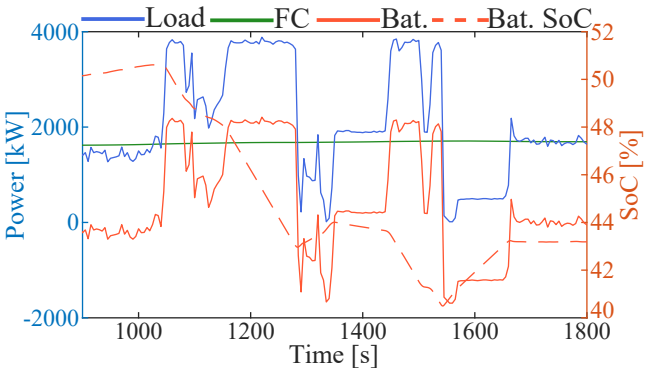


Figure 6.28: Power split between FC and battery, and battery SoC during high fluctuations with MPC and data-driven load prediction.

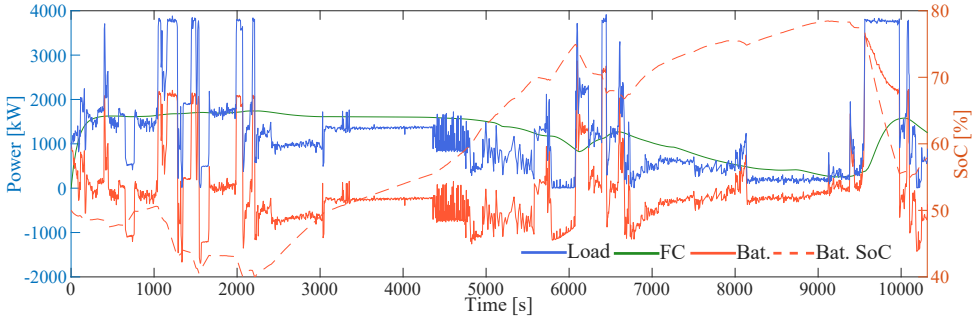


Figure 6.29: Power split between FC and battery, and battery SoC during mission simulation with MPC and data-driven load prediction.

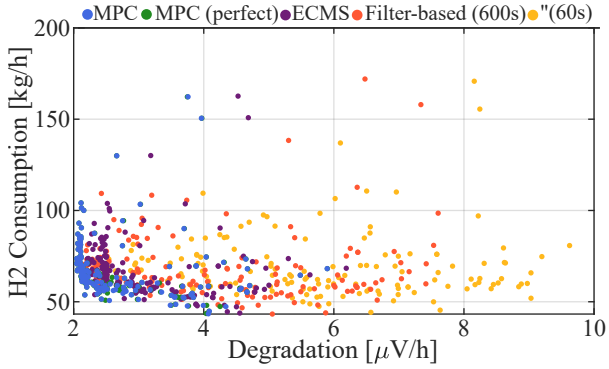


Figure 6.30: Hydrogen consumption rate versus fuel cell degradation rate for filter-based, ECMS, and MPC strategies for all mission profiles at BOL.

accumulated hydrogen consumption and degradation over all missions for these strategies. The comparison of simulation outcomes clearly shows the decrease in both cell degradation and hydrogen consumption that is achieved by the proposed strategies. At BOL, the benchmark controller with $\tau_{\mathrm{fd}} = 600\,\mathrm{s}$ yields 1422 μV cell degradation and 20.67 t hydrogen consumption, which is already a clear improvement over the faster filter-based controller (1838 μV;20.84 t). However, the ECMS (1041 μV;20.27 t) reduces these values by 26.8 % and 1.9 %, respectively. The MPC implementations with perfect prediction (946 μV;20.23 t) and data-driven prediction (945 μV;20.24 t) yield nearly identical results which are 33.5 % and 2.1 % under the benchmark. At EOL, it can be seen that the hydrogen consumption is generally higher. Whereas the filter-based approaches also show an increased degradation, the optimization-based approaches manage to limit or even reduce the latter. The MPC, compared to the benchmark, reduces total degradation by 36.4 %from 1460 μV to 928 μV and hydrogen consumption by 5.8 % from 22.35 t to 21.05 t. The results show that the proposed EMSs have high potential for improving the system performance, especially for the FC durability. Furthermore, the improvements become more significant when the FC's degradation is already in an advanced stage.

6.6.3 Variation of Prediction Horizon

As evaluated in Section 6.6.2, the results of MPC with data-driven load predictions are almost identical to those of MPC with assumed perfect predictions. This underlines the applicability of data-driven load predictions in real-time applications. In a next step, the effect of the prediction horizon on the control performance is analyzed. Since data-driven predictions are currently only available over 15 min, a comparison with a horizon of up to 60 min is conducted assuming perfect predictions. The results at BOL and EOL are shown in Fig. 6.32, indicating a significant boost in with an increased prediction horizon. At BOL with 15 min prediction horizon, a cell degradation of 945 μV and 20.24 t hydrogen consumption can be realized. An increased prediction horizon can decrease the degradation by up to 14.4 % to 809 μV and fuel use up to 3.6 % to 19.52 t with a 1 h horizon. At EOL the possible improvements are in a similar range with 14.0 % and 3.8 %, respectively. The graph shows that especially the degradation can be significantly lowered by including longer forecasting

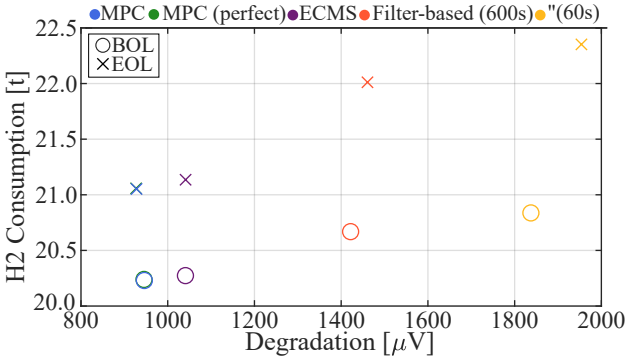


Figure 6.31: Cumulative hydrogen consumption versus fuel cell degradation for filter-based, ECMS, and MPC strategies over all mission profiles.

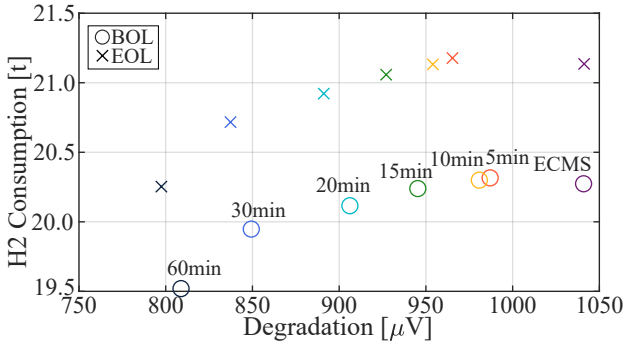


Figure 6.32: Cumulative hydrogen consumption versus fuel cell degradation for MPC with perfect prediction for varying prediction horizon.

periods. A prediction over 15 min has already been proven to be realistic in Section 6.4, while an increased horizon significantly increases the prediction error (Fig. 6.13). This comparison shows the expected benefits arising from an increased accuracy over longer horizons, e.g., due to more data or additional insights.

6.7 Conclusions

To increase the economic feasibility of FC-battery hybrid SPS, it is paramount to decrease its operating costs. A key factor in this is the design of the EMS, in which not only the hydrogen consumption but also the cell degradation, as a major contributor to the operating costs, must be considered. Leveraging data-driven load forecasting, this work implemented a degradation-aware predictive energy management that aims at minimizing the total operating costs of a zero-emission harbor tug. Using a degradation-aware equivalent cost approach for the instantaneous optimization of the energy management, a simultaneous decrease of both hydrogen consumption and cell degradation could be achieved compared to a filter-based benchmark. The data-driven load prediction, given the available data time-series of the tugboat, showed a fairly accurate load prediction with a MAPE of

2.8 % at 15 min. Leveraging this prediction, the degradation-aware predictive EMS yielded additional improvements in both fuel consumption as well as cell degradation over the ECMS-based method. It was further shown that an accurate load prediction over even longer predictions horizons of up to an hour could yield additional, significant performance gains. At an advanced aging state of the FC system towards its EOL, the relative difference in performance between the tested strategies increased, underscoring the potential benefits from the predictive strategy. By utilizing real measurement data and limiting the inputs to those available in the virtually retrofitted zero-emission tugboat, this work proved the real-time applicability of the predictive energy management in actual systems. This is essential to realize the expected reductions in fuel consumption and cell degradation, thereby lowering the operational costs and contributing to the cost-competitiveness of zero-emission ships.

For future work it is intended to expand this approach to further ship types. Whereas this study assumes a central control of a single FC and battery, larger system require the coordination of multiple parallel generation and storage devices. This will require to account for different component ratings and capabilities, potentially needing alternative control architectures, e.g. in a distributed architecture. Furthermore, this work expanded the equivalent cost approach of the ECMS to its MPC framework, including a terminal cost for the battery SoC. As a next step, it will be interesting to determine whether a multi-horizon approach with an outer mission-scale optimization will allow for an improved performance by computing a target SoC and on-off state of FC systems for the inner MPC. Whereas it seems that the minimization of both fuel consumption and cell degradation is favoring similar control strategies, i.e. steady operation within an efficient operation band, the inclusion of on-off switching of FC modules is expected to require a clearer trade-off between objectives. Furthermore, this work did not explicitly assign costs to the efficiency decrease due to degradation, but this warrants further exploration. In addition, the fixed 10 % performance drop for EOL definition of FCs is to be questioned for this application and instead be replaced by an optimization variable.

7

Distributed Energy Management for Modular Fuel Cell-Battery Power Systems

The previous chapter investigated a centralized controller for optimizing the power references for a fuel cell and a battery. This works well in such small scale power systems with limited number of components. This approach, however, is challenged in larger systems where communication-heavy computations come at a premium. Components do have individual characteristics and capabilities, and to include and update all of this information in a central controller becomes increasingly difficult. A system extension and reconfiguration after faults further complicates the energy management. In this chapter, I propose to solve this by introducing a distributed energy management architecture with a central coordinator to realize the same energy management strategy as before. However, the distributed architecture allows a plug-and-play extension of the system, a simple fault handling, and a local optimization of each module's power setpoint.

"Do not let your assumptions about a culture
block your ability to perceive the individual,
or you will fail."

— *Jasnah*, in *Words of Radiance*
by *Brandon Sanderson*

This chapter is submitted for publication with minor modifications as *Modular Energy Management via Distributed and Predictive Optimization for Fuel Cell-Battery Shipboard Microgrids, in: IEEE Open Journal of the Industrial Electronics Society, 2026* [262]

7.1 Introduction

The design of marine vessels sees a shift towards the electrification of the shipboard power system (SPS). An increased amount of different technologies is integrated into the system, such as fuel cells (FCs) [6, 68], energy storage systems (ESSs) [7], intermittent power generation, and electric propulsion [16], with a trend towards modularization and distribution of generation and storage units [263]. The increased system complexity makes the coordination of all energy resources a key challenge [100]. DC distribution technology is receiving interest as a solution to tie all different components together into a shipboard DC microgrid [10, 17]. Equipped with power electronics interfaces, the increased complexity of the shipboard microgrid can be met with the high controllability of power flows. Furthermore, increasing importance is attributed to the decarbonization of SPSs, for which hydrogen FCs offer a feasible approach [6]. Before this background, this article deals with the minimization of operational costs of hydrogen FC-based SPSs. The main drivers are the hydrogen cost and the effects of FC degradation [264], taking into account the unique challenges in maritime environments [265].

Automatic control for the energy management on-board maritime vessels is increasingly adopting optimization-based strategies[101]. The most widespread method for instantaneous optimization with a hybrid energy system (as described by [30]) is equivalent consumption minimization strategy (ECMS) [109]. For a diesel-hybrid tugboat, ECMS has been proposed in several works [127, 130]. [105] adopts this strategy for a hydrogen FC-based power system incorporating an additional cost-term for FC degradation. An adaptive ECMS implementation aiming for the modular integration of multiple FC and ESS modules is brought forward by [228].

However, the inherent drawback of this strategy is the neglect of any knowledge on future states and operation modes. An instantaneous optimization fails to properly account for dynamic costs and excludes insights on future disturbances, for which model predictive control (MPC) is a common solution [27]. Corresponding approaches in the literature differ strongly in their scope and time-scale. An ECMS that utilizes information (here: a target state-of-charge (SoC) for the ESS) from a mission-scale optimization, is developed by [140], shaping an example of long-term, static optimization. On the other end of the spectrum, [133] implements a predictive power management with short-term predictions for a diesel-hybrid tugboat, focusing on dynamic objectives. A multi-level MPC for efficient long-term power source dispatch and short-term dynamics is presented in [137], whereas the multi-level control by [53] focuses on generator set operation in DC SPSs. Predictive energy management, as opposed to the power management and low-level control loops, is often realized via a static, economic dispatch of power sources. The MPC in [134] features a static optimization for fuel consumption in a diesel-electric all-electric ship. For a similar vessel, [136] describes a two-level MPC where slow load fluctuations are handled by a static dispatch of generator sets and battery (dis-)charge. [239] implements a centralized, degradation-aware MPC for a hybrid tugboat, however only considering a single FC and battery, thus not incorporating different characteristics of parallel components. A further research trend combines the energy management strategy (EMS) with voyage scheduling or speed control in a hierarchical MPC [36, 38, 148].

One further aspect discussed in literature is the control architecture employed for the energy management. Generally, the EMS can be realized as a centralized optimization, assuming

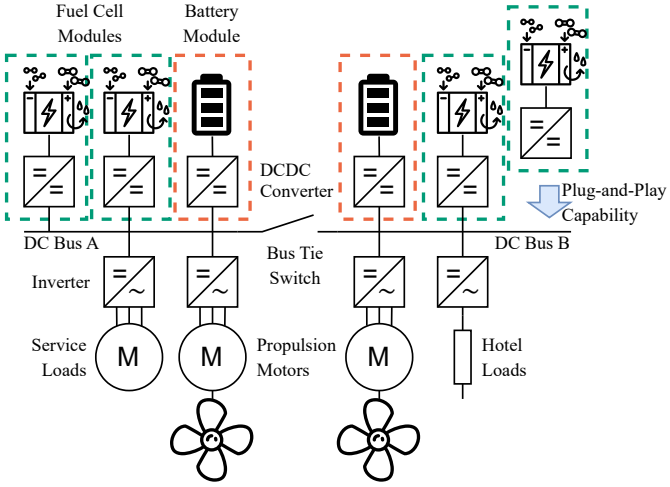


Figure 7.1: Modular FC-Battery Shipboard DC Microgrid with four FC modules and two battery modules

full knowledge of parameters and states of all components [239]. However, such a solution requires careful parameterization, a high computational burden, and lacks scalability [42]. An alternative lies in the shift towards a distributed architecture [45]. Distributed control and multi-agent systems offer increased resilience and survivability [43], and automatic reconfiguration capabilities [171]. [15] notes the plug-and-play characteristic of all-electric ships that facilitates the scalability of the power system. To this end, distributed control offers a suitable framework [166]. Moreover, local control algorithms for each agent may be highly complex and tailored to the source [163], which enables an adaptation to each component's characteristics. Based on these attributes, multi-agent systems meet the requirements for a modular control framework that handles a multitude of power system components with individual parameters [121]. Further advantageous features of the distributed architecture are the privacy-preservation [166] and the reduction of computational requirements in a centralized unit [45].

A multi-agent distributed control for the fuel consumption minimization with multiple diesel generators is investigated by [20]. [162] employs Lagrangian multipliers for the economic dispatch of generator sets and ESSs in a naval, all-electric ship. The authors note that the optimum is achieved when all units have the same marginal cost of power generation. Capitalizing on this, [153] utilizes the marginal cost of distributed generators as a consensus variable for distributed optimization in a microgrid, an approach which is applicable in both a federated and fully distributed architecture [44]. Multiple researchers present lambda iteration, a gradient-based method, to solve the Lagrangian dual decomposition. [154] presents this in a federated architecture for economic dispatch within a microgrid, while [155] showcases the use of lambda iteration in a fully distributed manner for managing various power generation and storage units. [173] employs this method to manage power exchange between microgrids, furthermore including loads and balancing the incremental cost per utility in the multi-microgrid system. [152] showcases that an approach based on Lagrangian decomposition is suitable for optimization in modular system topologies.

In SPS, distributed and multi-agent-based approaches have been applied to increase the resilience of naval ships [43] with a focus on power system reconfiguration [168], load management [175], and reserve power allocation [166]. Further research avenues delve into the coordinated control in DC SPS, dedicated to voltage regulation, accurate power sharing, and SoC balancing [20, 48] and power reference tracking [96]. For long-term objectives in ship energy systems, [20] utilizes a Lagrangian approach to balance the marginal cost of parallel diesel generators. [161] expands this approach to a ship-harbor energy system, leveraging the absence of a central coordinator. [176] uses a leader-follower approach for optimal distributed converter setpoints to achieve loss minimization and economic dispatch of parallel generators in an SPS.

In distributed optimization, the alternating direction method of multipliers (ADMM) [266] is often proposed as an alternative to lambda iteration, e.g., for the economic dispatch in microgrids [267]. An extension of this method to a multi-bus configuration is considered by[156]. ADMM is combined with a distributed resource allocation algorithm by [158] to include dynamic component characteristics in the optimization. A common prerequisite for both dual decomposition-based and ADMM-based consensus is the convexity of all local cost functions. As already shown in [239], the costs of FC and battery modules can be represented aptly via convex functions over their output power.

Combining distributed and predictive energy management [268] is receiving increasing interest for the control of SPS. For a fast-timescale subproblem, [97] implements distributed optimization via ADMM to ensure power servicing constraints. [165] employs ADMM for distributed MPC to manage the SoC of ESSs in a zonal SPS to minimize the load on generators with pulsed loads. For economic dispatch, [167] presents a static distributed optimization for an SPS using ADMM, leveraging short-term load forecasting. However, this work is not considering dynamic limitations and load fluctuations. [163] formulates an MPC aiming at fuel minimization while additionally including a battery degradation cost term. Coordination is realized via Lagrange multipliers while the authors note that local source-dependent optimization algorithms may be highly complex. An alternative approach to exact methods is offered via market- or auction-based algorithms which are less restrictive but compromise on the optimality of solutions [159, 160, 172]. Similarly, long-term dispatch is often approached via meta-heuristics, some of which can be implemented in a distributed fashion. [97] employs crow search for the distributed energy management in a multi-timescale strategy. For the same purpose, [93] implements a particle-swarm optimization.

For the modular integration of power generation and energy storage components in SPS, and specifically for the adaptive integration of multiple FC and ESS components with individual characteristics, the existing literature does not provide an EMS that matches the modular design and desired plug-and-play capability. Accordingly, this work proposes a distributed, model-predictive approach for the cost-optimal energy management in DC shipboard power systems with a modular FC-battery power system topology. To this end, we derive a distributed implementation of an optimization-based energy management which allows the integration of multiple power system components and an adaptation to their characteristics via local agents. In addition, the inclusion of load predictions in a predictive energy management allows for the anticipation and avoidance of increased operating costs due to dynamic operation, as well as an explicit formulation of operational

constraints. Finally, we define a localized decision-making heuristic for the state switching of FC modules, allowing a minimization of operating time and undesirable operating points. The proposed method is compared to a centralized MPC to evaluate the effect of the altered control architecture on the energy management performance. A demonstration at the example of a FC-battery hybrid tugboat highlights the benefits of a predictive, distributed and optimization-based energy management. For the use case both long-term simulation studies and control implementation on multiple real-time target machines, are presented.

The remainder of this chapter is organized as follows. Section 7.2 briefly describes the power system design and component models. Section 7.3 derives the proposed approach for the distributed ECMS and MPC for the control of modular FC-battery SPS and presents algorithms for the implementation in local and centralized controllers. In section 7.4, the performance of centralized and distributed energy management strategies as well as the performance of predictive control for different prediction horizons are evaluated numerically. This section further investigates the effect of local FC state decision-making. The deployment of the algorithms on real-time controller hardware and communication network is presented in section 7.5. Finally, section 7.6 reviews the contributions made in this work and gives an outlook on future research activities on this topic.

7.2 Modular Power System

We consider a shipboard DC microgrid whose primary equipment is comprised of parallel FC and battery modules that supply various power-controlled loads. Power generation and energy storage systems are connected to the DC bus via DC-DC converters, whereas loads are interfaced via inverters. Fig. 7.1 shows this topology, highlighting the plug-and-play characteristic offered by the DC distribution and power converters. The system model follows the approach described in [239].

7.2.1 Fuel Cells

Hydrogen proton exchange membrane FCs form the main power sources for supplying the SPS. Whereas these FCs convert hydrogen efficiently into electric energy, this efficiency drops with an increased power output. Hence, for the energy management it is a key challenge to keep the FCs within an efficient operating area. In addition, FC modules are subject to operation-dependent cell degradation, which decreases the performance and eventually requires a replacement of the affected stacks. In this work, we consider the cost of hydrogen, consumed by the FC modules, and the cost of degradation, necessitating a stack replacement, as the main drivers of operational costs for the vessel.

Table 7.1 lists hydrogen cost and degradation parameters used in this work, with values given in terms of units ([u]). The construction of the FC module degradation function is adapted from [121], and the calculation as well as the quadratic approximation of hydrogen and degradation costs are laid out in [239].

The FC and ESS (described below) modules are modeled via equivalent circuits, depicted in Fig. 7.2. The FC equivalent circuit consists of a current-dependent voltage source in series with an internal resistance. A degrading FC module is modeled through an increase of inner resistance, which leads to an additional drop of the module voltage proportional to its output current. The state-of-health of a module (given as a relative value) is reflected in

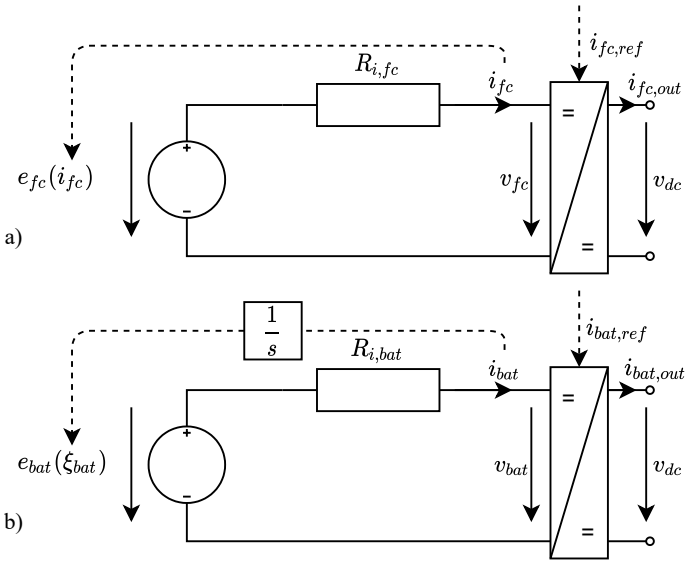


Figure 7.2: Equivalent circuit models including power converter for a) FC module, b) battery module, adapted from [239]

7

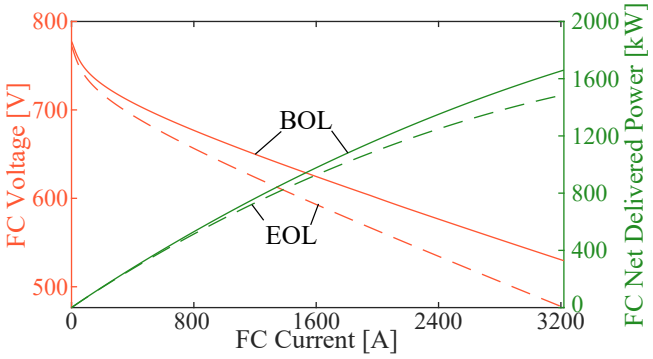


Figure 7.3: FC voltage and net output power as functions of output current at begin- and end-of-life, adapted from [239]

Table 7.1: FC Degradation Parameters (per cell), adapted from [239]

Param.	Description	Value
c_{h2}	Hydrogen costs	8 u/kg
$c_{\mathrm{fc,capex}}$	System cost	1500 u/kW
$r_{\mathrm{fc,stack}}$	Stack cost ratio	50 %
r_{eol}	Power loss at end-of-life	10 %
c_{deg}	Derived degradation cost	50.6 u/μV
p_{lo}	Low power threshold	20 %
p_{hi}	High power threshold	80 %
dv_{hi}	High power deg. ($> p_{\mathrm{hi}}$)	10.0 μV/h
dv_{lo}	Low power deg. ($< p_{\mathrm{lo}}$)	8.6 μV/h
dv_{base}	Base degradation	2.0 μV/h
dv_{sw}	Cyclic degradation	13.79 μV
dv_{dyn}	Dynamic degradation	0.5·19 μV
dt_{dyn}	Reference ramp time	10 s

the corresponding decrease of the module's output voltage at rated current relative to its value at begin-of-life (BOL). The voltage curve of an exemplary FC module at begin- vs end-of-life, based on manufacturer data from [218], is shown in 7.3.

7.2.2 Energy Storage Systems

Batteries are used as ESSs to complement the specific characteristics of FCs, as they are able to alter their power output quickly to match fast load power fluctuations [7]. Furthermore, ESS of sufficient sizing allow for load leveling and strategic charging, supporting the FC modules to operate in a more favorable operating points rather than following the load. However, a key challenge for ESS is the management of their SoC, as the amount of stored energy is a limited resource for the energy management. The equivalent circuit model of a battery, consisting of an SoC-dependent voltage source in series with an inner resistance, is depicted in Fig. 7.2.

7.2.3 DC System and Loads

The load power p_{load} is modeled as an external disturbance on the system. Its behavior is application-specific and differs in amplitude and volatility, among others factors. The power system components must be selected and sized appropriately for a given ship's load requirements. In this work, we consider a harbor tug boat, whose SPS design is detailed in [239].

The main constraint the energy system imposes on the control, is the power balance. This demands that the sum of all components' power outputs must equal p_{load} at all times. As the focus of this article is placed on the energy management, fast transients of the distribution system and power converter controls are neglected.

7.3 Modular Energy Management

This study focuses on the energy management task, responsible for determining the power dispatch for all power system components. This section introduces a generalized approach for the distributed optimization of the energy management in SPS with heterogeneous generation and storage modules with convex cost functions. For this, local optimizers for FC and battery modules, and a system-level coordinator are described. The approach is then extended into a predictive optimization framework. Finally, a non-convex decision-making heuristic is added to the EMS.

7.3.1 Instantaneous Optimization

We consider a power system equipped with a set of FCs I and a set of batteries J that make up all distributed generation modules ($I \cup J = M$). Each module's individual cost is a function of the system's parameters, states, and control inputs. Additionally, every component is subject to individual constraints, most notably on the power output, power gradient, and battery SoC. Each unit $m \in M$ has an individual cost function $f_m(p_m, x_m)$ that depends on is the unit's power output p_m (decision variable) and a state vector x_m. Power loads and intermittent generation pose disturbances on the power system that we aggregate as a scalar p_{load}.

Dual Decomposition

Regarding only one time instant, the energy management's goal is to minimize the total cost of power generation while meeting the power balance constraints:

$$\min_{p_m} \sum_{m \in M} f_m(p_m, x_m) \qquad s.t. \sum_{m \in M} p_m = p_{\text{load}} \tag{7.1}$$

This optimization problem is separable via dual decomposition [152], such that each unit solves a local optimization problem given a fixed Lagrange multiplier μ. The multiplier can be interpreted as a price for the output power. Each module maximizes its own utility, while respecting local constraints to maintain local feasibility:

$$\max_{p_m} \mu p_m - f_m(p_m, x_m), \forall m \in M \tag{7.2}$$

Local Optimization Problems

The operating cost of a FC module i is a function of its power level and power gradient, and incorporates both fuel costs as well as cost for the operation-dependent cell degradation. We formulate the costs as a time discrete function with an optimization time period Δt. Given the power $p_{i,k-1}$ of module i at time $k-1$ as a state, the cost function for transitioning to $p_{i,k}$ at the next time instant is

$$f_i(p_{i,k}, p_{i,k-1}) = k_{2,i} p_{i,k}^2 + k_{1,i} p_{i,k} + k_{0,i} + k_{d,i} \frac{(p_{i,k} - p_{i,k-1})^2}{\Delta t} \tag{7.3}$$

where $k_{x,i}$ are module-specific coefficients that realize a polynomial approximation of the actual costs. Fig. 7.4 shows exemplary static cost curves and their second-order polynomial

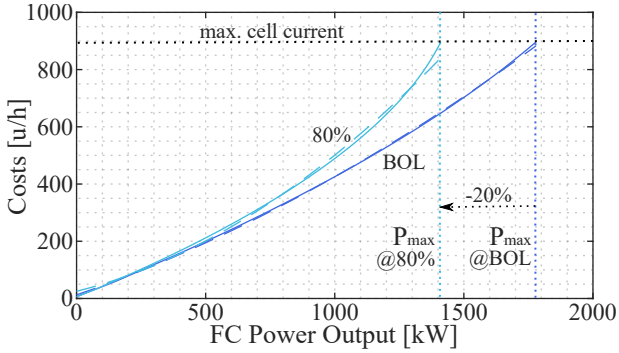


Figure 7.4: Cost model (solid) and second-order polynomial approximation dDashed) for PEMFC at BOL (blue) and 80% SoH (turquoise)

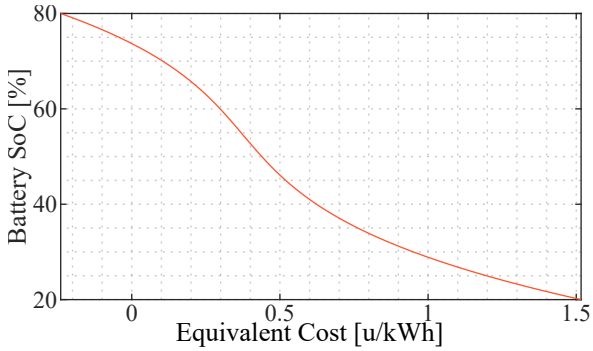


Figure 7.5: SoC-dependent equivalent cost of stored energy

approximations, of a new and an aged FC module. Note that the illustrated decrease to 80 % state-of-health is beyond the conventional end-of-life (EOL) definition of 10 % power loss [251].

Similar to a conventional ECMS-approach [109], the stored energy in an ESS is assigned an SoC-dependent equivalent cost. Fig. 7.5 shows an exemplary case of the value of stored energy. With this, we define the cost function of a battery as

$$f_j(p_{j,k}, \xi_{j,k-1}) = \lambda(\xi_{j,k-1})(p_{j,k} + k_{2,j} p_{j,k}^2) \tag{7.4}$$

which considers both the cost of discharge or revenue from charging, dependent on the sign of the power output, as well as quadratic power losses.

Using the local cost functions for FC and battery modules, a distributed ECMS can be derived via dual decomposition. Each FC module has a locally optimal power output $p_{i,k}^*(\mu_k)$ solving its specific optimization problem for the next time step k, and based on the current state variable at $k-1$:

$$\max_{p_{i,k}} \mu_k p_{i,k} - f_i(p_{i,k}, p_{i,k-1}) \tag{7.5}$$

The equivalent problem for a battery module yields $p^*_{j,k}(\mu_k)$:

$$\max_{p_{j,k}} \mu_k p_{j,k} - f_j(p_{j,k}, \xi_{j,k-1}) \tag{7.6}$$

It must be noted that all modules have additional local constraints on their power output range, power gradient (FC), and SoC range (batteries), that the local optimization steps are subject to.

Global Feasibility

For global feasibility, a central coordinator is required to adjust μ, functioning as a system wide price. All modules have convex cost functions, i.e., $p^*_{i,k}$ and $p^*_{j,k}$, and accordingly their sum, are monotonously increasing over μ:

$$\sum_{i \in I} \frac{dp^*_{i,k}}{d\mu_k} + \sum_{j \in J} \frac{dp^*_{j,k}}{d\mu_k} > 0 \tag{7.7}$$

Accordingly, using a gradient-based method, e.g. lambda iteration, lets us find a value μ^* that satisfies the power balance constraint:

$$\sum_{m \in M} p_m(\mu^*) = p_{\text{load}} \tag{7.8}$$

7.3.2 Predictive Optimization

Using time-series forecasting to predict the future load [108, 239], a set of predictions $\hat{p}_{\text{load},k} \forall k \in \{1, ..., N_\text{h}\}$ with prediction horizon N_h can be obtained. An expansion of the problem formulation for a series of discrete time intervals allows the optimization over the prediction horizon for the distributed system.

Local Optimization Problems

The instantaneous formulations of the local objective functions are extended to capture the costs of each module over a series of discrete time steps. Accordingly, the predictive objective functions for FC and battery modules are formulated as:

$$\max_{p_{i,k}} \sum_{k=1}^{N_\text{h}} \mu_k p_{i,k} - f_i(p_{i,k}, p_{i,k-1}) \tag{7.9}$$

$$\max_{p_{j,k}} \sum_{k=1}^{N_\text{h}} \mu_k p_{j,k} - f_j(p_{j,k}, \xi_{j,N_\text{h}}) + \lambda(\xi_{j,N_\text{h}}) E_{j,N_\text{h}} \tag{7.10}$$

where E_{j,N_h} and ξ_{j,N_h} are the terminal battery energy and SoC, respectively. $p_{i,0}$ denotes the FC power at time of optimization. Note that the battery cost function f_j takes the terminal SoC as an argument rather than the value corresponding to the respective time step. Eqs. (7.9) and (7.10), are subject to power and power gradient or SoC limits, as well as the module's state dynamics, as described in [239].

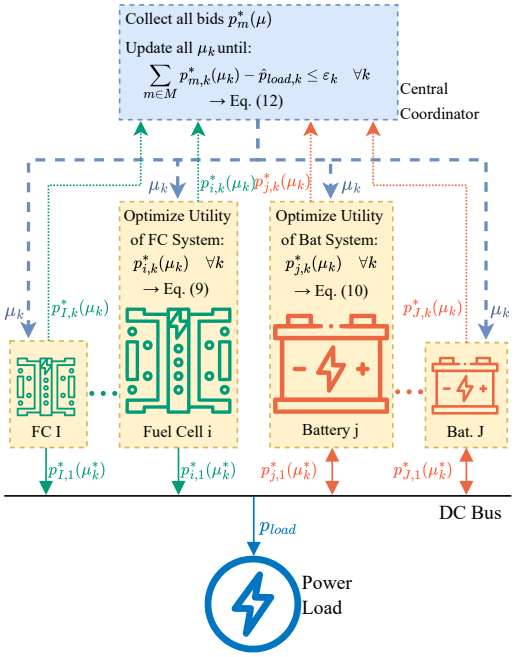


Figure 7.6: Control architecture for distributed optimization of modular FC-battery power system via price adjustment

Price Adjustment

We can interpret the local decision $p^*_{m,k}(\mu_k)$ as a power bid, responding to the externally set market price μ_k. It is the central coordinators' task to adjust the price such that the power balance constraint is fulfilled at each for each time step $k \in \{1, ..., N_\mathrm{h}\}$.. Due to the convexity of local functions, each μ_k can be adjusted via a gradient descent approach until the power balance constraint is fulfilled. I.e., there is an equilibrium for a vector of optimal Lagrange multipliers μ^*_k where the total distributed power generation $\sum_{m\in M} p^*_m(\mu_k)$ is equal to the load. With an iterative approach, we are looking for a value that is sufficiently close to this equilibrium:

$$\epsilon_k := |\hat{p}_{\mathrm{load},k} - \sum_{m\in M} p^*_m(\mu_k)| \leq \varepsilon \quad \forall k \in N_\mathrm{h} \tag{7.11}$$

where ε defines a small tolerance around the equilibrium.

The distributed MPC is solved iteratively following algorithms 1 and 2. Each μ_k is adjusted individually for time instant k until each module bids a discrete power trajectory such that the power balance constraint is below the tolerance threshold ε for each k. Accordingly, an individual market price is established at each time instant.

A generic FC-battery power system topology and the distribution of local and global optimization tasks is shown in Fig. 7.6. From the system perspective, the type and state of each unit is irrelevant as this information is included in the bids from each module. Hence, for the system level optimization it is sufficient to iteratively update μ_k until either a

convergence criterion is fulfilled or a maximum number of iterations is reached. The price adjustment algorithm, as shown in algorithm 1, is embedded in a central controller that broadcasts μ_k and sends a trigger signal to request power bids from all distributed modules. The parameter $\hat{\nabla}_\mu$ is a gradient estimate for the change in price over change in total power bid, α is a factor for the price adjustment step width, ε is the convergence tolerance, and it and $it_{\max}$ are iteration counter and maximum number of iterations, respectively. Upon receiving a trigger signal, each distributed unit updates its power bid according to algorithm 2. While not satisfying Eq. (7.11), μ_k is updated according to:

$$\mu_{k,it+1} = \mu_{k,it} + \alpha\hat{\nabla}_\mu\left(\hat{p}_{\text{load},k} - \sum_{m\in M} p^*_{m,k}\right) \tag{7.12}$$

where it is the iteration number of the update step. For gradient-based methods to work effectively, it is ideal to have the gradients at the current operating point available. To avoid a large amount of transmitted data, the distributed modules only share the bid for the currently shared price. It is then up to the central coordinator to update μ_k according to Eq. (7.11) while balancing convergence speed and stability. For this, it uses the estimate $\hat{\nabla}_\mu$, which approximates the average gradient over all k intervals:

$$E[\hat{\nabla}\mu] = \frac{1}{N_\text{h}}\sum_{k=1}^{N_\text{h}} \frac{d\mu_k}{dp_{\text{tot},k}(\mu_k)} \tag{7.13}$$

Algorithm 1 Price adjustment by central coordinator

Input: $p^*_{m,k}$, $\hat{p}_{\text{load},k}$
if New Optimization **then**
  $it \leftarrow 0$
  $\mu_k \leftarrow \mu^*_{k,\text{prev}}$ ▷ Start with Previous Equilibrium Price
  Send trigger **return**
end if
$\epsilon_k \leftarrow \hat{p}_{\text{load},k} - \sum_{m\in M} p^*_{m,k}$
if $\epsilon_k \leq \varepsilon \quad \| \quad it > it_{\max}$ **then**
  Stop trigger ▷ Converged or Max. Iterations Reached **return**
end if
$it \leftarrow it + 1$
$\mu_k \leftarrow \mu_k + \alpha\hat{\nabla}_\mu\epsilon_k$ ▷ Adjust Price
Send trigger **return**
Output: μ_k, trigger

Fuel Cell State Logic

In [269], it was generally assumed that all FC are switched on by default during a mission. To paint a complete picture of the power system operation, the start-up and shutdown of each FC module needs to be included in the energy management strategy. In [121] it has been shown that time-optimized on-off state switching of individual modules can significantly support in the reduction of cell degradation. To preserve the modularity of the distributed

Algorithm 2 Local bidding by distributed controllers

Input: μ_k, trigger

1: **if** trigger **then**

2: $p^*_{m,k} \leftarrow$ Eqs.(7.9) and (7.10) ▷ Optimal bid by Unit m

3: **end if**

Output: $p^*_{m,k}$

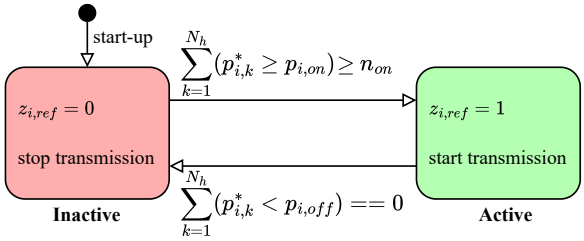


Figure 7.7: Local on-off switching logic for FC module

EMS in this work, we propose the implementation of a local state switching logic for each agent. In the distributed predictive EMS the state command $z_{i,\text{ref}}$ is determined based on the bids $p^*_{i,k}$ computed by each FC agent. The state reference must be computed outside of a regular optimization instance lest an integer-valued decision variable is introduced to the problem. Hence, the on-off decision is made only after an optimization sequence is complete, and is applied starting with the next optimization instance. The decision further needs to be subject to a hysteresis to avoid on-off toggling at each optimization instance.

The system switches on if the optimal bid $p^*_{i,k}$ is larger than the threshold $p_{i,\text{on}}$ in at least n_{on} prediction intervals. Contrary, the state reference toggles off when all $p^*_{i,k}$ are below a minimum value $p_{i,\text{off}}$. The state machine for each FC module is visualized in Fig. 7.7. While a FC module is off ($z_{i,\text{ref}} = 0$), the agent is not sharing its bids with the central coordinator. Thus, the module is not participating in the power dispatch. When the module switches off, it ramps down its power output with a fixed gradient.

7.4 Numerical Investigations

We investigate a tugboat whose power system design and operational data are described in [239]. The measurements have been cleaned and parsed into distinct mission profiles. For evaluating the performance of different strategies, we simulate the power system operation for a total of 167 missions recorded over the course of several months. The performance of a specific EMS implementation is evaluated based on the total accumulated cost for hydrogen consumption and degradation, using MATLAB/Simulink simulations. This section features a number of investigations that compare the performance of centralized and distributed architectures, and how different parameterizations of the distributed, predictive control can improve the performance.

7.4.1 Implementation

The implementation of the proposed EMS, low-level controllers, and power system simulations requires some considerations. These are described and evaluated in the following.

Time Scales: The distributed ECMS and MPC algorithms, low-level controllers, and possibly the power system simulation, require digital implementation. The various tasks of the simulation and control algorithms are running at different time steps, as listed in 7.2. The fastest dynamics are present in the simulation of the physical system and the primary control layer, running at T_{sim}. Testing on physical hardware presumably requires even faster low-level controllers, depending on switching frequency and current control bandwidths. Each optimization instance is initiated regularly with a time period T_{opt}. The MPC optimizes over N_{h} discrete intervals with an interval length of T_{mpc}. Each iteration of the distributed ECMS or MPC is completed at a rate of T_{com}, matching the communication bandwidth. The maximum number of iterations it_{max} is set such that an optimization instance is finished before the next optimization is triggered. To reduce the delay caused by a high number of iterations, all modules' power references are updated already during the optimization using the intermediate power bids of the ongoing optimization.

Initialization: A suitable initialization is crucial for the performance of the distributed optimization, considering the number of required iterations. While T_{opt} is significantly smaller than T_{mpc}, as realized in this work, an initialization with the final dual variables of the previous optimization instance is expected to minimize the number of required iterations. If T_{opt} approaches the value of T_{mpc}, an index shift or interpolation of values may lead to improved performance. For $T_{\text{opt}} = T_{\text{mpc}}$, the index shift for a new optimization would assign $\mu_k = \mu_{k+1} \forall k \in \{1, ..., N-1\}$.

Equivalent Cost Parameterization: As described in Section 7.3.1, the stored energy in batteries is assigned an SoC-dependent equivalent cost $\lambda(\xi)$. In the objective function (7.10), this term is a function of the SoC at the end of the horizon. Since the terminal SoC depends on the control input of all optimization intervals, the optimization complexity increases significantly. To mitigate this, λ is fed as a fixed parameter to the optimization, based on the terminal SoC of the previous optimization instance. This is viable, given that μ_k is updated in sufficiently small steps. Accordingly, difference of the terminal SoC between subsequent optimization instances, is minor. To further stabilize the behavior of the distributed optimization, λ is passed through a low-pass filter with a time constant of several seconds. Doing so avoids unstable bidding of multiple ESS. Otherwise, it is possible that ESS will alternate between extreme charge and discharge behaviors. Instead, the low-pass filter lets all ESSs find a consensus on an optimal terminal SoC, and thereby on an optimal equivalent cost of energy for a given optimization horizon.

Gradient Estimation: For a proper and stable convergence behavior, the update of the dual variables relies on the estimate of the global power bid gradient. In practice, the real gradient is unknown, unless explicitly shared by the agents, increasing the communication overhead and relaxing privacy conservation. In this work, the gradient is approximated based on the values of the dual variables and total power bids recorded over an optimization instance. Using these data-points, the gradient is approximated using linear regression with a least square error approach. To avoid unstable behavior, the gradient estimate is checked for feasibility and diffused with the previous gradient estimate.

The value of α must be smaller than 1.0. Values between 0.5-0.7 have shown adequate

Table 7.2: Default simulation and optimization parameters

Parameter	Description	Value
T_{sim}	Simulation step size	10 ms
T_{com}	Communication step size	100 ms
T_{opt}	Optimization step size	5 s
T_{mpc}	MPC optimization interval	30 s
N_{h}	Optimization horizon	30
ε	Constraint tolerance	10 kW
$it_{\max}$	Maximum iterations	45
α	Descent step size (decreasing)	0.7-0.07
$\xi_{\min}/\xi_{\min}$	Min./Max. battery SoC	20/80 %
$\dot{p}_{\text{fc,max}}$	Max. FC power gradient	$0.05\text{P}_i\text{SoH}_i\text{s}^{-1}$

convergence behavior. To further improve the convergence behavior by enforcing large steps in early iterations and smaller steps close around the solution, the step size is decreased for each iteration, with up to one order of magnitude at the final iteration.

Real-time power balancing: The EMS determines optimal power references for each module, averaged over the length of each MPC interval. In fact, the load changes continuous, yielding an imbalance between instantaneous demand and optimized power dispatch. This is compensated by fast-acting voltage controllers deployed in the battery modules, which realize the current sharing according to [187]. The battery modules dynamically adjust their available power based on their maximum rating and their power bid, and accordingly their power sharing gain is adjusted continuously to the operating conditions. It is key to do so for unpredicted load spikes not to lead to an overexertion of a battery system beyond its capacity.

7.4.2 Central vs Distributed

Initially, we consider a power system with only one FC and one battery, allowing the implementation of the centralized approach outlined in [239]. This source describes the power system design and a centralized ECMS and MPC for this case. The aim is to compare the performance of the centralized ECMS and MPC from [239] with the distributed strategy proposed in our study.

Fig. 7.8 shows the accumulated costs for hydrogen and cell degradation over all 167 simulated mission profiles. Results show nearly identical performance for centralized and distributed implementations of the MPC.

The comparison for ECMS strategies shows close results for the hydrogen costs. Only the degradation is higher with the distributed architecture, which can mainly be attributed to increased dynamic degradation effects. A reason for this lies in small deviations between consecutive optimization instances due to numerical tolerances in the convergence algorithm. This can be alleviated by tightening such tolerances at the expense of convergence behavior. However, results show that this is not present with the predictive strategy, which is the primal subject in this investigation.

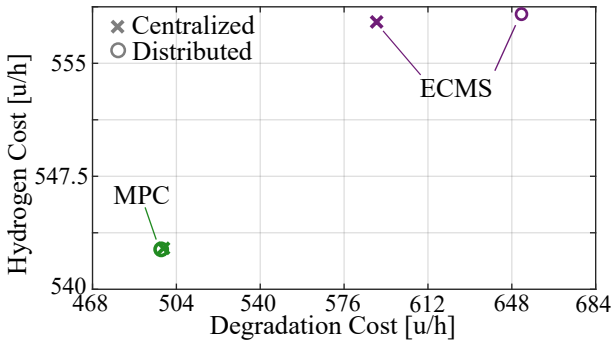


Figure 7.8: Hydrogen and degradation costs for all mission profiles with centralized versus distributed implementations of ECMS and MPC

This comparison underscores the ability of the distributed architecture to produce the same performance as a centralized implementation, but with the added benefits of the distributed architecture.

7.4.3 Modular System Topology

Next, we consider a system layout that reflects the modular design of modern, zero-emission SPS. The power system is equipped with four FC modules and two battery energy storage systems. Each FC module has an individual power rating and aging state, influencing its polarization curve. Each battery has an individual capacity and differs in cell-specific internal resistance. Accordingly each unit's cost function is unique, which should be reflected in its operation. The parameters of the system components are listed in Table 7.3. Conventionally, FC systems are considered to reach their end-of-life at 90 % state-of-health [251]. However, to explore further operation of modules beyond this point and to highlight discrepancies between local cost functions, we include FC modules who have passed the conventional end-of-life threshold.

7.4.4 Predictive Optimization

The results of one exemplary mission profile using the distributed MPC with a prediction horizon of 15 min are shown in Fig. 7.9. It can be seen that the FCs operate according to their respective marginal cost curves, whereas the power gradients are kept relatively low (Fig. 7.9b). Among the batteries, the SoCs are kept balanced while it is evident that battery B, which has a lower resistance relative to its capacity than battery A, is used more dynamically (Fig. 7.9c). The evolution of the optimal price in Fig. 7.9d gives an indication of the marginal energy cost at a given point in time. The bids for time instances over the prediction horizon additionally give an indication of the future cost. The latter can potentially serve as an input for the load management. Finally, Fig. 7.9e shows that the number of iterations required for completing each optimization is low, meaning that the needed data traffic and computational effort is within reasonable limits.

A reliable load forecast over 15 min has been proven possible in [239]. To gauge the potential benefits of an increased prediction horizon, Fig. 7.10 shows the costs with MPC

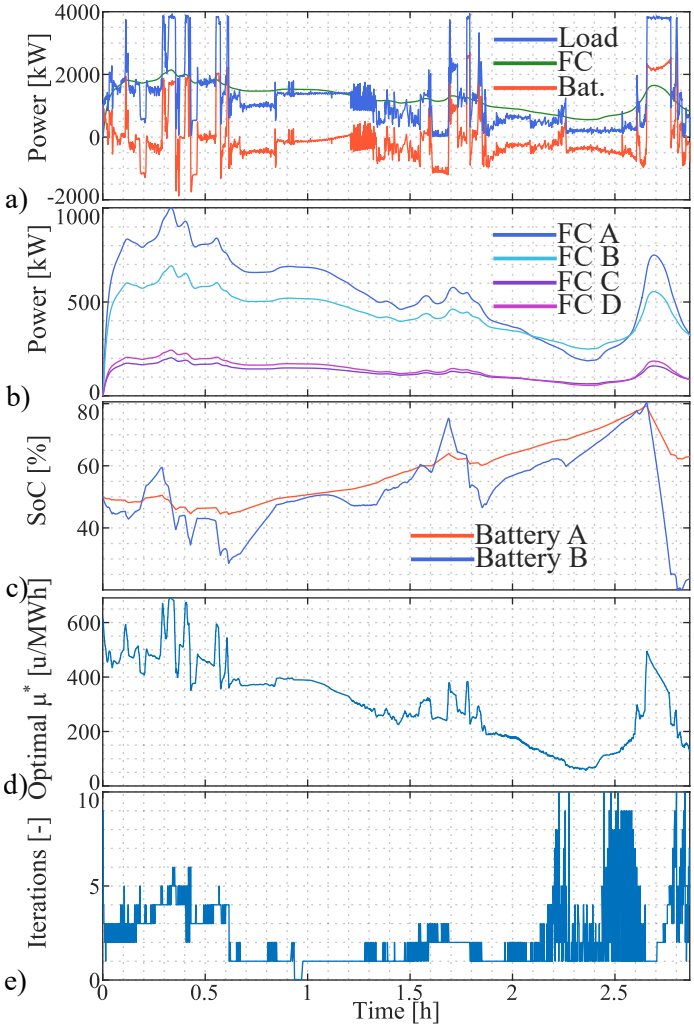


Figure 7.9: Exemplary results for one mission profile with distributed MPC with 15min load forecasting, showing a) the total power split, b) FC power per module, c) battery SoC per module, d) the optimal price, e) iterations required for solving the optimization.

Table 7.3: FC and battery parameters of modular power system

Parameter	Description	Value
$P_{\mathrm{fc,A}}$	Max. power FC A at BOL	1780 kW
$SoH_{\mathrm{fc,A}}$	State-of-health of FC A	100 %
$P_{\mathrm{fc,B}}$	Max. power FC B at BOL	1780 kW
$SoH_{\mathrm{fc,B}}$	State-of-health of FC B	80 %
$P_{\mathrm{fc,C}}$	Max. power FC C at BOL	445 kW
$SoH_{\mathrm{fc,A}}$	State-of-health of FC A	85 %
$P_{\mathrm{fc,D}}$	Max. power FC D at BOL	445 kW
$SoH_{\mathrm{fc,D}}$	State-of-health of FC D	95 %
$E_{\mathrm{bat,A}}$	Energy capacity battery A	1000 kWh
$R_{\mathrm{i,A}}$	Inner resistance battery A	19.2 mΩ
$E_{\mathrm{bat,B}}$	Energy capacity battery B	250 kWh
$R_{\mathrm{i,B}}$	Inner resistance battery B	15.4 mΩ

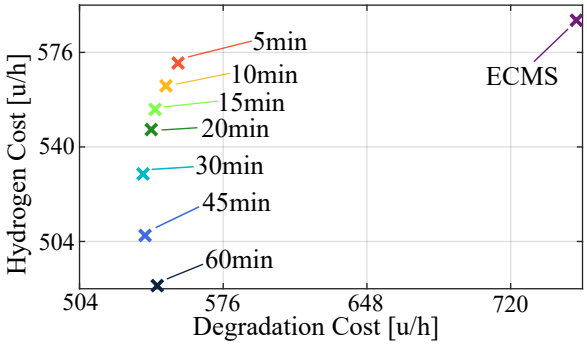


Figure 7.10: Accumulated hydrogen and degradation costs with distributed ECMS, and distributed MPC with different prediction horizons

for varying prediction horizons. The results show that the performance improves with an increasing prediction and optimization horizon. The differences are quite small between horizons of 5 min and 15 min. However, longer horizons promise significant gains for this specific case study. This highlights the importance of long prediction horizons for improving the operational efficiency of modular SPS.

Fig. 7.12 compares the time-series of load power vs total FC power and battery SoC for ECMS versus MPC with 15 and 60 min horizons. Fig. 7.12a shows how volatile the power output of the FCs is when using an instantaneous optimization, which immediately reacts to load changes. A predictive EMS flattens the FC power with an increasing horizon. In addition, with 60 min of prediction and optimization, the power output stays closer to the average required power than with a shorter horizon, which is more efficient with a quadratic cost function. The longer the horizon, the more extensive and effective the strategic charging of the ESSs can be realized (Fig. 7.12b).

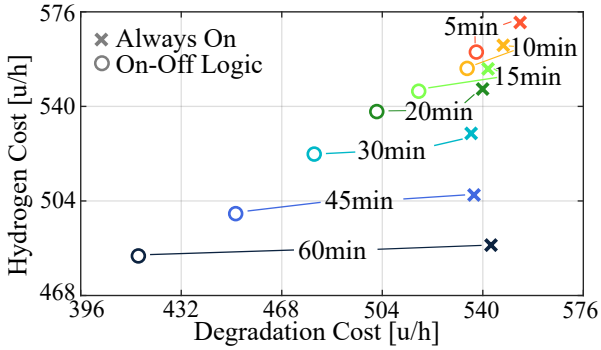


Figure 7.11: Accumulated hydrogen and degradation costs for distributed MPC with and without local on-off switching

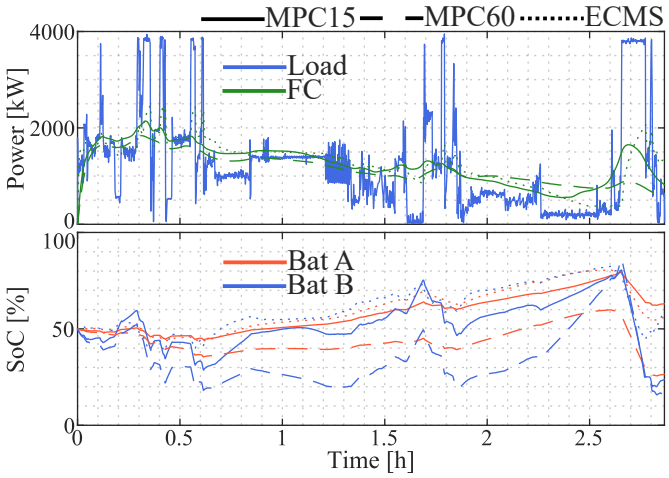


Figure 7.12: Time-series of simulation results for ECMS, and MPC with 15min and 60min horizon, showing a) Total FC vs. load power, b) SoC in the ESSs

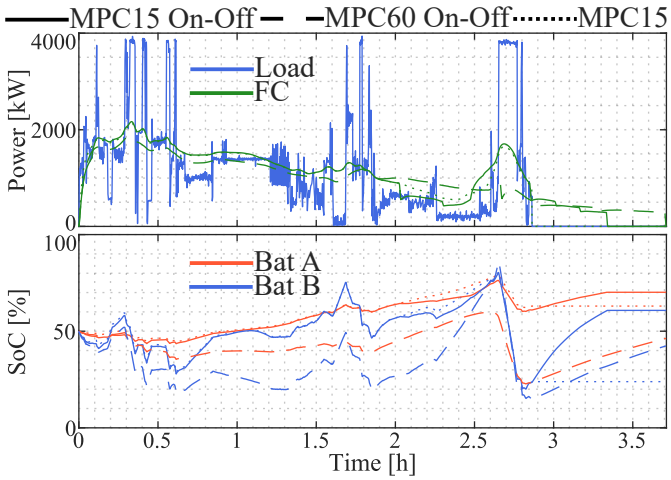


Figure 7.13: Time-series of simulation results for MPC with 15min horizon versus MPC with 15min and 60min horizon and individual FC state switching, showing a) Total FC vs. load power, b) SoC in the ESSs

Table 7.4: FC state switching heuristic parameterization

Parameter	Description	Value
$p_{i,\text{on}}$	On switch power threshold	$0.5\text{P}_i\text{SoH}_i$
$n_{i,\text{on}}$	On switch sample threshold	$\lceil 0.2N_\text{h} \rceil$
$p_{i,\text{off}}$	Off switch threshold	$0.2\text{P}_i\text{SoH}_i$

7.4.5 Individual FC State Switching

To assess the effect of allowing an individual on- and off switching of FC modules according to the method described in section 7.3.2. The parameters used for implementing the state switching heuristic are listed in table 7.4.

The graphs in Fig. 7.13 show a comparison of the distributed MPC with 15 min prediction horizon versus the MPC with added individual state-switching for horizons of 15 and 60 min. The comparison between the strategies with 15 min prediction horizon shows an overall more dynamic operation of the FC generation when enabling the state switching. The difference lies therein that the state switching is used for achieving the dynamics, whereas the strategy with all system on is required to apply higher power gradients to achieve the dynamics. Further, the state switching allows operation at lower total loads without running individual modules at detrimental low power outputs. The new strategy with the 60 min prediction horizon shows a very flat FC generation, and an overall lower average FC loading, resulting in higher efficiency. This also results in lower SoC of the batteries due to the decreased marginal cost of power generation. At the end of the mission profile, the switching logic allows to run FC modules longer for replenishing the battery charge. It must be noted that the final SoC is subject to the switching heuristics and not a result of a deterministic target value.

Fig. 7.14 shows more detailed results for the same mission with the 15 min MPC including state-switching. The time-series plots show clearly when each module switches on and off. The EMS allows a late start-up, an early shut-down, as well as an intermittent off-period for each module, as can be observed here. Further, the simulation is extended until all modules are switched off. Additional benefits from the on-off switching are the avoidance of very low FC loadings, as well as an improved convergence behavior in these operation zones. The graphs lay out in detail when individual modules are switched on and off, and what the effects are on power balance and on the equilibrium market price.
The cumulative results for all missions are shown in Fig. 7.11. This plot not only portrays the improvement of both hydrogen consumption and degradation for all horizons due to the added state-switching, but also the stark reduction in degradation costs with increasing horizon length. With the modules always on, only the hydrogen consumption saw high reductions with increasing length.

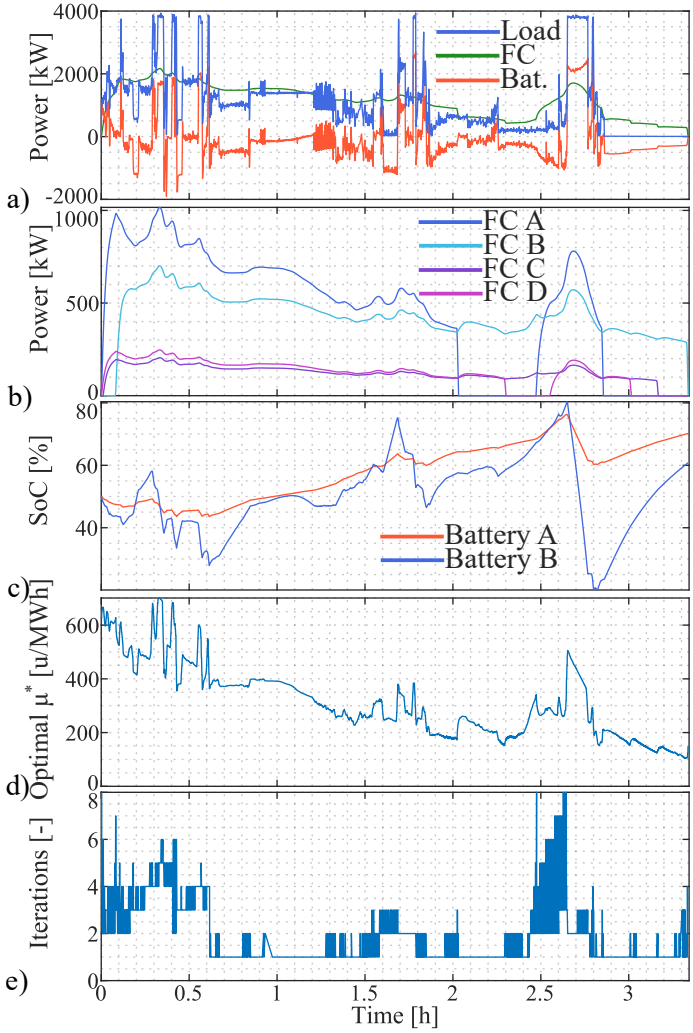


Figure 7.14: Exemplary results for one mission profile with distributed MPC with 15min load forecasting and individual on-off switching, showing a) the total power split, b) FC power per module, c) battery SoC per module, d) the optimal price, e) iterations required for solving the optimization.

7.5 Real-Time Controller Deployment

To demonstrate the application of the distributed energy management algorithm on multiple hardware components, we deploy the controllers on two real-time target machines (RTTMs) from Speedgoat. A schematic of this setup is displayed in Fig. 7.15.
The functional code on one machine, the Speedgoat Performance RTTM, is split into two parts, which run in parallel but without sharing any signals. On one part, we deploy the central coordinator that runs Algorithm 1 together with function which supplies the load predictions. On the second part, the power system simulation, including primary control loops, is realized. The second machine, the Speedgoat Baseline RTTM, runs all local agents. These run in parallel, without exchanging any signals between agents.
Communication between the machines is realized via UDP/IP over Ethernet. We connect two distinct communication lines for system level interaction, i.e. agent to central coordinator, and local interfaces, i.e. agent to component. The system level communication transmits the signals between agents and central coordinator, which are required for the algorithms 2 and 1. Over the local communication line, the agents send power references, and state references for the FC to their respective local control loops. The agents receive power, SoC and fault signals back, which they require for updating their local cost functions.

7.5.1 Optimal Dispatch

For testing the distributed optimization in real-time, we subject the power system to a load step. At time $t = 600\,\mathrm{s}$, the power steps up from 1300 kW to 3800 kW, which corresponds to an operational transition from transit to high assist. For the ease of demonstrating the predictive EMS, we limit the number of MPC intervals to $N_\mathrm{h} = 10$ and set the interval width $T_\mathrm{mpc} = 30\,\mathrm{s}$, resulting in a prediction horizon of 5 min. Further, the frequency of optimization instances is reduced with $T_\mathrm{opt} = 10\,s$. To showcase the convergence of the iterative optimization algorithm, all μ_k are initialized with the first element μ_1 at which the previous optimization instance has converged. It must be noted that this initialization method, as well as the reduced optimization frequency requires a higher number of iterations, compared to the approach described in section 7.4.1. Furthermore, we trigger a fault in FC A to capture the system response to a component fault at high, constant load. The power sharing between accumulated FC and battery power outputs against the load is displayed in Fig. 7.16.
The graph shows the power step occurring at 600 s. Before 300 s, the load steps enters the load prediction horizon. Before this time, only FC A has been active and slowly approached a quasi-static power sharing with the batteries. After, the FC power ramps up and the other FC modules sequentially switch on to supply the anticipated power load. At the time of the load step, only the batteries immediately adjust their power output to the new operation point, while the FC systems continue to increase their load. At 850 s, the FC systems supply the largest share of the load when a fault in FC A is triggered. Accordingly, the total FC power drops instantly. Immediately afterwards, the batteries compensate for the loss of generation and over minutes afterwards, FC and batteries find a new, efficient power dispatch. As a final note, it can be seen that the batteries' actual output power differs from the optimal reference values in-between optimization instances, and around high load steps. This is due to the batteries being utilized for instantaneous load-balancing as well as the limited optimization frequency.

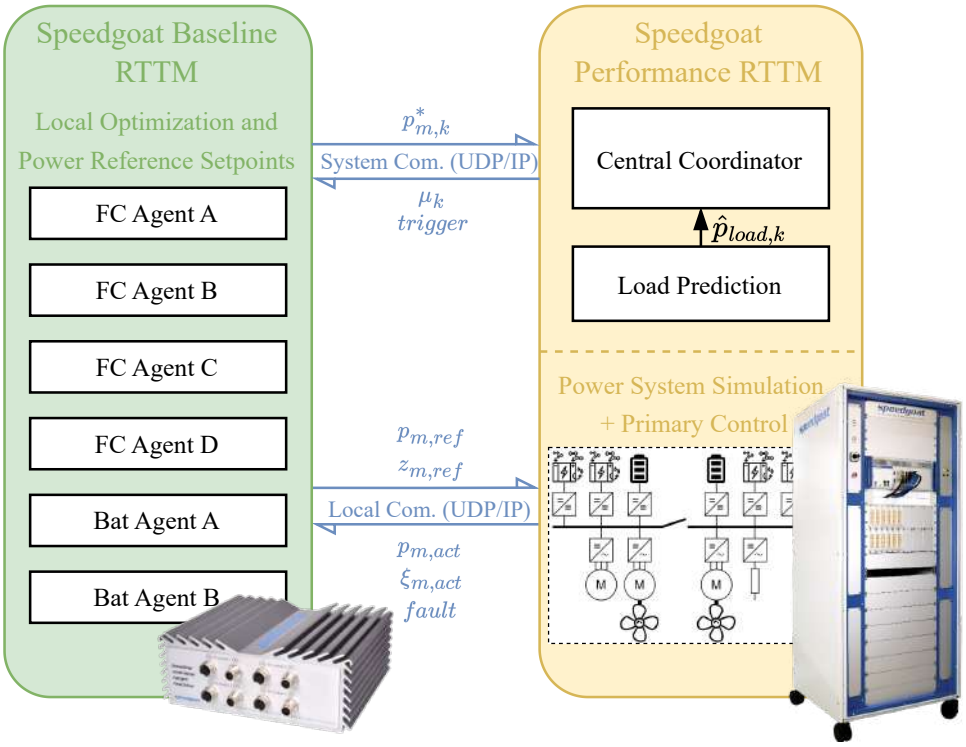


Figure 7.15: Deployment of distributed optimization on HiL setup with two Speedgoat real-time target machines (RTTM) and comunication via UDP/IP.

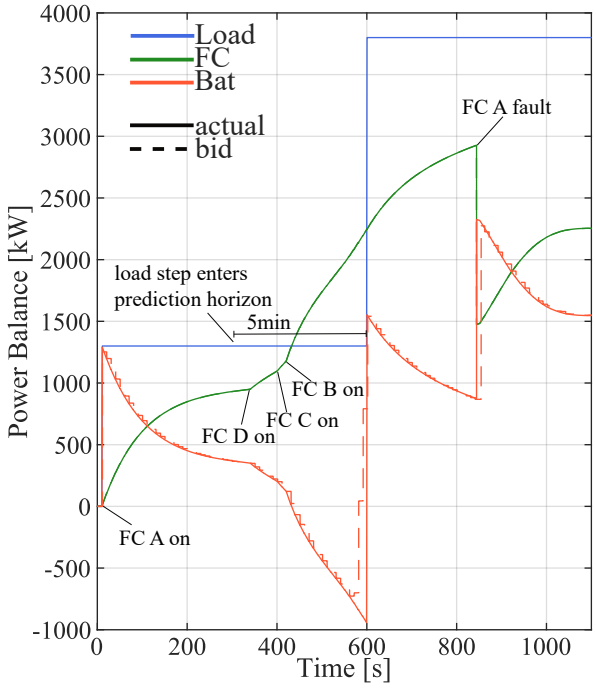


Figure 7.16: Cumulative FC and battery power references (final bid) and actual power for rectangular load step from 1300kW to 3800kW.

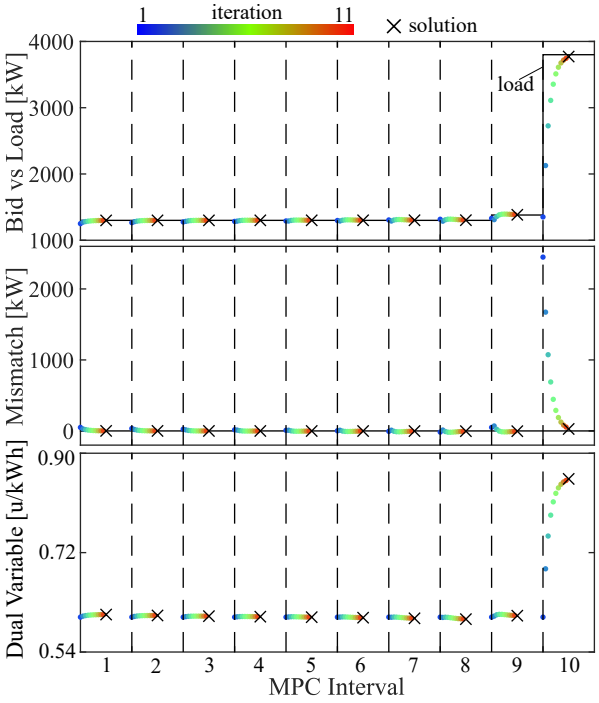


Figure 7.17: Convergence of distributed optimization during real-time simulation at t=330s, with the load step entirely predicted in the 10th MPC interval.

7.5.2 Convergence at Load Step

The advantage of the predictive optimization is that the algorithm can anticipate load changes before they occur. To investigate how the distributed optimization reacts to the prediction of the load step, we investigate the optimization instance occurring at time $t = 330\,\mathrm{s}$, at which the load step is fully captured within the final MPC interval. The corresponding evolution of accumulated bids from all power system components is shown in Fig. 7.17. The horizontal offset of bids within each interval is only for visualization. In the time domain, the dual variables and power bids are updated with the communication period T_{com}, which is 100 ms here. Showcased in this campaign via UDP/IP, this bandwidth, or even significantly faster, can be realized via various communication technologies.

The plot shows that the algorithm requires 11 iterations to converge. For the first 9 intervals, the initial dual variables from the previous optimization yield power bids that are sufficiently close to the power load. Only the 10th interval, for which now the stepped-up load to 3800 kW is predicted, requires multiple iterations, until the mismatch has dropped below the threshold. In accordance with the increased load requirement, the dual variable in interval 10 had to be increased significantly.

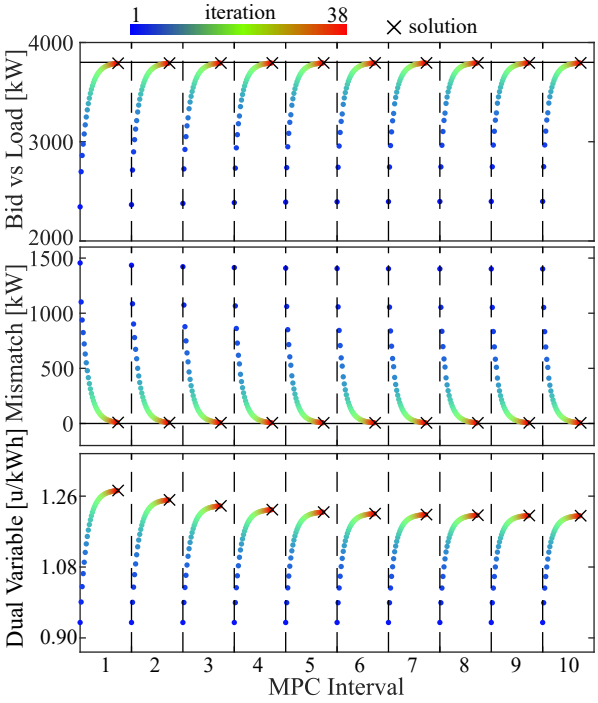


Figure 7.18: Convergence of distributed optimization during real-time simulation at time of FC fault (t=850s) during full load.

7

7.5.3 Convergence at Component Fault

Whereas the predictive optimization is able to anticipate the load step in the previous section, a component fault is typically an unforeseen event which requires immediate action. We assume that a fault occurs in FC module A, which is the largest power supply in the system, necessitating an sudden disconnect. Accordingly, the power output of the unit is reduced to zero within a short time period, and the FC agent is bidding 0 kW. Hence, the power bids from other components must compensate for the loss of generation. The convergence of the optimization algorithm immediately after the fault at $t = 850\,\mathrm{s}$ is shown in Fig. 7.18. We can observe that the algorithm requires 38 iterations until convergence. The loss of one large power supply leaves a large gap between initial power bid and power load. The dual variable highly increases in all intervals. The earlier intervals yield a slightly higher marginal cost than later intervals due to the high power gradients demanded from the FC systems.

The testing of these scenarios on multiple target machines showcases that the distributed optimization via Lagrangian dual decomposition in real-time, as proposed in this work, is suitable for deployment on actual control hardware. The distribution algorithm is converging in two extreme scenarios, even with non-ideal starting points. An initialization with the dual variables of the previous optimization instance, as well as a less frequent occurrence of

stark load changes will in practice significantly reduce the average number of iterations per optimization, as indicated by the results in Fig. 7.14. Finally, this demonstration underscores the adaptability of a distributed control approach for fault-tolerant system operation.

7.6 Conclusions and Discussion

Considering the increasing focus on modularity in shipboard power systems, the architecture and algorithms of the power system control and energy management must follow this trend and in turn become modular. This facilitates the integration of novel technologies, such as zero-emission power generation and storage systems. The way to achieve this is a shift from a centralized towards a distributed control architecture. Dual decomposition and predictive control allow for a flexible and and cost-optimized power dispatch, coordinated via a virtual market price. The deployment of distributed controllers and central coordinator on multiple RTTM, display the applicability of a predictive, distributed energy management for SPS on actual control and communication hardware. A further point is made by demonstrating the adaptation of the optimal power dispatch at the time of a generator fault, which is met by a re-optimization of the power dispatch adapted to the reconfigured power system.

Additional simulation results show the long-term performance of the proposed predictive and distributed energy management approach. These not only show that the distributed architecture is able to match the performance of a conventional, centralized approach, but also hint at possible gains that can be achieved by extending the load prediction horizons up to one hour. The cost-optimal power dispatch respects the parameterization and constraints of each module, proving the adaptability to individual characteristics. The cost-optimal results, combined with the added resilience, adaptability, and privacy-preserving aspect gained through the distributed architecture, shows that distributed power system control is a promising solution for the challenges in the operation of modern ships with an all-electric and integrated power system. The adaptation to each component's characteristics and to a topology alteration underscores the modularity of this control architecture.

A key challenge in the optimal power dispatch, present in centralized control but even more so in distributed architectures, is posed by discrete decision-making. In our investigations, a crucial decision-making lies in the modular on-off switching of FC systems, which adds a non-convex and discontinuous element to the agents' cost functions. A local heuristic has been applied in this work to handle this decision, generating promising results by adding the on-off switching as an additional degree of freedom in the energy management. A second key point in the EMS design lies in the adaptation of an equivalent cost approach for the construction of the ESS cost, which gives the energy management with short-term load forecasting an ECMS-like characteristic. Both mentioned aspects incentivize investigations into optimal mission-scale planning that would allow the adaptation of optimal FC state and ESS SoC references in favor of the employed heuristics.

An additional limitation of the proposed approach lies in the scope of the optimization objectives. Whereas we focused on the minimization of operational costs, considering only local constraints and global power balance, real SPS may be subject to further limitations, such as requirements on reserve power allocation and power availability. These potentially influence the optimal power dispatch, and are therefore worth including in detailed studies for specific ship types and sets of requirements. A possible opportunity arising from the

distributed approach via Lagrangian relaxation, lies in the information gained from the computed dual variable over the optimization horizon. It corresponds to the price of power generation at a given time. The utilization of this value in a feedback loop, e.g. for operator feedback on the expected power system efficiency or for an optimal load side management and voyage planning, warrants further investigations.
Further attention must be placed on the price adaptation mechanism, exploring its convergence behavior. Whereas the inclusion of convex and smooth cost functions is successfully handled with the approach presented in this study, the addition of non-convex modules (e.g. internal combustion engines), and more complex decision-making will require more sophisticated solutions. Alternative algorithms, such as ADMM, should be explored for applications in which the Lagrangian dual decomposition and gradient descent fall short.
An additional consideration lies in the opportunities and challenges arising from the flexible operation of complex and modular power system designs. More specifically, a distributed control architecture is promising for handling more complex networks, e.g. with a zonal or meshed layout, that allow flexible topology reconfiguration via bus-tie switches. This warrants further studies on the design of a distributed control and energy management architecture that incorporates topology-awareness.

8

Distributed Optimization in Multi-Bus DC Shipboard Power Systems

The previous chapter has introduced a framework for the energy management, which can be considered modular. It does not depend on a fixed topology and instead uses the resources which are available. Each component is included and operated based on its individual characteristics. The energy management adapts to parameter alterations of modules and even allows local decision-making on the operating state. But not everything is modular yet. The power system components are integrated in a modular fashion indeed, but what about the power system itself? We have, so far, assumed that there is one large, reliable power system to which we can connect, but reality is more nuanced. Power systems come in various topologies and have their own flaws. Focusing on DC technology, shipboard power system usually consist of multiple buses, connected and disconnected by switches. Buses and switches can fail. Depending on which switch connects which buses and based on which switches are closed at a given moment, the topology can change. To increase the resilience and adaptability of the distributed control approach, the work in this chapter adds topology-awareness to the energy management. The aim is to optimize not only the dispatch of units, but also the power flows between buses, and to adapt to the physical system topology.

"The purpose of a storyteller
is not to tell you what to think,
but to give you questions to think upon."

— *Wit*, in *The Way of Kings*
by *Brandon Sanderson*

This chapter is accepted for publication with minor modifications as *A Network-Coupled ADMM Framework for Distributed Energy Management in Multi-Bus Shipboard Microgrids, in: IFAC-PapersOnLine (In press)* [270]

8.1 Introduction

Electrified shipboard power systems (SPSs) are becoming increasingly complex, with a broadening variety of power system components incorporated into a single electric power network. Aiming at decarbonizing the maritime sector, hydrogen fuel cells (FCs) [68], energy storage systems (ESSs) [7], renewable power generation, and electric propulsion [16], are among the novel technologies brought on board. On top, there appears a trend toward modularization and distribution of generation and storage units [263]. Modern SPS with high reliability requirements incorporate multi-bus architectures with various power system modules spread over the electric network [271]. The increased system complexity makes the coordination of all energy resources a key challenge [100].

The energy management for ships shifts toward optimization-based techniques [101]. One overarching challenge discussed in current literature is the architecture employed for the power system control. Generally, the energy management strategy (EMS) can be realized as a centralized optimization, assuming full knowledge of parameters and states of all components [239]. However, such a solution requires careful parameterization, a high computational burden, and lacks scalability [42]. An alternative lies in shifting toward a distributed architecture [45]. Distributed real-time optimization and multi-agent systems offer an increased resilience and survivability [43], where the literature puts focus on power system reconfiguration [168], load management [175], and reserve power allocation [166]. [15] further note the plug-and-play characteristic in the design of all-electric ships which facilitates the scale-up of the SPS. Distributed EMS offer a pathway for meeting modular system designs with corresponding control strategies.

A widespread method of distributed optimization for real-time energy management is lambda iteration, based on Lagrangian dual decomposition. The optimal dispatch is found when all units have the same marginal cost of power generation [162]. [153] utilize the incremental cost of distributed generators as a consensus variable in a microgrid. For more complex microgrids, [154] employ lambda iteration in a federated architecture for economic dispatch. [155] showcase the application in a fully distributed architecture to manage a broad variety of power generation and storage units. The power exchange between microgrids lies in the focus of [173], whose method balances the incremental cost per utility in the multi-microgrid system. In SPS, [20] utilize lambda iteration for balancing the marginal cost of parallel diesel generators. [161] expand the application to a ship-harbor energy system, leveraging the absence of a central coordinator.

In distributed optimization, the alternating direction method of multipliers (ADMM) has emerged as a powerful alternative. It combines the decomposability of dual methods with the robustness of augmented Lagrangian techniques, leading to simple update rules with strong convergence guarantees for convex problems [266]. Like lambda iteration, ADMM has previously been employed for the economic dispatch in microgrids [267]. [156] further consider this method for the optimization in a multi-bus configuration. Common prerequisite for both dual decomposition-based and ADMM-based consensus is the convexity of all local cost functions. As already shown by [239], the costs for FC and battery modules can be represented via aptly convex functions over their output power.

DC distribution technology facilitates the use of meshed network topologies [271]. Their reconfiguration capabilities yield a high system reliability [272]. Such meshed SPS can be regarded as multi-bus microgrids connected via bus tie switches (BTSs). To achieve

both a resilient and plug-and-play integration of power generation and energy storage components in SPS requires adaptive strategies that match the modular system design, while accounting for the physical topology of the SPS. No existing work provides a topology-aware, distributed energy management formulation capable of handling DC shipboard multi-bus architectures with plug-and-play capability. To address this gap, we propose a network-coupled ADMM framework for the real-time dispatch of power and energy modules in multi-bus SPSs. Adapting to the physical network topology by considering BTS states in the distributed optimization allows for an efficient and adaptive dispatch of all power system resources. To realize this, we derive an implementation of federated bus-level ADMM instances, which additionally are coupled through BTS agents that participate in two optimization processes simultaneously to optimize inter-bus power flows. This enables the modular integration of various power system components on a bus-level and an adaptation to their characteristics via local agents. The inter-bus power flows through BTS is adapting to the actual network topology and are optimized to reduce overall power generation costs.

The remainder of this chapter is organized as follows. In section 8.2, we describe the energy management problem for FC-battery hybrid SPS and the ADMM-based distributed optimization on a single bus. Afterwards, in section 8.3, we extend this to our network-coupled ADMM framework for optimization over a multi-bus SPS architecture. In section 8.4, we showcase the application of the method in a case study, and conclude the findings in section 8.5.

8.2 Distributed Energy Management for Single-Bus Systems

As a first step, we derive an ADMM-based distributed EMS with central coordinator for an SPS consisting of multiple different power system modules. This method is intended for intra-bus optimization in the network-coupled distributed framework.

8.2.1 Problem Description

We consider an SPS equipped with a number of controllable power system modules $\mathcal{I}_b$ (generators, loads, storage, etc.), connected to a single bus b. Here, we limit the modules to FCs and batteries, which both have cost functions that can be approximated by convex functions of their output power $p_{b,i}$, as laid out by [239]. Fig. 8.1 shows an exemplary SPS topology with DC distribution system. A load d_b is imposed on the bus, which we assume to be an external disturbance on the system. The sum of each module's output power must match the load. The objective of the optimization is the minimization of the total cost of generation. Accordingly, the global problem is

$$\min_{\{p_{b,i}\}} \sum_{i \in \mathcal{I}_b} f_{b,i}(p_{b,i}) \qquad \text{s.t.} \qquad \sum_{i \in \mathcal{I}_b} p_{b,i} = d_b \tag{8.1}$$

where $f_{b,i}$ is the local cost of module i. In addition, each module's power output is limited to local constraints, such that $p_{b,i} \in \mathcal{P}_{b,i} = [P_{b,i,min}, P_{b,i,\max}]$.

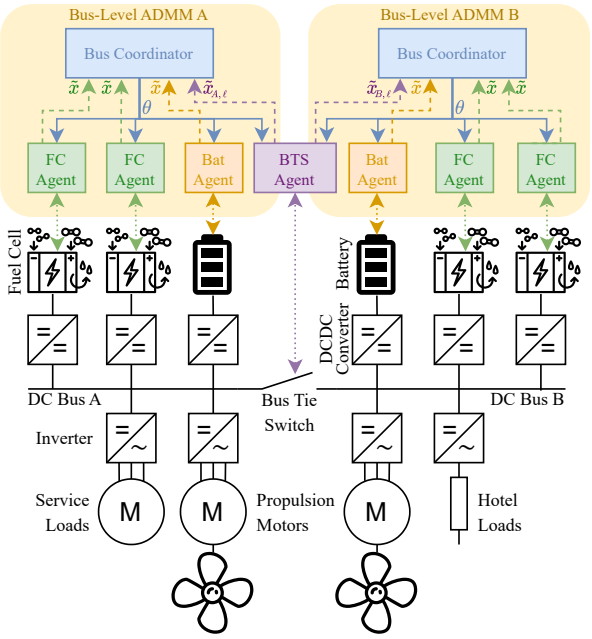


Figure 8.1: Proposed network-coupled ADMM for distributed energy management for dual-bus FC-battery DC shipboard power system

8.2.2 ADMM for Constrained Convex Optimization

The described problem is a constrained convex optimization problem, which can be approached using ADMM by employing an indicator function on the global power balance constraint [266]. The key idea of ADMM is to split the optimization problem into local subproblems, each solved by an agent, and then coordinate these subproblems through a consensus variable and a dual variable. Each iteration consists of three steps:

1. a **local update (x-update)**, where each agent optimizes its own cost subject to a quadratic penalty that keeps it close to the current consensus,
2. a **consensus update (z-update)**, where a central coordinator projects the agents' messages onto the global feasibility set, and
3. a **dual update (u-update)**, where accumulated mismatches are recorded and fed back into the next iteration.

Local x-update. Each agent solves a proximal problem to obtain its decision variable $x_{b,i}$, which serves as a proposed value for its output $p_{b,i}$:

$$x_{b,i}^{k+1} = \arg\min_{x \in \mathcal{P}_{b,i}} \; f_{b,i}(x) + \tfrac{\rho_b}{2} \left\| x - (z_{b,i}^k - u_{b,i}^k) \right\|^2 \tag{8.2}$$

which is equivalently written as

$$x_{b,i}^{k+1} = \operatorname{prox}_{f_{b,i}/\rho_b}^{\mathcal{P}_{b,i}} \left(z_{b,i}^k - u_{b,i}^k \right) \tag{8.3}$$

where ρ_b is the bus-specific penalty parameter originating from the augmented Lagrangian. The agent's proximal step ensures local feasibility and cost minimization. The agent then forms its shifted message

$$\tilde{x}_{b,i}^{k+1} = x_{b,i}^{k+1} + u_{b,i}^{k} \tag{8.4}$$

and transmits $\tilde{x}_{b,i}^{k+1}$ to the bus coordinator.

Coordinated z-update. The z-update forms a projection of the shifted messages $\tilde{x}_{b,i}^{k+1}$ onto the feasible set that fulfills the power balance constraint $\sum_{i\in\mathcal{I}_b} z_{b,i}^{k+1} = d_b$. The bus coordinator collects all shifted messages and broadcasts a uniform shift θ_b^{k+1} that realizes this projection:

$$\theta_b^{k+1} = \frac{\sum_{i\in\mathcal{I}_b} \tilde{x}_{b,i}^{k+1} - d_b}{|\mathcal{I}_b|} \tag{8.5}$$

The individual z-updates are finalized locally by each agent:

$$z_{b,i}^{k+1} = \tilde{x}_{b,i}^{k+1} - \theta_b^{k+1}, \qquad \forall i \in \mathcal{I}_b \tag{8.6}$$

Dual u-update. Finally, each agent updates its own dual variable, which is consequently required for the proximal step in the following iteration:

$$u_{b,i}^{k+1} = u_{b,i}^{k} + \left(x_{b,i}^{k+1} - z_{b,i}^{k+1}\right) \tag{8.7}$$

8.2.3 Stopping Criteria

The ADMM algorithm is stopped as soon as convergence is observed. For this, the bus coordinator monitors the average primal residuals

$$r_{b,i}^{k+1} = x_{b,i}^{k+1} - z_{b,i}^{k+1} \tag{8.8}$$

and the dual residuals

$$s_{b,i}^{k+1} = \rho_b \left(z_{b,i}^{k+1} - z_{b,i}^{k}\right) \tag{8.9}$$

which in turn are communicated by all agents. The convergence criterion is fulfilled if both the averaged absolute primal and scaled dual residuals, $\|r^{k+1}\|$ and $\frac{1}{\rho_b}\|s^{k+1}\|$, fall below a prescribed tolerance ε. Alternatively, the optimization instance may be stopped after a maximum amount of iterations. Upon finishing of an optimization instance, we assign the final value of the local decision variable to the power reference of the module, i.e. $p_{b,i} = x_{b,i}^{k,\max}$.

8.3 Network-Coupled ADMM for Optimization in Multi-Bus Systems

In a next step, we extend the method from section 8.2 to a multi-bus layout, coupled via BTSs. Each BTS is controlled by its own agent. As opposed to other local agents, the BTS agent is participating in two ADMM instances simultaneously, namely in those belonging to the two buses the switch connects. The network-coupled ADMM for a dual bus system is shown in Fig. 8.1.

8.3.1 Coupled Problem Description

BTS ℓ transfers power p_ℓ to bus m_ℓ from bus n_ℓ, the two buses it connects. It must respect its anti-symmetry constraint, i.e., the flow seen from m_ℓ is the negative of the flow seen from n_ℓ. In addition, the BTS agent has its own convex cost function $f_\ell(p_\ell)$. As opposed to the single bus problem, the need for bus-level power balance is relaxed. Instead, the BTS allow inter-bus power exchange and the load power can be met by the local power generation plus imported power from neighboring buses.

8.3.2 BTS Agent Updates

As before, each bus iteratively goes through its ADMM steps to find an optimal dispatch of all units $i \in \mathcal{I}_b$. From the perspective of each bus coordinator, the BTS agent acts equivalently to all other non-switch agents, with the exception that it communicates with the coordinators of both connected buses at the same time. Accordingly, the coordinator steps require no modification. However, we need to define the local ADMM updates done by the BTS agent.

The BTS determines its optimal decision variable x_ℓ with convex cost $f_\ell(x_\ell)$ on its locally feasible set $p_\ell \in \mathcal{P}_\ell = [-P_{\ell,\max}, P_{\ell,\max}]$. Since the BTS agent participates in two optimization instances, we create local copies $x_{m,\ell}$ and $x_{n,\ell}$, which denote the power flow directed at the respective buses m and n. The BTS agent further track separate consensus and dual variables $z_{m,\ell}$, $z_{n,\ell}$, $u_{m,\ell}$ and $u_{n,\ell}$, and we define specific cost functions $f_{m,\ell}(x_{m,\ell})$ and $f_{n,\ell}(x_{n,\ell})$. Both sides simultaneously update their local decision variable as

$$x_{b,\ell}^{k+1} = \operatorname{prox}^{\mathcal{P}_\ell}_{f_{b,\ell}/\rho_{b,\ell}}\left(z_{b,\ell}^{k} - u_{b,\ell}^{k}\right). \tag{8.10}$$

for $b = m, n$. Before the z-update, we enforce local feasibility through a projection on the anti-symmetry constraint ($x_{m,\ell} = -x_{n,\ell}$) via weighted averaging:

$$x_{\ell}^{k+1} = \frac{\rho_m x_{m,\ell}^{k+1} - \rho_n x_{n,\ell}^{k+1}}{\rho_m + \rho_n}. \tag{8.11}$$

The BTS forms its shifted messages to both buses using the projected x_ℓ^{k+1}:

$$\tilde{x}_{m,\ell}^{k+1} = x_{\ell}^{k+1} + u_{m,\ell}^{k} \tag{8.12}$$

$$\tilde{x}_{n,\ell}^{k+1} = -x_{\ell}^{k+1} + u_{n,\ell}^{k} \tag{8.13}$$

From the two adjacent buses, the agent receives different shift signals. Using these, the BTS agent updates its z- and u-variables, in the same manner as conventional agents:

$$z_{b,\ell}^{k+1} = \tilde{x}_{b,\ell}^{k+1} - \theta_b^{k+1}, \qquad u_{b,\ell}^{k+1} = u_{b,\ell}^{k} + \left(\pm x_{\ell}^{k+1} - z_{b,\ell}^{k+1}\right) \tag{8.14}$$

and updates its residual variables accordingly. As a result, the BTS internally has two local optimizers which are coordinated only by the anti-symmetry projection. Convergence must hence be guaranteed by a suitable design of the two cost functions for each BTS port.

8.3.3 BTS Cost Function

The cost functions of the BTS agent need to be designed such that convergence can be achieved while reflecting the actual costs of power transfer over the switch. We compute the marginal cost of power, which is a bus-specific quantity at equilibrium, and utilize it as a metric for determining the cost of transferred power. In addition, the estimated incurred transfer losses need to be accounted for. We use the information shared via the bus and the scaled dual variable u, computed by the agent. At equilibrium, we drop the superscript k since all variables are constant. With $x_{b,i} = z_{b,i}$, each agent reaches the condition

$$\nabla f_{b,i}(x_{b,i}) = -\rho_b u_{b,i} \tag{8.15}$$

which constitutes the marginal cost of power generation at bus b. From the definition of the ADMM steps in Eqs. (8.4)-(8.7), we can derive that $u_{b,i} = \theta_b$. Using this, we estimate the marginal cost at the bus before convergence as:

$$\hat{\nabla} f_b^k = -\rho_b \theta_b^k \tag{8.16}$$

The ohmic resistance of the switch R_ℓ yields losses quadratic with the power transfer, while the total voltage drop from diodes $V_{\mathrm{d},\ell}$ can be modeled as linear losses. Accordingly we model the losses as

$$p_{\mathrm{loss}}(p_\ell) = \frac{R_\ell}{V_{\mathrm{avg}}^2} p_\ell^2 + V_{\mathrm{d},\ell} p_\ell \tag{8.17}$$

Since the power supplied to bus m is "bought" from bus n, we use the "market price", i.e. the marginal cost, from the opposite bus to scale the power transfer and losses.

$$f_{m,\ell}^k(x_{m,\ell}) = \hat{\nabla} f_n^k(x_{m,\ell} + p_{\mathrm{loss}}(x_{m,\ell})) \tag{8.18}$$

Analogously, we switch indices m and n to obtain the cost function for the opposite port $f_{n,\ell}^k(x_{n,\ell})$. Upon convergence we assign the local consensus x_ℓ to the power flow reference p_ℓ.

8.3.4 Additional Stopping Criterion

It must be avoided that the optimization on one bus is stopped prematurely while that of a connected bus still requires changes of the transferred power through the BTS. To achieve this, we introduce a flag sent by the BTS which tells whether the convergence criterion of the neighboring bus has been reached. The ADMM is then stopped only as soon as the bus and all its neighbors signal the fulfillment of their respective stopping criteria.

8.4 Case Study

For demonstration of the proposed distributed energy management, the plant models, agent controllers, and bus coordinators are deployed in a simulation environment using Matlab/Simulink. The modeled SPS is equipped with four FC and two batteries in a dual bus configuration. The load power is taken from real measurements of a harbor tug, described in more detail in [239]. All components have unique parameters, due to differences in ratings and/or state-of-health. Parameters used for the plant models, power system simulation, and optimization are listed in Table 8.1.

Table 8.1: Power system, simulation, and optimization parameters

Parameter	Description	Value
$P_{\mathrm{fc,A}}$	Max. power FC A at BOL	1780 kW
$SoH_{\mathrm{fc,A}}$	State-of-health of FC A	100 %
$P_{\mathrm{fc,B}}$	Max. power FC B at BOL	1780 kW
$SoH_{\mathrm{fc,B}}$	State-of-health of FC B	80 %
$P_{\mathrm{fc,C}}$	Max. power FC C at BOL	445 kW
$SoH_{\mathrm{fc,C}}$	State-of-health of FC A	85 %
$P_{\mathrm{fc,D}}$	Max. power FC D at BOL	445 kW
$SoH_{\mathrm{fc,D}}$	State-of-health of FC D	95 %
$E_{\mathrm{bat,A}}$	Energy capacity battery A	1000 kWh
$R_{\mathrm{i,A}}$	Inner resistance battery A	6.1 mΩ
$E_{\mathrm{bat,B}}$	Energy capacity battery B	250 kWh
$R_{\mathrm{i,B}}$	Inner resistance battery B	12.2 mΩ
R_ℓ	BTS ohmic resistance	100 mΩ
$V_{\mathrm{d},\ell}$	BTS voltage drop	0 V
$I_{\mathrm{max},\ell}$	BTS Current limit	1000 A
T_{sim}	Simulation step size	10 ms
T_{com}	Communication step size	100 ms
T_{opt}	Optimization step size	5 s
ε	Constraint tolerance	0.5 kW
ρ_b	Penalty term	3×10^{-13}
$it_{\max}$	Maximum iterations	45

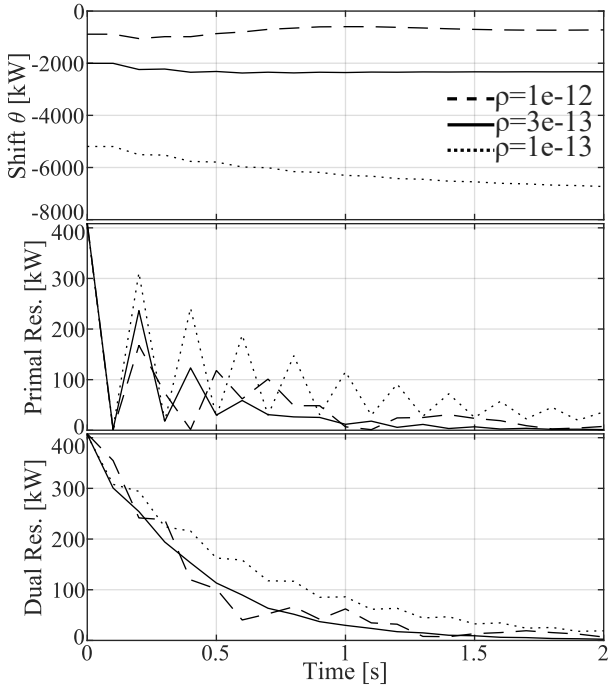


Figure 8.2: Shift message θ_b, mean primal residual $|r_b|$, and scaled dual residual $\frac{|s_b|}{\rho_b}$ for different ρ_b at time of load step application in single-bus topology.

8.4.1 Single Bus Topology

To demonstrate the behavior of the distributed energy management without network-coupling, we implement the single bus ADMM for the complete SPS, i.e. all four FC and two battery systems participate in one optimization instance, regardless of the physical layout. We investigate the convergence of the algorithm for a large load power step (from 1300 kW to 3800 kW). The values of the correcting shift θ_b, the mean absolute primal residual $|r_b|$, and the scaled mean absolute dual residual $\frac{|s_b|}{\rho_b}$ are shown in Fig. 8.2. The value of ρ_b is varied to find a value that balances the convergence speed of the primal and dual residuals. The graph shows that a low ρ_b leads to a slow convergence of the primal residual, and as a result the dual residual is asymptotically approaching a stable consensus. A high value leads to fast convergence of the primal residual, but it takes longer to find a stable consensus. Fig. 8.3 shows the convergence behavior for the individual components, i.e. four FCs and two battery systems. Early in the optimization instance, each module's local decision $x_{b,i}$ is at their previous operating point, while all modules equally contribute to the consensus on power balance with the projected consensus $z_{b,i}$. At convergence, predominantly the batteries have changed their power reference to compensate the load step. The change in θ_b indicates the increased marginal cost of generation at consensus. Further, both the primal residual, equal to all units, and scaled dual residuals converge below the threshold ε in less than 20 iterations.

8.4.2 Dual Bus Topology

In the next step, we apply the multi-bus ADMM with coupling via the BTS agent to a dual-bus topology with two FCs and one battery per bus. As listed in Table 8.1, the components have individual characteristics, which leads to a difference in generation costs between the buses. This imbalance incentivizes the BTS to transfer power between the buses for lowering the overall generation costs in the SPS. Figure 8.4 shows the convergence behavior of the BTS agent when the dual-bus system is subjected to the same load step as before. The load power is distributed evenly among the two buses. The plots show that all local decision variables xb,ℓ, the aggregated $x\ell$, and the consensus variables zb,ℓ converge. In equilibrium, the shift signals θ_b differ, with the power transfer reference depending on sign and magnitude on this difference.

Figs. 8.5 and 8.6 show the power balance and battery state-of-charge (SoC) during a mission simulation side-by-side for both buses with an open and closed BTS, respectively. Fig. 8.7 shows the bus-specific unscaled multiplier, indicating the marginal cost of power generation, as well as power flow through the switch toward bus A for both cases. With the switch disengaged, both buses operated autonomously and show different behaviors, especially regarding rate of FC power change and battery depth-of-discharge. The gap in marginal generation costs (Fig. 8.7) underscores these differences. Closing the BTS brings the behaviors closer together, with differences in FC dynamics and battery depth-of-discharge, decreasing. The closed BTS further pulls the marginal costs closer together, with power flows from the low cost to high cost bus through the BTS.

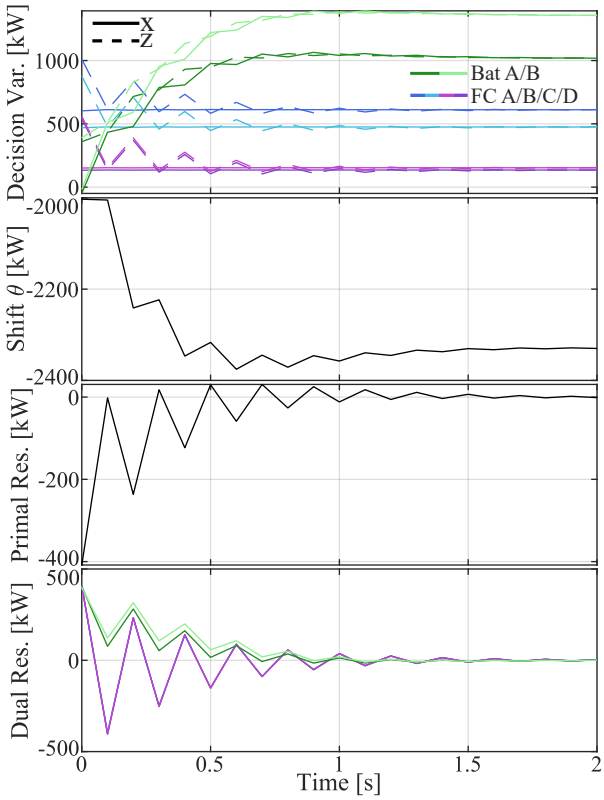


Figure 8.3: Local decision variables $x_{b,i}$ and $z_{b,i}$, broadcast shift message θ_b, primal residual $|r_{b,i}|$, and dual residuals $\frac{|s_{b,i}|}{\rho_b}$ at time of load step application in single-bus topology.

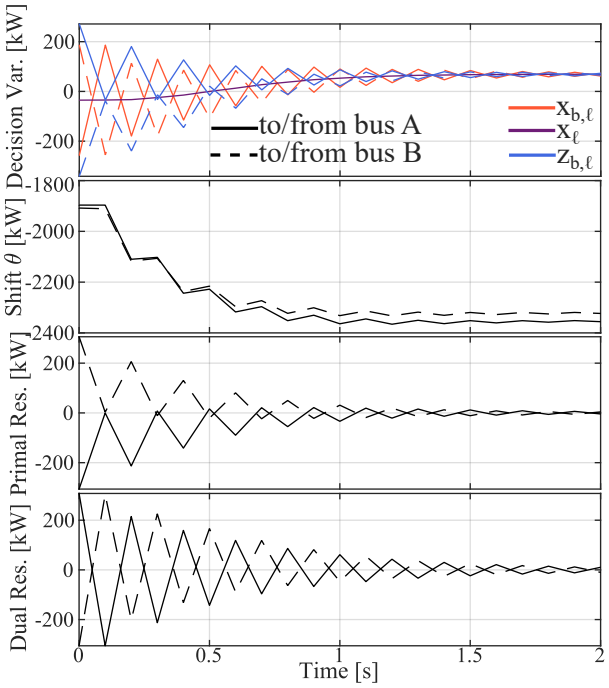


Figure 8.4: Local proximal steps $x_{b,\ell}$, anti-symmetric aggregate x_ℓ, and consensus variables $z_{b,\ell}$, and shifts θ_b received from bus agents and residuals $|r_{b,\ell}|$ and $\frac{|s_{b,\ell}|}{\rho_b}$ shared with both buses at time of load step in dual-bus topology.

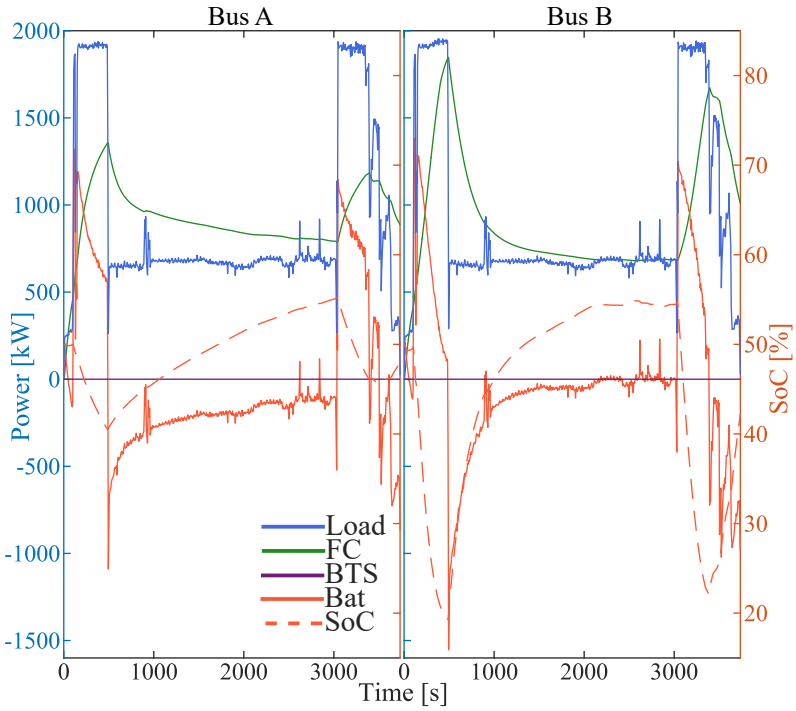


Figure 8.5: Power balance during mission simulation in dual bus system with open BTS, showing aggregated FC and battery power outputs, load power and battery SoC for both buses.

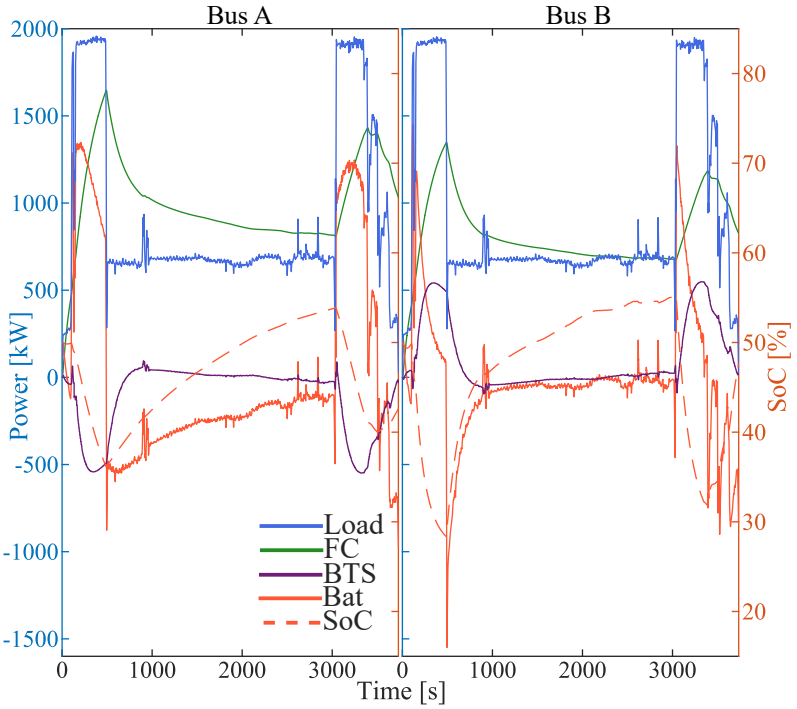


Figure 8.6: Power balance during mission simulation in dual bus system with closed BTS, showing aggregated FC and battery power outputs, load power and battery SoC for both buses.

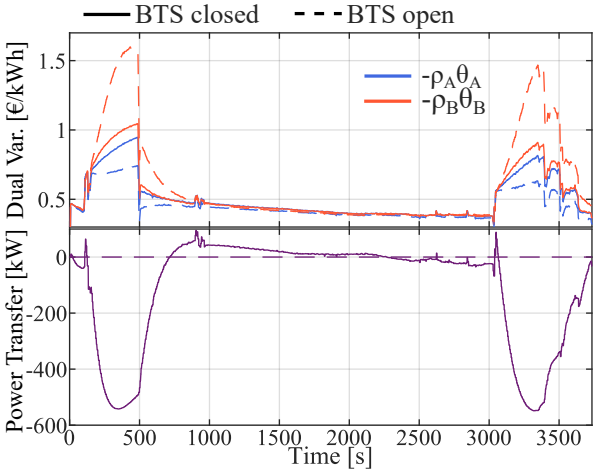


Figure 8.7: Unscaled multiplier $-\rho_b \theta_b$ (marginal cost of energy generation) and optimized power transfer through BTS from bus B to bus A during mission simulation for open (dashed) and closed (solid) BTS.

8.5 Conclusion

ADMM provides a powerful framework for distributed optimization in multi-agent systems. It converges to locally feasible and optimal decisions for all modules while maintaining global feasibility through a coordinated consensus step. In a single-bus system, this yields an optimal economic dispatch of power generation and storage units in a modular fashion. Through local optimization steps, each agent can adapt to individual component parameters and implement heterogeneous optimization algorithms. The shown ADMM algorithm minimizes the communication overhead and requires no sharing of sensible information through the network.

This work shows an extension to multi-bus architectures utilizing BTS agents that connect two buses on the energy management layer, without compromising the modular aspect of the single-bus optimization. We demonstrate the application of network-coupled ADMM for the real-time energy management in a dual-bus SPS, which flexibly adapts to the physical BTS switch state. This approach is also viable for more complex, meshed power networks and natively adapts to topology alterations arising from changing switch states. Through its high adaptability to changes in the network topology, connected modules, and local parameter changes, this energy management framework provides a highly resilient and optimization-based operation of complex SPS.

9

Synthesis and Future Directions

In the introduction of this thesis I mention the role of my work, namely to find answers. The content chapters of this thesis describe methods on the voltage stabilization in DC ships and real-time coordination between fuel cells and batteries; on the optimal and predictive energy management; and on distributed architectures, resilience, and adaptability of these functions. I thus touched all layers of the control hierarchy and revisited different architectures. With the progress I have made in the past years, I can finally answer the questions I set out with. In their entirety, my contributions form a modular approach to the optimization-based power system control and energy management for fuel cell-battery DC shipboard power systems. In this concluding chapter, I review the research questions one by one and connect them to the contributions from my investigations, to bring problem and solution together. With a set of recommendations, I then aggregate the most important insights from my work. Finally, while addressing the initial research questions, additional challenges came up which I did not cover yet, but that should be investigated in future work.

"The most important step a man can take.
It's not the first one, is it?
It's the next one."

— *Kaladin*, in *Oathbringer*
by *Brandon Sanderson*

This concluding chapter connects the original problem statement to the contributions made throughout this dissertation's investigations. Juxtaposing question and answer reveals the degree of success in finding a satisfactory response to each challenge. Section 9.1 provides an overview of the key findings of this work, and how they connect to the research questions. It then follows up with recommendations on how we can make use of these findings. Section 9.2, gives an overview of related challenges identified during the investigations but not yet addressed, and Section 9.3 concludes this chapter with a final reflection of this dissertation's contributions.

9.1 Contributions

Ship electrification, hybridization with energy storage systems, integration of fuel cells, DC distribution technology and power electronics converters are trends we see to varying degrees in modern vessels. Increasing system complexity and uncertainties meet high controllability and computational power. The challenge lies thus not in how the system can be controlled but in how it should be controlled. This Section summarizes the key contributions as an answer this challenge.

9.1.1 Findings

In the introductory chapter 1.3, the challenge of a modular, real-time control for hydrogen-based shipboard power systems (SPSs) has been broken down into a series of research questions. The following presents answers based on this dissertation's findings.

Research Question 1:

What are suitable methods and architectures for the power system control in shipboard DC distribution systems and for the energy management of fuel cell-battery ships?

In Chapter 2, an overview of state-of-the-art methods for coordinated control and energy management in SPS has been created. It could be shown that current literature on the integration of fuel cells (FCs) in electric ships is less mature than in conventional systems. However, much can be learned from established concepts in conventional ships, but also from other sectors, most notably the automotive and terrestrial power systems; especially considering hybrid electric vehicles and DC microgrids, respectively.

For the power system control, established methods from DC microgrids are applicable. This mainly revolves around droop-based methods for the parallel control of multiple power generation and energy storage components. However, compared to terrestrial systems, SPS need to handle additional challenges, such as pulsed and power-controlled loads, and high reliability and availability standards. In addition, considering a modular integration of multiple components with different characteristics, adaptive methods are promising. This demands low-bandwidth communication among the units, but allows the power system control to account for parameters changes and component faults, and to provide a more accurate power sharing and voltage regulation. Furthermore, the literature clearly indicates the need to utilize fuel cells and batteries differently. The former needs to be operated within viable limits and with possibly low power gradients, whereas batteries and especially ultra-capacitors (UCs) are able to supply high power gradients but introduce state-of-charge (SoC) management and balancing as additional challenges.

Most promising for the energy management are optimization-based methods and, if applica-

ble, predictive control. This allows both the formulation of objectives by associating inputs and states with costs, and an explicit formulation of constraints on the system and its components. In fuel cell-hybrid systems, the main cost drivers are the hydrogen consumption, and to a lesser extent the operation-dependent cell degradation. The optimization-based energy management should consider the system's total operation cost.

Finally, a truly modular approach can be realized via distributed control architectures, either with or without a central federating unit. In distributed methods, the main computations, e.g. optimization, are implemented on local controllers. Parameter changes can be processed locally, and thus the component-level problems can adapt the local algorithms, including cost functions and limitations without the need for extensive data sharing with a central unit. Coordination is then realized either via consensus algorithm or a federating agent. A distributed architecture is thus beneficial for enhanced resilience, scalability, adaptability, privacy-preservation, and vendor-agnostic integration of components.

In conclusion, the overview in Chapter 2 provides answers to research question 1, pointing out methods for the coordinated control and energy management in FC-battery DC SPSs that are promising for a modular power system control. Distributed architecture, adaptive control and coordination through low-bandwidth communication are key enablers for a modular power system control.

Research Question 2:

How can a stable bus voltage, in DC shipboard power systems with parallel converter-interfaced batteries, be ensured?

Chapter 3 presents a voltage stabilization method which is intended to be implemented in parallel DC-DC converters to connect fast-acting power system components, such as batteries and UCs. The energy-based approach shows improved dynamic stabilization speed and resilience towards power-controlled loads, compared to conventional voltage-based droop- and PI-controllers. Beyond a voltage stabilization, the control approach is also ensuring a restoration of the bus voltage to its nominal value.

This method is applicable for the parallel control of multiple battery DC-DC converters. It is shown how the local controllers can be tuned to achieve a power sharing ratio based on the available power of each unit. In addition, a low-bandwidth communication network is utilized to adapt parameters such that power sharing and voltage restoration are accurate and with the desired dynamics. This is key to avoid circulating currents since each unit relies on local measurements rather than global inputs, as demonstrated via hardware-in-the-loop (HiL) tests. The parameter adaptation also ensures that the overall system dynamics can be maintained under component faults or topology changes. Accordingly, the approach is modular since it adapts to the number and ratings of DC-DC-converter interfaced units. It further must be noted that the method is compatible with different local current controllers and with high-level energy management strategies (EMSs). Thus, this energy-based voltage stabilization method can be implemented as part of a complete control hierarchy with the task of providing a stable DC bus voltage and accurate power sharing, using the system's fast-acting power supplies and storage systems.

In summary, the method presented in Chapter 3 provides a solution for research question 2. It's deployment yields a stable foundation upon which higher-level control functionalities can be built. This is essential for improving quality of supply and power availability in electrified ships with DC distribution and power electronics-interfaced components.

Research Question 3:
How can the multiple fuel cells and batteries in a hybrid ship energy system be coordinated such that each component is operated based on its static and dynamic characteristics and constraints?

Chapter 4 includes components with different dynamic capabilities inf the coordinated control, namely batteries and FCs. The investigations focus on a decentralized approach that incorporates this fact. The solution is found in virtual impedance-based droop controllers that can be tuned locally based on the sources capabilities. The method implements a voltage stabilization and restoration while achieving a frequency decoupling between fast- and slow-responding power system resources.

In addition, the proposed method also focuses on further issues that needs to be addressed for forming a workable coordinated control. A key aspect of this is the balancing and management of battery SoC, whose limits are one of the main constraints on the overall power system control. Both the balancing and management are achieved through local sigmoid functions that account for the current SoC and its limits. It should be noted that this method can be implemented using an energy-based rather than a voltage-based approach and is therefore compatible with the method presented in the foregoing chapter. As before, the method employs low-bandwidth communication to adapt for parameters alterations and topology changes for maintaining the overall behavior of the DC distribution network.

This method allows each power system resource to be operated based on its own capabilities and limitations while ensuring sufficient power availability for the loads. This addresses research question 3, as the method in Chapter 4 is ready to use in complex FC-battery hybrid systems, featuring tailored static and dynamic power sharing controllers for each component.

Research Question 4:
How can the energy management in a fuel cell-battery shipboard power system be optimized under consideration of efficiency and component degradation?

Whereas previous chapters investigated short-term objectives and dynamic system behavior, the long-term optimization of a FC-battery SPS is investigated in Chapter 5. A dynamic programming algorithm is presented for the offline computation of the FC power and battery SoC over the course of a full mission. The algorithm minimizes the total operation cost of the system and includes hydrogen consumption and cell degradation as the main cost drivers. Moreover, it is designed to be computationally efficient, and is thereby applicable in a real-time multi-timescale model predictive control (MPC).

A particular point of interest in the context of modular energy management, is the individual on- and off-switching of multiple FC modules. It could be shown that the individual switching of modules allows a trade-off between total system efficiency and degradation, which in turn depend on the respective costs of these two factors.

Chapter 6 then investigates a real-time applicable optimized EMS. This includes an instantaneous optimization, based on the aforementioned factors. The lack of mission-scale foresight necessitates an equivalent cost approach for the energy storage system (ESS) deployment. In a second step, this is extended to an MPC with load predictions of up to one hour, still utilizing an equivalent cost for the terminal stored energy. The inclusion of load forecasts covering significant load fluctuations allows the EMS to significantly reduce operational cost with an increasing prediction horizon. In addition, an MPC approach

allows to explicitly incorporate system constraints, e.g. power gradient and SoC limits.

To address research question 4, Chapters 5 and 6 show that fuel consumption and component wear are the key indicators to minimize in order to optimize the operation cost of a FC-battery SPS. This is essential for making hydrogen-powered vessels more competitive and thereby driving their adoption. The developed, advanced EMSs and in particular predictive control strategies are elemental in fully exploiting the potential of hydrogen-based system designs.

Research Question 5:

How can an optimized energy management strategy be implemented in a modular DC shipboard power system considering its resilience towards parameter uncertainties, faults, and scalability?

Whereas the aforementioned studies on optimal EMSs assume a centralized control, subsequent investigations shifted the focus to the control architecture. In particular, distributed optimization was found to be promising for establishing a modular and optimization-based EMS framework. As described in Chapter 7, a distributed and predictive EMS based on dual decomposition and utilizing a central coordinator were developed.

The optimization-based MPC as in the previous chapter could be translated into a distributed architecture, with the same system performance regarding operational costs. However, the distribution of controllers achieves additional benefits. The transfer of component-level optimization to the local controller means that individual characteristics and limitations can be represented more easily, without the need for extensive information sharing with a central controller. An adaptation to parameter changes is implemented more easily and is isolated to the relevant local unit. Furthermore, this architecture is inherently scalable and can adapt to an extension and reconfiguration of the power system, and, most importantly, adapts online to component-faults. Hence, a distributed control approach offers in improved resilience of the power system by minimizing the effect of component-level faults and parameter alterations. With the insights from an individual on- and off-switching from the previous chapter, a local decision-making heuristic for the FC state was implemented. This is fully in line with the modular architecture and yields additional improvements, especially in terms of FC degradation, but also assists the distributed algorithm in improved convergence behavior.

Chapter 8 provides an improved, more robust distributed optimization method by deploying the alternating direction method of multipliers (ADMM) to the EMS formulation. In particular, this approach yields improved and more stable convergence. The presented study investigates an extension of the distributed optimization in a multi-bus framework that features bus-level coordinators which are organized in a distributed fashion. A key benefit over the previous formulation is the topology-awareness of the approach. Instead of considering the complete power system as a single node, the physical connection between buses, as well as the location of loads and power generation, are represented. This EMS optimizes the dispatch of resources per bus and additionally optimizes power flows between connected buses while taking into account the physical limitations and state of the system. Due to the inherent reconfiguration and handling of islanded subsystems, this topology-aware EMS provides a survivable method of power system operation.

To summarize and provide an answer to research question 5, distributed optimization, as proposed in Chapters 7 and 8, is most promising for a modular integration of power

system resources without compromising the performance of a centralized strategy. It ideally facilitates a local adaptation to each module's characteristics while ensuring system-level constraints. An additional topology-awareness expands the modularity aspect to the topology of meshed DC SPSs. The work presented in this dissertation presents a framework for efficient, resilient, and scalable SPS operation.

9.1.2 Recommendations

Isolating the findings from this research project to a set of conclusions raises the question what is to be done with the new knowledge. This Section breaks down the conclusions into a more tangible set of recommendations; with the hope that someone faced with the same challenge will make use of them.

DC Distribution and Power Converters: Chapters 3 and 4 show examples of electric power system designs incorporating batteries and FC systems. The integration of these technologies is eased using DC distribution and power electronics converters. The shift from conventional AC to DC distribution in electrified ships simplifies the integration of multiple different power system components. Moreover, the use of power electronics for interfacing each individual component yields full controllability of the system and standardizes the control interface of each connected module. Hence, the modularity and thereby the flexibility and resilience of the power system control is improved.

Voltage Stabilization: As shown in Chapter 3, a fast-acting power system component is required for stabilizing the bus voltage in a DC distribution system. To allow main power supplies to operate efficiently, it is advisable to provide a stable bus voltage with high quality of supply via the ESS, e.g. batteries or even ultra-capacitors. Moreover, for improving the power availability and system resilience, power sharing among parallel voltage stabilizing components should be allocated according to their power reserve.

Adaptive Control: The various methods presented throughout this dissertation are geared towards the aspect of modularity by implementing the main control functions locally. One key motivation for doing so is the increased adaptability of the local and system level controls. The local controller can flexibly adapt its parameters based on the current state of the component without any need for communication. Moreover, a low-bandwidth communication network for information exchange among parallel units to update coordinated control functionalities allows for an adaptive system control without a heavy reliance on central computation and high-speed communication.

Modular Control: A modular system design, e.g. with containerized power system components, mitigates uncertainties related to the adoption of novel technologies. This modularity expresses itself through parameter changes of individual components, a flexible number of power system components, as well as topology alterations of the distribution network. The power system control should be conceptualized to follow the modular design and adapt to the mentioned aspects without compromising its performance.

Optimization-based Energy Management: In chapters 5, 6, and 7, it could generally be shown that an optimization-based energy management strategy can significantly enhance the performance of the ship operation compared to conventional methods. If applicable, a predictive strategy is superior to instantaneous optimization and an effort in extending the optimization horizon promises further improvements. The optimization should be geared towards minimizing the overall operational costs while meeting system requirements. With

a FC-based system, the key drivers of operational costs lie in hydrogen consumption and component degradation.

Distributed Optimization: To combine a modular control approach with optimization-based energy management, a shift from a centralized to a distributed architecture is advisable. The distributed architecture handles the challenges introduced by the modular system design, allowing a plug-and-play system extension and fault-handling. It flexibly adapts to a multitude of power system components with individual characteristics, component faults, retrofits, and topology alterations. Overall, the resilience of the power system is improved compared to a centralized architecture. The key challenge for distributed optimization lies in the minimization of the required data exchange among units.

9.2 Future Research

Whereas the aim of a dissertation is to find answers to a specific challenge, it turns out that many more questions arise during that journey. With the completion of this research project comes a sense of what the real challenges are in this specific field. The following comprises a non-comprehensive list of key challenges to be addressed in future research, based on the findings of this dissertation.

Experimental Validation: The investigations in this work employ some validation equipment, namely a small HiL setup in Chapter 3 and a real-time target machine in Chapter 7. For control strategies, such validation is immensely important to optimize its parameterization, troubleshoot deployment issues and demonstrate its performance in a realistic setting. Offline simulations are not sufficiently realistic to uncover all possible problems whereas deployment in the field is too costly and time-consuming. For future research it is therefore advisable to incorporate on system and subsystem tests using appropriate laboratory and/or real-time simulation equipment for demonstrating the proposed methods.

Extension to More Components: The presented work focuses heavily on the system control of FC-battery systems. These are currently still considered novel technologies. The proposed modular approach for the system control, however, is intended to include a wider variety of system components. For this reason, an effort should be made to include conventional power supplies, e.g. gas turbines and diesel generator sets, fast-acting energy storage, e.g. ultra-capacitors, and renewable energy generation, e.g. photovoltaic panels, in the modular power system control and energy management concepts. A key challenge for the distributed optimization lies in the inclusion of non-convex cost functions and integer-valued decision-making.

Multi-Timescale Optimization: The MPC presented in Chapter 6 makes use of short-term load forecasting, considering dynamic limitations and costs. However, for long-term planning, e.g. on-off decision-making and an optimal SoC reference for the ESSs, the method relies on heuristics. For future research, a multi-timescale optimization that integrates mission-scale ahead-planning, similar to Chapter 5, promises improved results.

Distributed Decision-Making: The costs of FCs and ESSs were approximated via convex functions for the investigations in this thesis, specifically for the distributed methods. This challenge becomes significantly more complex by including discrete decision-making, such as the state switching in Chapter 5. The key will be to develop efficient distributed methods that enable optimal decision-making for distributed architectures.

Optimized and Distributed Coordinated Control: The application of distributed optimization in the dissertation is limited to the energy management aspect of the hierarchical control. The coordinated control and voltage stabilization methods are not optimization based. Especially for the coordinated control to achieve an efficient current sharing, voltage stabilization and SoC balancing, there is remaining potential to apply optimization-based methods with a distributed architecture.
Reserve Power Allocation: The proposed methods for the energy management are focused on creating a load balance as efficiently as possible. However, in real applications additional requirements apply. One important aspect is reserve power allocation in the context of contingency management to prevent insurmountable faults. Future work on the energy management and coordinated control should include application-specific operational constraints derived from the power system's requirements.
Load Management: The presented methods are fashioned to optimize the power output of the power generation and energy storage modules onboard the ship. Much potential, however, is on the load side. Depending on the specific application, the load power can be included in the optimal dispatch problem to increase system efficiency. Further, load management should be included in the fault-reaction, especially if the generation is unable to fully service all loads.
Interaction with Other Systems: The power system control and energy management do not exist in a vacuum. They interact with other automation systems and human operators. This leaves space for joint optimization of the energy management and operation of the ship and other equipment, whereas this work focused on the most efficient servicing of a fixed load profile.

9.3 Reflection

The initial ambition of this dissertation was to study the power system control and energy management for DC SPSs equipped with multiple FCs and battery modules. This endeavor delved into several aspects of the control hierarchy, starting from the voltage stabilization using battery DC-DC converters, via dynamic power sharing, up to predictive energy management and distributed optimization. In all these investigations, the aspects of modularity, adaptability, and optimization guided the approach. Across the different parts of the control hierarchy, the work demonstrates how voltage stabilization, coordinated control, and energy management can be realized in a way that accounts for the characteristics, limitations, and dynamics of each component while maintaining resilient system behavior. By combining fast-acting stabilization, capability-based power sharing, optimization of operational costs, and distributed methods that handle parameter changes, faults, and topology alterations, the contributions outline a modular approach that supports efficient, resilient, and scalable shipboard power system operation. The investigations contribute methods for control functionalities that are essential when it comes to the modular integration of FCs into electric systems onboard ships. The entirety of the contributions shall serve as a starting point for further refinement, deeper investigations and as a blueprint for practical applications. These efforts will ultimately lead to exploiting the full potential of modular power system control.

Bibliography

References

[1] "EU Climate Target Plan 2030: Building a modern, sustainable and resilient Europe," *European Commission*, https://climate.ec.europa.eu/eu-action/climate-strategies-targets/2030-climate-targets_en, (Accessed: 2026-03-11).

[2] "The Paris Agreement | UNFCCC," https://unfccc.int/process-and-meetings/the-paris-agreement/the-paris-agreement, (Accessed: 2026-03-11).

[3] "Transforming our World: The 2030 Agenda for Sustainable Development | Department of Economic and Social Affairs," https://sdgs.un.org/publications/transforming-our-world-2030-agenda-sustainable-development-17981, (Accessed: 2026-03-11).

[4] T.-H. Joung, S.-G. Kang, J.-K. Lee, and J. Ahn, "The IMO initial strategy for reducing Greenhouse Gas(GHG) emissions, and its follow-up actions towards 2050," *Journal of International Maritime Safety, Environmental Affairs, and Shipping*, Jan. 2020. doi: 10.1080/25725084.2019.1707938

[5] "Fourth Greenhouse Gas Study 2020," *International Maritime Organization*, https://www.imo.org/en/ourwork/environment/pages/fourth-imo-greenhouse-gas-study-2020.aspx, (Accessed: 2026-03-11).

[6] N. Shakeri, M. Zadeh, and J. Bremnes Nielsen, "Hydrogen Fuel Cells for Ship Electric Propulsion: Moving Toward Greener Ships," *IEEE Electrification Magazine*, Jun. 2020. doi: 10.1109/MELE.2020.2985484

[7] M. U. Mutarraf, Y. Terriche, K. A. K. Niazi, J. C. Vasquez, and J. M. Guerrero, "Energy Storage Systems for Shipboard Microgrids—A Review," *Energies*, Dec. 2018. doi: 10.3390/en11123492

[8] "REPowerEU: Affordable, secure and sustainable energy for Europe," *European Commission*, https://commission.europa.eu/strategy-and-policy/priorities-2019-2024/european-green-deal/repowereu-affordable-secure-and-sustainable-energy-europe_en, (Accessed: 2026-03-11).

[9] A. Haxhiu, A. Abdelhakim, S. Kanerva, and J. Bogen, "Electric Power Integration Schemes of the Hybrid Fuel Cells and Batteries-Fed Marine Vessels—An Overview," *IEEE Transactions on Transportation Electrification*, Jun. 2022. doi: 10.1109/TTE.2021.3126100

[10] L. Xu, J. Guerrero, A. Lashab, B. Wei, N. Bazmohammadi, J. Vasquez, and A. Abusorrah, "A Review of DC Shipboard Microgrids—Part II: Control Architectures, Stability

Analysis, and Protection Schemes," *IEEE Transactions on Power Electronics*, Apr. 2022. doi: 10.1109/TPEL.2021.3128409

[11] J. F. Hansen and F. Wendt, "History and State of the Art in Commercial Electric Ship Propulsion, Integrated Power Systems, and Future Trends," *Proceedings of the IEEE*, Dec. 2015. doi: 10.1109/JPROC.2015.2458990

[12] C. Nuchturee, T. Li, and H. Xia, "Energy efficiency of integrated electric propulsion for ships – A review," *Renewable and Sustainable Energy Reviews*, Dec. 2020. doi: 10.1016/j.rser.2020.110145

[13] J. Hou, J. Sun, and H. Hofmann, "Mitigating power fluctuations in electrical ship propulsion using model predictive control with hybrid energy storage system," in *Proceedings of the American Control Conference*, Portland, OR, USA, Jun. 2014. doi: 10.1109/ACC.2014.6858803

[14] S. Jayasinghe, L. Meegahapola, N. Fernando, Z. Jin, and J. Guerrero, "Review of Ship Microgrids: System Architectures, Storage Technologies and Power Quality Aspects," *Inventions*, Feb. 2017. doi: 10.3390/inventions2010004

[15] G. Sulligoi, A. Vicenzutti, and R. Menis, "All-Electric Ship Design: From Electrical Propulsion to Integrated Electrical and Electronic Power Systems," *IEEE Transactions on Transportation Electrification*, Dec. 2016. doi: 10.1109/TTE.2016.2598078

[16] L. Xu, J. Guerrero, A. Lashab, B. Wei, N. Bazmohammadi, J. Vasquez, and A. Abusorrah, "A Review of DC Shipboard Microgrids—Part I: Power Architectures, Energy Storage, and Power Converters," *IEEE Transactions on Power Electronics*, May 2022. doi: 10.1109/TPEL.2021.3128417

[17] A. Latorre, T. B. Soeiro, R. Geertsma, A. Coraddu, and H. Polinder, "Shipboard DC Systems—A Critical Overview: Challenges in Primary Distribution, Power-Electronics-Based Protection, and Power Scalability," *IEEE Open Journal of the Industrial Electronics Society*, Jul. 2023. doi: 10.1109/OJIES.2023.3294999

[18] Z. Jin, L. Meng, J. M. Guerrero, and R. Han, "Hierarchical Control Design for a Shipboard Power System With DC Distribution and Energy Storage Aboard Future More-Electric Ships," *IEEE Transactions on Industrial Informatics*, Feb. 2018. doi: 10.1109/TII.2017.2772343

[19] T. Dragicevic, X. Lu, J. Vasquez, and J. Guerrero, "DC Microgrids–Part I: A Review of Control Strategies and Stabilization Techniques," *IEEE Transactions on Power Electronics*, Sep. 2015. doi: 10.1109/TPEL.2015.2478859

[20] Y. Wang, S. Mondal, K. Satpathi, Y. Xu, S. Dasgupta, and A. K. Gupta, "Multiagent Distributed Power Management of DC Shipboard Power Systems for Optimal Fuel Efficiency," *IEEE Transactions on Transportation Electrification*, Dec. 2021. doi: 10.1109/TTE.2021.3086303

[21] L. Zhu, J. Han, D. Peng, T. Wang, T. Tang, and J.-F. Charpentier, "Fuzzy logic based energy management strategy for a fuel cell/battery/ultra-capacitor hybrid ship," in *2014 First International Conference on Green Energy ICGE 2014*, Sfax, Tunisia, Mar. 2014. doi: 10.1109/ICGE.2014.6835406

[22] A. M. Bassam, A. B. Phillips, S. R. Turnock, and P. A. Wilson, "An improved energy management strategy for a hybrid fuel cell/battery passenger vessel," *International Journal of Hydrogen Energy*, Dec. 2016. doi: 10.1016/j.ijhydene.2016.08.049

[23] F. Balsamo, C. Capasso, G. Miccione, and O. Veneri, "Hybrid Storage System Control Strategy for All-Electric Powered Ships," *Energy Procedia*, Sep. 2017. doi: 10.1016/j.egypro.2017.08.242

[24] L. Balestra and I. Schjølberg, "Energy management strategies for a zero-emission hybrid domestic ferry," *International Journal of Hydrogen Energy*, Nov. 2021. doi: 10.1016/j.ijhydene.2021.09.091

[25] T. Kopka, A. Coraddu, and H. Polinder, "Power System Control in DC Shipboard Power Systems: A Review of Methods and Architectures," *IEEE Access*, 2026. doi: 10.1109/ACCESS.2026.3702135

[26] J. M. Guerrero, J. C. Vasquez, J. Matas, L. G. de Vicuna, and M. Castilla, "Hierarchical Control of Droop-Controlled AC and DC Microgrids—A General Approach Toward Standardization," *IEEE Transactions on Industrial Electronics*, Jan. 2011. doi: 10.1109/TIE.2010.2066534

[27] J. Hu, Y. Shan, J. M. Guerrero, A. Ioinovici, K. W. Chan, and J. Rodriguez, "Model predictive control of microgrids – An overview," *Renewable and Sustainable Energy Reviews*, Feb. 2021. doi: 10.1016/j.rser.2020.110422

[28] O. Palizban and K. Kauhaniemi, "Hierarchical control structure in microgrids with distributed generation_ Island and grid-connected mode," *Renewable and Sustainable Energy Reviews*, Apr. 2015. doi: 10.1016/j.rser.2015.01.008

[29] M. Arnold, "On Predictive Control for Coordination in Multi-Carrier Energy Systems," PhD dissertation, ETH Zurich, 2011. doi: 10.3929/ETHZ-A-006712339

[30] R. Geertsma, R. Negenborn, K. Visser, and J. Hopman, "Design and control of hybrid power and propulsion systems for smart ships: A review of developments," *Applied Energy*, May 2017. doi: 10.1016/j.apenergy.2017.02.060

[31] A. Iovine, T. Rigaut, G. Damm, E. De Santis, and M. D. Di Benedetto, "Power management for a DC MicroGrid integrating renewables and storages," *Control Engineering Practice*, Apr. 2019. doi: 10.1016/j.conengprac.2019.01.009

[32] A. Haseltalab, "Control for autonomous all-electric ships: Integrating maneuvering, energy management, and power generation control," PhD dissertation, TU Delft, 2019. doi: uuid:82e02888-5f8d-4936-a33f-b1dcfad53b73

[33] P. Xie, J. M. Guerrero, S. Tan, N. Bazmohammadi, J. C. Vasquez, M. Mehrzadi, and Y. Al-Turki, "Optimization-Based Power and Energy Management System in Shipboard Microgrid: A Review," *IEEE Systems Journal*, Mar. 2022. doi: 10.1109/JSYST.2020.3047673

[34] A. Haseltalab, R. R. Negenborn, and G. Lodewijks, "Multi-Level Predictive Control for Energy Management of Hybrid Ships in the Presence of Uncertainty and Environmental Disturbances," *IFAC-PapersOnLine*, 2016. doi: 10.1016/j.ifacol.2016.07.016

[35] M. Babaei, J. Shi, and S. Abdelwahed, "A Survey on Fault Detection, Isolation, and Reconfiguration Methods in Electric Ship Power Systems," *IEEE Access*, Jan. 2018. doi: 10.1109/ACCESS.2018.2798505

[36] A. Haseltalab and R. R. Negenborn, "Model predictive maneuvering control and energy management for all-electric autonomous ships," *Applied Energy*, Oct. 2019. doi: 10.1016/j.apenergy.2019.113308

[37] A. Haseltalab, M. A. Botto, and R. R. Negenborn, "Model Predictive DC Voltage Control for all-electric ships," *Control Engineering Practice*, Sep. 2019. doi: 10.1016/j.conengprac.2019.06.018

[38] Y. Huang, L. Wang, Y. Zhang, L. Wang, and Z. Zhao, "An Overview of Multi-Energy Microgrid in All-Electric Ships," *Frontiers in Energy Research*, May 2022. doi: 10.3389/fenrg.2022.881548

[39] V. N. Coelho, M. Weiss Cohen, I. M. Coelho, N. Liu, and F. G. Guimarães, "Multi-agent systems applied for energy systems integration: State-of-the-art applications and trends in microgrids," *Applied Energy*, Feb. 2017. doi: 10.1016/j.apenergy.2016.10.056

[40] Z. Jin, G. Sulligoi, R. Cuzner, L. Meng, J. C. Vasquez, and J. M. Guerrero, "Next-Generation Shipboard DC Power System: Introduction Smart Grid and dc Microgrid Technologies into Maritime Electrical Netowrks," *IEEE Electrification Magazine*, Jun. 2016. doi: 10.1109/MELE.2016.2544203

[41] T. Vandoorn, J. De Kooning, B. Meersman, and L. Vandevelde, "Review of primary control strategies for islanded microgrids with power-electronic interfaces," *Renewable and Sustainable Energy Reviews*, Mar. 2013. doi: 10.1016/j.rser.2012.11.062

[42] D.-L. Nguyen and H.-H. Lee, "A survey on cooperative control strategies for DC microgrids," *Neurocomputing*, May 2022. doi: 10.1016/j.neucom.2021.11.036

[43] N. Doerry and K. McCoy, "Next Generation Integrated Power System: NGIPS Technology Development Roadmap," Defense Technical Information Center, Fort Belvoir, VA, Tech. Rep., Nov. 2007. doi: 10.21236/ADA519753

[44] S. Yang, S. Tan, and J.-X. Xu, "Consensus Based Approach for Economic Dispatch Problem in a Smart Grid," *IEEE Transactions on Power Systems*, Nov. 2013. doi: 10.1109/TPWRS.2013.2271640

[45] P. Xie, S. Tan, N. Bazmohammadi, Josep. M. Guerrero, Juan. C. Vasquez, J. M. Alcala, and J. E. M. Carreño, "A distributed real-time power management scheme for shipboard zonal multi-microgrid system," *Applied Energy*, Jul. 2022. doi: 10.1016/j.apenergy.2022.119072

[46] M. Mokhtar, M. I. Marei, and A. A. El-Sattar, "An Adaptive Droop Control Scheme for DC Microgrids Integrating Sliding Mode Voltage and Current Controlled Boost Converters," *IEEE Transactions on Smart Grid*, Mar. 2019. doi: 10.1109/TSG.2017.2776281

[47] S. Anand, B. G. Fernandes, and J. Guerrero, "Distributed Control to Ensure Proportional Load Sharing and Improve Voltage Regulation in Low-Voltage DC Microgrids," *IEEE Transactions on Power Electronics*, Apr. 2013. doi: 10.1109/TPEL.2012.2215055

[48] Y. Zeng, Q. Zhang, Y. Liu, X. Zhuang, X. Lv, and H. Wang, "An Improved Distributed Secondary Control Strategy for Battery Storage System in DC Shipboard Microgrid," *IEEE Transactions on Industry Applications*, May 2022. doi: 10.1109/TIA.2022.3153755

[49] F. Gao, R. Kang, J. Cao, and T. Yang, "Primary and secondary control in DC microgrids: A review," *Journal of Modern Power Systems and Clean Energy*, Mar. 2019. doi: 10.1007/s40565-018-0466-5

[50] Q. Xu, N. Vafamand, L. Chen, T. Dragičević, L. Xie, and F. Blaabjerg, "Review on Advanced Control Technologies for Bidirectional DC/DC Converters in DC Microgrids," *IEEE Journal of Emerging and Selected Topics in Power Electronics*, Apr. 2021. doi: 10.1109/JESTPE.2020.2978064

[51] M. R. Banaei and R. Alizadeh, "Simulation-Based Modeling and Power Management of All-Electric Ships Based on Renewable Energy Generation Using Model Predictive Control Strategy," *IEEE Intelligent Transportation Systems Magazine*, Apr. 2016. doi: 10.1109/MITS.2016.2533960

[52] M. A. Hassan, C.-L. Su, J. Pou, G. Sulligoi, D. Almakhles, D. Bosich, and J. M. Guerrero, "DC Shipboard Microgrids With Constant Power Loads: A Review of Advanced Nonlinear Control Strategies and Stabilization Techniques," *IEEE Transactions on Smart Grid*, Sep. 2022. doi: 10.1109/TSG.2022.3168267

[53] A. Haseltalab, F. Wani, and R. R. Negenborn, "Multi-level model predictive control for all-electric ships with hybrid power generation," *International Journal of Electrical Power & Energy Systems*, Feb. 2022. doi: 10.1016/j.ijepes.2021.107484

[54] M. H. Khooban, M. Gheisarnejad, H. Farsizadeh, A. Masoudian, and J. Boudjadar, "A New Intelligent Hybrid Control Approach for DC–DC Converters in Zero-Emission Ferry Ships," *IEEE Transactions on Power Electronics*, Jun. 2020. doi: 10.1109/TPEL.2019.2951183

[55] A. Accetta and M. Pucci, "Energy Management System in DC Micro-Grids of Smart Ships: Main Gen-Set Fuel Consumption Minimization and Fault Compensation," *IEEE Transactions on Industry Applications*, May 2019. doi: 10.1109/TIA.2019.2896532

[56] M. K. AL-Nussairi, R. Bayindir, S. Padmanaban, L. Mihet-Popa, and P. Siano, "Constant Power Loads (CPL) with Microgrids: Problem Definition, Stability Analysis and Compensation Techniques," *Energies*, Oct. 2017. doi: 10.3390/en10101656

[57] D. Radan, "Integrated Control of Marine Electrical Power Systems," PhD dissertation, Norwegian University of Science and Technology, 2008. ISBN 9788247166475

[58] M. Cupelli, F. Ponci, G. Sulligoi, A. Vicenzutti, C. S. Edrington, T. El-Mezyani, and A. Monti, "Power Flow Control and Network Stability in an All-Electric Ship," *Proceedings of the IEEE*, Dec. 2015. doi: 10.1109/JPROC.2015.2496789

[59] Y. Han, X. Ning, P. Yang, and L. Xu, "Review of Power Sharing, Voltage Restoration and Stabilization Techniques in Hierarchical Controlled DC Microgrids," *IEEE Access*, Oct. 2019. doi: 10.1109/ACCESS.2019.2946706

[60] M. U. Mutarraf, Y. Guan, Y. Terriche, C.-L. Su, M. Nasir, J. C. Vasquez, and J. M. Guerrero, "Adaptive Power Management of Hierarchical Controlled Hybrid Shipboard Microgrids," *IEEE Access*, Feb. 2022. doi: 10.1109/ACCESS.2022.3153109

[61] M. U. Mutarraf, Y. Terriche, K. A. K. Niazi, F. Khan, J. C. Vasquez, and J. M. Guerrero, "Control of Hybrid Diesel/PV/Battery/Ultra-Capacitor Systems for Future Shipboard Microgrids," *Energies*, Sep. 2019. doi: 10.3390/en12183460

[62] H. Park, J. Sun, S. Pekarek, P. Stone, D. Opila, R. Meyer, I. Kolmanovsky, and R. DeCarlo, "Real-Time Model Predictive Control for Shipboard Power Management Using the IPA-SQP Approach," *IEEE Transactions on Control Systems Technology*, Nov. 2015. doi: 10.1109/TCST.2015.2402233

[63] M. M. Mardani, M. H. Khooban, A. Masoudian, and T. Dragicevic, "Model Predictive Control of DC–DC Converters to Mitigate the Effects of Pulsed Power Loads in Naval DC Microgrids," *IEEE Transactions on Industrial Electronics*, Jul. 2019. doi: 10.1109/TIE.2018.2877191

[64] J. Kumar, A. Agarwal, and V. Agarwal, "A review on overall control of DC microgrids," *Journal of Energy Storage*, Feb. 2019. doi: 10.1016/j.est.2018.11.013

[65] H. Zhang, W. Xiang, W. Lin, and J. Wen, "Grid Forming Converters in Renewable Energy Sources Dominated Power Grid: Control Strategy, Stability, Application, and Challenges," *Journal of Modern Power Systems and Clean Energy*, Nov. 2021. doi: 10.35833/MPCE.2021.000257

[66] D. Kumar and F. Zare, "A Comprehensive Review of Maritime Microgrids: System Architectures, Energy Efficiency, Power Quality, and Regulations," *IEEE Access*, May 2019. doi: 10.1109/ACCESS.2019.2917082

[67] T. Fletcher, R. Thring, and M. Watkinson, "An Energy Management Strategy to concurrently optimise fuel consumption & PEM fuel cell lifetime in a hybrid vehicle," *International Journal of Hydrogen Energy*, Dec. 2016. doi: 10.1016/j.ijhydene.2016.08.157

[68] L. van Biert, M. Godjevac, K. Visser, and P. Aravind, "A review of fuel cell systems for maritime applications," *Journal of Power Sources*, Sep. 2016. doi: 10.1016/j.jpowsour.2016.07.007

[69] Z.-X. Xiao, Y.-Z. Guan, H.-W. Fang, Y. Terriche, and J. M. Guerrero, "Dynamic and Steady-State Power-Sharing Control of High-Efficiency DC Shipboard Microgrid Supplied by Diesel Generators," *IEEE Systems Journal*, Sep. 2022. doi: 10.1109/JSYST.2021.3111685

[70] B. Zahedi and L. E. Norum, "Voltage regulation and power sharing control in ship LVDC power distribution systems," in *15th European Conference on Power Electronics and Applications (EPE)*, Lille, France, Sep. 2013. doi: 10.1109/EPE.2013.6631763

[71] S. Faddel, T. A. Youssef, and O. Mohammed, "Decentralized Controller for Energy Storage Management on MVDC Ship Power System with Pulsed Loads," in *2018 IEEE Transportation Electrification Conference and Expo (ITEC)*, Long Beach, CA, USA, Jun. 2018. doi: 10.1109/ITEC.2018.8450147

[72] A. A. Jamil, W. F. Tu, M. U. Tahir, J. C. Lee, Y. Terriche, and J. M. Guerrero, "A decentralized control strategy for optimal operation of multi-sources in shipboard power systems," *Electrical Engineering*, Jul. 2025. doi: 10.1007/s00202-025-02990-3

[73] A. Haseltalab, L. van Biert, H. Sapra, B. Mestemaker, and R. R. Negenborn, "Component sizing and energy management for SOFC-based ship power systems," *Energy Conversion and Management*, Oct. 2021. doi: 10.1016/j.enconman.2021.114625

[74] Z. Jin, L. Meng, J. C. Vasquez, and J. M. Guerrero, "Specialized hierarchical control strategy for DC distribution based shipboard microgrids: A combination of emerging DC shipboard power systems and microgrid technologies," in *IECON 2017 - 43rd Annual Conference of the IEEE Industrial Electronics Society*, Beijing, China, Oct. 2017. doi: 10.1109/IECON.2017.8217191

[75] X. Chen, J. Zhou, M. Shi, L. Yan, W. Zuo, and J. Wen, "A Novel Virtual Resistor and Capacitor Droop Control for HESS in Medium-Voltage DC System," *IEEE Transactions on Power Systems*, Jul. 2019. doi: 10.1109/TPWRS.2019.2894754

[76] J. Khazaei, "Optimal Flow of MVDC Shipboard Microgrids With Hybrid Storage Enhanced With Capacitive and Resistive Droop Controllers," *IEEE Transactions on Power Systems*, Jul. 2021. doi: 10.1109/TPWRS.2021.3049343

[77] Y. Zhang and Y. Wei Li, "Energy Management Strategy for Supercapacitor in Droop-Controlled DC Microgrid Using Virtual Impedance," *IEEE Transactions on Power Electronics*, Apr. 2017. doi: 10.1109/TPEL.2016.2571308

[78] L. Xu, B. Wei, Y. Yu, J. Guerrero, and J. Vasquez, "Coordinated control of diesel generators and batteries in dc hybrid electric shipboard power system," *Energies*, Oct. 2021. doi: 10.3390/en14196246

[79] X. Lu, K. Sun, J. M. Guerrero, J. C. Vasquez, L. Huang, and R. Teodorescu, "SoC-based droop method for distributed energy storage in DC microgrid applications," in *2012 IEEE International Symposium on Industrial Electronics*, Hangzhou, China, May 2012. doi: 10.1109/ISIE.2012.6237336

[80] T. Dragičević, J. M. Guerrero, J. C. Vasquez, and D. Škrlec, "Supervisory Control of an Adaptive-Droop Regulated DC Microgrid With Battery Management Capability," *IEEE Transactions on Power Electronics*, Feb. 2014. doi: 10.1109/TPEL.2013.2257857

[81] M. U. Mutarraf, Y. Terriche, M. Nasir, Y. Guan, C.-L. Su, J. C. Vasquez, and J. M. Guerrero, "A Decentralized Control Scheme for Adaptive Power-Sharing in Ships based Seaport Microgrid," in *IECON 2020 The 46th Annual Conference of the IEEE Industrial Electronics Society*, Singapore, Oct. 2020. doi: 10.1109/IECON43393.2020.9255344

[82] K. Kwon, D. Park, and M. K. Zadeh, "Load Frequency-Based Power Management for Shipboard DC Hybrid Power Systems," in *2020 IEEE 29th International Symposium on Industrial Electronics (ISIE)*, Delft, Netherlands, Jun. 2020. doi: 10.1109/ISIE45063.2020.9152418

[83] Z.-H. Zhao, "Improved fuzzy logic control-based energy management strategy for hybrid power system of FC/PV/battery/SC on tourist ship," *International Journal of Hydrogen Energy*, Feb. 2022. doi: 10.1016/j.ijhydene.2022.01.040

[84] H. Chen, Z. Zhang, C. Guan, and H. Gao, "Optimization of sizing and frequency control in battery/supercapacitor hybrid energy storage system for fuel cell ship," *Energy*, Apr. 2020. doi: 10.1016/j.energy.2020.117285

[85] J. Hou, J. Sun, and H. Hofmann, "Adaptive model predictive control with propulsion load estimation and prediction for all-electric ship energy management," *Energy*, May 2018. doi: 10.1016/j.energy.2018.03.019

[86] D. Park and M. Zadeh, "Modeling and Predictive Control of Shipboard Hybrid DC Power Systems," *IEEE Transactions on Transportation Electrification*, Jun. 2021. doi: 10.1109/TTE.2020.3027184

[87] J. Hou, Z. Song, H. Park, H. Hofmann, and J. Sun, "Implementation and evaluation of real-time model predictive control for load fluctuations mitigation in all-electric ship propulsion systems," *Applied Energy*, Nov. 2018. doi: 10.1016/j.apenergy.2018.08.079

[88] J. Hou, Z. Song, H. Hofmann, and J. Sun, "Adaptive model predictive control for hybrid energy storage energy management in all-electric ship microgrids," *Energy Conversion and Management*, Oct. 2019. doi: 10.1016/j.enconman.2019.111929

[89] J. Hou, J. Sun, and H. F. Hofmann, "Mitigating Power Fluctuations in Electric Ship Propulsion With Hybrid Energy Storage System: Design and Analysis," *IEEE Journal of Oceanic Engineering*, Jan. 2018. doi: 10.1109/JOE.2017.2674878

[90] T. I. Bø and T. A. Johansen, "Battery Power Smoothing Control in a Marine Electric Power Plant Using Nonlinear Model Predictive Control," *IEEE Transactions on Control Systems Technology*, Jul. 2017. doi: 10.1109/TCST.2016.2601301

[91] X. Wang, J. Atkin, N. Bazmohammadi, S. Bozhko, and J. M. Guerrero, "Optimal Load and Energy Management of Aircraft Microgrids Using Multi-Objective Model Predictive Control," *Sustainability*, Jan. 2021. doi: 10.3390/su132413907

[92] V. Nasirian, S. Moayedi, A. Davoudi, and F. L. Lewis, "Distributed Cooperative Control of DC Microgrids," *IEEE Transactions on Power Electronics*, Apr. 2015. doi: 10.1109/TPEL.2014.2324579

[93] T. V. Vu, S. Paran, T. E. Mezyani, and C. S. Edrington, "Real-time distributed power optimization in the DC microgrids of shipboard power systems," in *2015 IEEE Electric Ship Technologies Symposium (ESTS)*, Old Town Alexandria, VA, USA, Jun. 2015. doi: 10.1109/ESTS.2015.7157872

[94] Q. Zhang, Y. Zeng, Y. Liu, X. Zhuang, H. Zhang, W. Hu, and H. Guo, "An Improved Distributed Cooperative Control Strategy for Multiple Energy Storages Parallel in Islanded DC Microgrid," *IEEE Journal of Emerging and Selected Topics in Power Electronics*, Feb. 2022. doi: 10.1109/JESTPE.2021.3072701

[95] Y. Zeng, Q. Zhang, H. Yu, H. H. C. Iu, X. Zhang, Y. Liu, H. Guo, F. Zhang, and S. Liu, "Multi-Objective Fusion Controller for Plug-and-Play Distributed Energy Storage Systems in Shipboard DC Microgrids Based on Dynamic Diffusion Algorithm," *IEEE Transactions on Transportation Electrification*, Aug. 2025. doi: 10.1109/TTE.2025.3604057

[96] T. V. Vu, S. Paran, F. Diaz-Franco, T. El-Mezyani, and C. S. Edrington, "An Alternative Distributed Control Architecture for Improvement in the Transient Response of DC Microgrids," *IEEE Transactions on Industrial Electronics*, Jan. 2017. doi: 10.1109/TIE.2016.2607681

[97] T. V. Vu, D. Perkins, D. Gonsoulin, C. S. Edrington, B. Papari, K. Schoder, M. Stanovich, and M. Steurer, "Large-Scale Distributed Control for MVDC Ship Power Systems," in *IECON 2018 - 44th Annual Conference of the IEEE Industrial Electronics Society*, Washington, DC, USA, Oct. 2018. doi: 10.1109/IECON.2018.8591346

[98] J. Han, J.-F. Charpentier, and T. Tang, "An energy management system of a fuel cell/battery hybrid boat," *Energies*, Apr. 2014. doi: 10.3390/en7052799

[99] C.-L. Su, X.-T. Weng, and Ching-Jin Chen, "Power generation controls of fuel cell/energy storage hybrid ship power systems," in *2014 IEEE Conference and Expo Transportation Electrification Asia-Pacific (ITEC Asia-Pacific)*, Beijing, China, Aug. 2014. doi: 10.1109/ITEC-AP.2014.6940639

[100] Y. Yuan, J. Wang, X. Yan, B. Shen, and T. Long, "A review of multi-energy hybrid power system for ships," *Renewable and Sustainable Energy Reviews*, Oct. 2020. doi: 10.1016/j.rser.2020.110081

[101] M. Jaurola, A. Hedin, S. Tikkanen, and K. Huhtala, "Optimising design and power management in energy-efficient marine vessel power systems: A literature review," *Journal of Marine Engineering & Technology*, May 2019. doi: 10.1080/20464177.2018.1505584

[102] M. F. Zia, E. Elbouchikhi, and M. Benbouzid, "Microgrids energy management systems: A critical review on methods, solutions, and prospects," *Applied Energy*, Jul. 2018. doi: 10.1016/j.apenergy.2018.04.103

[103] H. Fontenot and B. Dong, "Modeling and control of building-integrated microgrids for optimal energy management – A review," *Applied Energy*, Nov. 2019. doi: 10.1016/j.apenergy.2019.113689

[104] S. Ali, Z. Zheng, M. Aillerie, J.-P. Sawicki, M.-C. Péra, and D. Hissel, "A Review of DC Microgrid Energy Management Systems Dedicated to Residential Applications," *Energies*, Jul. 2021. doi: 10.3390/en14144308

[105] Z. Zhang, C. Guan, and Z. Liu, "Real-Time Optimization Energy Management Strategy for Fuel Cell Hybrid Ships Considering Power Sources Degradation," *IEEE Access*, 2020. doi: 10.1109/ACCESS.2020.2991519

[106] M. Banaei, J. Boudjadar, R. Ebrahimy, and H. Madsen, "Optimal Control Strategies of Fuel cell/Battery Based Zero-Emission Ships: A Survey," in *IECON 2021 – 47th Annual Conference of the IEEE Industrial Electronics Society*, Toronto, ON, Canada, Oct. 2021. doi: 10.1109/IECON48115.2021.9589512

[107] Y. Huang, H. Wang, A. Khajepour, B. Li, J. Ji, K. Zhao, and C. Hu, "A review of power management strategies and component sizing methods for hybrid vehicles," *Renewable and Sustainable Energy Reviews*, Nov. 2018. doi: 10.1016/j.rser.2018.07.020

[108] J. M. Walker, A. Coraddu, and L. Oneto, "Power Demand Forecasting for a Hybrid Marine Energy System with Shallow and Deep Learning," in *OCEANS 2024 - Singapore*, Singapore, Apr. 2024. doi: 10.1109/OCEANS51537.2024.10682263

[109] A. Sciarretta and L. Guzzella, "Control of hybrid electric vehicles," *IEEE Control Systems Magazine*, Apr. 2007. doi: 10.1109/MCS.2007.338280

[110] T. P. Fletcher, "Optimal energy management strategy for a fuel cell hybrid electric vehicle," PhD dissertation, Loughborough University, Jan. 2017.

[111] L. Serrao, S. Onori, and G. Rizzoni, "A Comparative Analysis of Energy Management Strategies for Hybrid Electric Vehicles," *Journal of Dynamic Systems, Measurement, and Control*, Mar. 2011. doi: 10.1115/1.4003267

[112] Y. Huang, H. Wang, A. Khajepour, H. He, and J. Ji, "Model predictive control power management strategies for HEVs: A review," *Journal of Power Sources*, Feb. 2017. doi: 10.1016/j.jpowsour.2016.11.106

[113] P. Pan, Y. Sun, C. Yuan, X. Yan, and X. Tang, "Research progress on ship power systems integrated with new energy sources: A review," *Renewable and Sustainable Energy Reviews*, Jul. 2021. doi: 10.1016/j.rser.2021.111048

[114] M. F. M. Sabri, K. A. Danapalasingam, and M. F. Rahmat, "A review on hybrid electric vehicles architecture and energy management strategies," *Renewable and Sustainable Energy Reviews*, Jan. 2016. doi: 10.1016/j.rser.2015.09.036

[115] T. J. McCoy, "Integrated Power Systems—An Outline of Requirements and Functionalities for Ships," *Proceedings of the IEEE*, Dec. 2015. doi: 10.1109/JPROC.2015.2480597

[116] X.-H. Yuan, G.-D. Yan, H.-T. Li, X. Liu, C.-Q. Su, and Y.-P. Wang, "Research on energy management strategy of fuel cell–battery–supercapacitor passenger vehicle," *Energy Reports*, Apr. 2022. doi: 10.1016/j.egyr.2021.11.244

[117] M. Butcher, R. Maltby, and P. S. Parvin, "Compact DC power and propulsion systems - the definitive solution?" in *2009 IEEE Electric Ship Technologies Symposium*, Baltimore, MD, USA, Apr. 2009. doi: 10.1109/ESTS.2009.4906561

[118] S. Wen, H. Lan, Y.-Y. Hong, D. C. Yu, L. Zhang, and P. Cheng, "Allocation of ESS by interval optimization method considering impact of ship swinging on hybrid PV/diesel ship power system," *Applied Energy*, Aug. 2016. doi: 10.1016/j.apenergy.2016.05.003

[119] M. Soleymani, A. Yoosofi, and M. Kandi-D, "Sizing and energy management of a medium hybrid electric boat," *Journal of Marine Science and Technology*, Dec. 2015. doi: 10.1007/s00773-015-0327-0

[120] B. Zahedi, L. E. Norum, and K. B. Ludvigsen, "Optimized efficiency of all-electric ships by dc hybrid power systems," *Journal of Power Sources*, Jun. 2014. doi: 10.1016/j.jpowsour.2014.01.031

[121] T. Kopka, A. Coraddu, and H. Polinder, "Optimal Energy Management of FC- Battery Shipboard Power System using Dynamic Programming," in *2024 IEEE International Conference on Electrical Systems for Aircraft, Railway, Ship Propulsion and Road Vehicles & International Transportation Electrification Conference (ESARS-ITEC)*, Naples, Italy, Nov. 2024. doi: 10.1109/ESARS-ITEC60450.2024.10819881

[122] A. Haseltalab, L. van Biert, and B. Mestemaker, "Energy Management for Hybrid Power Generation Using Solid Oxide Fuel Cell," in *International Ship Control Systems Symposium*, Online, Oct. 2020. doi: 10.24868/issn.2631-8741.2020.006

[123] M. Banaei, J. Boudjadar, T. Dragičević, and M.-H. Khooban, "Cost Effective Operation of a Hybrid Zero-Emission Ferry Ship," in *2020 IEEE 11th International Symposium on Power Electronics for Distributed Generation Systems (PEDG)*, Dubrovnik, Croatia, Sep. 2020. doi: 10.1109/PEDG48541.2020.9244456

[124] L. Serrao, S. Onori, and G. Rizzoni, "ECMS as a realization of Pontryagin's minimum principle for HEV control," in *2009 American Control Conference*, St. Louis, MO, USA, 2009. doi: 10.1109/ACC.2009.5160628

[125] A. Sciarretta, L. Serrao, P. Dewangan, P. Tona, E. Bergshoeff, C. Bordons, L. Charmpa, Ph. Elbert, L. Eriksson, T. Hofman, M. Hubacher, P. Isenegger, F. Lacandia, A. Laveau, H. Li, D. Marcos, T. Nüesch, S. Onori, P. Pisu, J. Rios, E. Silvas, M. Sivertsson, L. Tribioli, A.-J. van der Hoeven, and M. Wu, "A control benchmark on the energy management of a plug-in hybrid electric vehicle," *Control Engineering Practice*, Aug. 2014. doi: 10.1016/j.conengprac.2013.11.020

[126] H. Grimmelius, "Control of Hybrid Ship Drive Systems," PhD dissertation, TU Delft, Delft, 2011.

[127] L. C. W. Yuan, T. Tjahjowidodo, G. S. G. Lee, R. Chan, and A. K. Adnanes, "Equivalent Consumption Minimization Strategy for hybrid all-electric tugboats to optimize fuel savings," in *Proc Am Control Conf*, Boston, MA, USA, 2016. doi: 10.1109/ACC.2016.7526743

[128] J.-C. Guan and B.-C. Chen, "Adaptive Power Management Strategy Based on Equivalent Fuel Consumption Minimization Strategy for a Mild Hybrid Electric Vehicle," in *2019 IEEE Vehicle Power and Propulsion Conference (VPPC)*, Hanoi, Vietnam, Oct. 2019. doi: 10.1109/VPPC46532.2019.8952289

[129] L. Serrao, S. Onori, A. Sciarretta, Y. Guezennec, and G. Rizzoni, "Optimal energy management of hybrid electric vehicles including battery aging," in *Proceedings of the 2011 American Control Conference*, San Francisco, CA, USA, Jun. 2011. doi: 10.1109/ACC.2011.5991576

[130] L. C. W. Yuan, T. Tjahjowidodo, G. G. L. Seet, and R. Chan, "Implementation of Optimization-Based Power Management for All-Electric Hybrid Vessels," *IEEE Access*, Nov. 2018. doi: 10.1109/ACCESS.2018.2883324

[131] Y. Xiang and X. Yang, "An ECMS for Multi-Objective Energy Management Strategy of Parallel Diesel Electric Hybrid Ship Based on Ant Colony Optimization Algorithm," *Energies*, Feb. 2021. doi: 10.3390/en14040810

[132] S. Paran, T. V. Vu, T. E. Mezyani, and C. S. Edrington, "MPC-based power management in the shipboard power system," in *2015 IEEE Electric Ship Technologies Symposium (ESTS)*, Old Town Alexandria, VA, USA, Jun. 2015. doi: 10.1109/ESTS.2015.7157855

[133] T. L. Vu, A. A. Ayu, J. S. Dhupia, L. Kennedy, and A. K. Adnanes, "Power Management for Electric Tugboats Through Operating Load Estimation," *IEEE Transactions on Control Systems Technology*, Nov. 2015. doi: 10.1109/TCST.2015.2399440

[134] L. C. W. Yuan, T. Tjahjowidodo, G. S. G. Lee, and R. Chan, "Optimizing fuel savings and power system reliability for all-electric hybrid vessels using Model Predictive Control," in *2017 IEEE International Conference on Advanced Intelligent Mechatronics (AIM)*, Munich, Germany, Jul. 2017. doi: 10.1109/AIM.2017.8014236

[135] W. Wang and J. P. Koeln, "Hierarchical Multi-Timescale Energy Management for Hybrid-Electric Aircraft," in *ASME 2020 Dynamic Systems and Control Conference*, Online, Jan. 2021. doi: 10.1115/DSCC2020-3190

[136] Y. Zhang, Q. Xue, D. Gao, W. Shi, and W. Yu, "Two-level model predictive control energy management strategy for hybrid power ships with hybrid energy storage system," *Journal of Energy Storage*, Aug. 2022. doi: 10.1016/j.est.2022.104763

[137] G. Seenumani, J. Sun, and H. Peng, "A hierarchical optimal control strategy for power management of hybrid power systems in all electric ships applications," in

49th IEEE Conference on Decision and Control (CDC), Atlanta, GA, USA, Dec. 2010. doi: 10.1109/CDC.2010.5717035

[138] G. Seenumani, "Real-time Power Management of Hybrid Power Systems in All Electric Ship Applications." PhD dissertation, 2010.

[139] S. Antonopoulos, K. Visser, M. Kalikatzarakis, and V. Reppa, "MPC Framework for the Energy Management of Hybrid Ships with an Energy Storage System," *Journal of Marine Science and Engineering*, Sep. 2021. doi: 10.3390/jmse9090993

[140] P. Xie, S. Tan, J. M. Guerrero, and J. C. Vasquez, "MPC-informed ECMS based real-time power management strategy for hybrid electric ship," *Energy Reports*, Apr. 2021. doi: 10.1016/j.egyr.2021.02.013

[141] F. D. Kanellos, G. J. Tsekouras, and N. D. Hatziargyriou, "Optimal Demand-Side Management and Power Generation Scheduling in an All-Electric Ship," *IEEE Transactions on Sustainable Energy*, Oct. 2014. doi: 10.1109/TSTE.2014.2336973

[142] F. D. Kanellos, J. Prousalidis, and G. J. Tsekouras, "Optimal Active Power Management in All Electric Ship Employing DC Grid Technology," in *Operational Research in Business and Economics*, Jul. 2016. doi: 10.1007/978-3-319-33003-7_14

[143] F. D. Kanellos, "Optimal Power Management With GHG Emissions Limitation in All-Electric Ship Power Systems Comprising Energy Storage Systems," *IEEE Transactions on Power Systems*, Jan. 2014. doi: 10.1109/TPWRS.2013.2280064

[144] F. D. Kanellos, A. Anvari-Moghaddam, and J. M. Guerrero, "Smart Shipboard Power System Operation and Management," *Inventions*, Dec. 2016. doi: 10.3390/inventions1040022

[145] A. Anvari-Moghaddam, T. Dragicevic, Lexuan Meng, Bo Sun, and J. M. Guerrero, "Optimal planning and operation management of a ship electrical power system with energy storage system," in *IECON 2016 - 42nd Annual Conference of the IEEE Industrial Electronics Society*, Florence, Italy, Oct. 2016. doi: 10.1109/IECON.2016.7793272

[146] C. Shang, D. Srinivasan, and T. Reindl, "Economic and Environmental Generation and Voyage Scheduling of All-Electric Ships," *IEEE Transactions on Power Systems*, Sep. 2016. doi: 10.1109/TPWRS.2015.2498972

[147] S. Wen, T. Zhao, Y. Tang, Y. Xu, S. Fang, M. Zhu, and Z. Ding, "Joint Energy Management and Voyage Scheduling for All-Electric Ships Using Dynamic Real-Time Electricity Price of Onshore Power," in *2020 IEEE/IAS 56th Industrial and Commercial Power Systems Technical Conference (I&CPS)*, Jun. 2020. doi: 10.1109/ICPS48389.2020.9176793

[148] S. Wen, T. Zhao, Y. Tang, Y. Xu, M. Zhu, S. Fang, and Z. Ding, "Coordinated Optimal Energy Management and Voyage Scheduling for All-Electric Ships Based on Predicted Shore-Side Electricity Price," *IEEE Transactions on Industry Applications*, Jan. 2021. doi: 10.1109/TIA.2020.3034290

[149] K. Hein, Y. Xu, G. Wilson, and A. K. Gupta, "Coordinated Optimal Voyage Planning and Energy Management of All-Electric Ship With Hybrid Energy Storage System," *IEEE Transactions on Power Systems*, May 2021. doi: 10.1109/TPWRS.2020.3029331

[150] R. Tang, X. Li, and J. Lai, "A novel optimal energy-management strategy for a maritime hybrid energy system based on large-scale global optimization," *Applied Energy*, Oct. 2018. doi: 10.1016/j.apenergy.2018.06.092

[151] F. F. Angkasa, R. Zafar, and I.-Y. Chung, "Optimal Power Generation and Voyage Scheduling in Shipboard Power Systems Considering Load Characteristics-Based Operating Reserve Management," *Journal of Electrical Engineering & Technology*, Jul. 2023. doi: 10.1007/s42835-023-01544-6

[152] T. C. J. Romijn, T. H. Pham, and S. Wilkins, "Modular ECMS Framework for Hybrid Vehicles," *IFAC-PapersOnLine*, Jan. 2019. doi: 10.1016/j.ifacol.2019.09.021

[153] Z. Zhang and M.-Y. Chow, "Incremental cost consensus algorithm in a smart grid environment," in *2011 IEEE Power and Energy Society General Meeting*, Detroit, MI, USA, Jul. 2011. doi: 10.1109/PES.2011.6039422

[154] J. Hu, M. Z. Q. Chen, J. Cao, and J. M. Guerrero, "Coordinated Active Power Dispatch for a Microgrid via Distributed Lambda Iteration," *IEEE Journal on Emerging and Selected Topics in Circuits and Systems*, Jun. 2017. doi: 10.1109/JETCAS.2017.2676019

[155] S. Luo, K. Peng, C. Hu, and R. Ma, "Consensus-Based Distributed Optimal Dispatch of Integrated Energy Microgrid," *Electronics*, Jan. 2023. doi: 10.3390/electronics12061468

[156] C. Lyu, Y. Jia, and Z. Xu, "A Novel Communication-Less Approach to Economic Dispatch for Microgrids," *IEEE Transactions on Smart Grid*, Jan. 2021. doi: 10.1109/TSG.2020.3018622

[157] H. Liu, Y. Shi, Z. Wang, L. Ran, Q. Lü, and H. Li, "A distributed algorithm based on relaxed ADMM for energy resources coordination," *International Journal of Electrical Power & Energy Systems*, Feb. 2022. doi: 10.1016/j.ijepes.2021.107482

[158] L. Huang, W. Sun, Q. Li, and W. Li, "Distributed real-time economic dispatch for islanded microgrids with dynamic power demand," *Applied Energy*, Jul. 2023. doi: 10.1016/j.apenergy.2023.121156

[159] A. Dimeas and N. Hatziargyriou, "Operation of a multiagent system for microgrid control," *IEEE Transactions on Power Systems*, Aug. 2005. doi: 10.1109/TPWRS.2005.852060

[160] P. Xie, S. Tan, V. Liso, S. S. Araya, and S. L. Sahlin, "A Modular Digital Twin Framework for Robust Energy Management in Multi-Energy Systems," *SSRN (Pre-Print)*, Jul. 2025. doi: 10.2139/ssrn.5335328

[161] Y. Zhang, Q. Shan, F. Teng, and T. Li, "Coordinated Energy Management Scheme for Ship-Harbour Energy System Based on Economic Optimal Scheduling," in *2021 International Conference on Security, Pattern Analysis, and Cybernetics (SPAC)*, Chengdu, China, Jun. 2021. doi: 10.1109/SPAC53836.2021.9539984

[162] K. K. Tafanidis, K. D. Taxeidis, F. D. Kanellos, and G. J. Tsekouras, "Optimal Operation of War-Ship Electric Power System Equipped with Energy Storage System," *Journal of Computations & Modelling*, 2013.

[163] S. Vedula, S. S. Alaviani, and O. M. Anubi, "Distributed Model-Predictive Energy Management Strategy for Shipboard Power Systems Considering Battery Degradation," *IFAC-PapersOnLine*, Jan. 2024. doi: 10.1016/j.ifacol.2025.01.061

[164] Y. Zhang, J. Chen, and Y. Yu, "Distributed power management with adaptive scheduling horizons for more electric aircraft," *International Journal of Electrical Power & Energy Systems*, Mar. 2021. doi: 10.1016/j.ijepes.2020.106581

[165] C. S. Edrington, G. Ozkan, B. Papari, D. E. Gonsoulin, D. Perkins, T. V. Vu, and H. Vahedi, "Distributed energy management for ship power systems with distributed energy storage," *Journal of Marine Engineering & Technology*, Jan. 2020. doi: 10.1080/20464177.2019.1684122

[166] K. Lai and M. S. Illindala, "A distributed energy management strategy for resilient shipboard power system," *Applied Energy*, Oct. 2018. doi: 10.1016/j.apenergy.2018.06.111

[167] Y. Zhang, Q. Shan, F. Teng, and T. Li, "Distributed Economic Optimal Scheduling Scheme for Ship-Integrated Energy System Based on Load Prediction Algorithm," *Frontiers in Energy Research*, Sep. 2021. doi: 10.3389/fenrg.2021.720374

[168] K. Huang, S. K. Srivastava, D. A. Cartes, and L.-H. Sun, "Market-based multiagent system for reconfiguration of shipboard power systems," *Electric Power Systems Research*, Apr. 2009. doi: 10.1016/j.epsr.2008.06.020

[169] K. Huang, D. Cartes, and S. Srivastava, "A multiagent based algorithm for ring-structured shipboard power system reconfiguration," in *2005 IEEE International Conference on Systems, Man and Cybernetics*, Waikoloa, HI, USA, Oct. 2005. doi: 10.1109/ICSMC.2005.1571200

[170] X. Feng, K. L. Butler-Purry, and T. Zourntos, "A Multi-Agent System Framework for Real-Time Electric Load Management in MVAC All-Electric Ship Power Systems," *IEEE Transactions on Power Systems*, May 2015. doi: 10.1109/TPWRS.2014.2340393

[171] A. Feliachi, K. Schoder, S. Ganesh, and H.-J. Lai, "Distributed control agents approach to energy management in electric shipboard power system," in *2006 IEEE Power Engineering Society General Meeting*, Montreal, QC, Canada, Jun. 2006. doi: 10.1109/PES.2006.1708943

[172] H. S. V. S. Kumar Nunna and S. Doolla, "Multiagent-Based Distributed-Energy-Resource Management for Intelligent Microgrids," *IEEE Transactions on Industrial Electronics*, Apr. 2013. doi: 10.1109/TIE.2012.2193857

[173] L. Yan, X. Chen, D. Liu, J. Zhou, and Y. Chen, "Fully distributed energy management in smart grids based on diffusion strategy," *International Journal of Electrical Power & Energy Systems*, Jul. 2021. doi: 10.1016/j.ijepes.2020.106759

[174] Z. Zhao, J. Guo, X. Luo, C. S. Lai, P. Yang, L. L. Lai, P. Li, J. M. Guerrero, and M. Shahidehpour, "Distributed Robust Model Predictive Control-Based Energy Management Strategy for Islanded Multi-Microgrids Considering Uncertainty," *IEEE Transactions on Smart Grid*, May 2022. doi: 10.1109/TSG.2022.3147370

[175] X. Feng, K. L. Butler-Purry, and T. Zourntos, "Multi-Agent System-Based Real-Time Load Management for All-Electric Ship Power Systems in DC Zone Level," *IEEE Transactions on Power Systems*, Nov. 2012. doi: 10.1109/TPWRS.2012.2194314

[176] M. R. Hossain and H. L. Ginn, "Real-Time Distributed Coordination of Power Electronic Converters in a DC Shipboard Distribution System," *IEEE Transactions on Energy Conversion*, Jun. 2017. doi: 10.1109/TEC.2017.2685593

[177] T. V. Vu, D. Gonsoulin, F. Diaz, C. S. Edrington, and T. El-Mezyani, "Predictive Control for Energy Management in Ship Power Systems Under High-Power Ramp Rate Loads," *IEEE Transactions on Energy Conversion*, Jun. 2017. doi: 10.1109/TEC.2017.2692058

[178] L. Balestra and I. Schjølberg, "Modelling and simulation of a zero-emission hybrid power plant for a domestic ferry," *International Journal of Hydrogen Energy*, Mar. 2021. doi: 10.1016/j.ijhydene.2020.12.187

[179] H. Pourrahmani, M. Gay, A. Yavarinasab, and J. Van herle, "Optimization and dynamic responses of an integrated fuel cell and battery system for an 800 kW ferry: A case study," *Energy Reports*, Nov. 2022. doi: 10.1016/j.egyr.2022.07.144

[180] A. M. Bassam, A. B. Phillips, S. R. Turnock, and P. A. Wilson, "Development of a multi-scheme energy management strategy for a hybrid fuel cell driven passenger ship," *International Journal of Hydrogen Energy*, Jan. 2017. doi: 10.1016/j.ijhydene.2016.08.209

[181] M. Banaei, M. Rafiei, J. Boudjadar, and M.-H. Khooban, "A Comparative Analysis of Optimal Operation Scenarios in Hybrid Emission-Free Ferry Ships," *IEEE Transactions on Transportation Electrification*, Mar. 2020. doi: 10.1109/TTE.2020.2970674

[182] M. Banaei, J. Boudjadar, and M.-H. Khooban, "Stochastic Model Predictive Energy Management in Hybrid Emission-Free Modern Maritime Vessels," *IEEE Transactions on Industrial Informatics*, Aug. 2021. doi: 10.1109/TII.2020.3027808

[183] M. Gaber, S. El-Banna, M. El-Dabah, and M. Hamad, "Intelligent Energy Management System for an all-electric ship based on adaptive neuro-fuzzy inference system," *Energy Reports*, Nov. 2021. doi: 10.1016/j.egyr.2021.06.054

[184] S. Hasanvand, M. Rafiei, M. Gheisarnejad, and M.-H. Khooban, "Reliable Power Scheduling of an Emission-Free Ship: Multiobjective Deep Reinforcement Learning," *IEEE Transactions on Transportation Electrification*, Jun. 2020. doi: 10.1109/TTE.2020.2983247

[185] D. Pivetta, C. Dall'Armi, and R. Taccani, "Multi-objective optimization of hybrid PEMFC/Li-ion battery propulsion systems for small and medium size ferries," *International Journal of Hydrogen Energy*, Oct. 2021. doi: 10.1016/j.ijhydene.2021.02.124

[186] M. Rafiei, J. Boudjadar, and M.-H. Khooban, "Energy Management of a Zero-Emission Ferry Boat With a Fuel-Cell-Based Hybrid Energy System: Feasibility Assessment," *IEEE Transactions on Industrial Electronics*, Feb. 2021. doi: 10.1109/TIE.2020.2992005

[187] T. Kopka, A. Latorre, A. Coraddu, and H. Polinder, "Energy-Based Voltage Stabilization in DC Shipboard Power Systems With Dual Loop Control," *IEEE Access*, Jul. 2025. doi: 10.1109/ACCESS.2025.3586382

[188] F. Gao, S. Bozhko, A. Costabeber, C. Patel, P. Wheeler, C. I. Hill, and G. Asher, "Comparative Stability Analysis of Droop Control Approaches in Voltage-Source-Converter-Based DC Microgrids," *IEEE Transactions on Power Electronics*, Mar. 2017. doi: 10.1109/TPEL.2016.2567780

[189] X. Lu, K. Sun, J. M. Guerrero, J. C. Vasquez, L. Huang, and J. Wang, "Stability Enhancement Based on Virtual Impedance for DC Microgrids With Constant Power Loads," *IEEE Transactions on Smart Grid*, Nov. 2015. doi: 10.1109/TSG.2015.2455017

[190] P. Liutanakul, A.-B. Awan, S. Pierfederici, B. Nahid-Mobarakeh, and F. Meibody-Tabar, "Linear Stabilization of a DC Bus Supplying a Constant Power Load: A General Design Approach," *IEEE Transactions on Power Electronics*, Feb. 2010. doi: 10.1109/TPEL.2009.2025274

[191] J. Zeng, Z. Zhang, and W. Qiao, "An interconnection-damping-assignment passivity-based controller for a DC-DC boost converter with a constant power load," in *2012 IEEE Industry Applications Society Annual Meeting*, Las Vegas, NV, USA, Oct. 2012. doi: 10.1109/IAS.2012.6374043

[192] M. A. Hassan, E.-p. Li, X. Li, T. Li, C. Duan, and S. Chi, "Adaptive Passivity-Based Control of dc–dc Buck Power Converter With Constant Power Load in DC Microgrid Systems," *IEEE Journal of Emerging and Selected Topics in Power Electronics*, Sep. 2019. doi: 10.1109/JESTPE.2018.2874449

[193] M. A. Hassan and Y. He, "Constant Power Load Stabilization in DC Microgrid Systems Using Passivity-Based Control With Nonlinear Disturbance Observer," *IEEE Access*, May 2020. doi: 10.1109/ACCESS.2020.2992780

[194] W. He and R. Ortega, "Design and Implementation of Adaptive Energy Shaping Control for DC–DC Converters With Constant Power Loads," *IEEE Transactions on Industrial Informatics*, Aug. 2020. doi: 10.1109/TII.2019.2953694

[195] A. M. Rahimi and A. Emadi, "Active Damping in DC/DC Power Electronic Converters: A Novel Method to Overcome the Problems of Constant Power Loads," *IEEE Transactions on Industrial Electronics*, May 2009. doi: 10.1109/TIE.2009.2013748

[196] M. Wu and D. D.-C. Lu, "Active stabilization methods of electric power systems with constant power loads: A review," *Journal of Modern Power Systems and Clean Energy*, Sep. 2014. doi: 10.1007/s40565-014-0066-y

[197] S. Liu, P. Su, and L. Zhang, "A Virtual Negative Inductor Stabilizing Strategy for DC Microgrid With Constant Power Loads," *IEEE Access*, Oct. 2018. doi: 10.1109/ACCESS.2018.2874201

[198] T. L. Vandoorn, J. C. Vasquez, J. De Kooning, J. M. Guerrero, and L. Vandevelde, "Microgrids: Hierarchical Control and an Overview of the Control and Reserve Management Strategies," *IEEE Industrial Electronics Magazine*, Dec. 2013. doi: 10.1109/MIE.2013.2279306

[199] L. Meng, T. Dragicevic, J. C. Vasquez, and J. M. Guerrero, "Tertiary and Secondary Control Levels for Efficiency Optimization and System Damping in Droop Controlled DC–DC Converters," *IEEE Transactions on Smart Grid*, Nov. 2015. doi: 10.1109/TSG.2015.2435055

[200] T. Kopka, F. Mylonopoulos, A. Coraddu, and H. Polinder, "Decentralized Power Sharing with Frequency Decoupling for a Fuel Cell-Battery DC Shipboard Power System," in *Modelling and Optimisation of Ship Energy Systems 2023*, Delft, Netherlands, Oct. 2023. doi: 10.59490/moses.2023.670

[201] Y. Han, X. Ning, L. Li, P. Yang, and F. Blaabjerg, "Droop coefficient correction control for power sharing and voltage restoration in hierarchical controlled DC microgrids," *International Journal of Electrical Power & Energy Systems*, Dec. 2021. doi: 10.1016/j.ijepes.2021.107277

[202] X. Lu, J. M. Guerrero, K. Sun, and J. C. Vasquez, "An Improved Droop Control Method for DC Microgrids Based on Low Bandwidth Communication With DC Bus Voltage Restoration and Enhanced Current Sharing Accuracy," *IEEE Transactions on Power Electronics*, Apr. 2014. doi: 10.1109/TPEL.2013.2266419

[203] S. Liu, H. Miao, J. Li, and L. Yang, "Voltage control and power sharing in DC Microgrids based on voltage-shifting and droop slope-adjusting strategy," *Electric Power Systems Research*, Jan. 2023. doi: 10.1016/j.epsr.2022.108814

[204] O. Tremblay, L.-A. Dessaint, and A.-I. Dekkiche, "A Generic Battery Model for the Dynamic Simulation of Hybrid Electric Vehicles," in *2007 IEEE Vehicle Power and Propulsion Conference*, Arlington, TX, USA, Sep. 2007. doi: 10.1109/VPPC.2007.4544139

[205] S. N. Njoya, O. Tremblay, and L.-A. Dessaint, "A generic fuel cell model for the simulation of fuel cell vehicles," in *2009 IEEE Vehicle Power and Propulsion Conference*, Dearborn, MI, USA, Sep. 2009. doi: 10.1109/VPPC.2009.5289692

[206] B. Zahedi and L. E. Norum, "Modeling and Simulation of All-Electric Ships With Low-Voltage DC Hybrid Power Systems," *IEEE Transactions on Power Electronics*, Oct. 2013. doi: 10.1109/TPEL.2012.2231884

[207] H. Zeng, Y. Zhao, X. Wang, T. He, and J. Zhang, "Modeling of Ship DC Power Grid and Research on Secondary Control Strategy," *Journal of Marine Science and Engineering*, Dec. 2022. doi: 10.3390/jmse10122037

[208] A.-C. Braitor, G. C. Konstantopoulos, and V. Kadirkamanathan, "Current-Limiting Droop Control Design and Stability Analysis for Paralleled Boost Converters in DC Microgrids," *IEEE Transactions on Control Systems Technology*, Jan. 2021. doi: 10.1109/TCST.2019.2951092

[209] "RT Box User Manual," https://www.plexim.com/sites/default/files/rtboxmanual.pdf, 2024, (Accessed: 2026-03-11).

[210] "ST Microelectronics - STM32 Nucleo-64 Boards Data Brief," https://www.st.com/resource/en/data_brief/nucleo-g474re.pdf, (Accessed: 2026-03-11).

[211] "Pico Technology Ltd. - PicoScope 5000 Series Datasheet," https://www.picotech.com/download/datasheets/PicoScope5000ABSeriesDataSheet.pdf, (Accessed: 2026-03-11).

[212] T. Kopka, C. Andrea, and H. Polinder, "Virtual impedance-based frequency decoupling for modular fuel cell-battery DC shipboard power systems," *Journal of Marine Engineering & Technology*, Apr. 2025. doi: 10.1080/20464177.2025.2489313

[213] M. S. Sadabadi, Q. Shafiee, and A. Karimi, "Plug-and-Play Robust Voltage Control of DC Microgrids," *IEEE Transactions on Smart Grid*, Nov. 2018. doi: 10.1109/TSG.2017.2728319

[214] H. Xing, C. Stuart, S. Spence, and H. Chen, "Fuel Cell Power Systems for Maritime Applications: Progress and Perspectives," *Sustainability*, Jan. 2021. doi: 10.3390/su13031213

[215] Q. Xu, X. Hu, P. Wang, J. Xiao, P. Tu, C. Wen, and M. Y. Lee, "A Decentralized Dynamic Power Sharing Strategy for Hybrid Energy Storage System in Autonomous DC Microgrid," *IEEE Transactions on Industrial Electronics*, Jul. 2017. doi: 10.1109/TIE.2016.2608880

[216] Z. Jin, L. Meng, J. C. Vasquez, and J. M. Guerrero, "Frequency-division power sharing and hierarchical control design for DC shipboard microgrids with hybrid energy storage systems," in *2017 IEEE Applied Power Electronics Conference and Exposition (APEC)*, Tampa, FL, USA, Mar. 2017. doi: 10.1109/APEC.2017.7931224

[217] F. Mylonopoulos, T. Kopka, A. Coraddu, and H. Polinder, "A Model-based Parametric Study for Comparison of System Configurations and Control of a Hydrogen Hybrid Cargo Vessel," in *Modelling and Optimisation of Ship Energy Systems 2023*, Delft, Netherlands, Oct. 2023. doi: 10.59490/moses.2023.671

[218] Nedstack, "Nedstack | FCS 13-XXL," https://nedstack.com/sites/default/files/2019-11/20191105_nedstack_fcs_13-xxl.pdf, Jul. 2023, (Accessed: 2026-03-11).

[219] F. Barbir, *PEM Fuel Cells: Theory and Practice 2nd Ed.* Elsevier Academic Press, 2013. ISBN 978-0-12-387710-9

[220] K. W. Harrison, R. Remick, A. Hoskin, and G. D. Martin, "Hydrogen Production: Fundamentals and Case Study Summaries," National Renewable Energy Lab. (NREL), Golden, CO, USA, Tech. Rep. NREL/CP-550-47302, Jan. 2010.

[221] V. Ahmadi Sarbast, "Modeling of proton exchange membrane fuel cell performance degradation and operation life," PhD dissertation, University of Victoria, 2021.

[222] S. Peyghami, H. Mokhtari, P. Davari, P. C. Loh, and F. Blaabjerg, "On Secondary Control Approaches for Voltage Regulation in DC Microgrids," *IEEE Transactions on Industry Applications*, Sep. 2017. doi: 10.1109/TIA.2017.2704908

[223] L. Balestra, "Design of Hybrid Fuel Cell/Battery Systems for Maritime Vessels," PhD dissertation, Norwegian University of Science and Technology, 2022. ISBN 9788232661374

[224] SH2IPDRIVE, "Sustainable Hydrogen Integrated Propulsion Drives," *SH2IPDRIVE*, https://sh2ipdrive.com/, 2024, (Accessed: 2026-03-11).

[225] G. Tsakyridis, N. I. Xiros, M. Scharringhausen, and L. Witte, "Design and Control of a DC Boost Converter for Fuel-Cell-Powered Marine Vehicles," *Journal of Marine Science and Application*, Jun. 2020. doi: 10.1007/s11804-020-00140-8

[226] E. Pahon, S. Jemei, N. Y. Steiner, and D. Hissel, "Effect of Load Cycling on the Performance of Fuel Cell Stacks," in *2019 IEEE Vehicle Power and Propulsion Conference (VPPC)*, Hanoi, Vietnam, Oct. 2019. doi: 10.1109/VPPC46532.2019.8952418

[227] M. Jourdan, H. Mounir, and A. El Marjani, "Compilation of factors affecting durability of Proton Exchange Membrane Fuel Cell (PEMFC)," in *2014 International Renewable and Sustainable Energy Conference (IRSEC)*, Ouarzazate, Morocco, Oct. 2014. doi: 10.1109/IRSEC.2014.7059906

[228] T. Kopka, C. Löffler, A. Coraddu, and H. Polinder, "Hierarchical Control Strategy for Fuel Cell-Battery Shipboard Power System Utilizing a Modular Control Architecture," in *2023 IEEE Transportation Electrification Conference and Expo, Asia-Pacific (ITEC Asia-Pacific)*, Chiang-Mai, Thailand, Nov. 2023. doi: 10.1109/ITECAsia-Pacific59272.2023.10372342

[229] K. van Berkel, B. de Jager, T. Hofman, and M. Steinbuch, "Implementation of Dynamic Programming for Optimal Control Problems With Continuous States," *IEEE Transactions on Control Systems Technology*, May 2015. doi: 10.1109/TCST.2014.2357342

[230] S. Tao, W. Chen, R. Gan, L. Li, G. Zhang, Y. Han, and Q. Li, "Energy management strategy based on dynamic programming with durability extension for fuel cell hybrid tramway," *Railway Engineering Science*, Sep. 2021. doi: 10.1007/s40534-021-00247-w

[231] F. D. Kanellos, A. Anvari-Moghaddam, and J. M. Guerrero, "A cost-effective and emission-aware power management system for ships with integrated full electric propulsion," *Electric Power Systems Research*, Sep. 2017. doi: 10.1016/j.epsr.2017.05.003

[232] RS-PRO, "Rechargeable Lithiumion Iron Phosphate Battery (LiFePO4) - Datasheet," https://docs.rs-online.com/f4c2/A700000009327850.pdf, (Accessed: 2026-03-11).

[233] E. Wallnöfer-Ogris, F. Poimer, R. Köll, M.-G. Macherhammer, and A. Trattner, "Main degradation mechanisms of polymer electrolyte membrane fuel cell stacks – Mechanisms, influencing factors, consequences, and mitigation strategies," *International Journal of Hydrogen Energy*, Jan. 2024. doi: 10.1016/j.ijhydene.2023.06.215

[234] H. Chen, P. Pei, and M. Song, "Lifetime prediction and the economic lifetime of Proton Exchange Membrane fuel cells," *Applied Energy*, Mar. 2015. doi: 10.1016/j.apenergy.2014.12.062

[235] F. A. de Bruijn, V. a. T. Dam, and G. J. M. Janssen, "Review: Durability and Degradation Issues of PEM Fuel Cell Components," *Fuel Cells*, Feb. 2008. doi: 10.1002/fuce.200700053

[236] "Clean Hydrogen Monitor 2022," *Hydrogen Europe*, https://hydrogeneurope.eu/clean-hydrogen-monitor-2022/, Oct. 2022, (Accessed: 2026-03-11).

[237] "Clean Hydrogen Monitor 2023," *Hydrogen Europe*, https://hydrogeneurope.eu/wp-content/uploads/2023/10/Clean_Hydrogen_Monitor_11-2023_DIGITAL.pdf, Oct. 2023, (Accessed: 2026-03-11).

[238] "Clean Hydrogen Joint Undertaking - Strategic Research and Innovation 2021-2027," *Clean Hydrogen Partnership*, https://www.clean-hydrogen.europa.eu/system/files/2022-02/Clean%20Hydrogen%20JU%20SRIA%20-%20approved%20by%20GB%20-%20clean%20for%20publication%20%28ID%2013246486%29.pdf, Feb. 2022, (Accessed: 2026-03-11).

[239] T. Kopka, S. Tamburello, L. Oneto, L. van Biert, H. Polinder, and A. Coraddu, "Degradation-aware predictive energy management for fuel cell-battery ship power system with data-driven load forecasting," *arXiv*, Apr. 2026. doi: 10.48550/arXiv.2604.14994

[240] B. Lim and S. Zohren, "Time-series forecasting with deep learning: a survey," *Philosophical Transactions of the Royal Society A*, 2021. doi: 10.1098/rsta.2020.0209

[241] S. Shalev-Shwartz and S. Ben-David, *Understanding machine learning: From theory to algorithms*. Cambridge university press, 2014.

[242] C. M. Bishop and H. Bishop, *Deep learning: Foundations and concepts*. Springer Nature, 2023.

[243] R. J. Hyndman, *Forecasting: principles and practice*. OTexts, 2018.

[244] B. N. Oreshkin, D. Carpov, N. Chapados, and Y. Bengio, "N-beats: Neural basis expansion analysis for interpretable time series forecasting," *arXiv preprint arXiv:1905.10437*, 2019. doi: 10.48550/arXiv.1905.10437

[245] D. Salinas, V. Flunkert, J. Gasthaus, and T. Januschowski, "Deepar: Probabilistic forecasting with autoregressive recurrent networks," *International journal of forecasting*, 2020. doi: 10.1016/j.ijforecast.2019.07.001

[246] W. X. Zhao, K. Zhou, J. Li, T. Tang, and Others, "A survey of large language models," *arXiv preprint arXiv:2303.18223*, 2023. doi: 10.48550/arXiv.2303.18223

[247] M. Awais, M. Naseer, S. Khan, R. M. Anwer, and Others, "Foundational models defining a new era in vision: A survey and outlook," *arXiv preprint arXiv:2307.13721*, 2023. doi: 10.48550/arXiv.2307.13721

[248] N. Gruver, M. Finzi, S. Qiu, and A. G. Wilson, "Large language models are zero-shot time series forecasters," *Advances in Neural Information Processing Systems*, 2024. doi: 10.48550/arXiv.2310.07820

[249] Y. Liang, H. Wen, Y. Nie, Y. Jiang, and Others, "Foundation models for time series analysis: A tutorial and survey," in *ACM SIGKDD Conference on Knowledge Discovery and Data Mining*, 2024. doi: arXiv.2403.14735

[250] S. P. Adam, S. A. N. Alexandropoulos, P. M. Pardalos, and M. N. Vrahatis, "No free lunch theorem: A review," *Approximation and optimization*, 2019. doi: 10.1007/978-3-030-12767-1_5

[251] G. Kleen and W. Gibbons, "DOE Hydrogen Program Record: Heavy-Duty Fuel Cell System Cost – 2023," https://www.hydrogen.energy.gov/docs/hydrogenprogramlibraries/pdfs/review24/24004-hd-fuel-cell-system-cost-2023.pdf, Aug. 2024, (Accessed: 2026-03-11).

[252] L. Mao, L. Jackson, and T. Jackson, "Investigation of polymer electrolyte membrane fuel cell internal behaviour during long term operation and its use in prognostics," *Journal of Power Sources*, Sep. 2017. doi: 10.1016/j.jpowsour.2017.07.018

[253] K. Meng, H. Zhou, B. Chen, and Z. Tu, "Dynamic current cycles effect on the degradation characteristic of a H2/O2 proton exchange membrane fuel cell," *Energy*, Jun. 2021. doi: 10.1016/j.energy.2021.120168

[254] M. Jouin, M. Bressel, S. Morando, R. Gouriveau, D. Hissel, M.-C. Péra, N. Zerhouni, S. Jemei, M. Hilairet, and B. Ould Bouamama, "Estimating the end-of-life of PEM fuel cells: Guidelines and metrics," *Applied Energy*, Sep. 2016. doi: 10.1016/j.apenergy.2016.05.076

[255] T. Chen and C. Guestrin, "Xgboost: A scalable tree boosting system," in *acm sigkdd international conference on knowledge discovery and data mining*, 2016. doi: 10.1145/2939672.2939785

[256] S. Bai, J. Z. Kolter, and V. Koltun, "An empirical evaluation of generic convolutional and recurrent networks for sequence modeling," *arXiv preprint arXiv:1803. 01271*, 2018. doi: 10.48550/arXiv.1803.01271

[257] A. Das, W. Kong, R. Sen, and Y. Zhou, "A decoder-only foundation model for time-series forecasting," in *International Conference on Machine Learning*, 2024. doi: 10.48550/arXiv.2310.10688

[258] J. Herzen, F. Lässig, S. G. Piazzetta, T. Neuer, and Others, "Darts: User-friendly modern machine learning for time series," *Journal of Machine Learning Research*, 2022. doi: 10.48550/arXiv.2110.03224

[259] L. Oneto, *Model Selection and Error Estimation in a Nutshell*. Springer, 2020.

[260] M. Z. Naser and A. H. Alavi, "Error metrics and performance fitness indicators for artificial intelligence and machine learning in engineering and sciences," *Architecture, Structures and Construction*. doi: 10.1007/s44150-021-00015-8

[261] K. L. Sainani, "The value of scatter plots," *PM&R*, 2016. doi: 10.1016/j.pmrj.2016.10.018

[262] T. Kopka, A. Coraddu, and H. Polinder, "Modular energy management via distributed and predictive optimization for fuel cell-battery shipboard microgrids," *IEEE Open Journal of the Industrial Electronics Society*, 2026. doi: 10.1109/OJIES.2026.3710800

[263] S. Qazi, P. Venugopal, G. Rietveld, T. B. Soeiro, U. Shipurkar, A. Grasman, A. J. Watson, and P. Wheeler, "Powering Maritime: Challenges and prospects in ship electrification," *IEEE Electrification Magazine*, Jun. 2023. doi: 10.1109/MELE.2023.3264926

[264] A. Coraddu, S. Tamburello, C. Löffler, H. E. Ceyhun, L. van Biert, and L. Oneto, "State-of-Art Energy Management Strategies for Hybrid Fuel Cell Applications for Ships," in *Fuel Cell and Hydrogen Technologies in Maritime Transportation*, C. O. Colpan, S. A. Korkmaz, and O. Konur, Eds. Springer Nature Switzerland, 2025. ISBN 978-3-031-86110-9

[265] A. Broer, H. Polinder, and L. van Biert, "Polymer electrolyte membrane fuel cell degradation in ships — Review of degradation mechanisms and research gaps," *Journal of Power Sources*, Jun. 2025. doi: 10.1016/j.jpowsour.2025.236678

[266] S. Boyd, N. Parikh, E. Chu, B. Peleato, and J. Eckstein, "Distributed Optimization and Statistical Learning via the Alternating Direction Method of Multipliers," *Foundations and Trends® in Machine Learning*, Nov. 2010. doi: 10.1561/2200000016

[267] G. Chen and Q. Yang, "An ADMM-Based Distributed Algorithm for Economic Dispatch in Islanded Microgrids," *IEEE Transactions on Industrial Informatics*, Sep. 2018. doi: 10.1109/TII.2017.2785366

[268] R. Negenborn and J. Maestre, "Distributed Model Predictive Control: An overview of features and research opportunities," in *Proceedings of the 11th IEEE International Conference on Networking, Sensing and Control, ICNSC 2014*, Miami, FL, USA, Apr. 2014. doi: 10.1109/ICNSC.2014.6819682

[269] T. Kopka, A. Coraddu, and H. Polinder, "Distributed MPC for Cost-Optimal Control of FC-Battery Shipboard Microgrids," in *2025 IEEE Seventh International Conference on DC Microgrids (ICDCM)*, Jun. 2025. doi: 10.1109/ICDCM63994.2025.11144727

[270] ——, "A Network-Coupled ADMM Framework for Distributed Energy Management in Multi-Bus Shipboard Microgrids," in *IFAC-PapersOnLine [Under Review]*.

[271] R. Van Der Sande, A. Shekhar, and P. Bauer, "Reliable DC Shipboard Power Systems—Design, Assessment, and Improvement," *IEEE Open Journal of the Industrial Electronics Society*, Jan. 2025. doi: 10.1109/OJIES.2025.3532095

[272] ——, "Reliability Assessment of Meshed DC Shipboard Power Systems Using Stochastic Simulation," in *2024 IEEE Sixth International Conference on DC Microgrids (ICDCM)*, Columbia, SC, USA, Aug. 2024. doi: 10.1109/ICDCM60322.2024.10664918

[273] C. Löffler, T. Kopka, R. Geertsma, H. Polinder, and A. Coraddu, "Optimizing Energy Management for Full-Electric Vessels: A Health-Aware Approach with Hydrogen and Diesel Employing Equivalent Consumption Minimization Strategy," in *2023 IEEE Transportation Electrification Conference and Expo, Asia-Pacific (ITEC Asia-Pacific)*, Chiang-Mai, Thailand, Nov. 2023. doi: 10.1109/ITECAsia-Pacific59272.2023.10372270

Acronyms

ADMM	alternating direction method of multipliers
BOL	begin-of-life
BTS	bus tie switch
CI	cold ironing
CPL	constant power load
DG	diesel generator
ECMS	equivalent consumption minimization strategy
EMS	energy management strategy
EOL	end-of-life
ESS	energy storage system
FC	fuel cell
GT	gas turbine
HESS	hybrid energy storage system
HiL	hardware-in-the-loop
MPC	model predictive control
PEMFC	proton-exchange membrane fuel cell
PI	proportional-integral
PSO	particle swarm optimization
PV	photovoltaic
PWM	pulse-width modulation
RES	renewable energy source
RTTM	real-time target machine
SDP	sequential dynamic programming
SoC	state-of-charge
SPS	shipboard power system
UC	ultra-capacitor
ZES	zero emission ship

About the Author

Timon Kopka received the B.Sc. and M.Sc. degrees in electric energy technology from RWTH Aachen University, Germany, in 2015 and 2018, respectively, and the M.Sc. degree in electric power engineering as part of the T.I.M.E. Double Degree Program from KTH Royal Institute of Technology, Sweden, in 2018. In 2019 he worked at FEV GmbH in Munich, Germany, in the development and fault analysis of embedded software for electric vehicles. From 2019 to 2022, he was a development engineer for control and drive systems in automotive brake-by-wire applications at LSP GmbH, Munich. In 2022, he moved to the Netherlands to join the Department of Maritime and Transport Technology at Delft University of Technology, to pursue his doctoral studies on the topic of modular power system control for fuel cell-battery DC ships as part of the SH2IPDRIVE project. His research features voltage control and power sharing in DC microgrids, predictive energy management and optimization for shipboard power systems, and distributed control architectures, as well as degradation-aware operation of fuel cells and energy storage systems. Therein he focuses on resilient, adaptable, and scalable methods to achieve a modular control framework.

List of Publications

Journal Articles

1. ***Timon Kopka**, Alejandro Latorre, Andrea Coraddu, and Henk Polinder*: Energy-Based Voltage Stabilization in DC Shipboard Power Systems With Dual Loop Control. IEEE Access, 2025 [187]

2. ***Timon Kopka**, Andrea Coraddu, and Henk Polinder*: Virtual impedance-based frequency decoupling for modular fuel cell-battery DC shipboard power systems. Journal of Marine Engineering & Technology, 2025 [212]

3. ***Timon Kopka**, Sara Tamburello, Luca Oneto, Lindert van Biert, Henk Polinder, and Andrea Coraddu*: Degradation-aware Predictive Energy Management for Fuel Cell-Battery Ship Power System with Data-driven Load Forecasting. (Under review, preprint accessible on arXiv), 2025 [239]

4. ***Timon Kopka**, Coraddu Andrea, and Henk Polinder*: Modular Energy Management via Distributed and Predictive Optimization for Fuel Cell-Battery Shipboard Microgrids. IEEE Open Journal of the Industrial Electronics Society, 2026 [262]

5. ***Timon Kopka**, Coraddu Andrea, and Henk Polinder*: Power System Control in DC Shipboard Power Systems: A Review of Methods and Architectures. IEEE Access, 2026 [25]

Included in this thesis.

Conference Proceedings

1. ***Timon Kopka**, Foivos Mylonopoulos, Andrea Coraddu, and Henk Polinder*: Decentralized Power Sharing with Frequency Decoupling for a Fuel Cell-Battery DC Shipboard Power System. Modelling and Optimisation of Ship Energy Systems 2023, Delft, The Netherlands [200]

2. *Foivos Mylonopoulos, **Timon Kopka**, Andrea Coraddu, and Henk Polinder*: A Model-based Parametric Study for Comparison of System Configurations and Control of a Hydrogen Hybrid Cargo Vessel. Modelling and Optimisation of Ship Energy Systems 2023, Delft, The Netherlands [217]

3. ***Timon Kopka**, Charlotte Löffler, Andrea Coraddu, and Henk Polinder*: Hierarchical Control Strategy for Fuel Cell-Battery Shipboard Power System Utilizing a Modular Control Architecture. 2023 IEEE Transportation Electrification Conference and Expo, Asia-Pacific (ITEC Asia-Pacific), Chiang-Mai, Thailand [228]

4. Charlotte Löffler, ***Timon Kopka**, Rinze Geertsma, Henk Polinder, and Andrea Coraddu*: Optimizing Energy Management for Full-Electric Vessels: A Health-Aware Approach with Hydrogen and Diesel Employing Equivalent Consumption Minimization Strategy. 2023 IEEE Transportation Electrification Conference and Expo, Asia-Pacific (ITEC Asia-Pacific), Chiang-Mai, Thailand [273]

5. ***Timon Kopka**, Andrea Coraddu, and Henk Polinder*: Optimal Energy Management of FC-Battery Shipboard Power System using Dynamic Programming. 2024 IEEE International Conference on Electrical Systems for Aircraft, Railway, Ship Propulsion and Road Vehicles & International Transportation Electrification Conference (ESARS-ITEC), Naples, Italy [121]

6. ***Timon Kopka**, Andrea Coraddu, and Henk Polinder*: Distributed MPC for Cost- Optimal Control of FC-Battery Shipboard Microgrids. 2025 IEEE Seventh International Conference on DC Microgrids (ICDCM), Tallinn, Estonia [269]

7. Andrea Coraddu, ***Timon Kopka**, and Luca Oneto*: Hybrid Vessel Load Forecasting Leveraging Time Series Foundation Models. Modelling and Optimisation of Ship Energy Systems 2025, Genova, Italy (In Press)

8. ***Timon Kopka**, Andrea Coraddu, and Henk Polinder*: A Network-Coupled ADMM Framework for Distributed Energy Management in Multi-Bus Shipboard Microgrids. 23rd IFAC World Congress 2026, Busan, Republic of Korea (In press) [270]

Included in this thesis.

